UNIVERSITY *of the*
WESTERN CAPE

THE NATURE OF GEOCHEMICAL ANOMALIES ASSOCIATED WITH THE PGE MINERALIZATION IN THE STELLA LAYERED INTRUSION, NORTH WEST PROVINCE, SOUTH AFRICA

By

Nomagugu Nkomo

A thesis

Submitted to the Faculty of Natural Sciences

in partial fulfilment of the requirements

for a Master of Science Degree in Applied Geology

Supervisors

Dr A. M. Siad

Prof C. Okujeni

University of the Western Cape

PLAGIARISM DECLARATION

I hereby declare that "*The nature of geochemical anomalies associated with the PGE mineralization in the Stella Layered Intrusion, North West Province, South Africa*" is my work and that it has not been previously submitted for any degree or examination at any institution. All the ideas obtained from the work of various authors have been acknowledged using in-text citations and a complete reference list.

---------- ----------

Signature Date

KEYWORDS

Exploration

Regolith geochemistry

Partial leach techniques

PGE mineralization

Stella Layered Intrusion

Secondary dispersion

ACKNOWLEDGMENTS

Firstly, all reverence goes to the Almighty God who has sustained me and made all this possible.

To my supervisors, Dr A. M. Siad and Prof C. Okujeni, I am indebted to you. Without your invaluable wisdom and insight, all this would not have been possible; your help throughout this project is much appreciated. To Dr Mwenze Tshipeng, thank you for your contributions towards this work.

I cannot forget to thank my wonderful mother for the endless support and patience through all the tough times and to my late father; I know you are looking down at me with pride. Lastly, Arthur Chikware, my great friend, thank you for persuading me to do this and all the support through the difficult times, words can never be enough to thank you.

ABSTRACT

The redistribution patterns of trace elements related to ore mineralisation in the secondary environment are the foundation of regolith exploration geochemistry. Understanding the controls of these element patterns is important for the detection of underlying ore deposits, especially in areas where bedrock is concealed by extensive regolith. The study area, which hosts PGE and gold deposits within the Stella Layered Intrusion is one such area. A major aim of this study was to use major element data to characterise the regolith materials enclosing the PGE mineralisation in the Stella Layered Intrusion to ascertain the degree of weathering that has occurred. Furthermore, the study aimed to relate the weathering patterns in regolith to the distribution of pathfinder elements of PGEs and gold in areas proximal and distal to the mineralised zones.

The study was conducted using XRF data, which included major oxide and trace element data. These data were used to characterise regolith materials (scatter plots, K/Al versus Mg/Al plots) and calculating indices that determine the degree of weathering such as CIA and ICV indices as well as A-CN-K and A-CN-FM diagrams. Signatures of pathfinder/ trace elements were enhanced by hydroxylamine hydrochloride partial selective leach technique. The distribution patterns of the partial leach data were compared to the intensity of weathering and weathering products, e.g. manganese oxides, carbonates in areas proximal and distal to the ore zone.

In the Serpens North Prospect, the major horizons that were identified include saprolith, stone line and aeolian sands. Incipient calcrete formation occurs in some parts of the Sirius Prospect, while in some parts, well developed, thick calcrete layers are found interlayered with the saprolith and aeolian sand.

Most elements including the major oxides K_2O, CaO, Na_2O, MgO, MnO and the trace elements Cu, Co, and Ni are enriched in the lower aeolian sand and the upper saprolith (saprolite and saprock). The transported regolith (aeolian sand) is most enriched in SiO_2, with concentrations exceeding 60 wt.%, moderate Fe_2O_3 and Al_2O_3. The saprolith is mostly enriched in Fe_2O_3 with most samples having Fe_2O_3 concentrations greater than 30 wt.% and generally high Al_2O_3 and SiO_2. The lateral dispersion trains of Cu, Co and Ni only extend to distances proximal to the ore body (50m). The distribution of Pd and Pt extends to areas that are distal to the ore body in some cases (up to 100m), while the upward mobility is restricted to the saprolith in Serpens North. In Sirius elements As, Ni, Co, Pd, and Pt are enriched above the calcrete layer, within the aeolian sand, implying that the regolith carbonates were emplaced after the elements were mobilised.

CONTENTS

LIST OF FIGURES

LIST OF TABLES

LIST OF APPENDICES

1 INTRODUCTION

1.1 BACKGROUND

1.1.1 Platinum Group Element (PGE) Occurrence

PGE ore-bearing minerals are classified as strategic in the International Strategic Minerals Inventory because 96- 99% of the world's production of these minerals are only in five intrusive complexes. The PGE metals from these ores cannot be substituted in their various industrial uses. According to Zientek et al., 2010, the crustal abundance of PGEs is estimated to range from tens to a few hundred parts per trillion (ppt), thus making them a rare commodity. There is a consensus amongst most researchers that the largest contributors of PGEs worldwide are magmatic sulphide deposits (Maier, 2005). However, other modes of PGE concentration have been suggested, including post-cumulus mobilization and precipitation of PGEs by a late magmatic-derived fluid phase and hydrothermal fluid interactions (Maier, 2005). Before 1920, most of the world's PGEs came from native platinum alloys obtained from placer deposits derived from ultramafic plutons in Russia and Columbia (Zientek, et al., 2010). Thereafter, magmatic sulphide deposits became the major source of PGEs with the first deposits being discovered in Sudbury, Canada (Zientek, et al., 2010). To date, some of the primary sources of PGEs are Norilsk, Russia, the Bushveld Complex (BIC), South Africa and the Great Dyke, Zimbabwe (Zientek, et al., 2010) and Stillwater (USA) (Stribryn, et al., 2000).

In South Africa, the BIC consists of PGE reef- type deposits mined in the Merensky reef, the UG2, and Platreef (Zientek, et al., 2010). Other deposits that host PGE deposits include: the

Uitkomst complex (conduit type, sill deposit) which is related to the Bushveld complex, rich in Cu and Ni deposits and the Stella Layered Intrusion which is also a sill deposit (Zientek, et al., 2010).

Of particular interest is the Stella Layered Intrusion in the North West Province. The area of study is extensively covered by regolith, resulting in the sporadic occurrence of outcrops, which has made it difficult for mining companies to understand the underlying geology in the area and explore for PGEs (Anhaeusser & Walraven, 1997).

1.1.2 Regolith geology

In regolith, secondary dispersion patterns of elements are depended on the cumulative effect of successive weathering episodes that have operated over geological time (Butt, 2005). Generally, the most extreme, longest lasting or the currently operating climatic regime is likely to influence the geomorphology, regolith framework and geochemical dispersion of elements in an area (Butt, 2005). One appropriate method for exploration in such terranes is a regolith geochemical survey (Hall, 1998). The technique has been successfully used to discover concealed deposits through understanding elemental dispersion patterns of ore elements and pathfinder elements in regolith profiles that are associated with the underlying mineralisation (Hamilton, 2007). It is, however, important to consider the entire regolith profile and identify the horizons, which are most likely to have trapped elements migrating from the ore body when using regolith geochemistry as an exploration tool (Hall, 1998).

Element migration from the primary ore body into the overlying regolith against gravity requires a medium (water, air, mineral particles), and a force (concentration, electrical, temperature, pressure gradient) (Aspandiar, et al., 2008). According to Aspandiar et al. (2008), the mechanisms of element migration can be classified as either phreatic (within the zone of saturation) or vadose (within the unsaturated zone). The phreatic mechanism encompasses advection (groundwater flow and convection) and chemical/ electrochemical transport (diffusion along a concentration gradient and electro-migration as a result of redox or spontaneous gradients) (Aspandiar et al., 2008; Hamilton, 2007). Migration of elements in the vadose zone includes capillary action, gaseous processes, plant uptake, as well as bioturbation (Aspandiar et al., 2008; Hamilton, 2007). The elements that are precipitated in different regolith horizons provide the geochemical signatures that are useful in delineating underlying mineralised deposits (Hamilton, 2007). The precipitation of elements is dependent on the characteristics of the regolith materials.

The characteristics of the regolith depend on the parent rock (regolith can be “in situ” that is; the product of the bedrock or “transported” from a different area) and its composition, climate, topography and biological activity (Hall, 1998). Horizons with different characteristics are found in regolith profiles, some of these horizons may be absent in some areas depending on factors such as nature of the parent rock, topography, climate and biological activity (Hall, 1998).

Downward percolating rainwater tends to move dissolved elements down the soil profile (Hall, 1998). In climatic regions where evaporation exceeds rainfall, the effects of evaporation and root-zone transpiration cause the precipitation of these mobile elements in areas where

the highest moisture loss is within the soil profile (Fabris et al., 2009). Humid regions are characterised by soils that are thoroughly leached; hence they have a well-defined iron-rich horizon, while in semi-arid regions there is minimal extensive downward leaching, often resulting in the formation of calcareous soils known as calcrete due to precipitation of calcite and gypsum (Hall, 1998). Depending on the climate and local conditions, carbonates may become the major sink for the accumulation of trace elements (Hall, 1998). According to Hall, 1998; the main control of trace element uptake by carbonates (in their metastable or polymorphic forms) is pH. Trace elements may be co-precipitated as their carbonates or, for example, Cd can replace Ca^{2+} in the crystal lattice (Hall, 1998).

On the other hand, areas that receive high rainfall with good drainage systems have extensive leaching, hence the A- and B- horizons are well-differentiated (Hall, 1998). In case the drainage system is poor, and leaching is minimal, reducing conditions prevail, resulting in the formation of a thick organic-rich layer over mottled subsoil (Hall, 1998).

1.1.3 Regolith profiles in arid to semi-arid regions

a. Regolith carbonates

In arid to semi-arid regions, soils are usually characterised by minimal amounts of organic matter, the prevalence of authigenic carbonates (calcite and dolomite), poorly developed regolith profiles and low biological activity (van Berkel, 1982). According to Chen, 2010a; regolith carbonates, for example, calcretes have different varieties such as pisolitic, powdery, nodular, hardpan and mottled carbonates. The pisolitic variety is characterised by rounded carbonate concretions, with massive carbonate and/or detrital grains at the centre as

described (Netterberg, 1969; Chen, 2010a). Calcretes can also be classified as powdery, which refers to fine, loose calcite particles (Netterberg, 1967; Chen, 2010a), which according to Netterberg, 1969 represents the initial stages of calcrete development. Some calcretes are described as nodular, which means that they have soft to hard irregular shaped concretions of carbonate-cemented soil (Netterberg, 1969; Chen, 2010a). Previous work by Netterberg, 1969; Chen, 2010a; also discusses a calcrete variety called hardpan, which is defined as an indurated sheet-like horizon. Mottled carbonates are a variety that is formed when carbonates precipitate within the host material (Chen, 2010a).

The sources of calcium and magnesium for the formation of regolith carbonates can be Ca and Mg-rich bedrock, aeolian dust, and groundwater (which acts as a transport and redistribution medium for Ca^{2+}, Mg^{2+}, and HCO^{3-}ions (Chen, 2010b). According to McGillis (1967) as cited in Lintern (2010), calcretes were first used as a sample medium in Russia as early as the 1950s and successively in Yilgarn craton during the 1970s. Initially, calcrete was regarded as a diluent, and its association with Cu and Au was considered to be random as discoveries were not made using any systematic exploration techniques (Lintern, 2010). In later studies conducted by (Lintern, 1989) in Western Australia, calcrete was successfully used as a sample medium in Au exploration where an unquestionable correlation between Au and calcretes was demonstrated. In contrast, Fe and many other elements were diluted, which was consistent with studies previously conducted on base metals (Mazzucchelli, 1972).

Although calcretes provide an easily identifiable sample medium, they present some challenges for exploration. In addition to the fact that calcrete dilutes and depresses the geochemical signatures that are already low due to leaching that occurred before to the

formation of the calcretes, they also introduce an alkaline environment into the host regolith material which reduces the mobility of elements and restricts the formation of epigenetic anomalies (Lintern, 2010)

b. Saprolith (Saprolite/ Saprock)

Saprolith forms the lower part of regolith that has mostly retained the fabric of the parent rock (Anand & Paine, 2002). Saprock forms during the earlier stages of weathering of bedrock, and thus is partially weathered, consisting of both altered and some unaltered minerals and characterised by low porosity (Taylor & Eggleton, 2001; Anand & Paine, 2002). The horizon, therefore, still retains the fabric and structural features of the bedrock (Taylor & Eggleton, 2001). According to Anand & Paine, 2002; less than 20% of weatherable minerals are altered. The difference between saprock and the overlying saprolite is that saprock is physically strong compared to saprolite. Saprolite is more altered than saprock, but still maintains some of the fabric and structural features of the parent rock as well. In the saprolite horizon, the more resistant minerals largely remain unaltered while the less resistant minerals are partially or entirely pseudomorphed by clays, oxides, and oxyhydroxides (Taylor & Eggleton, 2001). Anand & Paine, 2002 suggest that more than 20% of weatherable minerals are altered in saprolite.

c. Aeolian sands

Aeolian sands are accumulations of wind-blown, fine-grained, uniformly graded materials that are mainly found in desert areas (Elipe & Lopez-Querol, 2014). The grain size of Aeolian sand particles ranges from 0.063 mm - 2mm (Pye & Tsoar, 2009). The chemical and

mineralogical composition of Aeolian sand is dependent on geographical location, but in general, the main chemical component is silica (Elipe & Lopez-Querol, 2014).

1.1.4 The behaviour of PGEs in the surficial environment

According to Butt et al., 1992; a limited number of studies have been conducted to investigate the behaviour of PGEs in the weathering environment in a range of climatic and geographic regions. Studies were conducted in humid temperate regions of Canada and USA, humid tropical environments in Sierra Leone, New Caledonia, cold semi-arid conditions in the USA, and lateritic regolith in the warm and semi-arid regions of Western Australia (Butt, et al., 1992).

Studies conducted in the Lac Sheen Cu-Ni-PGE deposit in Quebec suggest that organic matter and sulphides are responsible for the mobility and redistribution of PGEs (Cook, et al., 1992). Based on their results, the authors concluded that platinum is mobile in the surficial environment, although its dispersion halo was found to be smaller than that of palladium owing to its lower mobility. A study conducted in the humid tropical environments of Sierra Leone suggests that the soil contains organic species that have a high affinity for PGEs (Bowles, et al., 1994). According to Bowles et al. (1994); organic matter is responsible for chelating metals in the study area. Hence the main constraint for PGE mobility is pH. Studies carried out by Fuchs & Rose, 1974 suggest that the mobility of PGEs in the cold, semi-arid region of Stillwater complex, Montana is constrained by Eh, pH, chloride concentration of soil water, and mode of occurrence in the primary rock prior to weathering. They concluded that palladium is mobile under less extreme pH and Eh conditions compared to platinum, thus

palladium is mostly depleted from surface horizons. Based on these observations, palladium occurs in readily extractable form and in soil phases such as clays. Thus, palladium tends to be partitioned in a variety of forms in weathered materials, while platinum remains relatively immobile and remains close to the source. In the warm and semi-arid Western Australia, there was no significant dispersion of PGEs in the town of Ora Banda, which is characterised by the presence of laterites (Butt, et al., 1992). According to work done by Hattori, 2004; there is a contrast in the behaviour of palladium between the temperate regions of Ontario and the hot, dry regions of Western Australia. The cold, humid conditions in Ontario are conducive for the accumulation of soils rich in organic matter (Hattori, 2004). Therefore, according to Hattori, 2004; palladium is mobile in surface environments in temperate regions and is subsequently adsorbed by humus and organic-rich sediments in swamps and along drainages. In contrast, the hot, dry conditions in Western Australia which have led to the development of laterites have led to the hampering of the mobility of palladium by the Fe oxides that are found in these environments (Hattori, 2004).

There has been some controversy surrounding the dispersion of PGEs in the supergene environments (zones of oxidation of the primary ore body by meteoric water), with some authors (including Hattori & Cabri (1992) as cited in Bowles et al., 1994) suggesting that PGEs are resistant to weathering processes and therefore occur as a resistate phase. However, according to other studies, PGEs can be dissolved and transported in solution (Bowles, et al., 1994). Dissolution of metals can occur for example under acidic, highly saline and high Eh environments, while environments that are more alkaline, less saline or have low Eh, metals are precipitated (Bowles, et al., 1994). The mobility of PGEs can be influenced by the

formation of complex ions with chlorides, sulphur oxyanions, organic matter, and arsenious acids, in aqueous environments (Butt, et al., 1992).

1.1.5 Geochemical techniques used in areas characterised by extensive regolith cover

In temperate alluvial terrains, water-extractable and adsorbed or exchangeable forms of metals give the most prominent indicators of mineralization. In arid sandy desert terrains, water-extractable metals and metals bound to oxides (i.e., iron and manganese oxides) are the best indicators of underlying mineralization while in cold grasslands, organically bound and water-extractable metals are effective indicators of mineralization at depth (Xueqiu, 1998).

Manganese oxides are responsible for scavenging mobile elements. Although soils generally contain less Mn oxides relative to Fe oxides, they have a greater sorption capability for trace elements because manganese can exist in various oxidation states (ii, iii, iv) and they form non-stoichiometric oxides with different valences (Chao and Theobald, 1976 as cited in Hall, 1998). Mn oxides have surface areas of several hundreds of m^2/g and larger cation exchange capacity (CEC) than some clay minerals (Hall, 1998).

Trace elements can also be adsorbed to the surface of amorphous Fe oxides, co-precipitated, or strongly bound within the oxide structure (Hall, 1998). Amorphous Fe oxides are more reactive than pseudocrystalline and crystalline oxides, which is why they provide the basis for its chemical separation, i.e. the dissolution of amorphous Fe only requires moderate reducing

conditions, while the dissolution of crystalline oxides require a strongly reducing environment (highly acidic environments) (Hall, 1998).

According to Patchineelam (1978) as cited in Chao (1984); carbonates are not as effective as Fe and Mn oxides in scavenging metals, however in semi-arid and arid regions where Fe and Mn oxides may be less dominant, carbonates can be considered as scavengers of metals. Adsorption of metals can occur through co-precipitation, and formation of insoluble metal hydroxides (Chao, 1984). The metals that are likely to be adsorbed onto carbonates include Co, Cu, Cd, Fe, Mn, Ni, Pb, Sr, U, and Zn (Hall, 1998).

The challenges associated with exploration in areas characterized by the occurrence of thick regolith cover have resulted in the development of various geochemical techniques to detect anomalous concentrations of elements that are associated with ore deposits (Chao, 1984). These techniques were developed over three decades ago, and they were initially subdivided into (1) partial dissolution and (2) total dissolution techniques (Chao, 1984). In the latter technique, the entire soil sample, including the crystalline minerals that are part of the soil matrix, are dissolved (Chao, 1984). Total dissolution implies that elements that are part of the endogenic component of the soil; for example, those present in transported regolith will also be dissolved (Hamilton, 2007). Endogenic components refer to minerals that originate from sources unrelated to the underlying mineralization, such as transported material (Hamilton, 2007). In the partial dissolution techniques, however, a specific soil phase is dissolved (partial digestion) and includes part of the soil matrix OR only the adsorbed elements are extracted (partial extraction) (Mann, 2009).

Partial dissolution techniques have been widely used in geochemical prospecting because they involve the use of weak digestion/ extractions which attempts to selectively dissolve the exogenic component of the soil which is composed of the mobile metals that are loosely bound and adsorbed to the mineral grain (Hamilton, 2007). However, in partial digestion part of the soil matrix may be dissolved although to a lesser extent compared to total digestion (Mann, 2009). This exogenic component is potentially linked to the underlying mineralization.

1.1.5.1 Partial leach techniques

According to Mann (2009), there is a technical difference between partial digestion and partial extraction methods. In partial digestion, part of the soil matrix is dissolved, whereas, partial extraction causes the mobile element that is loosely bound to the surface of soil particles to be detached without dissolving the matrix of the sample. Partial digestion can be subdivided into selective leaches that digest one specific soil phase and non-selective leaches that dissolve more than one soil phase. Partial extraction is also divided into selective (targeting specific soil phases) and non-selective leaches (non-specific in extraction). Selective leaches involve the digestion/ extraction of one specific soil phase, but according to Chao (1984), the idea that a dissolution technique can isolate an individual component should be viewed with skepticism. The classification of partial leach techniques that are used in exploration is shown in Table 1.1 below.

The different selective digestion and extraction techniques target different soil phases. Hydrogen peroxide, for example, is used in the digestion of samples that contain organic

matter in order to liberate elements adsorbed to their surface (Chao, 1984). Sodium hypochlorite was also found to digest organic matter without digesting Fe and Mn oxides (Chao, 1984). The digestion of Fe and Mn oxides can be achieved by using hydroxylamine hydrochloride (Chao, 1984; Jenne, 1987; Hamilton, 2007; Mann, 2009). Ammonium oxalate is a weak acid that is also used for the extraction of amorphous Fe oxides (Jenne, 1987). However, Jenne, 1987 suggested that the method has some disadvantages as it **only** partially digests the amorphous Fe oxides and leads to partial dissolution of crystalline Fe. A method that is commonly used in commercial laboratories for the digestion of amorphous and pseudocrystalline Mn oxides is enzyme leach (Hall, 1998; Cameron et al., 2004). Carbonates commonly occur in arid and semi-arid environments, and ammonium acetate is mainly used in their digestion (Cameron et al., 2004).

Inorganic acids are used as non-selective leaches because they are strong acids (Chao, 1984). Some of the inorganic acids that have been widely used in exploration include hydrochloric acid, nitric acid, and aqua regia (a mixture of HCl and HNO_3) (Chao, 1984). Aqua regia is capable of digesting inorganic and organic colloids, oxide precipitates and minerals, as well as sulphides (Chao, 1984; Cameron et al., 2004). Complexing agents (ligands) are used in the extraction of metals (Jenne, 1987; Mann, 2009). One such ligand, EDTA has previously been used to extract metals from Fe oxides, but the rate at which Fe was removed proved to be extremely slow (Borggaard, 1981 as cited in Jenne, 1987). A more recently used ligand-based partial extraction technique is the mobile metal ion (MMI) technique, which consists of an extracting solution containing a strong ligand for each analyte (Mann, 2009). The ligand is responsible for chelating mobile ions adsorbed to soil phases and converting them to soluble

species (Hall, 1998; Mann, 2009). MMI has been used in Western Australia, Canada, with much success, although the actual procedure has never been revealed to the public (Mann, et al., 2005).

Table 1.1: Summary of some of the partial leach techniques used in exploration geology (after Mann, 2009).

Partial digestion		Partial extraction	
Selective leaches	Non-selective leaches	Selective leaches	Non-selective leaches
Ammonium oxalate, Hydroxylamine hydrochloride, Hydrogen peroxide, Sodium hypochlorite, Enzyme leach, Acid acetates, and Ammonium citrate.	Aqua regia, Hydrochloric acid (diluted), Nitric acid (diluted) and Sodium hydroxide.	EDTA and Sodium pyrophosphate	MMI, Magnesium chloride, Ammonium acetate, and, BLEG

1.1.5.2 Partial leach technique used in this study

In this study, hydroxylamine hydrochloride was used to leach Fe-Mn oxides from regolith samples for analyses by GFAAS. The technique was selected because it has been proven to be effective in leaching Fe-Mn oxides; which is a major phase that adsorbs trace elements in ferruginous soils (Chao, 1984; Jenne, 1987; Hall, 1998; Cameron et al., 2004).

Hydroxylamine Hydrochloride ($NH_2OH.HCl$) is a relatively mild reducing agent, which was initially used to extract cryptocrystalline Mn oxides. This method was originally developed by Chester and Hughes (1967) and was improved by Chao and Zhou (1983), as cited in Jenne, 1987 to include the extraction of amorphous Fe oxides. The advantage of the improved method is that it dissolves less than 1% of crystalline Fe (Jenne, 1987) and it has been widely used in the extraction of trace elements that are adsorbed by Fe and Mn oxides. The use of this technique to extract elements from samples that contain carbonates results in an undesirable outcome because the dissolution of carbonates results in pH increase and this leads to the re-adsorption of sorbed metals released from oxides during the initial stage of the leaching process (Jenne, 1987). In their work, Thompson-Becker & Luoma (1985), as cited in Jenne, 1987, titrated the hydroxylamine hydrochloride and sample mixture back to pH 2 after adding the sample in order to mitigate the effects of variable pH in samples. The technique requires acidic conditions to give a desirable outcome, hence the increased analytical effort required to adjust the pH during extraction (Jenne, 1987).

1.2 STUDY AREA

The Kalplats project area is located 25km north of Stella Township, in the North West Province of South Africa, as shown in Figure 1.1 below (Lewins, et al., 2008). The study area is located on the southern part of the Kalahari and forms part of the savannah biome. The area is described as a semi-arid to an arid environment that is prone to droughts (Department of Rural, 2015). The landscape is characterised by slightly undulating to flat topography (elevation ranges from 1245 to 1275m) (Lewins, et al., 2008). Rainfall patterns vary across the Province, ranging from less than 300mm per annum in the west to 550mm per annum in the

central part of the region and 600m per annum in the eastern and south-eastern parts hence the province is classified as a semi-arid region with an average rainfall of about 539mm per annum (Department of Rural, 2015). Evaporation exceeds rainfall in most parts of the Northwest Province, and as a result, the province is highly dependent on groundwater to meet its needs (Department of Rural, 2015).

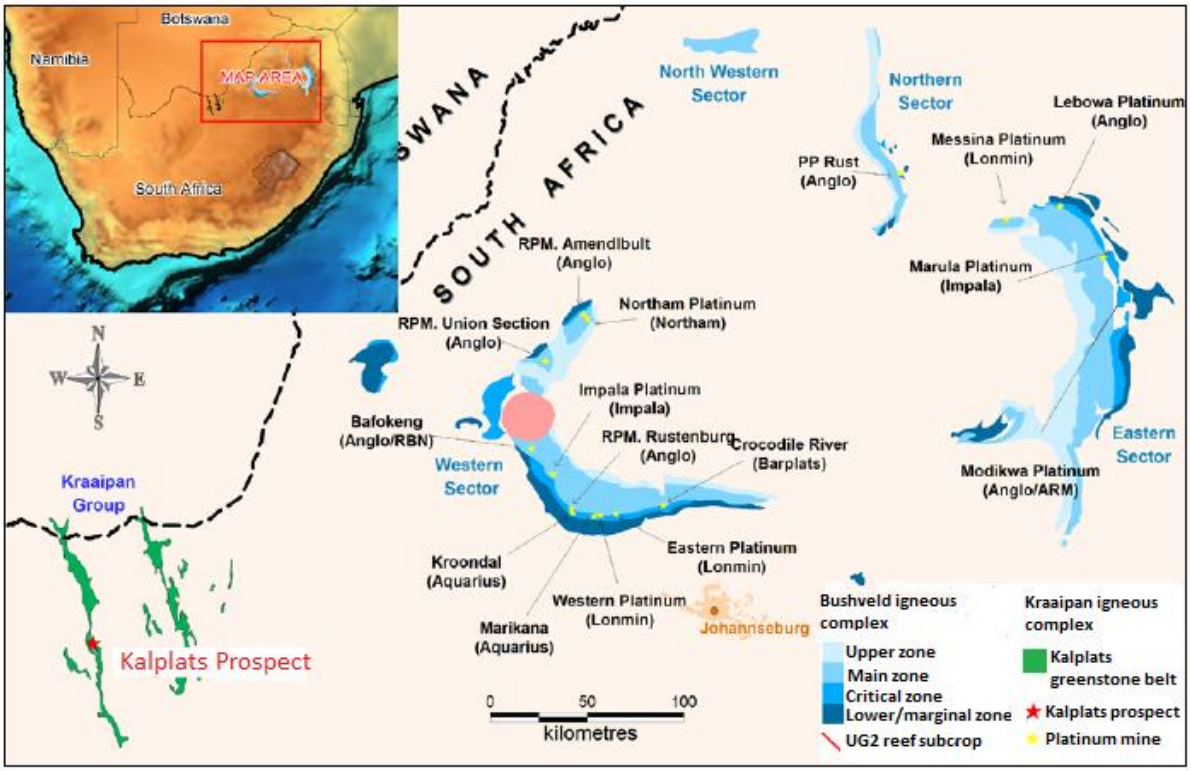

Figure 1.1: Location map of the area of study (Kalplats) (Platinum Australia Limited, 2007)

The temperatures vary daily and seasonally, with very hot summers (average temperature ranges of 17-32^{o}C in October-April) and mild to cold winters (average minimum temperatures of 4-20^{o}C in May-September (Department of Rural, 2015). The area is characterised by the occurrence of red-yellow aeolian Kalahari sands (Lewins, et al., 2008).

1.3 RATIONALE

Regolith geochemistry has played a major role in delineating concealed ore deposits. Such studies have been extensively conducted in Australia and Canada by various authors including, Loftus-Hills and Solomon, 1967, Butt et al., 1997; Anand, 2001; McQueen, 2006; Hall, 1998; Hamilton, 2007; Cameron, et al., 2004 and many others. However, there is a consensus that to delineate the underlying mineralisation successfully; it is important to successfully characterise regolith materials (Arhin, 2013). This is important because regolith materials are very complex, and elements will tend to undergo fractionation during weathering or be retained in particular regolith components to form characteristic geochemical signatures (Arhin, 2013). The nature of regolith was identified as a major control in the secondary dispersion of ore-related pathfinder elements and target elements (Arhin, 2013). Generally, in order to characterise regolith materials, it is important to understand the mineral composition of regolith. However, it is difficult to identify minerals in regolith because they are either very fine-grained or pulverised in drill cuttings (McQueen, 2006). Thus, methods such as X-Ray diffraction and Infra-red spectral analysis are usually used in order to identify minerals in such cases (McQueen, 2006). Where X-ray diffraction and Infra-red spectral analysis are unavailable, geochemical data can be used as a surrogate because minerals have a definite chemical composition (McQueen, 2006).

In the study area, studies have previously been conducted on the secondary dispersion of ore-related pathfinder elements and target elements in Sirius and Crater (Leuta, 2009). In the Kraaipan belt adjacent to the area of study, the controls of element dispersion on regolith were explained, with the emphasis of the role regolith materials play in the dispersion of trace

elements in the secondary environment (Okujeni et al., 2005). However, there has been no characterisation of the regolith materials using major element geochemical data. As a result, there is no literature explaining the mechanisms that control the secondary dispersion patterns of pathfinder elements and target elements.

1.4 PROBLEM STATEMENT

The regolith materials in Serpens North and Sirius have not been characterised using major element geochemical data. As a result, their influence/ control (these materials are responsible for retaining or releasing trace elements) on the secondary dispersion of pathfinder elements and target elements is not clearly defined.

1.5 AIMS AND OBJECTIVES

The main aim of this study was to use major element data to characterise the regolith materials enclosing the PGE mineralisation in the Stella Layered Intrusion and ascertain the degree of weathering that has occurred. Furthermore, the study aimed to relate the weathering patterns in regolith to the distribution of pathfinder elements of PGEs and gold in areas proximal and distal to the mineralised zones. In addition, the study aimed to determine which horizon is most ideal for sampling in future exploration work. The aims were achieved through:

- Investigation of the characteristics of the regolith materials from the bulk geochemical data using scatter plots, box plots, and principal component analysis;

- Investigation of the intensity of weathering that has occurred in the area from the bulk geochemical data, using K/Al versus Mg/Al ratios, CIA and ICV indices; A-CN-K and A-CNK-FM plots.
- Using available geochemical data obtained from using hydroxylamine hydrochloride partial leach technique which enhances geochemical signatures, to determine the mobilization and redistribution patterns of pathfinder elements and ore elements by modelling the spatial distribution of these elements.

Bulk geochemical data can be used to understand the composition of fresh rocks and to classify them. Additionally, the bulk composition of weathered materials can be used to understand the characteristics of regolith profiles, how weathering has influenced the mobilisation and redistribution of elements and subsequent formation of secondary minerals. Statistical analysis has been widely used to identify meaningful trends in geochemical data. A combination of graphic and text-based data summaries provide a foundation for context and comparison of different data types (Grunsky, 2010). Univariate data summaries such as box plots and statistical summary tables are useful when analysing data because they provide a summary of the distribution of data. While a single box plot provides a quick visual of the frequency distribution, multiple box plots can be used to provide summaries of comparisons between groups of data (Grunsky, 2010). Scatter plots are also a form of data representation that is useful in providing graphical representations used to assess the relationship between two variables visually. A multivariate plot that has been used across different fields of study is the principal component analysis. Principal component analysis can simplify a large set of data by decreasing the number of variables required to describe variations observed within a data set (Grunsky, 2010).

The use of geochemical indices was initially conducted by Nesbitt and Young (1982). In their work, they state that feldspars are the most abundant of the labile minerals. As a result, the degradation of feldspars during chemical weathering dominates, leading to the formation of clays. The highly mobile elements in the weathering environment include calcium, potassium, sodium, which results in the increased ratio of the relatively immobile aluminium to these alkalis in the weathering products (Nesbitt & Young, 1982). The Chemical Index of Alteration (CIA) was developed using the molecular proportions of these elements to determine the degree of weathering (Nesbitt & Young, 1982). In their successive work, Nesbitt & Young, 1984; developed A-CN-K plots to describe weathering trends. Further work conducted by Nesbitt & Young (1989) employed A-CNK-FM diagrams which were initially used to show the relationship between leucocratic and melanocratic constituents in the weathering environment. The use of bulk element composition of weathered materials in order to understand weathering trends using the above-mentioned indices was subsequently used in geochemical studies by authors such as Cox et al., 1995; McQueen, 2006; Goldberg & Humayun, 2010; Valiani & Rezaee, 2014; Arhin, et al., 2017; among others.

Spatial interpolation is a tool that is widely used by geoscientists to predict the values of a variable within the perimeter of a sampled location, where samples were not actually taken (Mitas & Mitasova, 1999; Li & Heap, 2014). The tool can be based on geostatistics (for example; ordinary kriging, simple kriging, dual kriging) or it can be non-geostatistical (such as; nearest neighbour, inverse distance weighting, regression models), while others are based on mixed methods (Li & Heap, 2014). The factors that influence the performance of spatial interpolation methods include; complexities of sample locations and spatial distribution of samples, as well as data nature and quality (Li & Heap, 2014).

Inverse-distance weighting (IDW) is a widely used spatial interpolation method by geoscientists because it is implemented in software packages such as many GIS packages (Lu & Wong, 2008) and Rockworks. This method is deterministic because it produces estimates without necessarily incorporating uncertainties (Li & Heap, 2014). In general, IDW is based on the idea that the attribute values of two sample points are related to each other. However, their similarity is inversely proportional to the distance between them (Lu & Wong, 2008). According to Fotheringham and O'Kelly, 1989, as cited in Lu & Wong, 2008, however, the relationship between any two locations in space is more complex than just being inversely proportional to the distance between two points. Thus, an exponential function or power is used to improve on this method (Lu & Wong, 2008).

2 GEOLOGY

2.1 OVERVIEW

The Kaapvaal craton forms the basement rocks in South Africa, and in the study area, these basement rocks are referred to as the Kraaipan granite-greenstone terrane (Anhaeusser & Walraven, 1999). The greenstone belt is comprised of iron formations, schists, and associated mafic volcanic rocks. However, its age is not well constrained (Brandl et al., 2006). The Stella Layered Intrusion, which hosts the Pt, Pd, and Au deposits intruded the Kraaipan granite-greenstone terrane at about 3.03 Ga (Anhaeusser & Walraven, 1999). Occasional occurrences of the neo-Archaean rocks of the Ventersdorp Supergroup have also been reported (Anhaeusser & Walraven, 1999). Overlying these rocks are the younger Tertiary Kalahari sediments.

Table 2.1: The sequence of rock emplacement in the Kraaipan granite-greenstone terrane (modified after Hunter, et al., 2006).

Geological Time (Ma)	**Event**
1-1.2	Deposition of the Kalahari Group sediments
2840-2700	The collision of the Kaapvaal and Zimbabwe cratons, Ventersdorp Supergroup deposition
3033±0.3	Stella Layered Intrusion emplacement
3644- 3100	Emplacement of Kraaipan greenstones TTG gneisses

The study area is located in the North West Province of South Africa. According to Anhaeusser and Walraven (1997), the literature available on the geology of this area has been inferred from the information obtained from the Witwatersrand basin by various mining companies that conducted studies in the area. This is partly because of the extensive regolith cover and

the scarcity of exposures which has hindered the construction of a complete stratigraphic sequence of the area (Anhaeusser & Walraven, 1997). However, because the underlying rocks are magnetic, this has enabled the extent of the Kraaipan granite-greenstone terrane to be mapped through airborne geophysical surveys (Haddon, 2005).

2.2 REGIONAL GEOLOGY

2.2.1 Southern African basement rocks (Kaapvaal craton)

The Kaapvaal craton, which was formed and stabilized between 3700 and 2700 Ma, is an Archaean granite-greenstone belt located in Southern Africa (Anhaeusser & Walraven, 1999). Rocks of Neoarchean and Proterozoic ages, as well as younger sequences of Cenozoic age, overlie the craton (Anhaeusser & Walraven, 1999). The extent of the Kaapvaal craton is shown in Figure 2.1 below.

The craton is largely comprised of tonalitic and trondhjemitic granodioritic gneisses (TTG) and subordinate volumes of metamorphosed volcano-sedimentary rocks (forming the greenstone terranes) (Haddon, 2005). A significant number of studies which provide information about the basement rocks have been carried out on the eastern and northern parts of the craton; in the southern part of Swaziland and to the north, the Barberton, Murchison, Pietersburg, and Sutherland granite-greenstone terranes (Anhaeusser & Walraven, 1999).

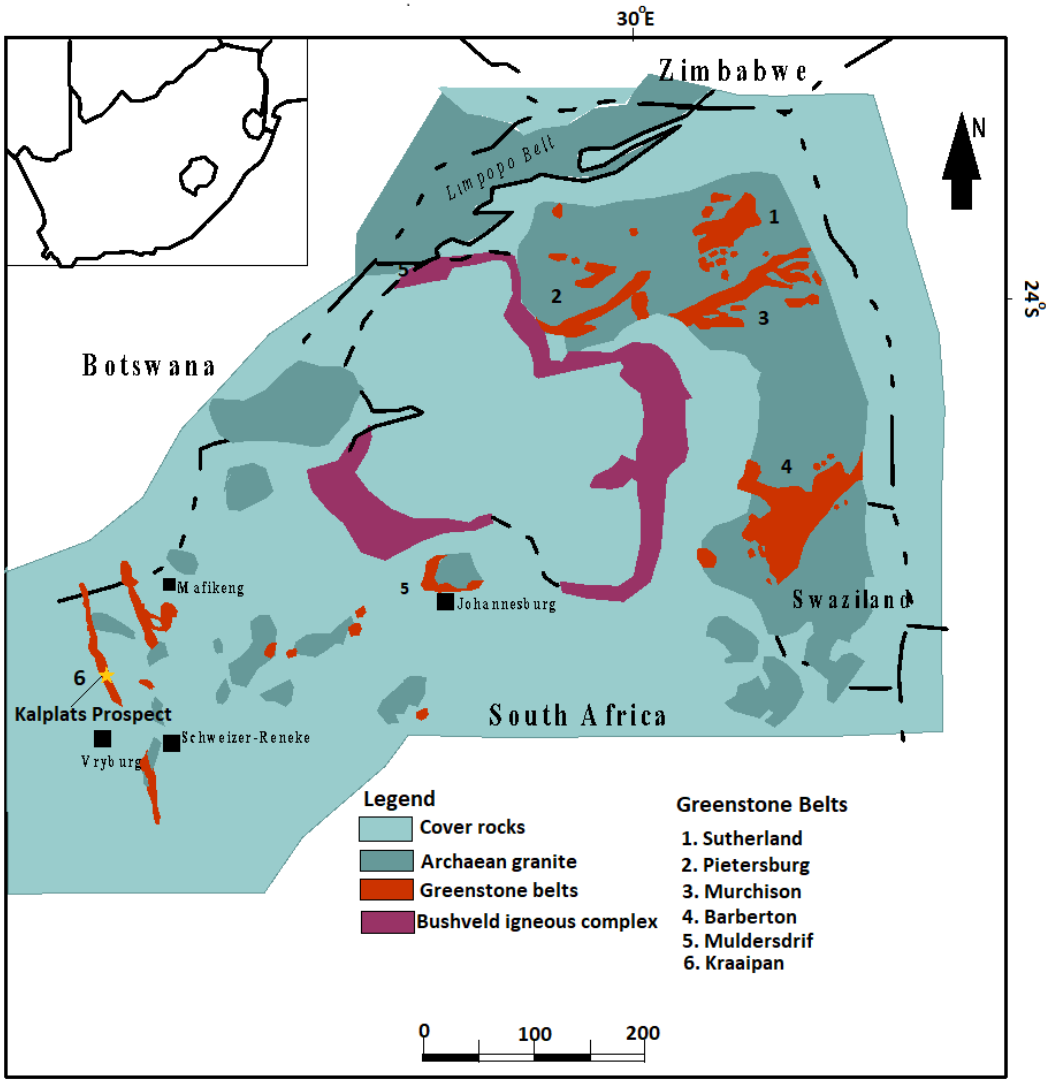

Figure 2.1: Geological map of the Kaapvaal craton, showing the distribution of Archaean basement rocks and greenstone terranes (after Anhaeusser and Walraven, 1999).

Earlier studies have suggested that the greenstones were part of the primordial crust and that the TTGs were derived from the partial melting of the oceanic basalts within these belts (Hunter, et al., 2006). The occurrence of xenoliths of the greenstones within the TTGs further reinforces the idea that the greenstones are older than the TTGs (Brandl, et al., 2006). However, successive radiometric dating has suggested that most of the TTG terranes may be older than the greenstones, although more studies need to be conducted to validate these results (Hunter et al., 2006). Another model was proposed to explain the evolution of the

craton, and it suggests that intra-oceanic obduction caused the imbrication and thickening of the oceanic crust which was then partially melted and formed the TTG (Hunter et al., 2006). This process was coupled with the initial continental lithosphere separation (Hunter et al., 2006). As repeated consolidation continued, the lithospheric plates eventually formed the more widespread and more stable Kaapvaal craton (Hunter et al., 2006).

The western part of the craton is characterized by limited exposures, stretching from the western part of Johannesburg and extending to Schweizer Reneke (Anhaeusser & Walraven, 1999). Intermittent outcrops of granitoids have been reported to occur in the Northwest province beneath the Neo-Archean rocks of the Ventersdorp Supergroup and the relatively younger Tertiary to recent sediments of the Kalahari Group (Anhaeusser and Walraven, 1999).

2.2.2 The Kraaipan Granite-Greenstone Belt

2.2.2.1 The greenstone belt

The Kraaipan greenstone belt is located in the North West Province of South Africa (Lewins, et al., 2008). It is one of the greenstone belts that form the Kaapvaal craton along with five other well know greenstone belts, as illustrated in Figure 2.1 above. The belt is comprised of three NNW trending belts shown in Figure 2.2 below (Brandl, et al., 2006).

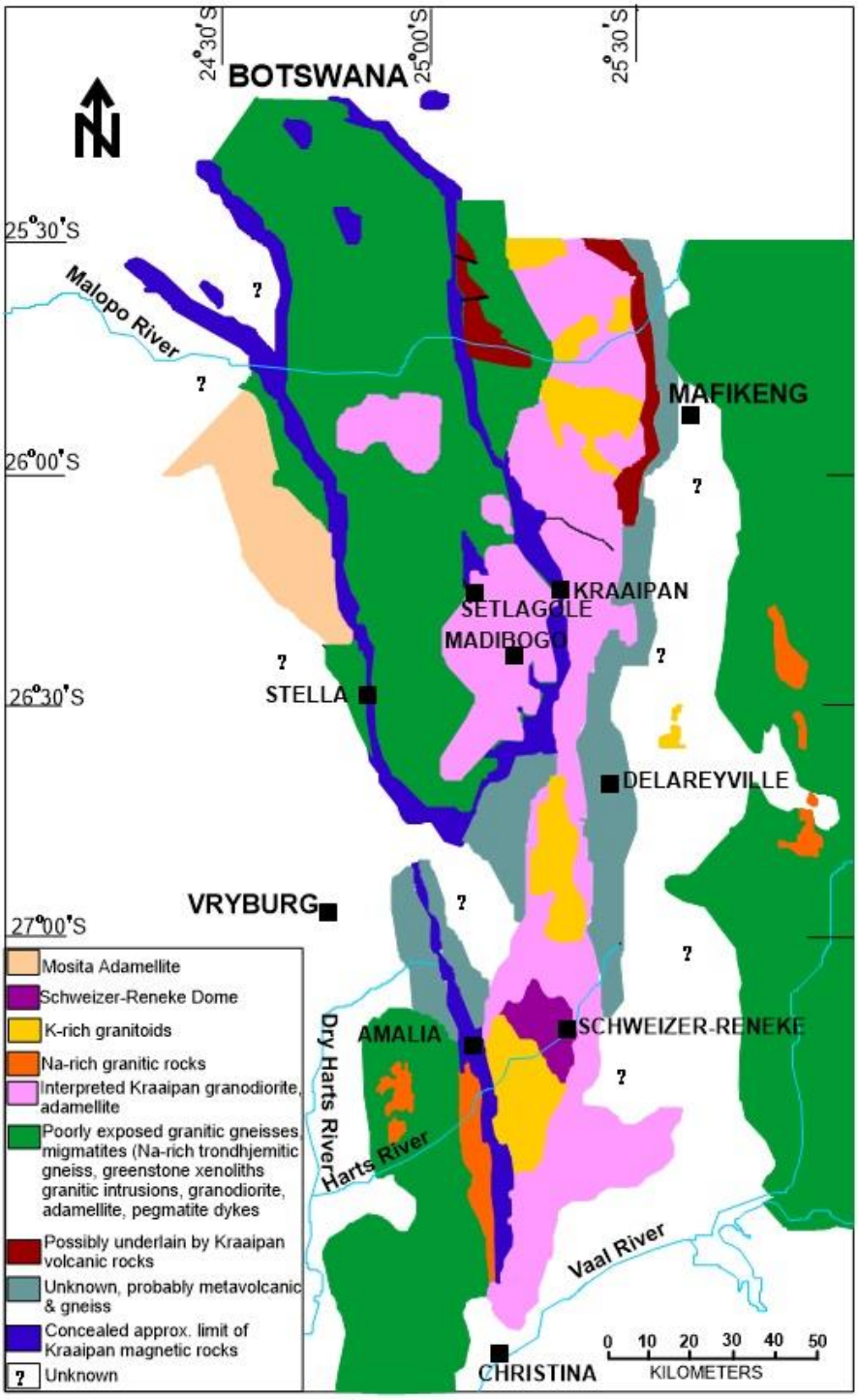

Figure 2.2: A map showing the extent of the Kraaipan greenstone belt (Poujol et al., 2002; Anhaeusser & Walraven, 1999).

To the east is the Kraaipan belt (passing through the Kraaipan settlement) which consists of the most continuous stratigraphic succession in the Kraaipan greenstone belt (Brandl, et al., 2006). Smaller fragments of the belt are found to the west, 20km from Kraaipan in Setlagole

(Brandl, et al., 2006). The westernmost part of the belt is the Stella belt which trends in a SSE direction in the vicinity of the Stella township and continues into Botswana for 110km where it has NNW trend (Brandl, et al., 2006). A third discontinuous belt is located to the south, and it passes through the town of Amalia

The greenstone belt is largely comprised of volcano-sedimentary rocks outcropping occasionally over a distance of 250km from the southern parts of Botswana in the north and nearly to the Vaal River in Christina to the south along with the associated granitoids (Anhaeusser & Walraven, 1999). The exact age of the Kraaipan greenstones is not well known. A whole rock Pb-Pb age of 3410Ma was obtained from the BIFs from the central belt (Brandl, et al., 2006). The age of some phyllites from Madibe was found to be c. 3407 Ma and 3344 Ma using SHRIMP 11 zircon dating ($^{207}Pb/^{206}Pb$) (Brandl, et al., 2006).

According to S.A.C.S., 1980 (as cited in Brandl et al., 2006), the greenstone succession can be subdivided into three distinct formations. Forming the base of the succession is the ***Gold Ridge Formation*** which is comprised of amphibolites that are saussuritised with chlorite-actinolite-epidote assemblages, and clinopyroxene preserved only at the residual phase (Brandl, et al., 2006). Iron formations are found associated with minor phillitic, chloritic and calcareous schists and clastic sediments (Brandl, et al., 2006). In some areas, the interlayered iron formations are associated with ultramafic rocks including serpentinites, talc, talc-carbonate or talc chlorite schists (Brandl et al., 2006). Alternating laminae of chert and hematite+goethite+magnetite characterise the iron formations, which are sometimes

jaspalitic especially in the Stella belt, and in some areas, they display isoclinal folding (Brandl, et al., 2006).

The ***Ferndale Formation*** forms the intermediate layer of the succession and is characterised by the occurrence of laminated iron-rich chert and jaspalitic chert which have been intensely folded with some local brecciation (Brandl et al., 2006). Interlayered with the chert are felsic volcanic rocks which are rhyolitic in composition with a mineral assemblage, which includes quartz, sericite, and, plagioclase (Brandl, et al., 2006).

The uppermost succession is the ***Khunwana Formation,*** which resembles the Gold Ridge Formation in terms of lithology (Brandl et al., 2006). However, the metavolcanic rocks in this formation are amygdaloidal and have pillow structures in some areas (Brandl et al., 2006). These pillow structures become younger towards the east (Brandl, et al., 2006). Unlike the Gold Ridge Formation, this Formation is entirely undeformed in some areas (Brandl, et al., 2006).

Table 2.2: A stratigraphic table summarising the Kraaipan greenstone belt geology.

Formation	**Description**
Khunwana	Amphibolites; phyllitic, calcareous and chloritic schists and talc-chlorite schists; iron formations; serpentinite; cherts; isoclinal folding
Ferndale	Laminated iron-rich chert; jaspalitic cherts; rhyolites; intense folding and local brecciation
Gold Ridge	Amphibolites; schists and talc-chlorite schists; iron formations, serpentinites; cherts; completely undeformed in some areas

2.2.2.2 The granitoids

Three distinct granitoids have been identified within the Kraaipan terrane and these include; the tonalitic and trondhjemitic granodioritic gneisses (TTG) and migmatites; granodiorite-adamellite suite and the Mosita adamellite, located in the areas shown in Figure 2.2 above (Anhaeusser & Walraven, 1999).The TTGs are the oldest granitoids to intrude the Kraaipan volcano-sedimentary sequence forming the ancient basement in the region (Anhaeusser & Walraven, 1999) and the dating of the oldest gneisses gave an age of c. 3008 Ma (Robb, et al., 2006). These granitoids are largely foliated, and they have sub-vertically trending mineral fabric that is parallel to the generally north-trending Kraaipan greenstone rocks (Anhaeusser & Walraven, 1999). In some areas, the TTG rocks exhibit a migmatitic texture (Anhaeusser & Walraven, 1999). The rocks are characterised by the occurrence of xenoliths of the Kraaipan amphibolites and BIF (Anhaeusser & Walraven, 1999). Some leucocratic dykes and aplitic veins also occur, and they are parallel to the foliation. TTG rocks occur throughout the region (Anhaeusser & Walraven, 1999). The granodiorite- adamellite suite intruded the TTG sequence (Anhaeusser & Walraven, 1999). This suite is composed of grey to massive pink granites that are homogenous and weakly foliated in some areas, and they have a fine-medium-grained texture (Anhaeusser & Walraven, 1999).

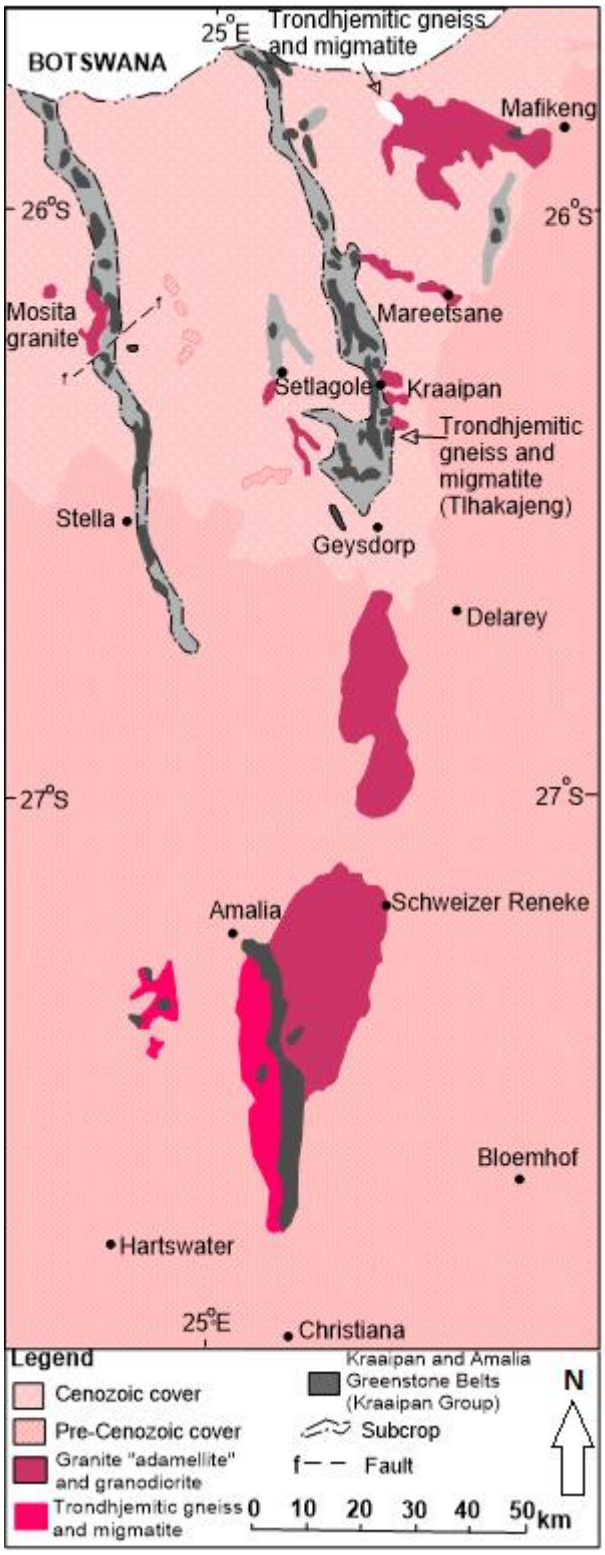

Figure 2.3: A map showing the extent of the Kraaipan greenstone belt (Brandl et al., 2006).

Some cross-cutting pegmatitic dykes and veins can be observed, especially in the central part of the belt (Robb, et al., 2006). The age range for this granitoid is between c. 2915 and 2879,

Ma. These rocks can be found outcropping sporadically from the north to south of the Kraaipan greenstone terrane (Anhaeusser & Walraven, 1999). The Mosita adamellite is another type of granitoid occurring in the area, and it is pinkish in colour and differs from the other granitoids because it is much more coarse-grained (Anhaeusser & Walraven, 1999). The estimated age of the rocks is 2791 ±8 Ma (Robb, et al., 2006) The minerals present in the rocks include quartz, perthite, microcline and albite and accessory minerals including zircon, chlorite, magnetite, myrmekite, and carbonates that form cross-cutting veins (Anhaeusser & Walraven, 1999).

2.2.3 The Venterdsdorp Supergroup

The Ventersdorp Supergroup rocks were deposited on the Kaapvaal craton approximately 2.64 Ga ago (Burke, et al., 1985). However, the literature about the existence of the Ventersdorp Supergroup rocks in the study area is limited, but its presence has been suggested (Anhaeusser & Walraven, 1999). According to Platinum Australia Limited (2007), rocks of the Ventersdorp Supergroup have been identified to the east and west of the Kraaipan granite-greenstone terrain, and in some areas, they are found interlayered with the greenstones and the SLI rocks as a result of deformation. The supergroup is subdivided into three groups, namely, the Klipriviersberg group, Platberg group and the Pniel series (Burke, et al., 1985).

According to the S.A.C.S, 1980, as cited in Burke et al., 1985, the Klipriviersberg group attains a thickness of 1830m and consists of a monotonous sequence of alkali-rich tholeiitic flood

basalt (Tankard et al., 1982, as cited in Burke et al., 1985). Conformably overlying the Klipriviersberg is the Platberg group which is composed of fanglomerate-type sediments, mafic and silicic (bimodal) volcanic rocks, immature sands and lake sediments and is approximately 4510m in thickness (Burke, et al., 1985). The youngest sequence in the supergroup is the Pneil series which is comprised of mature sandstones, conglomerate, quartzites and alkali-rich continental tholeiitic flood basalts (S.A.C.S, 1980; Winter, 1976; as cited in Burke et al., 1985).

2.3 LOCAL GEOLOGY

The western belt of the Kraaipan granite-greenstone terrane was intruded by the Stella Layered Intrusion (SLI) about 3.03 billion years ago (Anhaeusser & Walraven, 1999). The intrusion is one of the oldest known hosts of PGE deposits in the world, which is characterised by the occurrence of titanium and vanadium-rich magnetite horizons, and also hosts Cu and Au deposits (Brandl et al., 2006). According to Harmony Gold (and referenced therein Lewins et al., 2008), the intrusion has a strike length of 12km and a width of 1.5km. The Kalahari Platinum Project (Kalplats) is found in this terrane and is located approximately 25km north of Stella Township within the westernmost Stella belt (Lewins et al., 2008). The project area has been divided into eight deposits, which include Sirius, Serpens North, Serpens South, Crater, Vela, Orion, Crux, and Mira.

2.3.1 The Stella Layered Intrusion

The Stella Layered Intrusion is a mafic, sill intrusion, which intruded the Kraaipan greenstone belt approximately 3.03 billion years ago (Lewins, et al., 2008). It hosts some of the well-known magmatic reef deposits in South Africa (Lewins, et al., 2008). The intrusion is composed of layered gabbroic and magnetite-rich gabbroic material, and it stretches over 12 km in length and is 1.5 km in width (Lewins, et al., 2008). The lithologies that form the intrusion include non-foliated cumulate textured gabbro, leucogabbro, and magnetite gabbro (Lewins, et al., 2008). The magnetite content of the various lithologies ranges from low disseminated (1-2%) to strong segregations that form magnetite layers (up to 50-90%) (Lewins, et al., 2008). Mafic diabase dykes are found associated with shear zones that are sub-vertically dipping and trending in the NNW direction (Lewins et al., 2008), a relationship that could suggest that the dykes intruded much later, following the existing crustal weakness of the shear zones. The non-magnetic dykes are greenish in colour, and they range in width from 0.5- 3m (Lewins et al., 2008).

The SLI and the Kraaipan greenstone belt were subjected to some extensive deformation during an eastward verging orogenic event, which resulted in widespread folding and faulting (Lewins, et al., 2008). The complex faulting resulted in the disruption and duplication of the reef zone in some areas (Lewins, et al., 2008). There was an intense alteration of rocks of the SLI that can be attributed either too high temperatures associated with a magmatic source or deformation of the greenstone belt (Lewins, et al., 2008). Epidotization, chloritisation, sericitization and carbonate alteration characterise the Stella Layered Intrusion (Lewins, et

al., 2008). Carbonate alteration was more intense and resulted in the complete alteration of the precursor lithologies, forming some breccia-like textures or complete limestone/ dolomite like features (Lewins, et al., 2008).

The deep footwall, which forms the base of the Stella Layered Intrusion is comprised of non-foliated, fine-grained, homogenous gabbro which does not contain any magnetite, and is highly chloritised (Lewins, et al., 2008). A feldspar-rich pegmatoid occurs above the deep footwall, and it is coarse-grained, with occasional magnetite segregations (Lewins, et al., 2008). The footwall above is composed of feldspathic rich gabbro, and occasional magnetite bearing leucogabbro is present. From the easternmost contact of the mineralized package, the rocks have a cumulate texture for several tens of meters (Lewins, et al., 2008). The lithologies of the hanging wall higher up are mainly comprised of homogenous, magnetite-rich gabbro displaying some chlorite alteration with no distinctive zones (Lewins, et al., 2008). A later phase of pegmatoidal gabbro, which is feldspar-rich, with occasional occurrence of magnetite forming coarse intercumulate segregations, intruded and cross-cut the cumulate textured gabbro (Lewins et al., 2008). The pegmatoidal gabbro is estimated to be about 20-30m (Lewins, et al., 2008).

2.4 REGOLITH GEOLOGY IN STUDY AREA

The study area is characterised flat relief, with some low lying BIF outcrops being the prominent topographic features (Leuta, 2009; Mpuru, 2009). The BIF ridges are, however, partly obscured by the occurrence of brick red aeolian sand mixed with scree derived from the BIF ridges and remnants of the greenstones (Ackon, 2001; Leuta, 2009; Mpuru, 2009).

2.4.1 Regolith overlying the Serpens North deposit

The regolith overlying this deposit is characterized by the occurrence of aeolian sand, stone line, and saprolite. According to Mpuru (2009), the regolith in Serpens North extends to approximately 30 – 40 m. In situ regolith, comprised of saprock and saprolite (saprolith) occur at the base of the framework, and overlying the saprolith is transported regolith comprised of aeolian sand and stone lines (Mpuru, 2009). Mpuru (2009, p 14) proposed that the main regolith units found in the Serpens North Prospect could be classified into three units including; 1. "*an erosional area of exposed bedrock and skeletal soils"*, 2. "*a shallow depositional area mostly covered by up to 2-3 m of aeolian sand"*, 3. "*a depositional area with overburden of more than 3 m*".

The saprock horizon consists of partly weathered bedrock and directly overlies fresh bedrock (Mpuru, 2009). According to Mpuru (2009), this horizon is comprised of consolidated fragments of chloritic greenstone, medium to fine-grained, altered magnetite gabbro that has been mottled by iron and manganese oxides.

Overlying the saprock is the saprolite horizon, which still retains some of the primary fabric of the bedrock (Mpuru, 2009). Based on studies conducted by Mpuru (2009), the horizon has a characteristic light brown to grey colour, and is composed of sandy clay and significantly weathered chloritic greenstone, magnetite, gabbro, hematite nodules, and siliceous materials mottled with Fe and Mn oxides. The upper saprolite is highly mottled and is comprised of residual ferruginous sand and mottled quartz associated with carbonate granules (Mpuru, 2009).

The stone-lines overlying the saprolite represent a paleo-surface which consists of course to medium-grained pebbles and cobbles derived from the BIF and iron-rich debris (Mpuru, 2009). Based on observations made by Mpuru (2009), the main regolith material found in the horizon consists of sandy-clay goethite matrix with concretions of Fe and Mn oxide nodules, quartz, and chert in the matrix.

Wind-blown aeolian sand overlies the stone-lines and covers the entire area and ranges in thickness from < 0.5 m in areas of higher elevation and can reach up to 3 m in some low lying areas (Mpuru, 2009). The aeolian sand has a characteristic reddish colour due to the presence of ferruginous quartz (Mpuru, 2009). At the base, the horizon is characterised by the occurrence of Fe concretions, which change to a reddish-brown colour at the top (Mpuru, 2009).

2.4.2 Regolith overlying the Sirius deposit

At the base of the regolith profile is the saprolith which forms a significant part of the regolith profile. Based on some samples observed, in Sirius, the saprolith horizon is much more developed than in the boreholes drilled in Serpens North. The stone-line layer is absent from most of the boreholes, although it is has been suggested that it is present in some areas (Leuta, 2009). In Sirius, the regolith in this area is characterized by the occurrence of a calcrete horizon with a characteristic whitish colour, attaining a thickness of up to 5 meters in some places (for example borehole KP098). In some boreholes aeolian sand pinches out, leaving the calcrete layer exposed as the uppermost horizon (Leuta, 2009). The aeolian sand layer pinches out in borehole KP096. The thickness of the calcrete layer increases from the west part of the study area to the east and is absent in KP090.

2.5 NATURE OF MINERALISATION IN THE STUDY AREA

The Stella layered intrusion hosts some PGM, specifically Pt and Pd as well as minor Au and Cu (Lewins, et al., 2008). Mineralization is discontinuous, forming seven distinct entities namely, Crater, Vela, Mira, and Sirius; found in the northern part of the Kalplats with a NNW strike and to the south the Orion, Serpens North, Serpens South, and Crux; with an NW strike (Lewins, et al., 2008). The magnetite-rich gabbro hosts the mineralization at about 150-230m above the contact with the Kraaipan greenstone rocks, although in some areas the footwall gabbro has been completely sheared, such that the proximal footwall rocks to the mineralised package consist of floor rocks (Lewins, et al., 2008). Remnants of the deposit are found in the area, and they are thought to have once been part of a continuous reef (Lewins, et al., 2008). The fragmentation of the reef is due to the complex faulting, and north-easterly trending, sub-vertical shear zones, and low angle thrust that characterise the area (Lewins, et al., 2008). The footwall contains low PGE and Au mineralization (Lewins, et al., 2008).

The mineralized package is comprised of a magnetite-rich gabbro and magnetitite layer forming the alpha reef (~2m thick), which has elevated PGE (Pd: Pt ratio of 3:1) concentrations found within the footwall rocks (Platinum Australia Limited, 2007). A low-grade layer is found to the east of the Alpha reef (***pre-low grade reef***) consisting of magnetite gabbro (Platinum Australia Limited, 2007). The reef consists of a magnetitite layer attaining a thickness of 1-2m. A low-grade magnetite gabbro separates the pre-LG reef from the reef above (Platinum Australia Limited, 2007). The lowermost reef to the mineralized package, referred to as the lower grade reef (LG) is characterised by less feldspar-rich gabbro, a moderate amount of chloritisation and weak to moderate amount of shearing and is magnetite poor and has an

average grade of 1.0g/t. The mid-reef (MR) higher up is characterized by higher magnetite concentrations with up to 20% of its mineral assemblage being magnetite. The minerals have an anhedral shape, and the chlorite alteration and shearing starts to increase. This zone is divided into the MR1 and MR2, and the low-grade layers in between called the mid-reef low grade (MRLG). MR2 represents the continuous high-grade zone found at the top of the mid-reef, while MR1 represents the lensoidal unit within the mid-reef (Lewins et al., 2008).

The reef higher up is the main low-grade unit (MLG), which is a feldspathic unit with very low magnetite concentrations. This zone is not sheared and has minor chlorite alteration. The uppermost part of the mineralized package is termed the ***main reef,*** and it has been subdivided into the lower-main (LM), mid-main (MM) and upper-main (UM) mineralized units. The lower-main is about 4-5m thick and has up to 20% magnetite in its mineral assemblage and is usually sheared and shows some chlorite alteration. The mid-main resembles the lower main in mineral composition but is characterized by lower P t+ Pd + Au grades. The upper-main zone is the uppermost part of the reef, and it is characterized by the occurrence of chalcopyrite towards the top of the unit, with high Cu and Au grades but with a drop in Pd concentrations (Lewins et al., 2008).

The hanging wall lithologies are magnetite-rich compared to the lower units, and the presence of chalcopyrite continues for approximately 50m. There is a gradual decrease in the Au concentration from the UM to the hanging wall, although some anomalous Au values continue to occur in the hanging wall. PGEs occur within Ti-magnetites, the cracks within the Ti-magnetites and occurring as occlusions in gangue minerals (amphiboles, carbonates, and

chlorite). Chalcopyrite is possibly the most common sulphide that was part of the primary Pt/Pd paragenesis (Lewins et al., 2008).

3 METHODOLOGY

3.1 OVERVIEW

The initial phase of this study encompassed a desktop study aimed at gathering literature on the geology of the study area, regolith geology, and exploration methods that are used in areas concealed by extensive regolith. This study is based on data that was acquired from field and laboratory studies that were conducted by Mpuru (2009) and Leuta (2009). In this chapter, field surveys, laboratory work, and analysis, as well as data quality control measures as discussed by Mpuru (2009) and Leuta (2009) will be outlined. Additional analysis for the hydride-forming elements arsenic and mercury, as well as Pt and Pd, were conducted in the Earth Sciences Department, University of the Western Cape.

This study will re-evaluate and re-interpret the data that was prepared by Mpuru (2009) and Leuta (2009), in view of the newly acquired arsenic, mercury, and PGE data. This will be achieved by reviewing the core logging originally conducted by Mpuru (2009), and Leuta (2009). In addition, the whole-rock geochemical data obtained from Mpuru (2009) and Leuta (2009), will be used for data analysis in order to understand weathering patterns. In addition, trace element data obtained through the hydroxylamine hydrochloride partial leach technique will be used to model the dispersion of pathfinder and ore elements, for the purposes of analysis and interpretation of the data.

3.2 ORIGINAL DATA PROVIDED

3.2.1 Field Surveys

The samples used for this study were collected from the Kalplats, located 25 km north of Stella Township in the North West Province of South Africa between the months of March and June in 2007 (Leuta, 2009; Mpuru, 2009). The boreholes were drilled in traverses that are 200m apart, with boreholes in each traverse spaced 50m apart (Leuta, 2009; Mpuru, 2009). These boreholes were drilled across the mineralised zone, intercepting the regolith at depths of 15m and 10m in Serpens North and Sirius, respectively (Leuta, 2009; Mpuru, 2009). In Serpens North boreholes KP048, KP054, KP058, KP063, and KP067 were drilled directly over the mineralized zone (Mpuru, 2009), while in Sirius, boreholes KP092, KP094 and KP095 were drilled directly above the mineralised zone (Leuta, 2009), where the parent rocks are gabbro and magnetite gabbro. According to Leuta (2009) and Mpuru (2009), samples were taken at one-meter intervals downhole, thus a total of 150 and 100 samples were collected from Serpens North and Sirius respectively. Boreholes were drilled using an earth auger along NE-SW traverses (Leuta, 2009; Mpuru, 2009).

3.2.2 Laboratory analysis

The laboratory analysis was divided into two steps, as outlined in Leuta, 2009 & Mpuru, 2009. The first step involved the analysis of soil samples for major and minor elements, using XRF analysis (Leuta, 2009; Mpuru, 2009). In Serpens North Prospect, samples from 24 boreholes were analysed for the major oxides including; SiO_2, Al_2O_3, Fe_2O_3, MnO, MgO, CaO, K_2O, Na_2O, P_2O_5, SO_3 and trace elements including Ba, Ce, Co, Nd, Ni, Pb, Rb, Sr, Y, V, Zn and Zr (Mpuru,

2009). Samples from ten boreholes obtained from Sirius were also analysed for the abovementioned elements (Leuta,2009). This geochemical analysis is essential for the determination of the parent rock, understanding weathering patterns and identifying the regolith materials that form the regolith.

The second stage encompassed the use of the partial leach solution, hydroxylamine hydrochloride (0.05M) to digest Fe and Mn oxides in order to release adsorbed and exchangeable mobile trace elements from the soil phases. Hydroxylamine hydrochloride is a weak acid that selectively digests Fe and Mn oxides in order to liberate trace elements that are adsorbed or loosely bound to the surface of the soil phases (Chao, 1984; Jenne, 1987; Mann, 2009). A weak acid is an acid that does not dissociate fully in aqueous solution, thus the non-ionised acid still occurs in abundance, along with a hydronium ion and the conjugate base of the acid (Flowers et al., 2015). However, Luoma and Bryan, 1981 as cited in Jenne, 1987; Xueqiu, 1998; suggested that carbonates are also digested by hydroxylamine hydrochloride although this brings about an undesirable effect. The dissolution of carbonates results in pH increase, which leads to the re-adsorption of sorbed metals released from oxides during the initial stage of the leaching process (Luoma and Bryan, 1981 (as cited in Jenne, 1987; Xueqiu, 1998). Adsorbed trace elements do not form part of the soil matrix. Hence they are considered as the mobile elements that are liberated from the underlying bedrock during weathering processes and are subsequently adsorbed by Fe, Mn, and carbonate phases. This type of geochemical analysis is essential for understanding the secondary dispersion of elements associated with PGE and Au mineralisation in the secondary environment. The hydroxylamine hydrochloride leach solution is appropriate for both Serpens North and Sirius because of the presence of Fe oxides in the soil profiles.

3.2.3 Sample preparation for XRF analysis

The samples collected were damp, thus they had to be dried overnight in an oven at 105^{o}C in order to remove excess moisture (Leuta, 2009; Mpuru, 2009). After that, portions of the sample were crushed to very fine grains using an Agate mortar, thoroughly cleaning the apparatus after every sample was crushed to prevent any cross contaminations (Leuta, 2009; Mpuru, 2009). The resultant fine grain samples were then milled into a very fine powder using a Planetary Ring Mill (Leuta, 2009; Mpuru, 2009). In order to prevent the disintegration of the pellets, the samples were mixed with a binder in the ratio of 9g of the sample to 1g of binder (Leuta, 2009; Mpuru, 2009). The binder is a mixture of Wax-C (one part) and EMU powder (nine parts) (Leuta, 2009; Mpuru, 2009). The resulting mixture was then pelletized at 15 kilo-bars of pressure. This process was repeated for all samples, and the pellets were subsequently analysed for major and trace elements using an XRF apparatus.

3.2.4 Measuring Loss on Ignition (LOL)

The only data available for LOI analysis was obtained from samples from Sirius that were prepared by Leuta, 2009. As outlined by Leuta, 2009; the first step was to measure the weight of the crucibles on a scale, and the weights were recorded. After that, the weight of the crucible was cancelled upon placing the crucible on the scale, and 1g of each sample was measured in the crucible. The samples were then dried in an oven for 30 minutes at a temperature of 120^{o}C. Thereafter, the samples were transferred into a pre-heated oven at 1000^{o}C for 45 minutes. The contents were then allowed to cool down, and they were subsequently measured. The weight of each crucible was then subtracted from the combined

weights of the crucibles and samples after the ignition of samples. The difference between the initial sample weight (which is 1g) and the weight of the sample after ignition represents the LOI.

3.2.5 Partial leach techniques

3.2.5.1 Cold hydroxylamine hydrochloride leach

A 0.05M hydroxylamine hydrochloride solution was prepared by adding 3.5 grams of hydroxylamine hydrochloride crystals to a 1000 ml measuring cylinder. Nitric acid (10%) was prepared by diluting 65% nitric acid; which was achieved by mixing 13 ml of 65% HNO_3 and 117 ml of distilled water (Leuta, 2009). A portion of 5 ml dilute HNO_3 was then added to the hydroxylamine hydrochloride solution and shaken. Thereafter, 80 ml of the hydroxylamine hydrochloride solution was added to 5 grams of the soil sample in a sample bottle. The mixture was sealed and placed on a horizontal shaker for 1 hour. Filter paper was then used to filter the contents to obtain a clear solution, which was then analysed using the GFAAS. A portion of 0.8 ml of 65% nitric acid was added to each sample before analysis for calibration of the GFAAS machine (Leuta, 2009).

3.2.6 Analysis by Vapour Generation AAS

Atomic absorption spectrometry is a more readily available, robust and cost-effective method for analysis compared to equipment such as ICP-MS which are more sensitive, perform multi-element analysis, but generally more expensive (Tsalev, 2010). Vapour generation AAS is a combination of the hydride generation AAS (HG-AAS) (used in the analysis for hydride-

forming elements such as As, Sn, Pb, etc.) and cold vapour AAS (for mercury analysis) (Tsalev, 2010; D'Ulivo, 2018). The poor sensitivity associated with mercury detection using a traditional flame AAS led to the development of CV-AAS which improved the limits of detection a hundred times or more (McCurdy & Sibakoti, 2011). The HG-AAS allows for a spectral interference-free analysis because only the analyte of interest reaches the atomizer as a gaseous metal hydride (Analytikjena, 2014). The separation of the analyte from the matrix leads to improved accuracy of the method (D'Ulivo, 2018).

In this study, the HydrEA (developed by Analytikjena) was used for analysis. The technique combines hydride, or Hg cold vapour method with the graphite tube method (Analytikjena, 2014). In the Hg cold vapour technique, mercury liberated from compound associations through digestion methods is converted to elemental mercury using reducing agents such as stannous chloride or sodium tetrahydroborate. A gas, such as nitrogen is then passed through the solution, carrying the Hg atomic vapour through a flow cell placed in the light path in the AAS apparatus, recording the absorption signal (Amos, 2006). The methods used for mercury and arsenic analysis was adopted from the Chemical Engineering Department in CPUT.

3.2.6.1 Mercury analysis procedure

Aqua regia, a leach solution prepared by mixing HNO_3 and HCl in a 1:3 ratio was used in mercury analysis. A portion of 20ml of the aqua regia solution was added to one gram of sample in a sealable vessel. The mixture was allowed to digest overnight in a sand bath at 80 - 90°C. Filter paper was used to filter out the remaining solid. The filtrate was diluted using distilled water in a 1:1 ratio. In order to prevent complexation, 3ml of 6M HNO_3, two drops of

10% permanganate, 5ml of 9M H_2SO_4, and 5ml of 1.5M hydroxylamine hydrochloride were added to the diluted filtrate. The reductant was prepared by adding 9 grams of sodium borohydride ($NaBH_4$) and 3 grams of sodium hydroxide to 300ml of 1.5% HCl. Using a dispensing bottle, 5ml of the reductant was pumped to the reaction beaker, a carrier gas (argon) was blown into the sample, resulting in volatilisation of the mercury atoms. The Hg vapour was then enriched in a gold-coated graphite tube at a pre-heating temperature of 150°C. Subsequently, the mercury atoms deposited on the gold coating were then atomized at 800°C. The resulting atomic vapour cloud absorbs the primary radiation at the resonance line of 253.7nm to be detected. After the analysis of each sample, the reaction vessel was cleaned using 10% HNO_3.

3.2.6.2 Arsenic analysis procedure

In the arsenic analysis, 20ml of aqua-regia was added to one gram of sample in a closed vessel and placed in a water bath (100-120°C) and allowed to digest for two hours. The mixture was then filtered using filter paper. The filtrate was then diluted with distilled water in a ratio of 1:1. In order to reduce arsenic from As^{+3} to the more mobile As^{+5}, a pre-reduction solution was prepared by adding 100 grams of both 10% potassium iodide and 10% ascorbic acid were dissolved in 1000ml of distilled water. Thereafter, 5ml of the pre-reduction solution was added to the samples and subsequently placed in the reaction beaker in the HydrEA system. A reductant was prepared by adding 9 grams of sodium borohydride ($NaBH_4$) and 3 grams of sodium hydroxide to 300ml of 1.5% HCl. A portion of 5ml of the reductant was pumped from the reductant dispensing bottle into the reaction beaker in order to volatilise arsenic. The

graphite tube was coated with a 1ppm Iridium solution in order to improve the sensitivity of analysis. After the analysis of each sample, the reaction vessel was cleaned using 10% HNO_3.

3.2.7 Analysis for platinum and gold (Fire assay technique)

The technique outlined below was adopted from Mintek Laboratories. In the fire assay technique, high temperatures and a flux are used to melt and collect precious metals. A fire assay flux is comprised of litharge (provides Pb for collecting precious metals and acts as a flux), soda ash (reacts with silica to form a slug), borax (lowers fusion point of slugs), silica (prevents attack on crucibles), nitre (oxidising agent used when handling sulphide-rich samples), flour (reductant of litharge to Pb), and silver (collects precious metals) (ALS Minerals, 2012). For this study, the flux was prepared by mixing 720g of sodium carbonate, 470g of lead monoxide, 90g silica, 30g borax, 70g maize meal, and 70g fluorspar (Mahala, 2008).

In the first stage of the fire assay procedure is **fusion**, a weighed sample (30 grams), was mixed thoroughly with the flux (144g) and 0.2g of silver nitrate (Mahala, 2008). The mixture was placed in a pre-heated furnace at 1040 °C for 60 minutes. Thereafter, a hammer was used to separate the lead button from the slug. In the second stage (**cupellation**), the resulting lead button is placed in a cupel and placed in a pre-heated furnace at 1000 °C for an hour. The cupel absorbs the lead, and the resulting PGMs, Au, and Ag (added as a collector) prill was transferred into a sealable container. Aqua regia (50ml), was then added to the prill and placed in an oven at 220 °C for 8 hours in order to dissolve the prill. The solution was then analysed for Pt, Pd, and Au using the GFAAS.

3.2.8 Quality Assurance/ Quality Control of geochemical data

The laboratory work executed by Leuta, 2009 and Mpuru, 2009 also included quality control measures such as duplication of selected samples. In addition, standards were prepared for XRF analysis, and these were used to calibrate the XRF machine. According to Leuta (2009), the control standards used for the XRF machine were; bauxite (BX-N), iron formation (FER-1), feldspar (FK-N), feldspathic sand (FK), deposit type (GXR-3), dunite (NIM-D), syenite (STM1), lujavrite (NIML), albite (AL-I), basalt (BHVO), gabbro (MRG-1) and syenite (NIM-S). This choice of standards was based on the fact that they allow for a wide range of elements and include both hard rock and soil sample types (Leuta, 2009).

An important part of handling geochemical data is to examine and assess the quality of data generated from the experiments. In order to determine the precision of the data univariate statistical data analysis, specifically, precision scatter-plots were plotted to ascertain whether the data falls within the acceptable confidence intervals. When analysing the samples, two standards were placed after every six samples. Precision control plots for the major element SiO_2 showed a precision of ± 7% and a plot for Co gave a precision of ± 5% (Leuta, 2009). In general, major elements had a precision of between ± 2,5 to ± 7.5%; while minor elements had a precision range between ± 5% and 7.5% (Leuta, 2009).

Reference standards and blanks were also used for quality control in GFAAS analysis. These were placed after every 20 samples. Duplicates of 24 samples were leached using hydroxylamine hydrochloride and were analysed to monitor the precision of the data (Leuta,

2009). Precision scatter-plots of the original samples plotted against the duplicate samples gave a precision range between ± 5% to ± 7.5% for the trace elements Pt, Co, Cu and As while the precision of Fe, Ba, Zn, and Mg was approximately ± 10% (Leuta, 2009).

3.3 DATA ACQUISITION ASSUMPTIONS

The data used in this study was acquired from work that was conducted by Mpuru (2009) and Leuta (2009). Quality assurance measures are an important part of sample collection and handling. During laboratory analysis, the necessary precautions are generally taken in order to avoid contamination. This includes the careful labelling of samples in order to avoid confusing samples. The laboratory equipment used while conducting the experiments has to be thoroughly washed before use. Double distilled water should be utilised in dilutions that required the use of distilled water. Thus, the assumption in this study is that these measures were adhered to.

3.4 DATA ANALYSIS AND EVALUATION

In this study, the evaluation techniques outlined below were employed with the aim of reinterpreting the existing data and incorporating the newly acquired As, Hg, Pt, and Pd data in the analysis and evaluation.

3.4.1 Univariate data analysis

Summary statistical tables were created using a statistical analysis software called SPSS. Summary statistics are useful when analysing data because they provide a summary of the distribution of data (Grunsky, 2010). Ranges, geomeans and standard deviations of the major and trace elements were calculated for each regolith horizon. The range and standard deviation are measures of spread and provide an idea of the dispersion of data. The statistical geomean is a measure of the central tendency of a set of data and gives insight into where data seems to cluster (Grunsky, 2010; Sykes et al., 2016).

3.4.2 Multivariate data analysis

Box plots were also generated on SPSS to further understand the variability of different major elements within different regolith horizons. Box plots are a good way of summarising variations between groups of data (Grunsky, 2010).

The major and trace geochemical element data was also used to conduct a principal component analysis (PCA) using SPSS. Representing data using the PCA ensures the reduction of dimensionality of the data, which means that the number of variables required to explain variability within a data set is reduced (Grunsky, 2010).

Geochemical data were analysed using a statistical analysis software package *ioGAS.* Bivariate plots were generated using ioGAS in order to demonstrate relationships between two variables (major elements) and identify trends in the various regolith horizons. The software

was also used to generate diagrams that aid the understanding of weathering intensities and these include; Mg/Al vs K/Al plots (after McQueen,2006), A-C-K and A-CK-FM diagrams (after Nesbitt & Wilson, 1992). The Zr vs Ti plots were also generated in order to discriminate the bedrock from which the regolith was derived. Titanium and zirconium are relatively immobile elements that reside in rutile and zircon, minerals that are highly resistant to weathering (McQueen & Scott, 2008). Titanium can also be found in less stable minerals such as pyroxene, amphibole, sphene, ilmenite, and micas, but after it is released, the Ti re-precipitates as anatase (McQueen & Scott, 2008). The chemical index of alteration (CIA) calculated using the formula [$100*Al_2O_3/(Al_2O_3+CaO+Na_2O+K_2O$) (Nesbitt & Wilson, 1992) and the index of chemical variability (ICV) calculated as follows; [Fe_2O_3+ CaO+ Na_2O+ K_2O+ MgO+ MnO+ TiO_2]/Al_2O_3 (Cox et al., 1995), were calculated in Excel. These indices reflect the weathering of feldspars and micas to kaolinite (McQueen & Scott, 2008). Compositionally immature regolith is mostly characterised by non-clayey primary minerals, and therefore lower CIA (Nesbitt & Young, 1982; McQueen, 2006) and higher ICA values (Cox et al., 1995; McQueen, 2006), due to the abundance of mobile elements. In areas where intense weathering has occurred, high CIA indices and low ICV indices are characteristic, because of higher Al_2O_3 concentrations relative to mobile elements such as Na_2O, K_2O, CaO (more clayey regolith) (McQueen, 2006).

Earthworks Downhole explorer was used to represent the regolith horizons and the associated element concentrations in each borehole in order to understand the downhole trends of elements.

3.4.3 Spatial analysis using 2D modelling

In this study, inverse distance modelling was used to create the models. In this method, a grid node is assigned a value based on the average of all data points or some directionally distributed neighbours (Rockware, 2017). The value of the data point is then weighted as the inverse of its distance from the grid node, to the power of a value selected by the user (Rockware, 2017). This method of gridding is ideal because it produces smooth and continuous grids, and it does not exaggerate the extrapolations beyond the given data points (Rockware, 2017). Anisotropic inverse distance modeling was used because the program searches for the closest control point in each 90-degree quadrant around the node (Rockware, 2017). This method, which employs a directional search, improves the interpolation of voxel values that lie between data point clusters and is a useful method for modelling drill-hole based data (Rockware, 2017).

For this particular work, however, only 2D sections were plotted in order to aid the visualisation of the subsurface spatial concentration of pathfinder elements, gold, platinum, and palladium through interpolation methods. Such diagrams can interpolate dispersion trains, secondary halos, and show the patterns of mobility of elements in the subsurface. The HH data saved on Excel was imported to Rockworks 15. The element concentration data was named interval data, a name that the program recognises. In Rockworks, the concentration data collected at intervals is referred to as I-data, which is defined as data that is measured at depth intervals rather than at depth points (Rockware, 2017). Sections were created based on the traverses along which samples were collected. The NNE-SSW sections traverse the mineralised zone which has a NNW strike. The 2D sections constructed along traverses give a

visual representation of the lateral dispersion of elements from the ore body, while at the same time showing the vertical dispersion patterns across the boreholes. The sections, which in this case represent the traverses of sampling were labelled from the NW to the SE using letters A-A' – H-H' and A-A' – B-B' in Serpens North and Sirius Prospects respectively.

4 RESULTS

4.1 OVERVIEW

In arid to semi-arid environments, weathering tends to be shallow as evidenced by the thin nature of soil profiles in these areas (van Berkel, 1982). The reason for minimal weathering is largely due to high evaporation rates, which exceed precipitation. According to van Berkel (1982), the strong surface heating and characteristic low humidity in such environments cause minimal penetration of water into the bedrock and rapid upward capillary movement of water. As a result, mechanical weathering is the dominating weathering process in these regions (van Berkel, 1982). However, the action of chemical weathering cannot be completely dismissed. Hence the weathering processes operating particularly in the study area can be described as both physical and chemical. Chemical weathering in the study area is however limited by the restricted amount of time the water resides in the weathering front due to evaporation, the low content of humic acids and CO_2 due to sparse vegetation, which results in oxidising, alkaline conditions unfavourable for chemical weathering. Furthermore, physical weathering is also limited by the thick aeolian cover that characterises the area.

In this chapter, geochemical data acquired from the analysis of samples obtained from two of the eight reef fragments that comprise the Kalplats deposit, specifically, Serpens North and Sirius Prospects were analysed. The analysis was carried out according to the following steps:

- **Characterisation of regolith using major element chemistry**

  Summary statistical tables are useful when analysing data because they provide a summary of the distribution of data (Grunsky, 2010). Ranges, geomeans and standard

deviations of major and trace elements were calculated for each regolith horizon. The range and standard deviation are measures of spread of data and they provide an idea of the dispersion of data. The statistical geomean is a measure of the central tendency of a set of data and gives insight into where data seems to cluster (Grunsky, 2010; Sykes et al., 2016). A comparison of the mobilisation and redistribution of elements in different regolith horizons will be made based on the measures of variability and central tendency (Sykes, et al., 2016). Various authors have previously used statistical summary tables for comparing element concentrations in different horizons, (for example, Anand, 2001; Brand & Butt, 2001; Anand & Paine, 2002).

- **Characteristics of regolith based on XRF data (major and trace elements)**

  Firstly, the variability of different major elements within different regolith horizons will be discussed based on box plots. Box plots are a good way of summarising variations between groups of data (Grunsky, 2010). Anand (2001) classified ferruginous materials using box plots in order to compare Au concentrations in different regolith materials. In a subsequent study, Anand and Paine (2002); used box plots to compare the distribution of the elements including Fe_2O_3, K_2O, SiO_2, and Cr in different regolith horizons. Studies conducted by Lett, 2010 also used box plots to represent fire assay and aqua regia data in order to compare the distribution of trace elements, as well as a comparison of element concentrations in different regolith horizons. Similarly, the element distributions in different horizons in Serpens North and Sirius Prospects will be compared using box plots.

The second evaluation technique employed is the principal component analysis (PCA). Representing data using the PCA ensures the reduction of dimensionality of the data, which means that the number of variables required to explain variability within a data set is reduced (Grunsky, 2010). A study conducted by Grunsky et al. (2009) used PCA to demonstrate the winnowing and sorting of heavy metals in soils and stream sediments. In addition, the use of the PCA was employed in the classification of samples according to the mineral composition of the sediments, i.e. clays or feldspars and carbonates (Grunsky, 2010). In a similar study conducted by Towett et al. (2015); the PCA was also used to demonstrate the clustering of elements based on their atomic weight, elements that are likely to partition into clays, or feldspars and carbonates.

Thirdly, bivariate plots will be used to demonstrate relationships between two variables (major elements), and identify trends in the various regolith horizons. Regassa et al. (2014); used bivariate plots to show the trends in major oxides with increase in weathering intensity. Bivariate plots have also been used in numerous studies to determine major oxide trends in sediments by authors such as Varga et al., 2005; Ma et al., 2007; Brand & Butt, 2001.

- **Weathering trends and indices**

  Major element data can be used to determine the intensity of weathering. The intensity of weathering can be determined using weathering indices such as the chemical index of alteration (CIA) and the index of chemical variability (ICV). In addition, A-CN-K, A-CNK-FM, Mg/Al versus K/Al plots can also be used to determine

the degree of weathering. Various authors have used this approach to understand the mobility and redistribution of elements in the surficial environment and determine the regolith frameworks of particular areas. The CIA, A-CN-K, and A-CNK-FM were initially developed by Nesbitt and Young (1982) and Nesbitt and Young (1984). Thereafter, the methods have been used extensively to understand weathering in various environments by authors including Nesbitt & Young (1989); Cox et al. (1995); Price & Velbel (2003); Arhin et al. (2017); Khider & McQueen (2005); McQueen (2006); Regassa et al. (2014); Valiani & Rezaee (2014).

- **Determination of protolith**

  The parent rock from which weathered material is derived from can be determined using ratios of some elements which are relatively resistant to weathering such as Ti and Zr. Using Ti and Zr is based on the idea that during weathering of parent rock, these elements will maintain their concentration as weathering progresses, which implies that their concentration even after weathering is still characteristic of their parent rock. Anand & Paine (2002), and Khider & McQueen (2005) for example, used the Zr- Ti plot to classify weathered bedrock samples in order to determine the bedrock from which they were derived from.

- **Ore- and ore-related trace element associations based on HH data**

  Some of the techniques used for the evaluation of XRF data were also employed in the evaluation of HH data. Statistical summary tables were produced in order to summarise the HH data using a measure of central tendency (geomean) and the measures of the spread of the data (standard deviation and range).

Box plots were also used to illustrate the variability in element concentrations within different horizons. Also, the PCA was performed in order to determine element associations. The major oxides including Fe_2O_3, MnO, Al_2O_3, CaO, and SiO_2 were also included in the plots in order to determine whether the adsorbed elements are associated with any of the soil phases that are known to scavenge trace elements. Pearson's correlation matrix was also used to quantify the relationship between different pairs of elements.

- **Modelling the dispersion of ore elements in the weathering environment**

  Inverse distance modelling techniques use interpolation to predict the dispersion of elements within a sampled area, where samples were not actually taken (Mitas & Mitasova, 1999; Li & Heap, 2014). This method was used by Anand & Butt (2010), to interpolate the regolith patterns using 3D block models and fence diagrams, as well as the dispersion of nickel using fence diagrams. In this study, cross-sections will be created in order to interpolate the spatial dispersion of ore and ore- related elements.

The nature of regolith plays an important role in controlling the dispersion of ore elements in the weathering environment. The geochemistry of regolith, therefore, influences the expression of geochemical signatures. Different soil phases tend to scavenge certain trace elements, hence the understanding of the soil phases constituting the regolith is necessary for better insight into the occurrence of anomalies in the weathering environment. The intensity of weathering influences the geochemistry of the regolith because, during weathering, elements are mobilised and redistributed. Evaluation techniques such as summary statistics, boxplots, scatter plots, PCA, A-CN-K and A-CNK-FM plots, Mg/Al vs K/Al

plots, CIA, and ICV are all important in the understanding of the nature of regolith in Serpens North and Sirius Prospects. Determining the parent rock is also important because in-situ regolith is derived from the underlying bedrock which influences the composition of weathering products. For instance, lateritic residuum is strongly developed where bedrock is mafic or ultramafic and may never develop in felsic rocks (Anand & Butt, 2010). Silcretes are likely to be formed on granitoid and felsic rocks (Butt, 1995 as cited in Anand & Butt, 2010). An understanding of the nature of regolith is essential for understanding the behaviour of pathfinder and ore elements. The cross-sections plotted on Rockworks are important for the visualisation of the dispersion of pathfinder and ore elements, as well as identifying the extent of dispersion of these elements from the orebody laterally as well as vertically.

The results will, therefore, be presented in sections. Section 4.1 will discuss the characterisation of regolith using major element chemistry in Serpens North and Sirius Prospects. A section discussing the characteristics of regolith in Serpens North will follow (Section 4.2 and 4.3). Thereafter, weathering trends and indices in the Serpens North prospect will be presented in Section 4.4. Section 4.5 provides a summary of the findings of the Serpens North data. Sections 4.6 and 4.7 will address the characteristics of regolith in Sirius Prospect and its weathering trends and indices respectively. A summary of the findings for the Sirius Prospect data will be discussed in Section 4.8. In section 4.9, the major difference between major element distributions in Sirius and Serpens North Prospect will be outlined. The distribution of pathfinder and ore- forming elements analysed using the HH leach technique will be discussed in Section 4.10.

4.2 CHARACTERISATION OF REGOLITH MATERIALS USING MAJOR ELEMENT CHEMISTRY

4.2.1 Summary statistics of major element chemistry in Serpens North Prospect

The statistical summary table in Table 4.1 below shows the ranges, geomeans and standard deviations in the three regolith horizons found in the Serpens North Prospect. The geomean concentrations of the major elements that constitute the bulk weight percentage of the samples in aeolian sand include SiO_2, Fe_2O_3, and Al_2O_3. Stone-lines are mainly composed of SiO_2, Al_2O_3, Fe_2O_3, and to a lesser extent, MgO and CaO. The saprolith horizon is mostly composed of SiO_2, Al_2O_3, Fe_2O_3, and to a certain extent, MgO, CaO, and TiO_2. Silica concentrations are lower in the saprolith, increase towards the stone-line and are highest in the aeolian sand. In contrast, the Fe_2O_3 concentrations are relatively high in the saprolith, but are highest within the stone-line, while concentrations are lowest in the aeolian sand. According to Brand & Butt, 2001; the concentrations of SiO_2 and Fe_2O_3 generally increase towards the upper parts of a profile, due to progressive loss of MgO. Brand and Butt's findings are consistent with the trends observed in Serpens North, because SiO_2 concentrations increase upwards, while MgO concentrations decrease upwards from a mean of 3.69 wt.% in the saprolith to 1.32 wt.% in the stone-line, and 0.78 wt.% in the aeolian sand, due to progressive leaching. Potassium oxide exhibits a different trend, showing lower concentrations in the saprolith and increasing slightly upwards, from the stone-line to the aeolian sand. However, the concentration of Fe_2O_3 only increases into the stone-line, suggesting ferruginisation in this horizon, but concentrations then decreases upwards into the aeolian sand.

The Al_2O_3 concentrations are highest in the saprolith, and decrease upwards into the stone-line and are lowest in the aeolian sand. Based on the fact that clays are characterised by the loss of more mobile elements and a corresponding enrichment of Al_2O_3, the low Al_2O_3 up in the profile in Serpens North suggests low clay contents in the profile. The geomean concentration of TiO_2 is, however, relatively high within the aeolian sand, decreasing in the stone-line and increases again in the saprolith. In contrast, the geomean concentration of Zr is lowest within the saprolith horizon and increases upwards, with the highest concentration in the aeolian sand. According to Brand & Butt (2001); Ti, Al, and Zr tend to be enriched in ferruginous materials, in resistate and secondary phases. According to studies conducted in Mt. Keith, Western Australia; high Zr concentrations were observed within transported regolith, similar to the observations made in Serpens North, which they attributed to an external origin. Similar trends in Zr were also observed in Ora Banda (Anand & Paine, 2002). Contrary to observations made by Brand and Butt in Mt. Keith, the mean concentration of Zn is highest in the saprolith and decreases upwards, being lowest in the aeolian sand. In the Mt. Keith case study, Brand and Butt attributed the Mn enrichment in the saprolith-pedolith boundary to the precipitation of secondary oxides at a past redox front. The mean concentration of MnO is lowest within the saprolith, increases in the stone-line (which could also be attributed to precipitation of secondary oxides in this horizon), but concentrations decrease in the aeolian sand horizon. Based on the summary statistics, CaO concentrations are generally higher in the saprolith (geomean of 2.45 wt%.), and decrease upward in the stone-line and is lowest in the aeolian sand (geomean of 0.57 wt%.). A high Ca concentration can be attributed to a calcium-rich bedrock. The concentrations of Ni are significantly lower than those observed in by Brand & Butt, 2001 in Mt. Keith where the protolith is dunite.

However, the geomean of Ni slightly increases from the saprolite to the stone-line and then decreases in aeolian sand.

4.2.2 Summary of major element chemistry in Sirius Prospect

The elements that form the bulk concentration of aeolian sand samples in the Sirius Prospect are the oxides of Si, Al, Fe, and to a lesser extent Mg. A summary statistics tableis shown in Table 4.2 below. The calcrete horizon is largely composed of SiO_2, Al_2O_3, Fe_2O_3, MgO and CaO. The saprolith horizon is dominated by elements including SiO_2, Fe_2O_3, Al_2O_3, and to a certain extent, Ca and Mg oxides. The geomean concentration of LOI is relatively high (>6 wt.% in the aeolian sand and saprolith),suggesting that most samples have a high LOI, which is an indication of the abundance of carbonates in the horizons. The LOI geomean in the aeolian sand is lower than in the underlying horizons. The geomean of SiO_2 (42.23 wt.%) is lower within the saprolith and progressively increases upwards and is highest within the aeolian sand horizon. Iron and Mg oxides, as well as Co, all display high concentrations within the saprolith, and concentrations progressively decrease upwards. There is a lower CaO concentration within the aeolian sand as indicated by the low geomean, while concentrations are elevated within the calcrete horizon, and slightly decrease in the saprolith possibly due to partial loss during the initial breakdown of plagioclase and amphiboles which are among the first minerals to break down to form clays and carbonate minerals. Calcrete horizons usually develop on Ca-rich bedrock and saprock (Anand & Paine, 2002).

Table 4.1: Summary statistics of regolith overlying the Serpens North prospect.

	Range				Geomean				Std. Dev.			
	All	Aeolian	Stone line	Saprolith	All	Aeolian	Stone line	Saprolith	All	Aeolian	Stone line	Saprolith
Major elements (wt.%)												
SiO_2	68.05	34.97	25.43	63.09	56.39	72.3	59	50.98	13.19	8.86	8.01	10.64
Al_2O_3	20.9	17.08	20.22	18.48	11.49	8.9	9.11	13.16	4.78	3.54	5.59	4.4
Fe_2O_3	53.38	24.67	33.07	53.38	18.81	12.38	22.82	21.26	10.56	6.85	10.12	10.4
MnO	0.95	0.78	0.93	0.83	0.1	0.07	0.14	0.12	0.14	0.15	0.23	0.11
MgO	22.42	5.88	5.53	22.4	1.68	0.58	0.87	2.81	3.32	1.02	1.44	3.71
CaO	7.59	7.43	5.48	7.59	1.52	0.57	0.81	2.45	2.11	1.31	1.41	1.99
Na_2O	2.96	1.41	2.6	2.96	0.23	0.17	0.2	0.27	0.63	0.29	0.88	0.66
K_2O	6.1	1.33	1.99	6.1	0.52	06	0.54	0.48	0.86	0.27	0.52	1.03
TiO_2	5.2	2.45	1.23	5.2	0.8	0.91	0.59	0.81	0.84	0.45	0.4	0.98
P_2O_5	0.09	0.05	0.09	0.06	0.01	0.04	0.02	0.01	0.02	0.01	0.02	0.01
SO_3	0.14	0.13	0.09	0.01	0.01	0.02	0.01	0.01	0.01	0.02	0.02	0.003
Trace elements (ppm)												
Ba	1470	627	501	1470	228.7	149.81	258.89	262.08	205.57	162.27	149.03	220.57
Ce	256	244	125	171	46.81	55.69	29.33	48.16	46.55	55.59	43.1	44.5
Co	271	191	119	271	31.84	17.92	35.19	38.54	43.98	35.79	37.47	45.3
Nd	72	68	27	49	14.55	19.01	10.84	14.43	13.3	17.22	8.85	12.85
Ni	519	268	346	519	57.23	47.84	75.61	58.2	91.04	54.85	94.2	100.29
Pb	39	37	14	25	11.35	11.8	10.85	11.28	5.7	6.84	4.18	5.51
Rb	157	111	150	156	23.33	27.66	20.93	22.32	24.54	19.26	35.57	24.25
Sr	432	249	309	432	70.91	42.75	75.41	84.74	82.69	75.79	87.64	81.61
V	3601	2779	1071	3601	493.34	414.51	382.47	550.6	686.78	526.34	352.01	763.03
Y	134	126	122	134	12.02	11.28	13.32	12.08	20.72	21.08	29.27	18.96
Zn	174	143	73	168	36.67	18.97	27.34	49.72	44.22	41.3	29.01	44.27
Zr	273	271	174	220	51	104.03	47.62	39.55	67.7	75.61	58.81	50.14

Table 4.2: Summary statistics of regolith overlying the Sirius Prospect.

	Range				Geomean				Std. Dev.			
	All	**Aeolian**	**Calcrete**	**Saprolith**	**All**	**Aeolian**	**Calcrete**	**Saprolith**	**All**	**Aeolian**	**Calcrete**	**Saprolith**
Major oxides & LOI (wt.%)												
SiO2	57.53	37.6	38.133	53.62	47.15	66.7	47	43.8	15.65	9.057	12.709	14.74
Al2O3	15.31	3.19	5.725	13.25	10.22	11.3	7.3	10.7	2.68	0.897	2.143	2.63
Fe2O3	45.97	25.54	12.17	45.72	18	11.7	9.6	22.6	12.45	6.5	3.366	12.14
MnO	*	*	*	0.4	*	*	*	0.07	*	*	*	0.1
MgO	8.85	4.36	2.325	8.67	2.87	1.01	2.4	3.7	2.55	1.121	0.66	2.53
CaO	30.75	1.08	28.960	6.55	1.86	0.4	11.1	1.8	6.44	0.314	10.463	1.5
Na2O	2.05	1.07	0.173	1.97	0.24	0.12	0.06	0.4	0.51	0.219	0.054	0.54
K2O	1.9	0.32	0.475	1.9	0.35	0.6	0.5	0.3	0.36	0.089	0.129	0.41
TiO2	2.94	0.4	0.58	2.93	0.76	0.6	0.5	0.9	0.55	0.103	0.178	0.6
P2O5	0.06	0.03	0.054	0.03	0.01	0.02	0.02	0.004	0.01	0.009	0.015	0.005
SO3	0.11	0.03	0.027	0.11	0.01	0.01	0.02	0.004	0.01	0.008	0.007	0.02
LOI	23.67	4.5	21.673	11.68	7.81	5.1	12.8	7.7	4.36	1.258	6.801	2.77
Trace elements (ppm)												
Ba	1099	445	193	1099	228.56	157.8	151.5	270.2	177.48	119.16	63.495	186.73
Ce	198	118	79	198	53.71	52.5	38.6	57.5	40.98	48.21	24.446	41.11
Co	433	144	70	429	65.92	36.1	25	92.8	119.71	42.54	22.018	127.32
Nd	28	8	*	28	7.03	5.7	*	7.5	8.85	4.037	*	9.44
Ni	*	*	*	*	*	*	*	*		*	*	*
Pb	29	11	11	29	14.16	14.9	12.8	14.3	4.04	3.26	2.99	4.3
Rb	86	20	14	86	22.16	33.5	23.66	19	15.06	4.99	4.18	17.23
Sr	260	48	75	258	70.65	25.9	72.5	85.7	68.34	13.38	25.75	72.02
V	2885	1330	677	2829	1002.24	743	765.1	918.1	631.80	350.52	214.64	677.03
Y	21	14	9	21	11.08	11.8	11.6	15	4.12	3.89	2.62	4.42
Zn	176	49	15	172	35.51	18.1	12.7	48.2	50.87	12.82	5.2	52.04
Zr	256	196	128	252	76.01	198.6	159.2	46.2	88.64	59.17	39.98	84.58

Compared to various calcrete forms that were studied by Anand & Paine (2000) in the Yilgarn Craton; the calcrete horizon from the Sirius Prospect is characterised by slightly lower CaO with a geomean concentration of 11.1 wt.%. compared to the 14.10 wt.% - 42.19 wt.% in various calcrete forms. While the mean concentration of Na_2O decreases upwards, the concentration of K_2O shows the opposite trend, decreasing downhole. According to Brand & Butt, 2001; TiO_2 and Zr tend to concentrate on ferruginous materials within resistate primary and secondary phase minerals. In Sirius, however, these elements do not show a similar trend. Titanium has a higher concentration in the saprolith and decreases upwards, while Zr shows an opposite trend, showing a lower concentration at the base and increases upwards.

4.3 CHARACTERISTICS OF REGOLITH IN SERPENS NORTH PROSPECT

4.3.1 Variation patterns of major elements- Box plots

The variations in major oxide concentrations in different horizons are shown in Figure 4.1 below. From the boxplots, it can be deduced that aeolian sand has the highest SiO_2 concentrations, with a geomean value of 72.3 wt.% (Table 4.1 above). The high concentrations persist into the stone-line and saprolith horizon. Some examples of studies conducted in Mt. Keith where the underlying protolith is a komatiite, the SiO_2 mean concentration in the regolith is less than 35 wt.% (Brand & Butt, 2001); in South China, regolith underlain by basalt has mean concentrations of silica oxide ranging from 17wt.% - 34 wt.% (Ma et al., 2007), while the upper soils overlying gabbro and talc-chlorite schist in Ora Banda, have mean SiO_2 contents ranging from approximately 40 wt.% - 54 wt.% (Anand & Paine,

2002). Compared to the results from these studies, the saprolith in the Serpens North Prospect has SiO_2 contents that are in the ranges similar to those observed in Ora Banda.

The Fe_2O_3 and Al_2O_3 concentrations are also high within the aeolian sand, although they are slightly less than those observed in the two underlying horizons. However, the mean concentrations of the two oxides only differ slightly across the different horizons. The concentrations of MgO and CaO are slightly higher within the saprolith, which can be attributed to a bedrock that is slightly Mg and Ca-rich.

The stone-line is characterised by a lower geomean concentration of Mg and Ca oxides, but with more variability amongst different samples, which can be attributed to variations in weathering intensity. However, the aeolian sand has low Mg and Ca oxide concentrations, with very low variability between samples, which suggests that these relatively mobile oxides have possibly been leached from the horizon. The concentration of Ti_2O varies slightly in different horizons but is highest within the aeolian sand. While Na_2O and K_2O concentrations are generally very low; K_2O concentrations are highest in the aeolian sand, where samples show less variability. The Na_2O concentrations show less variability in the aeolian sand and stone-line, but the saprolite is characterised by variable concentrations, although in general, all the horizons show lower concentrations in this oxide.

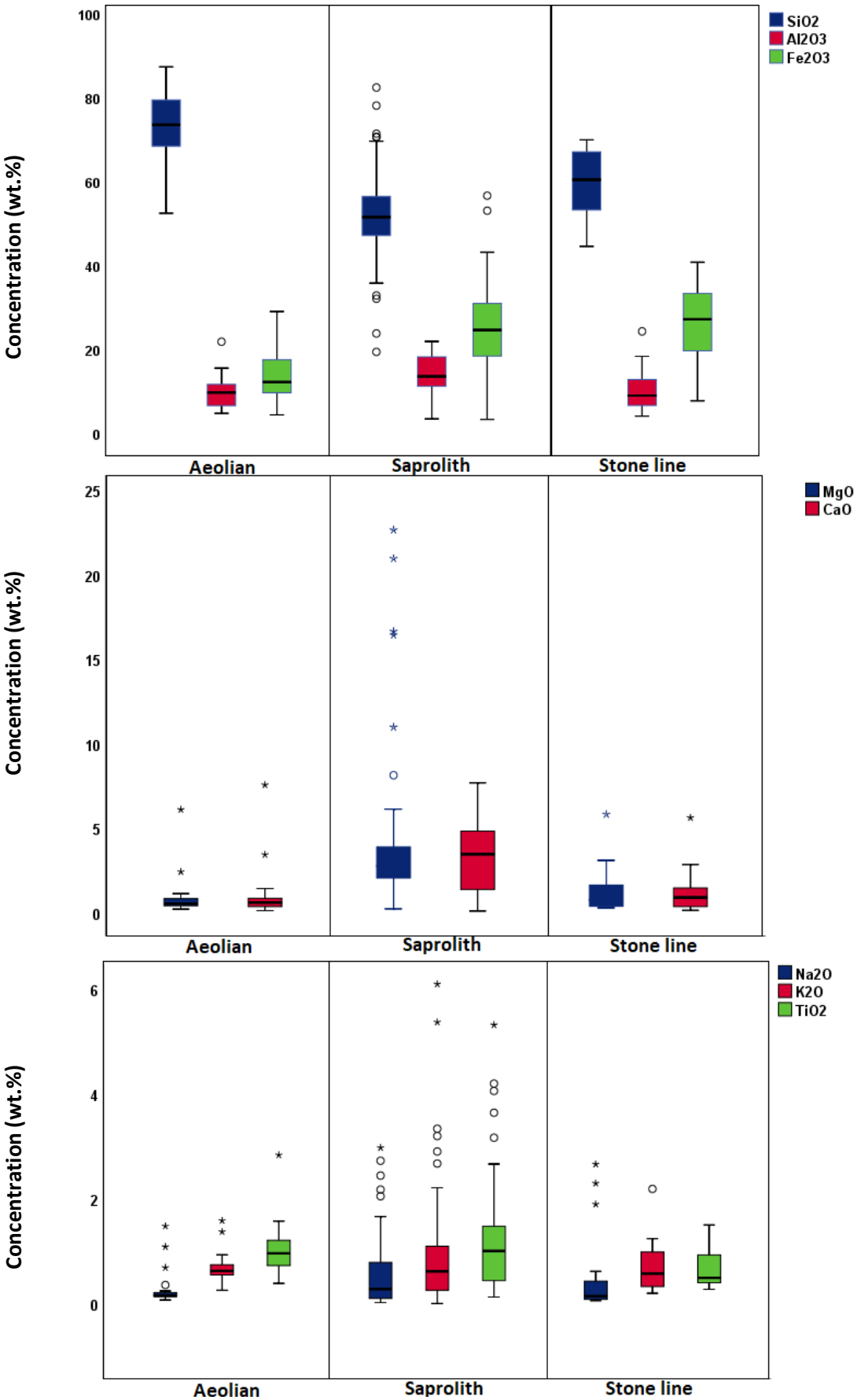

Figure 4.1: The distribution of major oxides in aeolian sand,stone-line and saprolith in the Serpens North Prospect.

4.3.2 Major and trace element associations in the regolith

A principal component analysis (PCA) of the geochemical data in Figure 4.2 below further reinforces the close associations between certain elements and groups of elements based on different clusters. The element associations vary within the different regolith horizons. Within the aeolian sand horizon, there are four distinct clusters of elements (Figure 4.2b). The first group of elements found in close association includes Zn, V, Sr, Rb, Ni, Co, and Ba. Secondly, there is an association between K_2O, Na_2O, Al_2O_3, MgO, CaO, Pb, and Y. The third association of elements includes SiO_2, TiO_2, P_2O_5, SO_3, Nd, Ce. Finally, Fe and Mn oxides show a close association, which could represent the precipitation of these elements to form oxy-hydroxides, although elements that are known to be found associated with these oxides do not appear to be associated with the oxides (e.g. Co, Cu, Ni). According to Pearson's correlation, SiO_2 only has a strong positive correlation with Zr (Appendix 6). There is, however, a strong negative correlation between SiO_2 with the majority of elements including Al_2O_3, Fe_2O_3, MnO, CaO, Na_2O, Ba, Ni; while there is a weaker negative correlation between SiO_2 and MgO, K_2O, Co, and Zn (Appendix 6). A strong positive correlation between Al_2O_3 and elements such as CaO, Na_2O, K_2O, Ba, and Pb, suggests that the regolith is immature and has not experienced significant weathering based on the association of Al_2O_3 with relatively mobile major oxides. There is a significant positive correlation between Fe and Mn oxides, but these two elements have no significant correlations with any other elements, suggesting that they are not responsible for scavenging any trace elements (Appendix 6).

The stone-line layer is comprised of five clusters of elements (Figure 4.2c). The first cluster of elements includes Na_2O, Al_2O_3, K_2O, Ce, Nd, Co, and Ba. In arid environments, some major elements can be retained in smectites or concentrated by high evaporation and

reprecipitation leading to their enrichment (McQueen & Scott, 2008), which is why oxides such as MgO and CaO occur in close association, along with Zr, forming another cluster. The other cluster of elements consists of Fe_2O_3, P_2O_5, Ni, and to a lesser extent, TiO_2. There is also an association between MnO, SO_3, Sr, Rb, and Y. Finally, there is a close association between SiO_2, Pb, and V. Based on the Pearson's correlation matrix, there are no significant correlations between SiO_2 and most of the elements, other than a positive correlation with Co, which is an unusual occurrence considering that the element is usually associated with ferromagnesian elements. In addition, there is a significant negative correlation between SiO_2 and Fe_2O_3 (Appendix 7). A negative correlation also exists between Al_2O_3 and Fe_2O_3, oxides that commonly occur concurrently in weathering products. The trend also differs from observations made in Thunderdome Prospect (Tonui, et al., 2003). There is also a significant correlation between Al_2O_3 and the oxides of Ca, K, and Na, which suggests less intense weathering.

The saprolith horizon is characterised by four distinct clusters of elements (Figure 4.2d). The first cluster of elements is comprised of Al_2O_3, Na_2O, CaO, Zn, V, Ni, and Co, which possibly represent incipient weathering of ferromagnesian minerals and feldspars. This implies that the more mobile elements such as CaO and Na_2O are still retained, along with aluminium and trace elements hosted by ferromagnesian minerals. This cluster of elements has a diametric relationship with a set of elements including MnO, P_2O_5, Rb, Zr. The third association of elements includes MgO, Fe_2O_3, TiO_2, SO_3, and Sr. The third group of elements has a diametric relationship with SiO_2, K_2O, Ba, Pb, Ce, Nd, and Y. According to Middelburg et al. (1988), Land & Ohlander (2000), potassium will persist in the weathering environment because it is likely to reside in K-feldspars, which are more resistant to weathering than plagioclase, hence its association with the less mobile SiO_2.

4.3.3 Pearson's correlation of major and trace elements in the Serpens North prospect

Pearson's correlation coefficient was used to determine the strength of associations between certain elements (Appendices 36-38). In the aeolian sand horizon, SiO_2 shows a strong, statistically significant, negative correlation with major oxides including Al_2O_3, Fe_2O_3, MnO, CaO, Na_2O, and trace elements Ba and Ni. The only element that has a strong, statistically significant, negative correlation with SiO_2 is Zr. Aluminium oxide has a strong, positive association with elements such as CaO, Na_2O, and K_2O, suggesting that the transported regolith has only undergone incipient weathering, and thus still retains these relatively mobile elements. The trace elements that are associated with Al_2O_3 include Pb and Ba. There are no significant associations between Fe_2O_3 and all elements, except for a weak correlation with Ni. An association between MgO and Ni could possibly be indicative of a mafic mineral, rich in magnesium (e.g. olivine), where Ni is a minor element. Calcium oxide is strongly associated with major oxides including Na_2O and K_2O, as well as trace elements such as Ba and Pb. The trace elements that are strongly associated with Ba include Co, Rb, Sr, V, and Zn.

Within the stone-line horizon, Al_2O_3 shows a strong correlation with the major oxides Na_2O, CaO, and K_2O, as well as the trace elements Ce and Nd. The association between Al_2O_3 and mobile oxides on the horizon also suggests minimal weathering. There are no trace elements that exhibit any statistically significant correlations with Fe_2O_3, while MnO only shows a strong association with Y.

In the saprolith horizon, Al_2O_3 is associated with major oxides CaO (weak correlation), Na_2O, and K_2O, as well as a weak correlation with Sr. There are no significant correlations between iron and manganese oxides with any trace elements in this horizon, which is unusual

considering that iron-rich minerals that form mafic rocks usually contain trace elements such as Ni and Co.

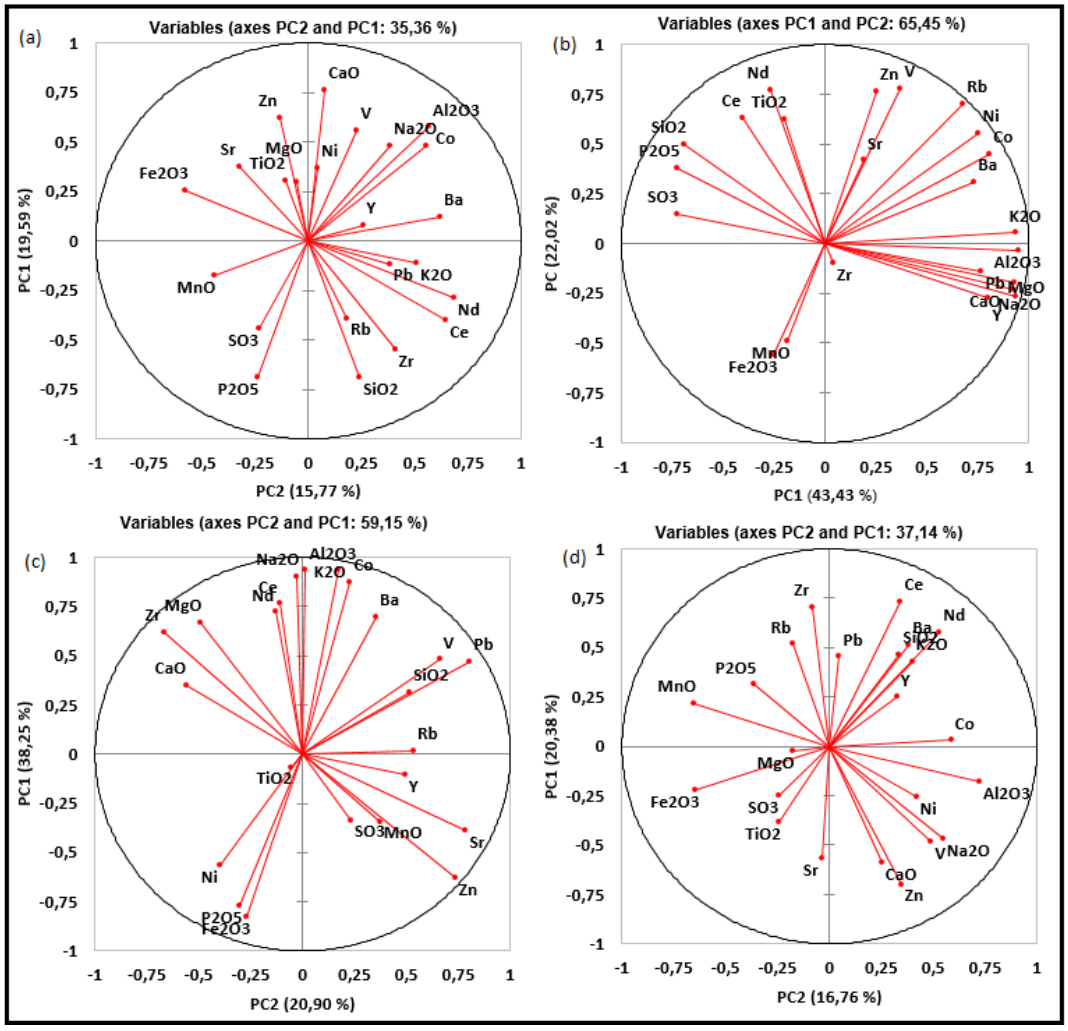

Figure 4.2: A principal component analysis of the major and trace elements of the samples within the different regolith horizons; (a) all samples, (b) aeolian sand, (c) stone lines, (d) saprolith.

4.3.4 Interpretation of major element associations using bivariate plots

In general, regolith profiles are characterised by the progressive loss of alkali and alkaline earth elements such as Ca, K, Na, Mg and the retention of Al, Fe, and partial retention of Si (Anand & Butt, 2010). The bivariate plots of major oxides within the three different horizons (Figures 4.3 & 4.4 below) show that aeolian sand has a significantly high concentration of SiO_2 (>70 wt.% in most samples), and the Fe_2O_3 concentrations in this horizon are also relatively

high. This is because samples are characterised by coarse quartz grains that are resistant to weathering. According to a study conducted by Kelly & Anand, 1995 (as cited in (Anand & Paine, 2002) in Forrestania, Yilgarn Craton, a similar range of concentrations of SiO_2 can be attributed to granitic-derived aeolian sand. However, the Fe_2O_3 concentrations in Serpens North are slightly high compared to Forrestania. Aeolian sand samples also exhibit low concentrations in the oxides of Ca, K, Na, Mg, which suggests that these highly mobile elements are leached from the horizon onto the underlying horizon during rainy seasons. The concentrations of these mobile oxides are within ranges similar to those observed in areas such as Forrestania, as well as Kanowna and Bounty (areas characterised by the occurrence of calcrete) (Anand & Paine, 2002).

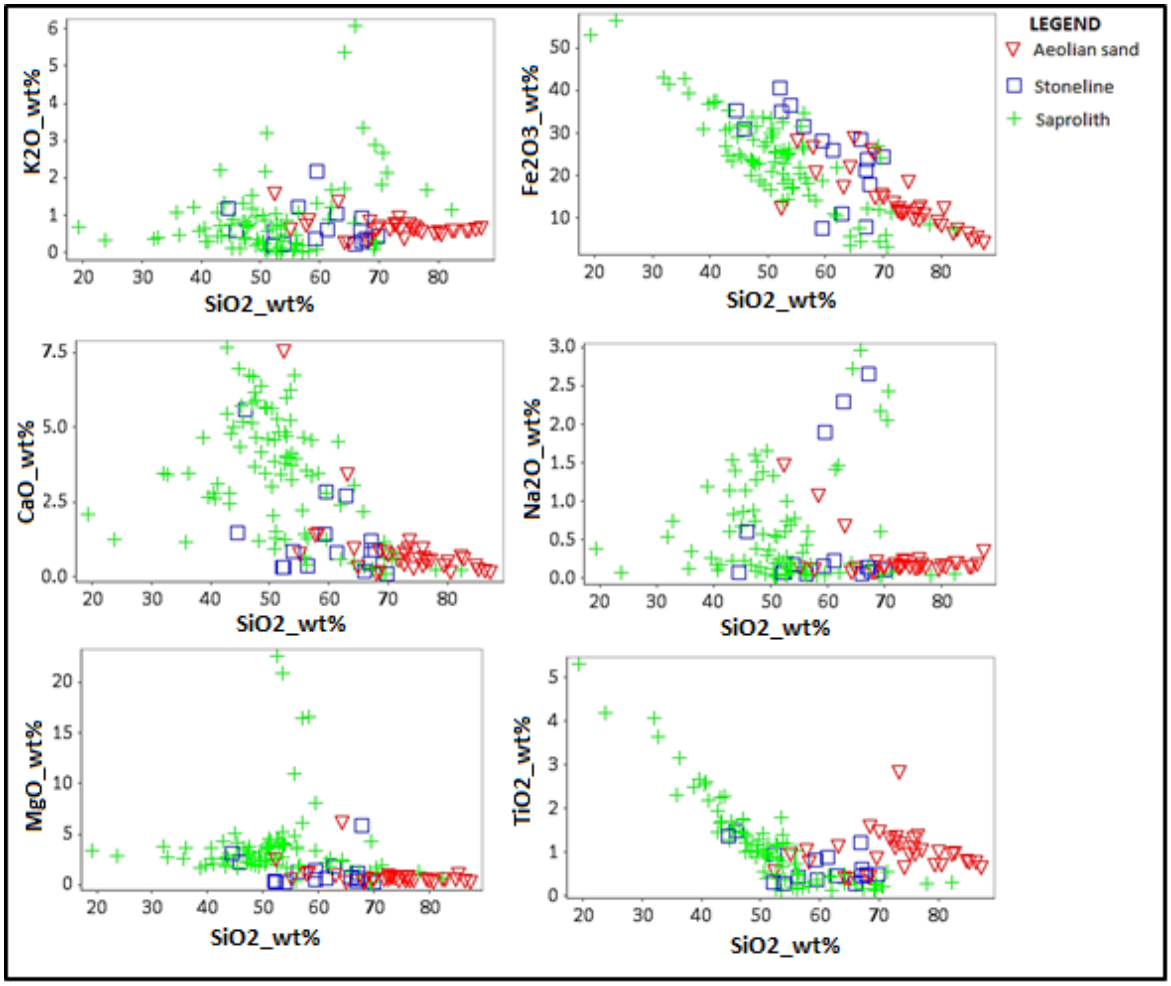

Figure 4.3: A plot showing the relationship between SiO_2 and various major oxides in the three regolith horizons.

The stone-line horizon is characterised by moderate enrichment in both SiO_2 and Fe_2O_3. Three of the stone-line samples, however, show slightly lower concentrations of the two oxides and a corresponding enrichment of CaO and Na_2O. All the other samples generally show low concentrations of Mg, K, Ca, Ti, and Na, almost similar to the trends observed in the aeolian sand except the Si concentrations which are generally lower than in aeolian sand.

The saprolith samples are characterised by variable concentrations of SiO_2, with some samples showing significant enrichment of up to 70 wt.% while some samples have SiO_2 concentrations as low as 20 wt. % which can be attributed to variabilities in weathering and loss of Si in some areas. Although some saprolith samples show lower Fe_2O_3 concentrations (below 10 wt.%), most samples are characterised by high concentrations (ranging from 10-40 wt.%), owing to the mafic nature of the protolith. The progressive decrease in SiO_2 concentration in saprolith samples is accompanied by an increase in Al_2O_3 and Fe_2O_3 concentrations, which according to Tonui et al. (2003); is a result of the enrichment of the two latter oxides in Fe- oxides and clay minerals. Compared to the aeolian sand and stone-lines, the saprolith is characterised by higher Na and K oxides, suggesting that there is retention of these elements possibly within feldspars which are not significantly altered in the early stages of weathering.

Most of the samples are characterised by enrichment in MgO and CaO, which suggests that the protolith is rich in these oxides, while TiO_2 shows variable concentrations in different samples. According to Butt et al. (2000); the saprolith is characterised by the loss of SiO_2 and MgO, except where they are retained in smectites, kaolinite, and quartz, which is contrary to

the observed high concentrations in these elements in the study area. The abundance in these elements suggests that minimal weathering has taken place, as also evidenced by the higher concentration of even more mobile elements such as Na, Ca and K. The high Fe_2O_3 concentrations within the saprolith are within the ranges observed in the goethite-rich ferruginous saprolite Matt Dam gold prospect in the Yilgarn Craton (Anand, 2001).

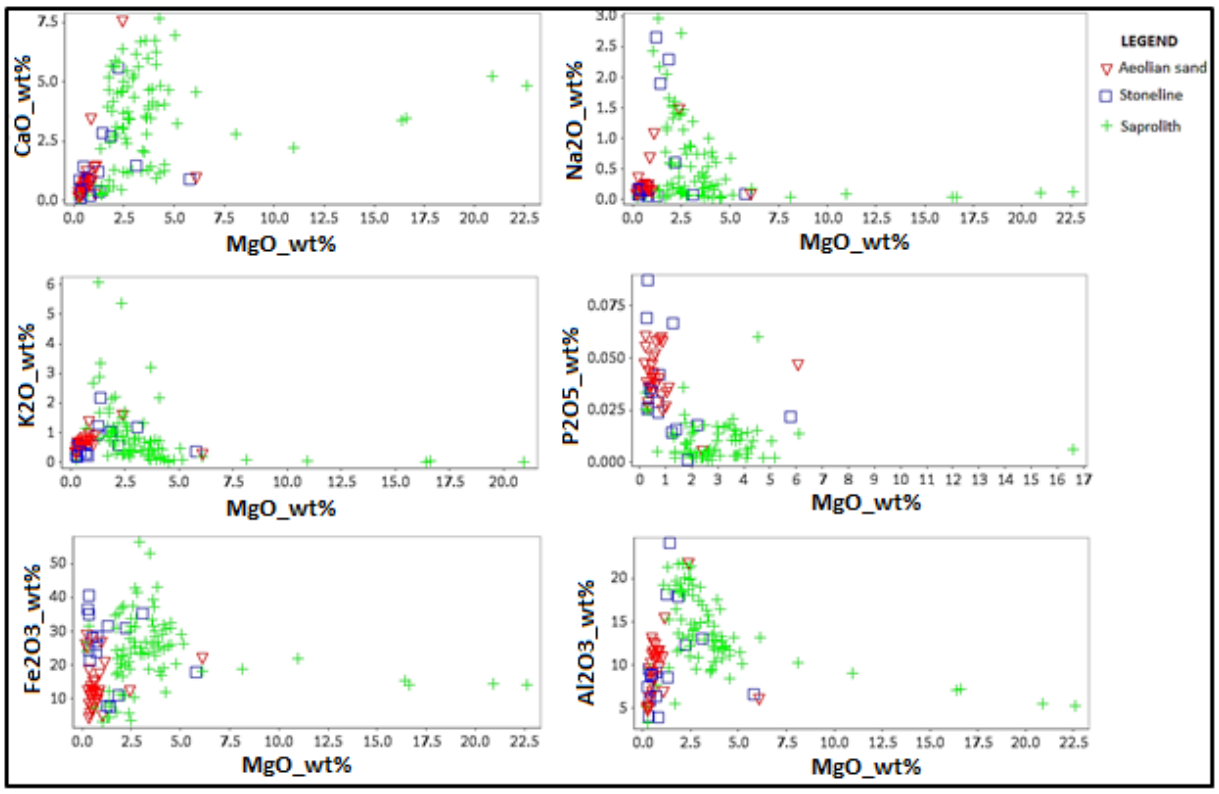

Figure 4.4: The relationship between MgO and various other major oxides within different horizons down the soil profile.

4.4 WEATHERING TRENDS AND INDICES

Weathering indices have been widely used to characterise regolith derived from parent rock with different compositions and to determine the degree of weathering (Nesbitt & Young, 1982; Nesbitt & Young, 1984; Nesbitt & Young, 1989; Cox, et al., 1995; Khider & McQueen, 2005; McQueen, 2006; McQueen & Scott, 2008; Goldberg & Humayun, 2010; Valiani &

Rezaee, 2014; Arhin et al., 2017). The mobilization of cations such as Na^{+}, Ca^{2+}, K^{+}, and Mg^{2+}, (partly Si^{4+}), and the retention of cations such as Si^{4+}, Fe^{3+}, and Al^{3+} during weathering processes can be used for characterization of regolith materials that are at different stages of chemical evolution (McQueen & Scott, 2008). Ratios of K/Al were plotted against Mg/Al ratios based on data from the Serpens North Prospect, and the results are shown in Figure 4.5. Based on samples from three different types of regolith from the Cobar and Kalgoorlie regions, Australia; McQueen calculated the ratios of K/Al and Mg/Al and plotted them on a cartesian plane. He proposed that samples obtained from transported regolith, ferruginous alluvium, and saprolite developed on mafic rocks should have K/Al ratios ranging from 0.00-0.16; 0.15-0.28; 0.16-0.4; respectively. The ratios of Mg/Al in the aforementioned regolith horizons would range from 0.00-0.15; 0.05-0.35; 0.07-0.2, respectively (McQueen, 2006).

Most of the saprolith data (Figure 4.5) shows a trend towards Mg enrichment relative to Al and a corresponding depletion in K, which according to McQueen (2006), is characteristic of smectite/ chlorite/ dolomite minerals. According to Butt et al. (2000), continued weathering at the base of the profile in arid and semi-arid environments leads to the formation of smectites and accumulation of Si, alkali and alkaline earth elements. Therefore, the enrichment of Mg is consistent with the formation of smectite. Some of the saprolith samples, however, have higher K/Al ratios and moderate Mg/Al ratios. The reason for the previously mentioned trend is that these samples still retain some primary minerals such as muscovite suggesting that there is variable weathering. Additionally, these samples may represent newly weathered samples closer to the bedrock, meaning they have not been subjected to extensive weathering. A few samples, however, plot towards the kaolinite direction of weathering, mostly characterised by Al_2O_3 enrichment and a corresponding depletion in mobile elements such as potassium and magnesium, hence the low K/Al and Mg/Al ratios. Aeolian sand

samples are characterised by both low Mg and K relative to Al, implying that there is a depletion in these mobile elements relative to Al. Like the aeolian sand samples, stone-line samples are largely characterised by Al enrichment and a corresponding depletion in K and Mg as evidenced by the low K/Al and Mg/Al ratios.

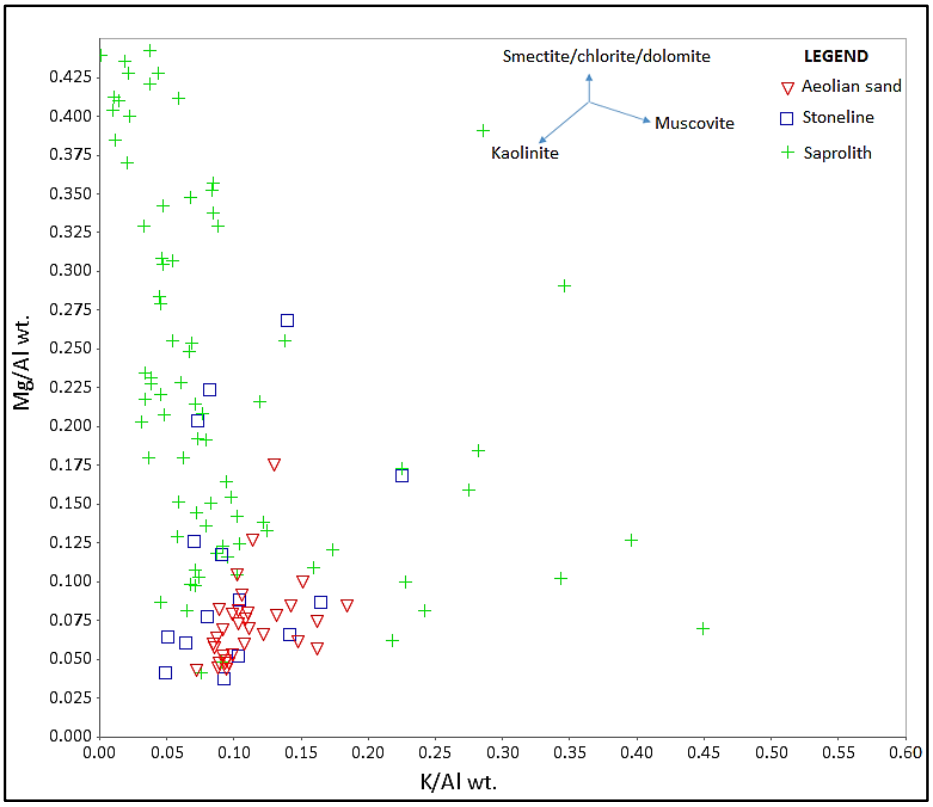

Figure 4.5: A plot of the ratios of mobile elements Mg and K to the relatively immobile Al plotted against each other to show weathering trends based on samples obtained from Serpens North (McQueen (2006)).

Data was also presented using downhole plots in order to show the element trends in individual boreholes (Appendices 5-27). Additionally, the geometric mean concentrations of the different elements were also calculated in order to summarise the data (Table 4.3). Based on the geomean statistics, it is evident that SiO_2 fractionates downwards, with the highest concentration occurring in the aeolian sand layer, where it is partly retained and forms the major component of the samples due to the loss of more mobile elements. There seems to be an abundance of quartz throughout the profile as evidenced by the high concentrations of SiO_2 throughout the profile.

The geomean concentration of Al_2O_3 is highest within the lower and mid saprolith, where, according to Butt et al. (2000), there is initial destruction of primary minerals (feldspars and ferromagnesium minerals) and the formation of clay minerals and subsequent retention of Al_2O_3 in this zone. The weathering of less stable ferromagnesian minerals during the early stages of weathering results in the formation of iron oxides, which scavenge trace elements (Butt, et al., 2000). The high concentrations of elements including Ni and Zn within the lower saprolith suggest that these trace elements are adsorbed by iron oxides, while there seems to be a loss of Co within the lower saprolith and its enrichment in the upper saprolith. The highest geomean of Fe_2O_3 occurs within the upper saprolith and stone-line, suggesting that these are zones of ferruginisation, and these are coupled with Co, Ba, Rb, Sr, V, Y, and Pb enrichment.

The lower aeolian sand is also characterised by a high concentration of trace elements such as Ba, Co, Ni, Rb, Sr, V, and Zr, relative to the overlying upper aeolian sand, suggesting that elements that are mobilised from the upper aeolian sand during rainy seasons, precipitate in the lower aeolian sand. The concentrations of these trace elements are generally higher than those in the lower and mid-saprolith.

Table 4.3: Geometric mean concentrations of major and trace elements in various regolith horizons in Serpens North Prospect.

	Geomean					
	Upper aeolian	**Lower aeolian**	**Stone lines**	**Upper saprolith**	**Mid saprolith**	**Lower saprolith**
Major oxides (wt.%)						
SiO2	76,35	64,52	59,54	53,47	50,49	50,11
Al2O3	7,84	11,59	10,31	11,59	13,88	13,81
Fe2O3	10,69	16,84	25,38	22,6	20,62	19,97
MnO	0,04	0,15	0,21	0,14	0,11	0,12
MgO	0,54	0,68	1,32	2,01	2,97	3,38
CaO	0,45	0,95	1,29	1,71	2,62	3,19
Na2O	0,15	0,23	0,55	0,18	0,31	0,36
K2O	0,55	0,74	0,68	0,45	0,54	0,47
TiO2	0,9	0,92	0,68	0,74	0,85	0,8
P2O5	0,04	0,03	0,03	0,01	0,01	0,01
SO3	0,02	0,02	0,01	0,01	0,004	0,003
Trace elements (ppm)						
Ba	110,23	284,53	292,13	236,64	260,18	260,68
Ce	54,63	57,31	50,75	57,75	50,52	37,32
Co	11,3	41,45	53,43	48,86	32,19	35,31
Nd	20,64	17,5	14,55	12,16	16,89	14,32
Ni	34,6	88,58	104,86	38,48	69,13	76,46
Pb	12	11,31	11,81	13,50	10,14	10,46
Rb	25,21	33,55	31,13	19,82	21,45	24,18
Sr	25,74	123,47	106,94	60,65	85,91	114,75
V	328,11	675,75	526,25	592,18	436,02	557,23
Y	10,5	13,02	19,44	12,6	11,89	12,5
Zn	10,72	62,57	43,81	36,67	43,9	65,19
Zr	169,2	37,62	71,44	47,76	46,74	31,82

4.4.1 Determining the degree of weathering using weathering indices

The two indices that were used to determine the maturity of the regolith are the CIA (Nesbitt & Young, 1982), calculated using the formula [100*Al_2O_3/(Al_2O_3+CaO+NaO+K_2O) and ICV (Cox et al., 1995), calculated as follows; [Fe_2O_3+ CaO+ Na_2O+ K_2O+ MgO+ MnO+ TiO_2]/Al_2O_3 (results are shown in Appendices 1, 2 & 3). These indices are used to determine the abundance of Al_2O_3 relative to the other major oxides. The indices are based on the premise that the breakdown of feldspars (most abundant mineral in the earth's crust), liberates some mobile elements such as CaO, Na_2O, K_2O to form clays (Price & Velbel, 2003). According to Cox et al.

(1995); non-clay silicates are characterised by lower Al_2O_3 concentrations compared to clay minerals; hence, their higher ICV index. The ICV index is higher where less stable minerals such as pyroxenes and amphiboles are present (>1), and decreases significantly in more stable alkali feldspars and micas (between 0.54 – 0.87), and is lowest where clay minerals such as illite, montmorillonite, and kaolinite are abundant (0.03 – 0.78) (Cox, et al., 1995). The CIA is generally < 50 for unweathered igneous and metamorphic rock, while the index can reach 100 in weathered aluminosilicates (Nesbitt & Wilson, 1992; Valiani & Rezaee, 2014).

The ICV calculated for the in-situ regolith (saprolith), shows that most of the samples have indices greater than one, implying that the regolith has only undergone incipient chemical weathering (Appendix 1-3). Furthermore, the indices indicate that the samples are immature and characterised to a certain extent by non-clay, primary minerals. However, some clay minerals are present as evidenced by CIA indices above 70 and ICV indices less than one, as shown in Appendices 1-3. The presence of clays can be attributed to some form of chemical weathering which occurs during wet summer seasons, which subsequently leads to the mobilization and redistribution of elements.

The A-C-K diagram, initially proposed by Nesbitt & Young, 1984; was modified by Lambe (1996) (and cited therein Regassa et al., 2014). The A-C-K diagram in Figure 4.6 shows that the majority of the saprolith samples are characterised by low-moderate CaO because most of the samples have percentage molar concentrations that are less than 50 mol%. The K_2O concentrations in most of the saprolith samples are lower, because they plot away from the K_2O apex of the diagram, although some samples show a slight increase in the oxide (over 50 mol.%). Almost all of the samples are characterised by moderate-high Al_2O_3 concentrations

greater than 50 mol.%, characteristic of a moderate degree of weathering. The stone-line and aeolian sand samples show lower CaO concentrations and therefore, plot towards the upper apex of the triangle. These two horizons are also characterised by relatively low K_2O concentrations. According to the general classification of weathering materials which was used to modify the A-C-K diagram to include the CIA by the Geological Society of London, (Lambe, 1996 (as cited in Regassa et al., 2014)), samples with a CIA less than approximately 63 represent fresh rocks - rocks that are slightly discoloured by weathering. In their classification, samples that have a CIA that is between approximately 63 -81 indicate decomposition of up to 50% of the primary minerals, while a CIA greater than 81 indicates residual materials with no remnants of the primary minerals. The majority of samples from Serpens North prospect have CIA values greater than 63, while a few of the samples have a CIA greater than 81 (Figure 4.6).

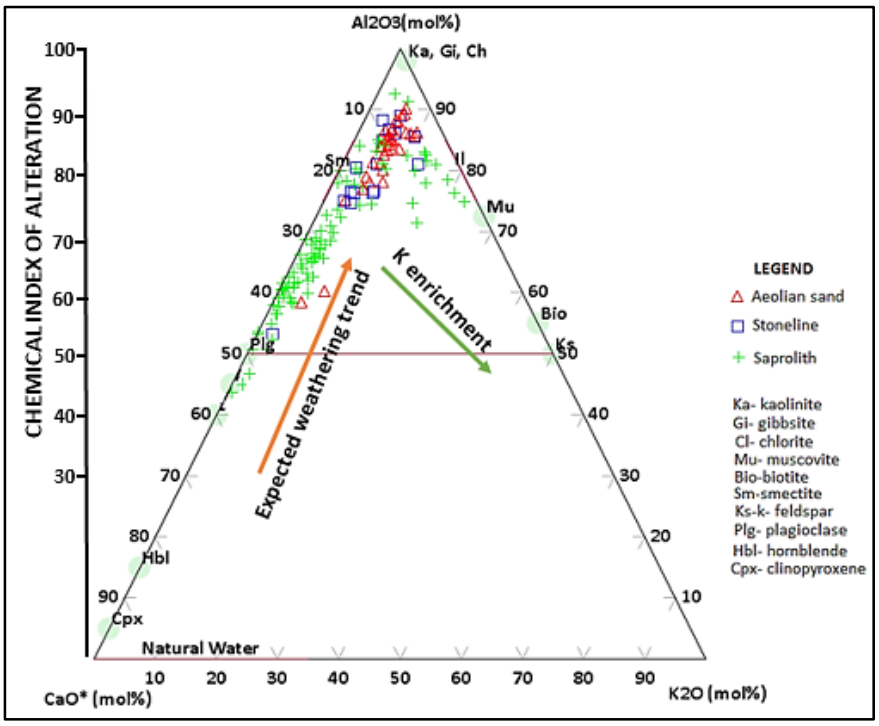

Figure 4.6: Weathering trend in Serpens North obtained from the chemical index of alteration (adopted Nesbitt & Young, 1982).

The A-CNK-FM diagram in Figure 4.7 below shows that most of the samples have high FeO + MgO* and low – moderate Al_2O_3 and CaO*+ Na_2O + K_2O, characteristic of mafic rocks. Furthermore, the progressive decrease in SiO_2 concentrations in the saprolith horizon is accompanied by an increase in Fe_2O_3 concentrations, which Tonui et al. (2003) attributed to the enrichment of iron in secondary Fe- oxides. Some of the samples plot close to the biotite field, which suggests that these samples have concentrations of FeO and MgO characteristic of primary minerals of mafic nature and possibly the accumulation of iron oxyhydroxides in the weathering environment. A large number of samples plot in the field proximal to gabbro (Ga), which suggests concentrations of the oxides of iron and magnesium that are characteristic of residual regolith from a mafic bedrock that has been weathered slightly, to form clays. Some soil samples have characteristics of a more intermediate protolith because they plot in the area around diorite. Lower FeO + MgO characterises a few of the samples because they plot higher up, suggesting significant weathering. The majority of the stone-line and a few aeolian sand samples have similar geochemical characteristics with the saprolith, being characterised by high FeO + MgO contents, while most aeolian sand samples have a more intermediate composition.

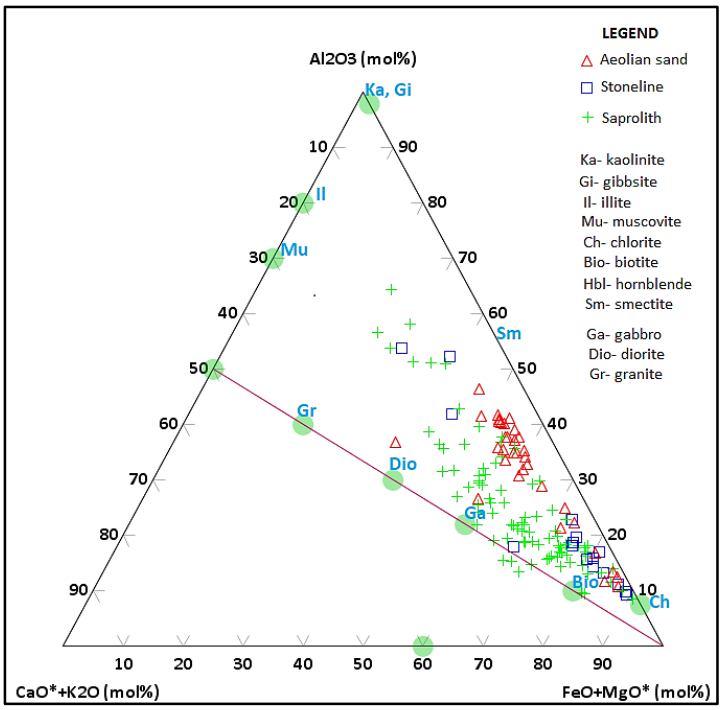

Figure 4.7: The distribution of regolith samples on an A-CNK-FM diagram indicating the composition of the samples and the degree of weathering (adopted from Nesbitt & Young, 1982).

4.4.2 Determining the protolith of samples

While regolith loses most elements during pedogenic processes, particularly the more mobile ones, it is the more immobile elements that are retained even after extensive weathering that can be used to determine the original bedrock of the residual regolith including zircon and titanium. In the Zr vs Ti plot in Figure 4.8 below, the saprolith samples mostly plot within the gabbro field, while a few of the samples plot within the more intermediate field of diorite and a few more within granodiorite which is intermediate between diorite and granite in composition. The stone-line and aeolian sand, although transported were also plotted and they are characterised by both intermediate and mafic parent rocks.

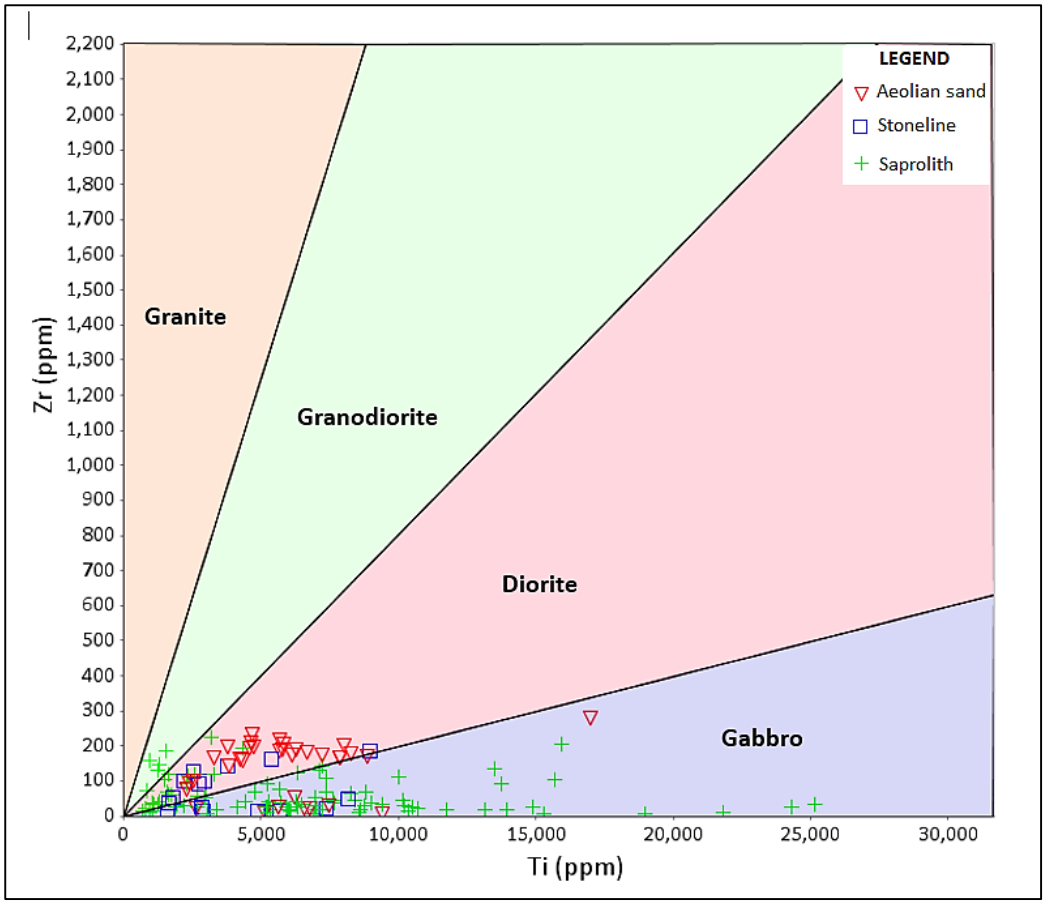

Figure 4.8: A plot showing the possible parent rocks of regolith samples from Serpens North (after Hallberg. 1984).

4.5 SUMMARY OF FINDINGS

Based on the different analytical techniques performed on the data, the main findings can be summarised as follows:

- The bulk composition of the aeolian sand horizon includes SiO_2, Fe_2O_3, and Al_2O_3. The remaining elements all have geomean concentrations that are below 1 wt%. The associations within the aeolian sand include; (a) Zn, V, Sr, Rb, Ni, Co, and Ba; (b) K_2O, Na_2O, Al_2O_3, MgO, CaO, Pb, and Y; (c) SiO_2, TiO_2, P_2O_5, SO_3, Nd, Ce; (d) Fe_2O_3 and MnO. The absence of any other elements besides Fe_2O_3 and MnO in the fourth cluster suggests that these oxides are not responsible for scavenging any elements in this horizon. According to Jenne, 1987, Al_2O_3 and SiO_2 have the ability to scavenge trace

elements, although less emphasis is placed in determining the trace element associations with these oxides. In addition, organic matter also scavenges trace elements (Jenne, 1987; Chao, 1984). All these phases are possibly responsible for scavenging trace elements because Fe and Mn oxides do not play a role in scavenging trace elements in this horizon.

- Stone-lines are mainly composed of SiO_2, Al_2O_3, Fe_2O_3, while all the other elements also have a geomean concentration that is less than 1 wt%. The highest concentration of Fe_2O_3 is within this horizon, which suggests that this is the ferruginised zone. The element associations within the stone-line horizon include; (a) Na_2O, Al_2O_3, K_2O, Ce, Nd, Co, and Ba; (b) MgO, CaO, and Zr; (c) Fe_2O_3, P_2O_5, Ni, and to a lesser extent TiO_2; (d) MnO, SO_3, Sr, Rb, and Y; (e) SiO_2, Pb, and V.
- The saprolith horizon is mostly composed of SiO_2, Al_2O_3, Fe_2O_3, and to a certain extent, MgO and CaO. All the other elements have geomean concentrations below 1 wt%. The upper saprolith can be classified as ferruginous because the Fe_2O_3 concentrations are highest within this zone. The element associations with the saprolith include; (a) Al_2O_3, Na_2O, CaO, Zn, V, Ni, and Co (b) MnO, P_2O_5, Rb, Zr; (c) MgO, Fe_2O_3, TiO_2, SO_3, and Sr; (d) SiO_2, K_2O, Ba, Pb, Ce, Nd, and Y.
- Magnesium oxide and Al_2O_3 show some fractionation, indicating a progressive loss upwards, while the SiO_2 and K_2O fractionation is opposite, increasing in concentration upwards.
- The decoupling of elements that are characteristic of mafic minerals (for example Co and Ni) from Fe and Mg oxides in in-situ regolith suggests that trace elements have been released from primary minerals by weathering processes and adsorbed into the complex structures of aluminium rich clays, hence their association with Al_2O_3. In the

in-situ regolith, SiO_2 and K_2O are associated with a number of trace elements, and this group possibly represents the primary feldspars that have not undergone weathering, thus retaining some trace elements. Iron oxides (such as goethite and hematite), do not seem to retain any trace elements, except Sr.

- Based on weathering indices, the degree of weathering in the Serpens North Prospect can be characterised as incipient – moderate.

4.6 CHARACTERISATION OF REGOLITH MATERIALS IN SIRIUS PROSPECT

4.6.1 Variation patterns of major elements- Box plots

The aeolian sand horizon (Figure 4.9) shows high concentrations of the Si, Fe, and Al oxides, while the concentrations of Na, K, Mg, and Ca oxides are less than 1 wt.%, but Na_2O is the most leached from the horizon with a geomean concentration of 0.1 wt.%.

The concentrations of the oxides of Na and K do not show a marked increase in the calcrete horizon, probably because the elements are leached from the horizon. The concentrations of Ca and Mg oxides show a significant increase in the calcrete horizon (geomean concentrations of 11.1 wt.% and 2.4 wt.% respectively), with Si, Fe, and Al also forming a major component of the samples. The high CaO concentrations within the horizon are within ranges similar to those observed in Ora Banda in the Yilgarn Craton (CaO= 9.5-14.1 wt.%) (Anand & Paine, 2002), although the MgO ranges are lower in the Sirius Prospect. The parent rock in Ora Banda is gabbro (Anand &Paine, 2002), similar to the parent rock of the regolith in the Sirius Prospect. The occurrence of calcretes in the Sirius Prospect is characteristic of arid

environments, where excess evaporation leads to accumulation of carbonates which would otherwise be leached from upper horizons in humid regions and the presence of a Ca and Mg-rich bedrock (Anand & Paine, 2002). However, the composition of the calcretes found in the Sirius Prospect differs from the chemical composition standards of different forms of calcretes that were proposed by Anand & Paine, 2002 (especially the CaO mean concentration). According to Anand & Paine, 2002; the CaO mean concentrations range from 14.10 wt.% in powdery calcretes to 42.19 in boulder calcretes. Compared to the classification of calcretes based on chemistry proposed by Anand & Paine (2002), the calcretes from Sirius are characterised by slightly lower average Ca and LOI while Mg concentrations conform to the values proposed in the classification. Based on the classification by Anand & Paine (2002), the calcretes in the Sirius Prospect are also characterised by slightly elevated Si, Fe, and Al.

The saprolith horizon shows a higher and great variability in concentrations of the oxides of Si, Fe, Na, K, Mg, and Ti, indicating the accumulation of these oxides in this horizon. In general, the regolith profiles show very little fractionation, unlike the significant fractionation observed in the deeply-weathered terrain in the Yilgarn craton (Anand & Butt, 2010).

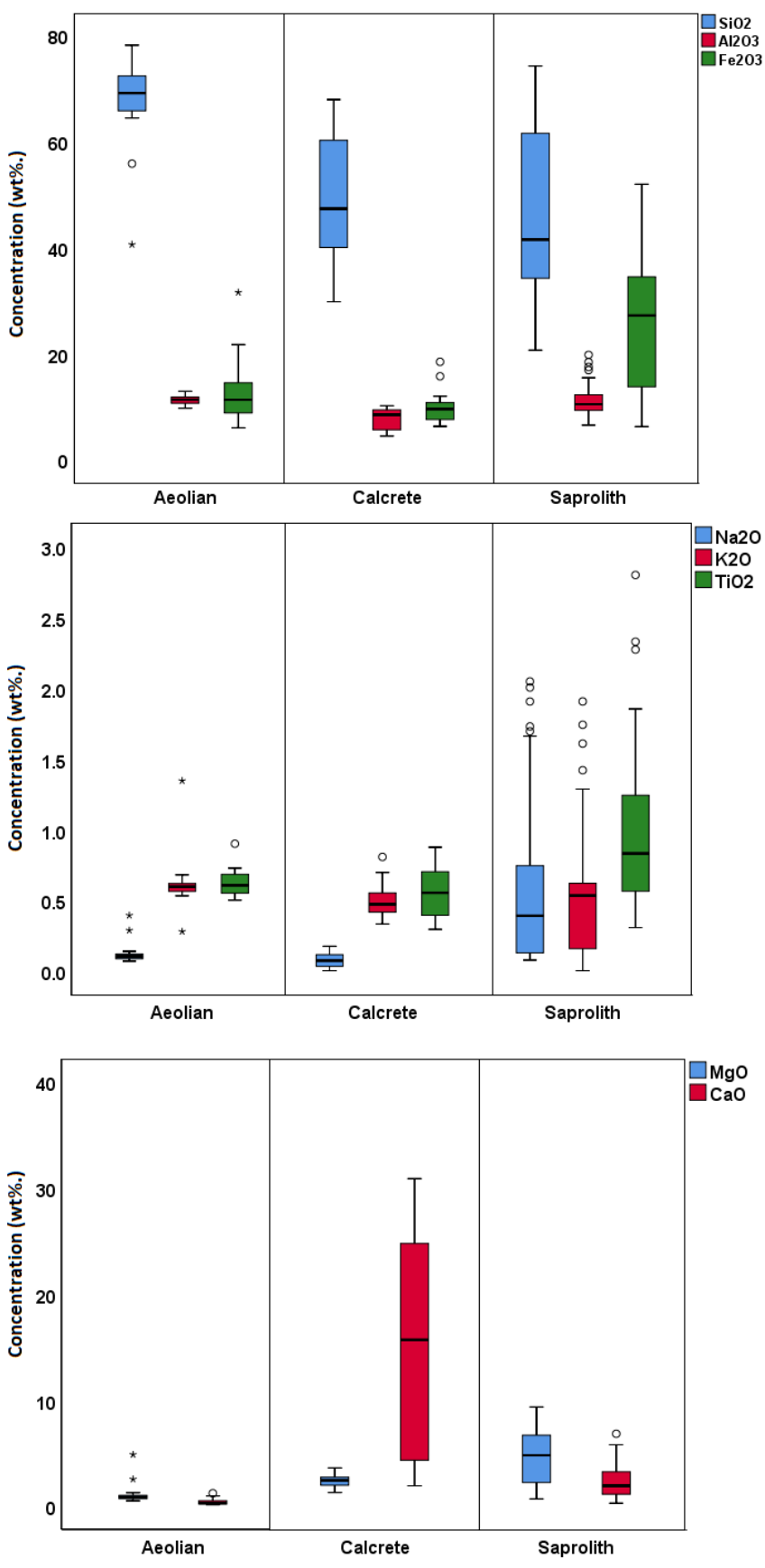

Figure 4.9: Distribution of major oxides in aeolian sand, calcrete, and saprolith in the Sirius Prospect (concentrations of oxides in wt.%).

4.6.2 Major elements associations in regolith - PCA plots

The PCA plotted for aeolian sand indicates the presence of four distinct clusters of elements (Figure 4.10b). The first cluster of elements includes LOI, Na_2O, Pb, Ce, and Nd. The second cluster of elements includes Fe_2O_3, MgO, CaO, Sr, V, Zn, Co, Ba, and Y, which suggests that the protolith from which the transported regolith is derived is also mafic in nature as shown by the Fe and Mg oxides, but also calcium-rich. An association between iron oxides and trace elements such as Zn, V, Co, Ba, and Y indicates the ability of iron oxides to adsorb these trace elements (Tonui et al., 2003). Another association of elements includes Al_2O_3, TiO_2, P_2O_5, K_2O. Finally, there is an association between SiO_2, SO_3, Zr, Rb, which gives an indication of the presence of sulphates within the quartz-rich aeolian sand. Based on Pearson's correlation matrix, associations of elements established were consistent with the PCA, compared to Serpens North (Appendix 12).

Within the calcrete horizon (Figure 4.10c), there is an association between MgO, P_2O_5, CaO, LOI, SO_3, Sr. The second cluster of elements includes Fe_2O_3, TiO_2, Na_2O, Zn, Co, Ba, Ce, and Pb, which suggests that at this stage, trace elements such as Co, Zn, Ba, Ce, and Pb are hosted by iron oxides rather than carbonates because the trace elements are found associated with Fe_2O_3. Thirdly, there is an association between K_2O, Rb, Al_2O_3, SiO_2, and Zr, a group mainly composed of less mobile elements which will tend to be retained in the weathering profile. Pearson's correlation produced results that are consistent with those of the PCA, indicating that there are strong and statistically significant associations between elements (Appendix 13).

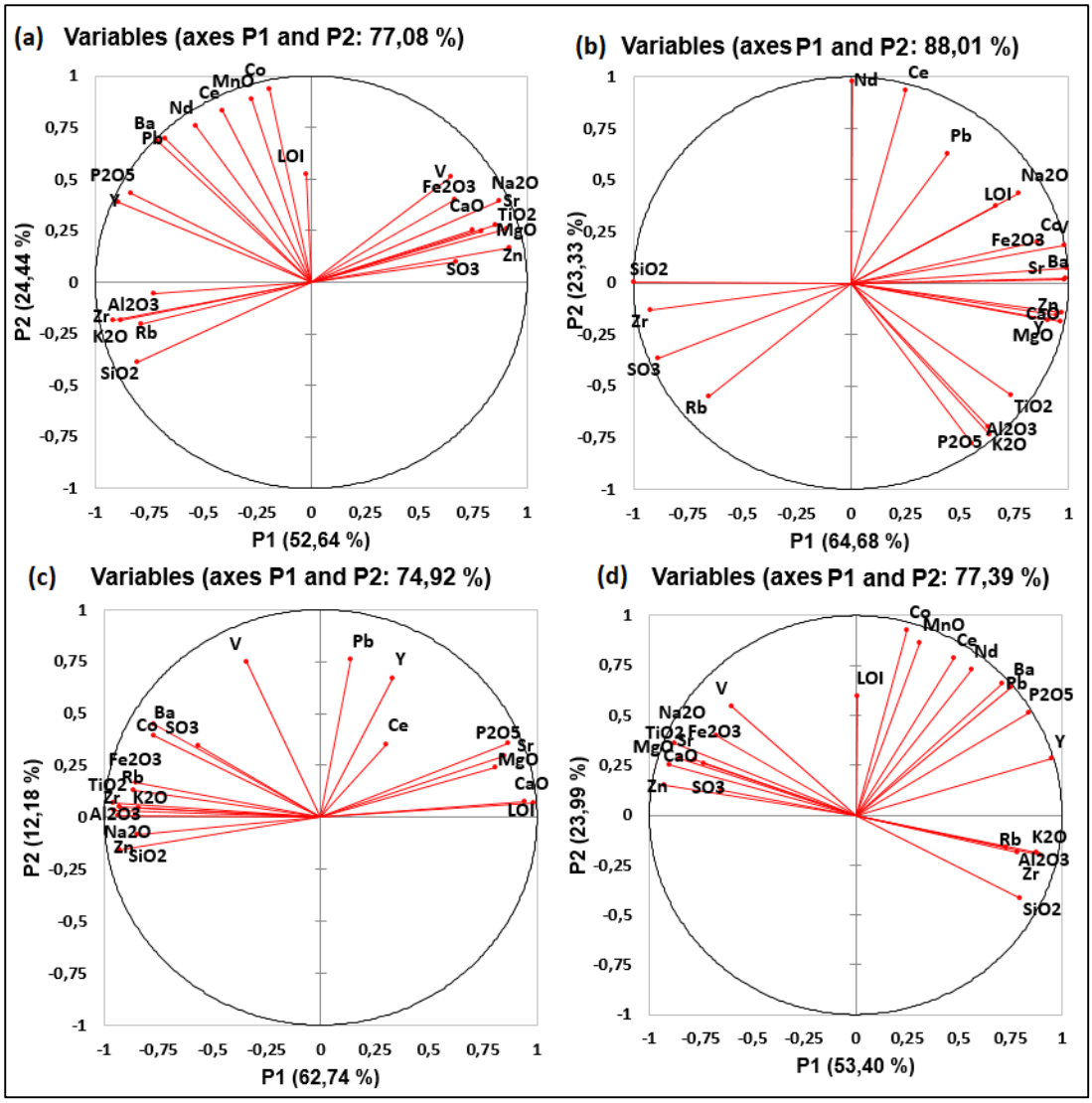

Figure 4.10: Element associations in the different regolith horizons in Sirius; (a) all horizons, (b) Aeolian sand, (c) calcrete, (d) saprolith.

Elemental associations within the saprolith include three clusters (Figure 4.10d). The first cluster includes LOI, MnO, P_2O_5, Co, Ce, Nd, Pb, Ba, and Y. The association of the trace elements such as Co, Pb, Ba, Ce, and Nd with LOI could be an indication that these trace elements are hosted in carbonates because the high LOI in the saprolith can be attributed to the presence of carbonates rather than organic matter (because of the sparse vegetation) (Heiri et al., 2001; Frangipane et al., 2009). According to Pearson's correlation, however, Co has a significant, strong positive correlation with Fe oxides, suggesting that the trace

element's enrichment is also dependent on the oxide. Secondly, there is a close association among elements that include Fe_2O_3, MgO, Na_2O, CaO, TiO_2, SO_3, Zn, Sr, and V, indicating regolith that has only undergone incipient weathering as evidenced by the coexistence of more mobile elements in this group. The group also represents a mafic protolith which is also rich in plagioclase feldspars as indicated by the association of iron oxides with Na and Ca oxides. The previously mentioned elements have a diametric relationship with a group of elements which includes Al_2O_3, SiO_2, K_2O, Zr, and Rb. A similar trend was also observed in the calcrete horizon, which represents the less mobile elements such as Al and Si oxides, and K_2O which persists in the weathering environment (in K-feldspars). According to Middelburg et al. (1988); Land & Ohlander (2000); these oxides are more resistant to weathering. Pearson's correlation matrix was used to also determine the degree of correlation between elements in different regolith horizons and the results are shown in Appendices 11-14.

4.6.3 Pearson's correlation of major and trace elements in the Sirius Prospect

The Sirius Prospect, unlike Serpens North, is characterised by numerous significant correlations between various elements. For example, in the aeolian sand horizon, Si_2O shows a strong correlation with Rb and Zr. Iron oxides also show a strong correlation with trace elements including Ba, Co, V, Pb, Y, and Zn, as well as the major oxides of Na, K, Mg, and Ti.

Similar associations are observed in the calcrete horizon, with iron oxides seemingly scavenging trace elements such as Co, Ba, V, Y, and Zn, as evidenced by their strong association with the oxide. In addition, MnO shows strong associations with elements such as Ce, Co, Sr, and Zn. A major component of this horizon, CaO is strongly associated with Sr and

Nd, suggesting that these trace elements are scavenged by this oxide. In this horizon, Si_2O and Al_2O_3 have a strong association and both oxides are strongly associated with trace elements Rb and Zr.

Within the saprolith, Fe_2O_3 exhibits strong associations with trace elements which include Sr, Co, Zn, and V. Manganese oxides are strongly correlated with Ba, Co, Nd, and Pb. The association between the iron and manganese oxides with all these trace elements suggest that during weathering of the bedrock, the trace elements are incorporated into secondary minerals such as goethite and hematite. The oxides of aluminium and silica show a strong association with Rb and Sr, respectively, with Si_2O also showing a weak but statistically significant correlation with Rb.

4.6.4 Interpretation of major element associations using bivariate plots

Bivariate plots of the major elements in Figure 4.11 & 4.12 below show that aeolian sand samples are characterised by lower concentrations of CaO, MgO, and to a certain extent, TiO_2; while SiO_2, Fe_2O_3, LOI, and Al_2O_3 concentrations are generally high. The aeolian sand horizon is also characterised by higher P_2O_5 concentrations relative to other horizons.

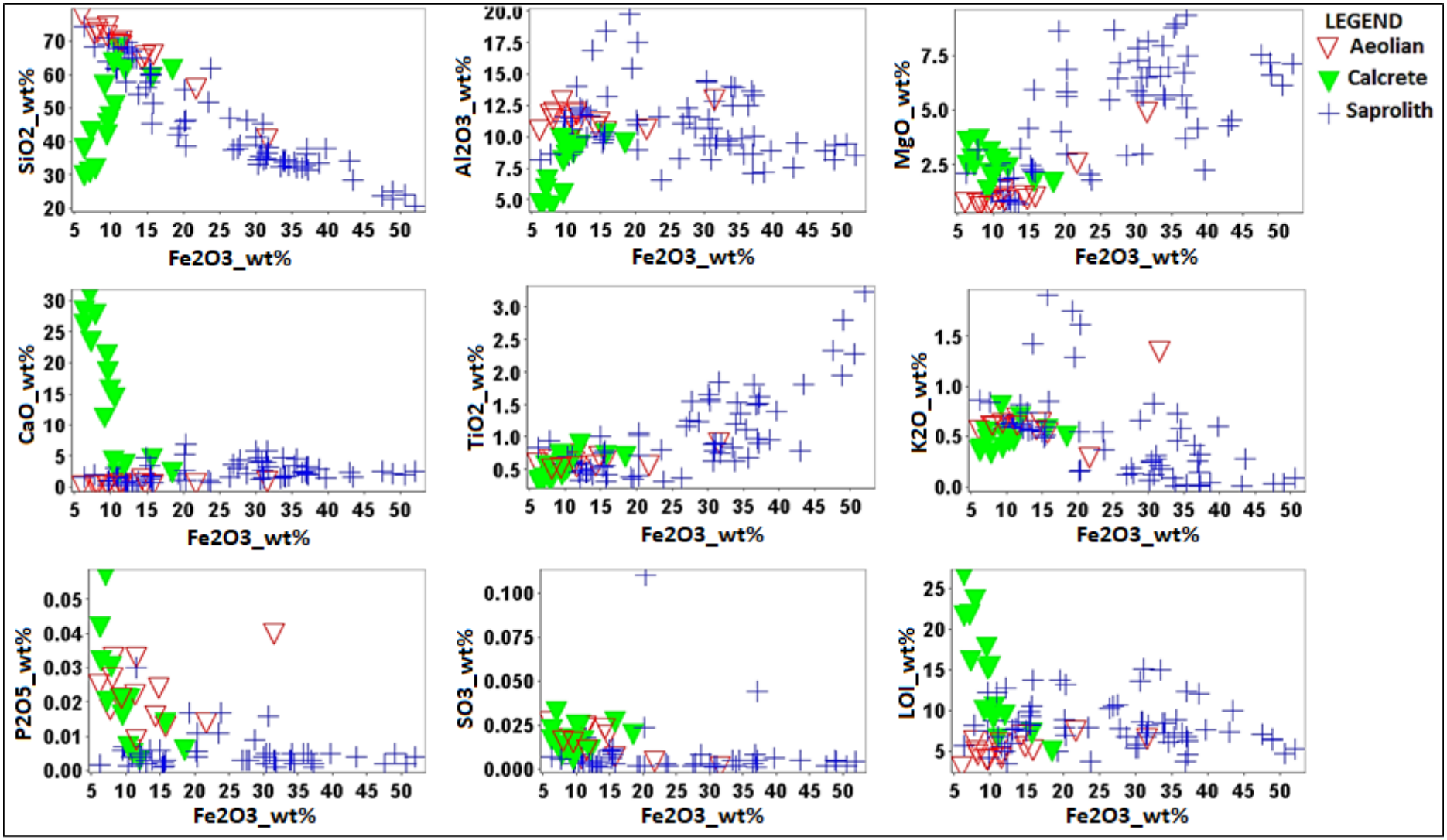

Figure 4.11: A plot showing the relationship between iron oxide and various major elements.

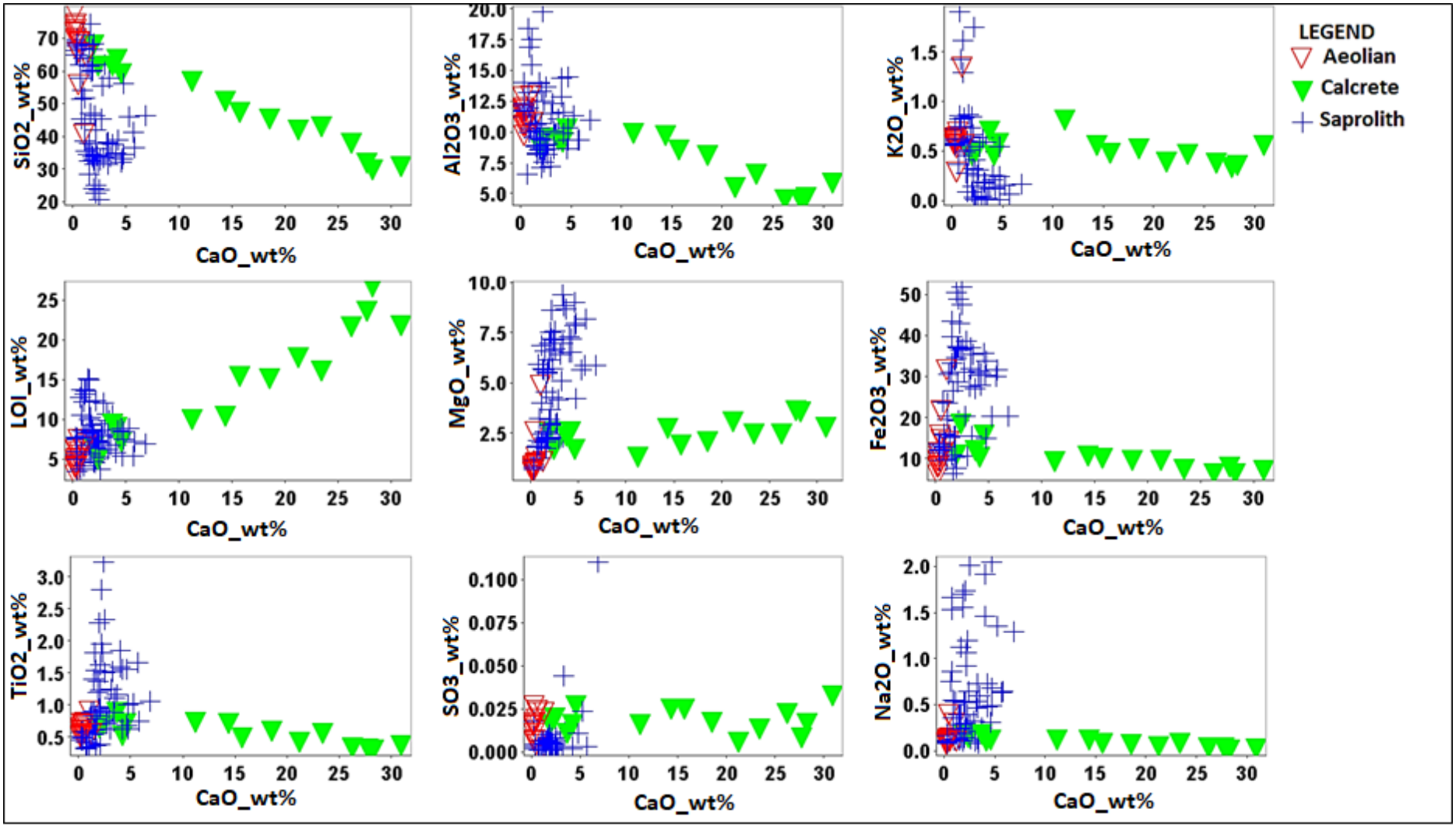

Figure 4.12: A bivariate plot showing the relationship between calcium oxide and other major oxides.

Within the calcrete horizon, there are two distinct groups. The first group is characterised by much higher LOI and corresponding higher CaO concentrations >10wt%, and up to 30 wt.% as shown in Figure 4.11. However, the geomean concentration within the entire horizon is slightly lower (11.1 wt.%), especially considering the standard mean concentrations of calcretes outlined by Anand & Paine, 2002. This group of samples is also characterised by a slightly higher P_2O_5, MgO, and Al_2O_3 concentrations, while the Fe_2O_3 concentrations are lower.

The second group of samples is characterised by low CaO concentrations (<5 wt.%). The entire calcrete horizon is mostly characterised by high Fe_2O_3, Al_2O_3, and SiO_2 concentrations. There is a large variation in Fe_2O_3 concentrations in the saprolith, with some samples having concentrations as low as 5wt.%; while some samples have concentrations up to >50wt.%. The saprolith horizon is characterised by relatively high concentrations of Al_2O_3, MgO, LOI, and TiO_2. A display of the borehole data using downhole plots is shown in Appendices 27-30**.**

4.7 WEATHERING TRENDS AND INDICES

The ratios of mobile elements to less mobile elements can be used to determine the degree of weathering. Ratios of both K and Mg to Al were plotted to show how weathering has influenced the geochemistry of regolith in Sirius, as shown in Figure 4.13. The concentrations of Mg are higher relative to Al in all horizons, as shown by the elevated Mg/Al ratios. Aeolian sand generally has the lowest K/Al and Mg/Al ratios, but the ratios of these elements increase within the calcrete and saprolith horizons; with some saprolith samples having very high

ratios. In general, all samples are also characterised by low K, as evidenced by the relatively low K/Al ratios in all samples. Based on the regolith classification diagram by McQueen (2006), most of the calcrete and saprolith samples have Mg/Al and K/Al ratios characteristic of weathering towards smectite/chlorite/dolomite. This gives an indication that the regolith carbonates in Sirius are also dolomitic due to the high magnesium relative to aluminium.

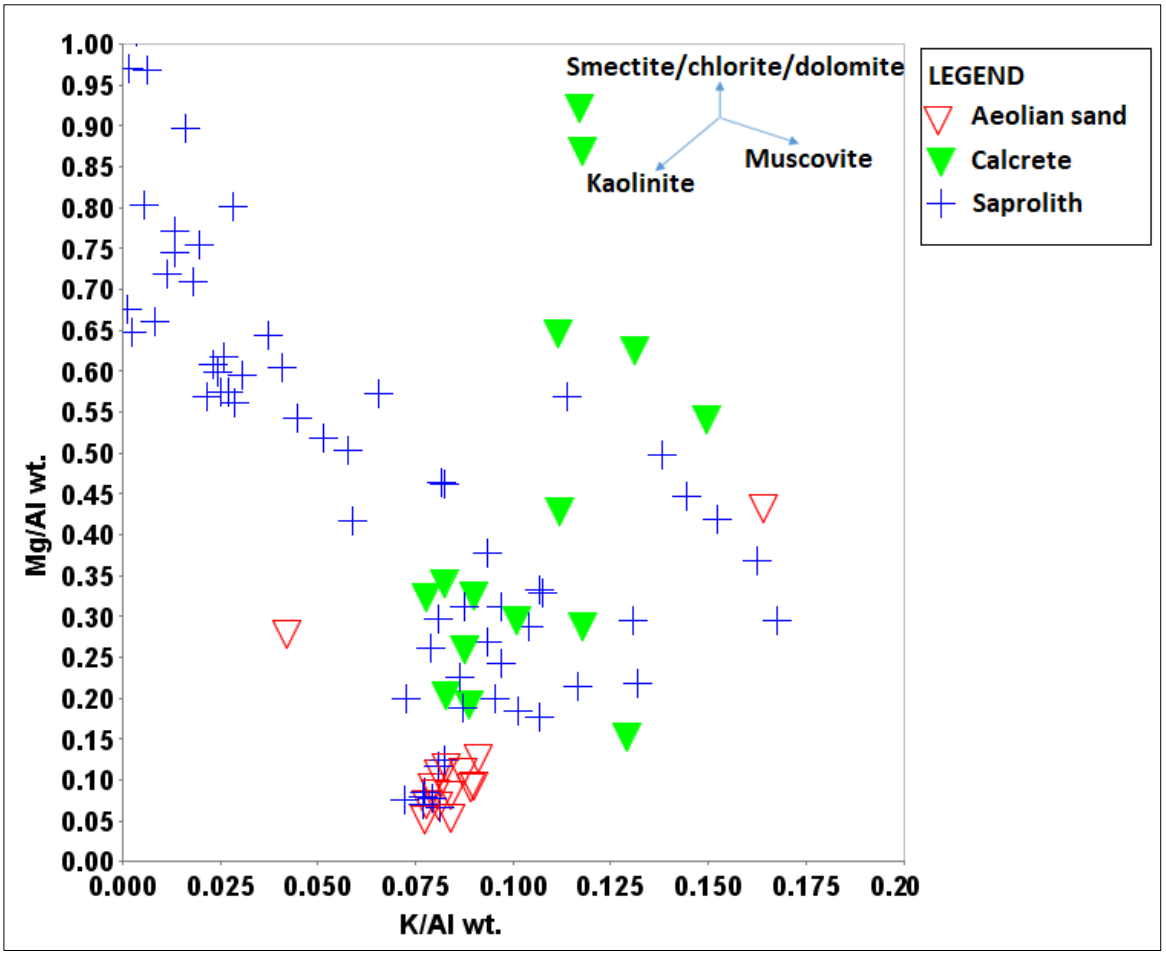

Figure 4.13: A classification of regolith samples using McQueen's classification of regolith materials (adopted from McQueen, 2006).

The geomean data shown in Table 4.4 below indicates that there is a general fractionation of certain elements. The concentrations of the elements including Fe_2O_3, MgO, CaO, and Na_2O are highest in the lower saprolith and decrease upwards as a result of progressive weathering

which has led to the loss of these relatively mobile elements in the regolith profile. The concentration of SiO_2 shows an opposite trend, being highest in the aeolian sand and progressively decreasing downhole to its lowest concentration in the lower saprolith. The upward increase in SiO_2 concentrations can be attributed to the gradual loss of some more mobile components of the regolith thereby increasing the proportion of this oxide relative to other elements (Anand & Paine, 2002). The lower parts of each of the three horizons seem to have high concentrations of the oxides of Fe and Al relative to the upper parts suggesting the accumulation of Fe and Al oxides in these zones. In addition, the trace elements Co and Zn are highly concentrated in these areas of ferruginisation, suggesting that they are hosted by these oxides.

Table 4.4:: Geomean concentrations of various elements in the different regolith horizons found in the Sirius Prospect.

	Geomean						
	Upper aeolian	**Lower aeolian**	**Upper calcrete**	**Lower calcrete**	**Upper saprolith**	**Mid saprolith**	**Lower saprolith**
Major oxides and LOI (wt.%)							
SiO2	61,82	63,29	50,49	56,65	50,78	40,48	36,8
Al2O3	10,3	12,15	7,96	8,97	10,51	10,96	11,21
Fe2O3	10,44	12,36	10,98	15,01	18,4	24,92	27,43
MgO	1,14	1,09	2,23	2,18	2,36	4,72	5,74
CaO	0,91	0,3	6,14	1,78	1,42	2,26	2,25
Na2O	0,1	0,11	0,07	0,14	0,21	0,45	0,73
K2O	0,57	0,71	0,47	0,38	0,4	0,26	0,21
TiO2	0,59	0,63	0,56	0,69	0,8	0,91	0,9
P2O5	0,03	0,02	0,01	0,005	0,004	0,004	0,004
SO3	0,02	0,007	0,01	0,06	0,005	0,003	0,006
LOL	6,42	5,27	11,31	7,53	7,48	7,93	7,96
Trace elements (ppm)							
Ba	127,15	172,34	177,49	213	279,72	296,85	249,33
Ce	43,62	101,5	40,02	53,79	60,36	56,76	54,35
Co	21,37	45,39	30,14	39,74	68,74	117,25	133,59
Nd	6,63	3,46			5,14	5,99	8,66
Pb	12,93	14,39	13,57	13,21	14,73	14	14,91
Rb	30,43	34,31	24,73	22,93	24,78	19,13	16,15
Sr	32,46	25,08	66,43	51,74	64,43	105,89	118,38
V	702,41	706,55	777,98	826,34	960,44	1249,29	1380,34
Y	10,42	13,12	10,81	10,68	11,68	12,14	9,51
Zn	16,98	21,4	13,61	19,85	32,04	67	83,04
Zr	183,5	181,06	166,28	153,22	113,47	41,87	21,34

The intensity of weathering in the Sirius Prospect can be described as incipient to intermediate. This deduction is based on CIA values, which range from as low as 44.8 to about 92 (Appendix 4). The lower CIA values suggest an occurrence of primary minerals, more stable secondary minerals such as kaolinite, secondary silica, as well as quartz which tends to retain the mobile elements that would otherwise be leached from these horizons (McQueen & Scott, 2008). The high CIA values of about 92 indicate the presence of some clay minerals. The variability in the CIA values shows the heterogeneity of weathering intensity across the area, as suggested by McQueen & Scott, 2008. In general, the degree of weathering increases upwards in the saprolith horizon as indicated by the lower CIA values at the base of the boreholes and their increase upwards in the profile. Thus the lower parts of the saprolith are less weathered relative to the upper parts.

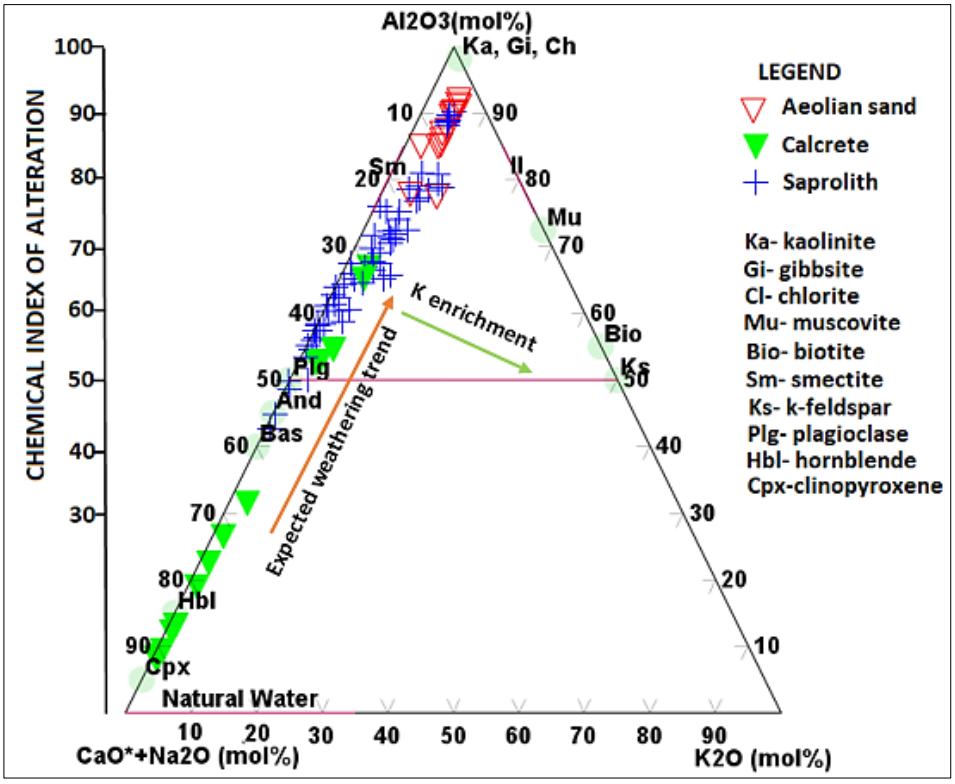

Figure 4.14: Weathering trend in the Sirius deposit regolith samples and the chemical index of alteration of the in-situ regolith, adopted from (Nesbitt & Young, 1982).

An ICV calculated on this data reinforces this deduction because there are a few samples that have ICV values that are as low as 0.7, which suggests slightly intense weathering while values greater than one are mostly observed, indicating the abundance of primary minerals. The intensity of weathering of the saprolith samples (Figure 4.14 & Appendix 4), indicating that most of the samples have CIA values of between 50 and 80, while a few samples are on the extreme ends. In general, all the samples are characterised by K_2O depletion, while Al_2O_3 and CaO vary from sample to sample, with calcrete samples plotting towards the CaO apex of the triangle.

Based on the A-C-K diagram above (Figure 4.14), most of the samples are characterised by CIA values greater than approximately 63. As suggested by Lambe, 1996 (as cited in Regassa et al., 2014), such high CIA values indicate significant degrees of weathering (more than 50% of the primary minerals). According to Nesbitt & Wilson, 1992; samples plotting towards the Al_2O_3 apex indicate significant weathering and a corresponding loss of Ca, K, and Na. The geochemical data plotted on an A-CK-FM diagram shown in Figure 4.15 below also indicates that the soil samples are derived from a mafic parent rock as most samples plot towards the FeO + MgO* apex of the triangle. A cluster of samples plots towards the bottom left side of the diagram and this group represents samples that have a high Ca concentration, low Al and low to moderately low FeO + MgO*.

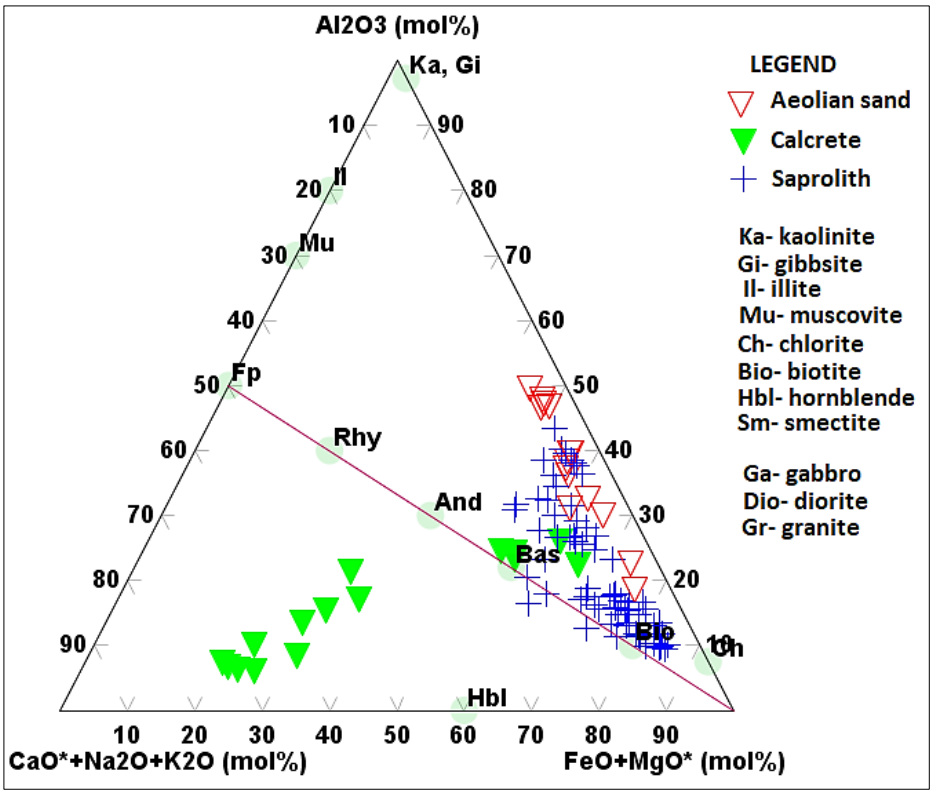

Figure 4.15: Samples from Sirius plotted on an A-CNK-FM plot to determine the possible mineral composition and the maturity of the regolith in the area.

4.7.1 Determining the protolith

Based on the concentrations of Ti and Zr, which are more resistant to weathering and tend to be retained even after extensive weathering, the parent rock of the samples was determined, as shown in Figure 4.16. Most of the saprolith samples are characterised by high Ti concentrations and low Zr concentrations, characteristic of mafic rocks. However, some of the saprolith samples have slightly higher Zr and lower Ti concentrations characteristic of intermediate rocks. Most of the calcrete and aeolian sand samples are also characterised by Zr and Ti concentrations characteristic of intermediate rocks.

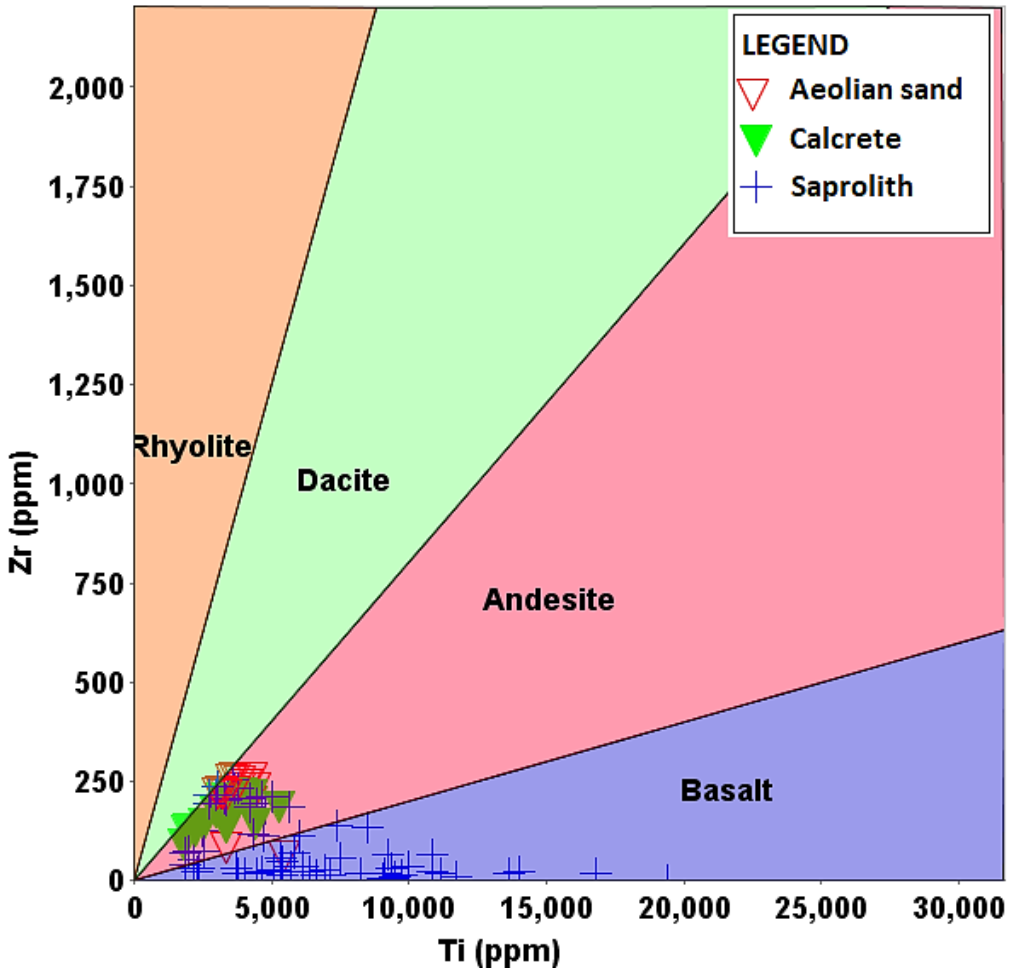

Figure 4.16: Classification of samples from Sirius according to parent rock from which they were derived using the relatively immobile Zr and Ti.

4.8 SUMMARY OF FINDINGS

The main findings on the Sirius Prospect can be summarised as follows:

- The bulk concentration of aeolian sand samples in the Sirius Prospect are Si, Al, Fe, and to a lesser extent Mg oxides. The element associations within the aeolian sand include; (a) LOI, Na_2O, Pb, Ce, and Nd; (b) Fe_2O_3, MgO, CaO, Sr, V, Zn, Co, Ba, and Y; (c) Al_2O_3, TiO_2, P_2O_5, K_2O; (d) SiO_2, SO_3, Zr, and Rb.
- The bulk concentration of the calcrete samples is comprised of the oxides of Si, Al, Fe, and to a lesser extent Mg and Ca. Within the calcrete horizon the associations among

the elements include; (a) MgO, P_2O_5, CaO, LOI, SO_3, and Sr; (b) Fe_2O_3, TiO_2, Na_2O, Zn, Co, Ba, Ce, and Pb; (c) K_2O, Rb, Al_2O_3, SiO_2, and Zr.

- The saprolith horizon is dominated by elements including Si, Fe, Al, and to a certain extent, Ca and Mg. Elemental associations within the saprolith include three clusters; (a) LOI, MnO, P_2O5, Co, Ce, Nd, Pb, Ba, and Y; (b) Fe_2O_3, MgO, Na_2O, CaO, TiO_2, SO_3, Zn, Sr, and V; (c) Al_2O_3, SiO_2, K_2O, Zr, and Rb.
- There is a fractionation of MgO, Fe_2O_3, Na_2O, TiO_2, and Co, due to the progressive loss of the elements upwards. The fractionation of SiO_2, K_2O, and Zr is opposite, showing a general increase in concentration upwards in the regolith profile.
- In the Sirius prospect, there are significant positive correlations between Fe-Mn oxides and Ba, Co, Nd, Pb, Sr, V, and Zn, suggesting that the enrichment of the trace elements is dependent on the availability of these oxides.
- The weathering intensity in the Sirius prospect can be classified as incipient – moderate. The calcrete is derived from the weathering of the Ca-rich, mafic parent rock.

4.9 MAJOR DIFFERENCES IN ELEMENT CHEMISTRY AROUND THE SERPENS NORTH AND SIRIUS PROSPECTS

The major difference between the geochemistry of the Serpens North and Sirius prospects is that there is a greater fractionation in elements in Sirius compared to Serpens North. The only elements that show any significant fractionation in Serpens North Prospect are MgO and Al_2O_3 which show a progressive loss upwards, while SiO_2 and K_2O show an upward enrichment. In the Sirius Prospect, there is a fractionation of MgO, Fe_2O_3, Na_2O, TiO_2, and Co, due to the progressive loss of the elements upwards, while SiO_2, K_2O, and Zr show an upward

enrichment. In addition, although geochemical data from Serpens North reveals that the bedrock is Ca and Mg-rich, there is no development of the calcrete horizon in Serpens North while in the Sirius prospect, there is a well-developed calcrete horizon. Based on Pearson's correlation matrix (Appendices 6, 7, and 8), there are no significant associations between the major soil phases (Fe and Mn oxides) and trace elements, which implies that the enrichment of trace elements is not controlled by these soil phases in the Serpens North prospect. For instance, Fe_2O_3 only has a weak positive correlation with Ni (0.38), while MnO shows a weak positive correlation with Sr and Zn (0.38 and 0.37 respectively). On the contrary, in the Sirius Prospect, there are significant positive correlations between Fe-Mn oxides and Ba, Co, Nd, Pb, Sr, V, and Zn, suggesting that the enrichment of the trace elements is dependent on the availability of these oxides and possibly, a bedrock that is enriched in these trace elements.

4.10 DISTRIBUTION OF ORE AND ORE-RELATED TRACE ELEMENTS

Hydroxylamine hydrochloride (HH) was used to enhance the geochemical signatures in the Serpens North Prospect. In this section, the secondary dispersion of Pt, Pd, Au and the pathfinder elements (Cu, Co, Ni, As, and Hg) based on data obtained from HH selective leach technique will be analysed.

4.10.1 Summary of trace elements in regolith and regolith units in Serpens North Prospect.

The summary statistical data from Serpens North is shown in Table 4.5 below. The geomean concentration of adsorbed Fe is lowest within the saprolith horizon. A significant increase in

concentration is observed in the stone line horizon. There is a slight decrease in Fe concentrations in the aeolian sand, as evidenced by the lower geomean concentration. Other trace elements that show a similar trend to Au are Cu, Co, and Ni. Gold and Hg exhibit similar trends, with their geomean concentrations being lowest in the saprolith horizon. The two

race elements attain their highest concentration within the stone-line horizon; however, concentrations decrease again in the aeolian sand horizon. The geometric mean concentrations of Mn and arsenic are highest within the saprolith horizon and decrease upwards, indicating a loss of these elements upwards. Platinum and Pd exhibit similar trends, with geomean concentrations that show to be higher within the saprolith. The geomean concentrations of the two elements is lowest within the stone-line horizon but increases again in the aeolian sand. Based on Pearson's correlation (Appendices 55-58), there are no statistically significant, strong, positive relationships between most adsorbed trace elements and the oxides of Fe, Mn, and Al, which suggests that the enrichment of trace elements is not dependent on the availability of these soil phases (Fe, Mn, and Al oxides) in regolith. There are, however weak, positive correlations between Fe_2O_3 and Au (0.224) and between MnO and Pt (0.308), within the saprolith. This suggests that the enrichment of adsorbed trace elements is possibly controlled by other soil phases, possibly carbonates, secondary sulphides and in upper horizons, organic matter.

4.10.2 Summary of trace elements in regolith and regolith units in Sirius Prospect

The summary statistics for the Sirius Prospect data are given in Table 4.6. In Sirius, the geomean value of adsorbed Fe is lowest within the saprolith. However, Mn has a geometric

mean that is highest within this horizon. Other trace elements that exhibit higher concentrations in the horizon are Cu, Co, and Pt.

The geomean concentration value of Fe increases significantly within the calcrete horizon, accompanied by a slight increase in the geomean concentrations of arsenic and Pd. However, the geomean of the other trace elements including Cu, Co, Ni, Pt, and Au significantly decreased in the horizon suggesting a dilution of element concentrations in the horizon resulting in attenuation of geochemical signatures these trace elements.

Within the aeolian sand, lower concentrations of Fe along with the trace elements Pt, Au, Ni, and As, compared to the other two horizons were observed, suggesting that the underlying calcrete horizon hinders the vertical dispersion of these trace elements. Manganese, Cu, and Pd concentrations are slightly elevated compared to the underlying calcrete horizons. The presence of a carbonate-rich layer increases the pH of water as it migrates upward by capillary action and results in the precipitation of most trace elements. However, the dispersion of palladium is not hindered by the alkalinity of the transporting medium because according to Hattori (2004) & Cook et al. (1992); Pd is relatively mobile even under alkaline conditions. The higher Cu concentrations within the aeolian sand in Sirius are however unusual, because the carbonate-rich horizon buffers the transporting medium (water) which is expected to result in the precipitation of Cu, an element which is only soluble under acidic conditions (pH 5-6) (Reeder et al., 2006; McQueen, 2008).

Table 4.5: Statistical summary of selected trace elements in the different regolith horizons from Serpens North, based on HH data (in pbb).

	Range				Geomean				Std. Dev			
Element	All	Aeolian	Stone line	Saprolith	All	Aeolian	Stone line	Saprolith	All	Aeolian	Stone line	Saprolith
As	22,86	9,53	10,97	22,86	1,53	1,28	1,50	1,58	3,28	1,67	2,22	3,58
Fe	328,83	306,67	294,19	328,83	35,27	42,40	45,90	33,09	85,94	95,29	76,78	85,08
Mn	147,40	119,30	105,70	147,40	138,82	135,20	136,40	139,72	28,45	32,48	32,10	27,34
Cu	117,50	95,90	77,10	117,50	7,88	12,80	10,40	7,02	22,20	28,86	18,83	20,85
Co	270,20	266,40	242,50	250,40	40,42	44,00	44,36	39,40	60,11	69,94	57,80	58,66
Ni	303,88	303,41	290,95	277,78	13,21	15,50	18,19	12,36	40,82	69,53	55,59	29,70
Pd	103,40	69,60	56,45	103,40	26,83	27,30	20,37	27,59	19,88	18,54	17,71	20,32
Au	37,27	12,43	10,93	37,27	1,42	1,58	1,83	1,35	2,98	2,38	3,34	3,02
Pt	313,80	307,99	22,89	313,80	4,48	3,46	2,72	4,91	48,46	57,30	5,84	49,62
Hg	64,26	51,62	50,14	64,26	7,89	7,39	8,69	7,90	11,37	11,44	10,20	11,54

Table 4.6: Statistical summary of selected trace elements in the different regolith horizons found in Sirius, based on HH data (in ppb).

	Range				Geomean				Std Dev			
	All	Aeolian	Calcrete	Saprolith	All	Aeolian	Calcrete	Saprolith	All	Aeolian	Calcrete	Saprolith
As	27,5	3,4	26,80	6,30	2,3	1,7	2,9	2,3	2,8	0,9	5,4	1,0
Fe	325,1	311,5	317,60	325,10	37,9	28,2	72,1	32,8	127,3	119,6	111,7	133,0
Mn	121,2	102,8	109,50	121,20	104,7	90,5	84,5	116,7	43,4	37,7	41,4	42,3
Cu	116,2	78,3	81,60	116,20	22,1	22,4	15,9	24,8	31,7	24,5	26,5	34,8
Co	282,5	129,2	134,30	274,80	36,8	27,9	17	51,1	53,8	42,7	30,8	58,5
Ni	32,6	17,8	15,70	32,60	5,4	4,1	6,3	5,5	5,4	5,9	4,5	5,7
Pd	324,3	323,6	76,70	82,20	39,0	46,3	41,7	36,4	35,0	75,9	20,6	18,6
Au	41,0	2,6	40,99	20,62	1,5	1,2	1,3	1,7	4,8	0,7	8,5	3,4
Pt	308,5	87,1	81,80	308,20	8,0	6,6	7,9	8,6	38,0	23,2	17,4	46,7

Based on Pearson's correlation (Appendices 59-62), there is a statistically significant, weak correlation between Al_2O_3 and adsorbed elements including Mn, Cu, and Co (0.33, 0.303, and 0.331 respectively), within the saprolith horizon. In this horizon, Fe_2O_3 has a positive correlation with adsorbed Mn, while MnO has a strong, positive correlation with arsenic (0.64).

The calcrete horizon is characterised by strong, positive correlations between Fe_2O_3 and Au (0.716), and between CaO and Pt (0.7). Within the aeolian sand horizon, Fe_2O_3 is strongly correlated with arsenic (0.577). Most trace elements do not seem to be associated with the major soil phases in the Sirius Prospect.

4.10.3 Variation patterns of trace elements- box plots

The variability of trace elements in Serpens North (Figure 4.17) is greatest for elements such as Co and Hg. Most of the elements are characterised by outliers and extreme outliers, which is indicative of anomalous concentrations of the elements across the regolith profile.

Within the aeolian sand horizon, elements that show significantly high outliers are Co, Ni, Au, Fe, and Hg. The stone-line horizon is not characterised by any significant outliers in the data. In the saprolith, the elements that show extreme outliers are Co, Cu, Pt, Ni, As, Au, Hg, and Fe.

The distribution of trace elements in Sirius is shown in Figure 4.18 below. There is significant variability in concentrations of most trace elements (Fe, Mn, Cu, Co, Pd, and Ni). The mean concentrations of Fe and Mn seem to have opposite trends. The mean concentration of Fe is highest within the calcrete horizon and decreases significantly in the aeolian sand and saprolith. Manganese mean concentrations, on the other hand, are lowest in the calcrete horizon and are slightly higher in the saprolith and aeolian sand. The trace element data for Pt, Au, and arsenic shows less variability, although Pt and Au consist of some extreme outliers.

Within the saprolith, samples that are enriched along with Mn are Co and Ni. In the calcrete horizon, Ni seems to be associated with Fe. However, there are no significant trends visible in the different horizons as the different horizons do not show significant differences in element concentrations.

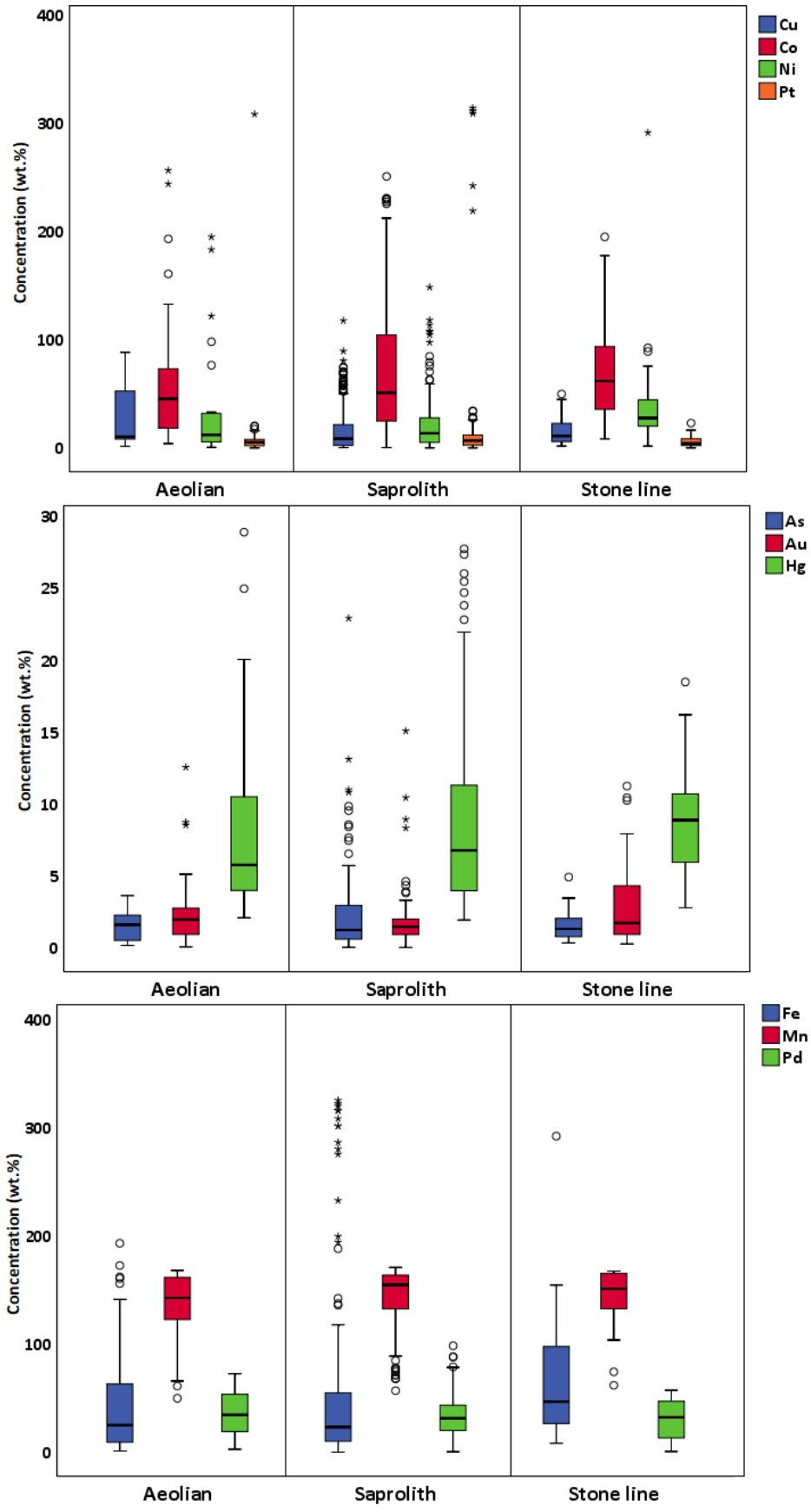

Figure 4.17: Distribution of trace elements in aeolian sand, stone-line, and saprolith, in the Serpens North Prospect, based on HH data.

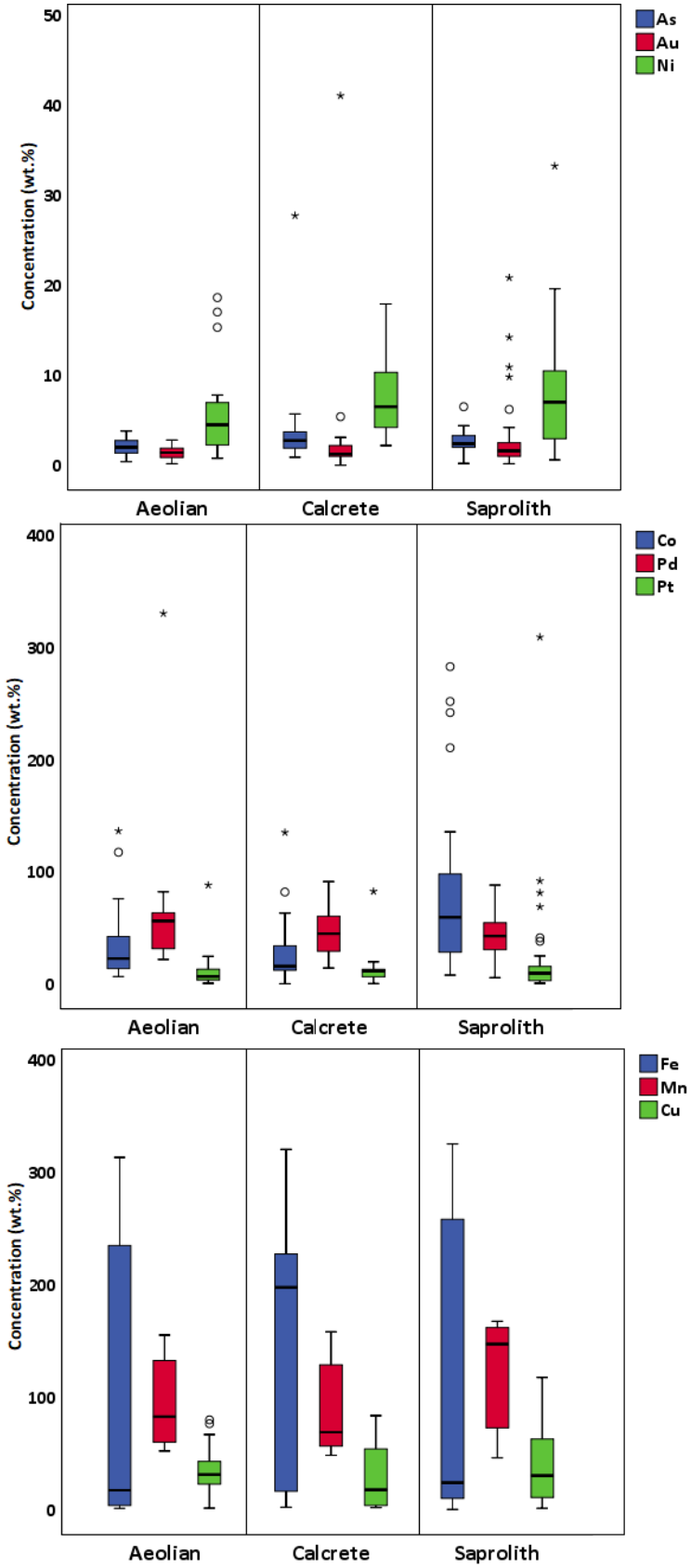

Figure 4.18: Distribution of trace elements in the aeolian sand, calcrete, and saprolith in the Sirius Prospect, based on HH data.

4.10.4 Trace elements associations using PCA plots in the Serpens North Prospect

The overall data shows three distinct groups of element associations (Figure 4.19a). While data from the aeolian sand horizon shows the same number of clusters as the overall data, the elements contained in each cluster vary slightly (Figure 4.19b). For example, one of the clusters of elements includes CaO, Al_2O_3, MnO, Au, and Pt. Based on Pearson's correlation, there is a statistically significant, strong correlation between MnO and Pt, however the oxide's correlation with Au is statistically insignificant. The association of Pt and MnO (one of the major phases that adsorbs trace elements), as well as CaO and Al_2O_3, suggests that these oxides adsorb Pt and Au. Also, there is an association between elements including; Fe_2O_3, Co, Cu, Ni, Fe, and Mn. The association between Fe_2O_3 and the trace elements suggests that in this horizon, the oxides of Fe are responsible for adsorbing the trace elements. According to Pearson's correlation (P-test), MnO also has statistically significant, strong positive correlations with Co, Cu, Ni, Fe and Fe_2O_3, suggesting that both Fe_2O_3 and MnO play a role in the adsorption of the trace elements (also shown by the proximity of MnO to these elements although they are in different quadrants). The other cluster of elements includes Pd, Hg, and As, which suggests that they were adsorbed by a different phase, possibly organic matter since this is the uppermost horizon. According to Pearson's correlation the association between these elements is not statistically significant.

Within the stone-line horizon, there is a different association of elements (Figure 4.19c). The first group of elements that form a cluster includes; Ni, Cu, Co, Pt, Fe, and MnO. In this horizon, the trace elements are dependent on the availability of MnO. However, the only

statistically significant, strong correlation is between MnO and both Co and Pt. The second cluster of elements includes Mn, Pd, and Hg, and Fe_2O_3, although according to the P-test, the correlations are not statistically significant. The oxides of calcium and aluminium, and Au form a cluster. Although Pearson's correlation suggests that there is a statistically significant, strong correlation between Au and Al_2O_3, there is no statistically significant correlation between MnO and Au. Thus, in this horizon, the oxide responsible for the adsorption of Au is mainly Al_2O_3.

The saprolith horizon is also characterised by one distinct cluster of elements (Figure 4.19d). The cluster is comprised of Co, Cu, Ni, Fe, Mn and the oxides of Fe and Mn. This association coincides with Pearson's correlation in which the P-test suggests that the correlations of these elements are statistically significant, although the correlations are weak. Therefore, the adsorption of Co, Cu, Ni, Fe, Mn in the saprolith is controlled by the presence of Fe and Mn oxides. The remaining elements do not form a distinct group and based on Pearson's correlation, there are no significant correlations among any of the elements. Therefore, these elements are not found in association and their adsorption does not seem to be dependent on Fe and Mn oxides.

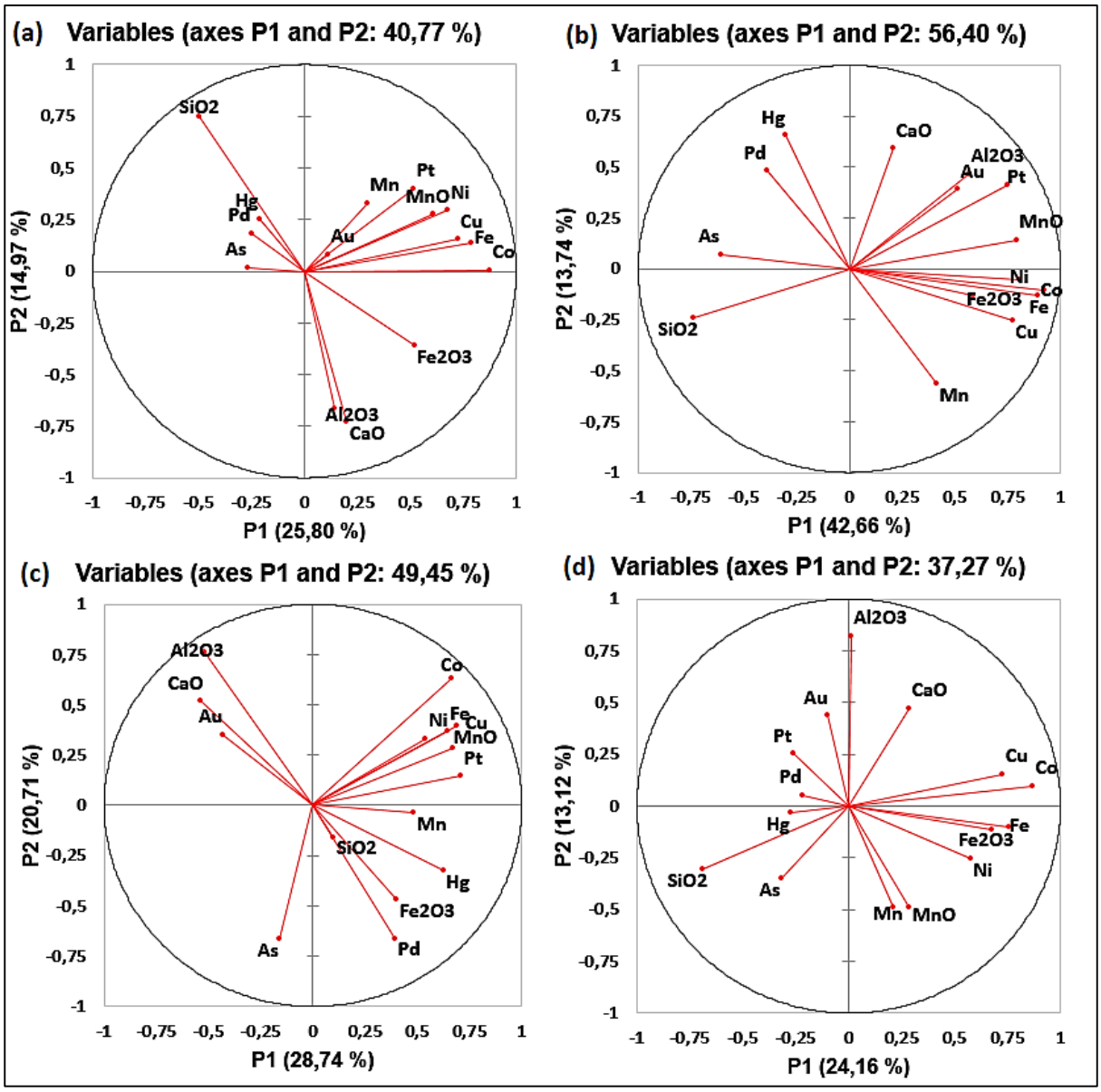

Figure 4.19: Trace element associations in different regolith horizons in Serpens North based on HH data; (a) all horizons, (b) aeolian sand, (c) stone-line, (d) saprolith.

In the Sirius prospect, there is an association between the elements Fe, Pt, and Al_2O_3 in the aeolian sand horizon. The association between Fe and Pt with Al_2O_3 suggests that the enrichment of the trace elements is dependent on the availability of Al_2O_3, as this is one of the soil phases that is responsible for scavenging trace elements. However, this soil phase has received less attention in studies compared to major soil phase Fe and Mn oxides that commonly adsorb trace elements. Manganese, Au, and Ni are closely associated within the

aeolian sand suggesting that the enrichment of the elements is likely to be unrelated to Fe and Mn oxides, but perhaps another phase, such as organic matter. In this horizon, the oxides of Ca and Fe are associated with Pd and arsenic, while SiO_2, Co, and Cu form a diametric relationship with these elements (Figure 4.20b). However, based on Pearson's correlation, there are no statistically significant correlations between all elements except between arsenic and Fe_2O_3; Pt and Co; as well as Ni and Mn.

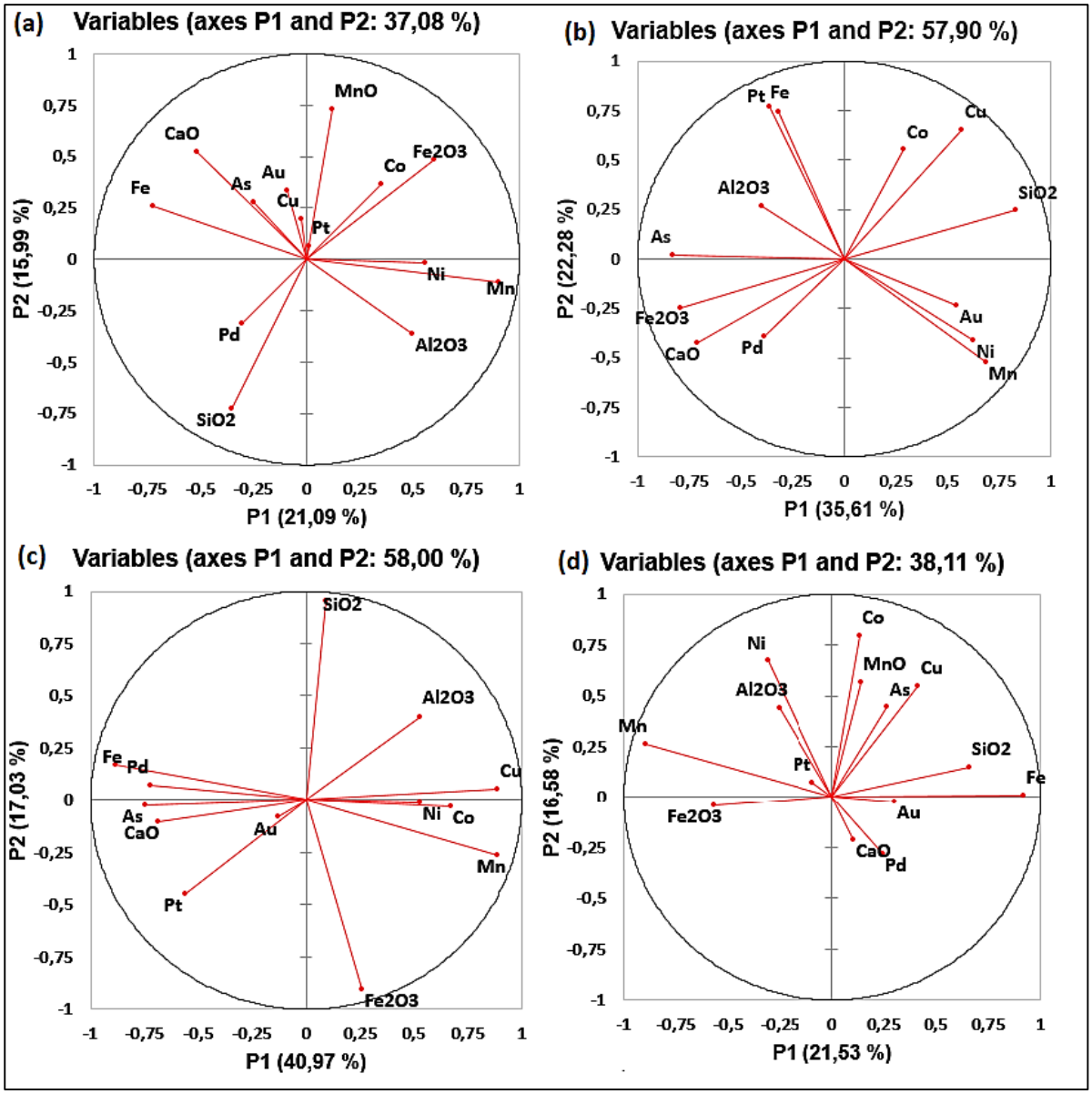

Figure 4.20: Trace element associations in different regolith horizons in Sirius based on HH data; (a) all horizons (b) aeolian sand, (c) calcrete, (d) saprolith.

Within the calcrete horizon, there is an association between the elements Fe, Pt, Pd, As, Au, and CaO (Figure 4.20c). There is a close relationship between Cu, Co, Ni, Mn, and Al_2O_3 within this horizon. However, according to Pearson's correlation, the only statistically significant, strong correlations are between Fe_2O_3 and Au, as well as between CaO and Pt. Therefore, in this horizon, Fe_2O_3 and CaO control the enrichment of Au and Pt respectively.

The saprolith horizon is characterised by three clusters of elements including; 1. As, Cu, Co, MnO, 2. Ni, Pt, Mn, Al_2O_3, and Fe_2O_3 3. CaO and Pd 4. SiO_2, Fe, Au (Figure 4.20d). In this horizon, the availability of Fe and Al oxides affects the enrichment or depletion of Pt and Ni. The enrichment or depletion of As, Cu and Co are influenced by the availability of MnO. Calcium oxides play a major role in the adsorption and enrichment of Pd, while SiO_2 seems to control the enrichment of Au and Fe.

4.10.5 Geochemical dispersion of trace elements in the Serpens North and Sirius Prospects

Chemical weathering, due to groundwater interaction with the bedrock results in the release of trace elements. In arid to semi-arid environments, where evaporation is relatively high meaning that groundwater levels drop significantly during dry seasons, trace elements released during chemical weathering are mobilised for example, by capillary action or electrochemical migration from the redox zone upwards (Hamilton, 2007). In general, semi-arid to arid environments receive minimal rainfall, and thus, the amount of downward leaching is also minimal. Mobile elements released through these processes are adsorbed to

Fe and Mn oxides, carbonates and organic materials (Hall, 1998). In this section, data obtained from hydroxylamine hydrochloride partial leach technique, which is used to selectively leach trace elements adsorbed to Fe and Mn oxides, will be interpreted.

In order to better understand the dispersion of elements, a statistical analysis was performed to determine the background and anomalous ranges for selected elements, as shown in Table 4.1. The anomalies are classified as “anomaly” and “strong anomaly”. Thereafter, cross-sections were generated using the statistical summaries to show trace element trends and better visualisation of the dispersion trains of the various trace elements. Some of the pathfinder elements of PGEs and Au, which include As, Cu, Co, and Ni and ore elements Pt, Pd, and Au were used to create the cross-sections.

Table 4.7: Estimation of background and anomalous values based on the statistical summaries in the Serpens North and Sirius.

Element	Background	Anomaly	Strong Anomaly
Serpens North Prospect			
As	0 - 6	6 - 9.2	9.2 - 23
Fe	0 - 161	161 - 247	247 - 329
Mn	23 - 170.3	170.3 - 171	*
Cu	0 - 40	40 - 62	62 - 118
Co	0 - 125	125 - 186	186 -271
Ni	0 - 45	45 - 109	109 - 304
Pd	0 - 54	54 - 74	74 - 104
Au	0 - 5	5 - 8	8 - 38
Pt	0 - 65	65 - 113	113 - 314
Hg	0 - 22.5	22.5 - 34	34 - 65
Sirius Prospect			
As	0 -3.6	3.6 - 4.7	4.7 - 7
Fe	0 - 240	240 - 326	*
Mn	40 - 157	157 - 168	*
Cu	0 - 69	69 - 100	100 - 118
Co	0 - 111	111 - 164	164 - 283
Ni	0 - 12.7	12.7 - 18.2	18.2 - 33.5
Pd	0 - 62.5	62.5 - 82	82 - 91
Au	0 - 4.5	4.5 - 12	12 - 41
Pt	0 - 40	40 - 85	85 - 309

4.10.5.1 Geochemical dispersion of pathfinder elements (As, Cu, Co, Ni) in Serpens North Prospect

Arsenic (As) is a chalcophile element and is mostly partitioned into various sulphoarsenide minerals including arsenopyrite (FeAsS), realgar (AsS) and orpiment (As_2S_3) (Reeder, et al., 2006). Additionally, it occurs as an accessory element in other sulphide minerals such as galena, sphalerite and pyrite (Reeder, et al., 2006). Weathering processes occurring in the weathering front result in the release of arsenic from the above-mentioned minerals. Thus, secondary dispersion and anomalous concentration of arsenic can be attributed to underlying sulphide mineralisation.

The cross-sections in Figure 4.21 below showing the dispersion of arsenic indicate that the concentrations of the element are mostly within the background range (0 -6ppm), in four traverses (B-B', D-D', E-E', F-F') across the mineralised zone. However, some areas are characterised by anomalous concentrations, as shown in Figure 4.21 below. The boreholes to the extreme southeast and northwest; (KP051, KP052, and KP089) and (KP075, KP082, and KP084) respectively show anomalous arsenic concentrations (6 - 9.2ppm), with some parts of the lower saprolith having strong anomalous values (KP051, KP075, and KP084) (>9.2ppm). Anomalous concentrations of arsenic are mainly within the saprolith horizon, while the aeolian sand and stone-line are mostly characterised by background concentrations except for borehole KP089, where the enrichment of the element extends into these two horizons. The depletion of arsenic within the upper horizons may be linked to the fact that, while the element can exist as a cation, it can also form oxyanions (Torres et al., 2017; Cameron et al., 2004). The negatively charged arsenic species tend to be less adsorbed, especially when pH increases and the surfaces of Fe and Mn oxides become negatively charged (Torres, et al.,

2017), and are subsequently lost. From the cross-sections, it is clear that arsenic signatures are more pronounced in the saprolith and attenuate in the upper horizons in some boreholes. However, in other boreholes, the element has been completely removed from the profile. In general, the boreholes drilled directly over mineralisation (KP058, KP063, KP067, KP079, and KP087), do not show any arsenic enrichment except in KP052. A few boreholes drilled on regolith proximal to mineralisation (KP075 and KP084), and distal to mineralisation (KP051, KP072, KP082, KP089) are characterised by arsenic enrichment, suggesting more pronounced lateral dispersion of the element rather than vertical dispersion.

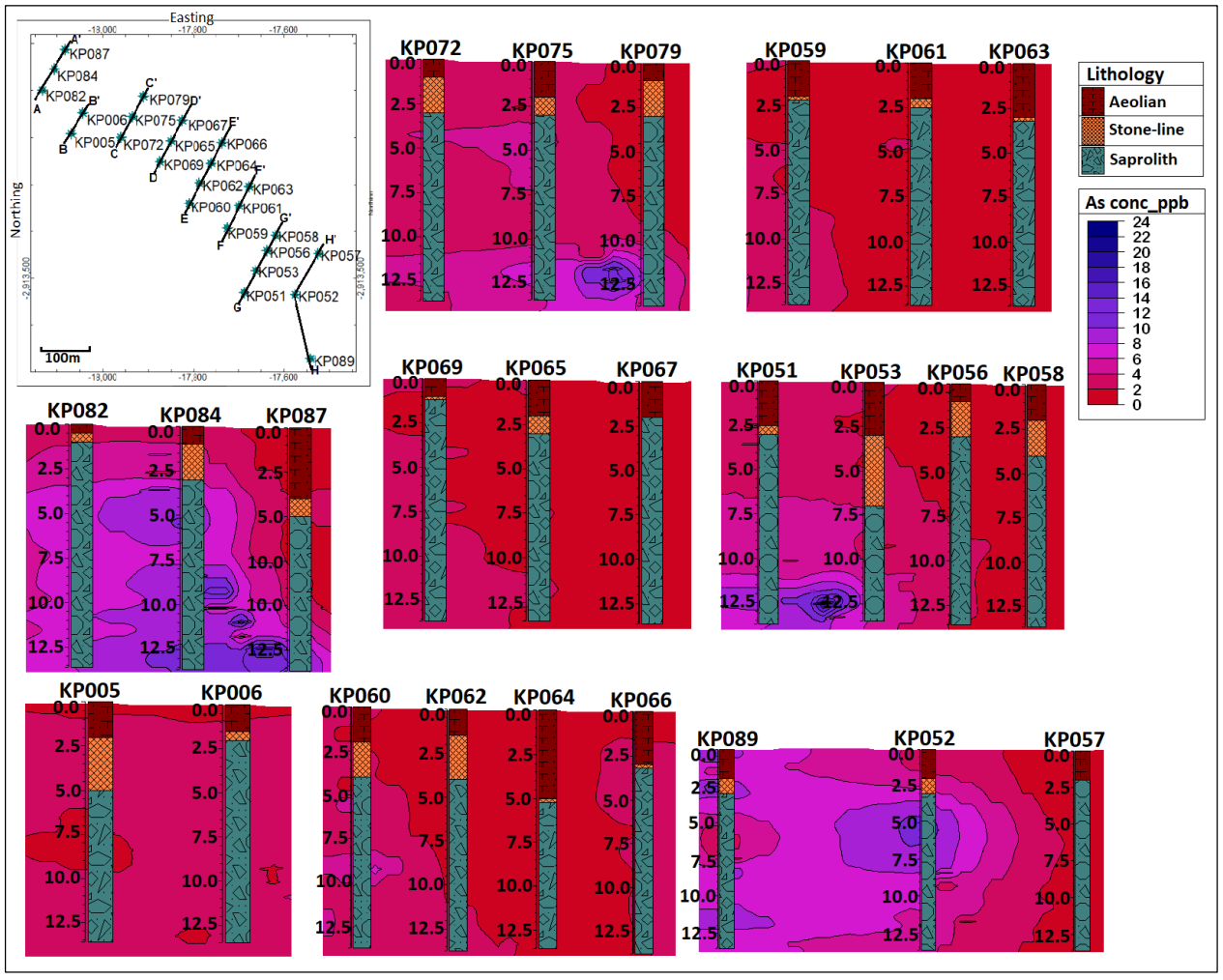

Figure 4.21: Geochemical distribution of arsenic across the Serpens North deposit and the corresponding horizons down the soil profile.

Copper (Cu) is a chalcophile element which occurs mainly in chalcopyrite ($CuFeS_2$), covellite (CuS) and malachite (Cu_2CO_3 $(OH)_2$), and minor concentrations occur in biotite, pyroxene, and amphibole, hence it is mainly found in mafic rocks rather than felsic rocks (Reeder, et al., 2006). This element is regarded as a pathfinder element for gold deposits, although it is most likely to indicate the presence of mafic rocks. Copper is relatively mobile under oxidising and acidic conditions (ph 5-6), and can easily be scavenged by the secondary mineral, goethite (Anand, 2001).

In the sections across the mineralised zone and shown in Figure 4.22, there are Cu anomalies (>40ppb) throughout the profile in KP063 and KP067(directly over mineralization) and KP066 (proximal to mineralisation). In KP058, KP057, and KP087, anomalous concentrations occur within the upper saprolith, stone-line, and lower aeolian sand. The profiles located within the mid-section of the study area have occasional anomalies. Additionally, the distribution of Cu shows secondary dispersion trains, with lower concentrations in the stone-lines and saprolith, and enrichment towards the aeolian sand, although some anomalies occasionally occur in the lower saprolith. In general, Cu shows more vertical dispersion from the orebody rather than lateral dispersion. Hence there are no wide dispersion halos.

Based on the calculated background concentrations (0 - 40ppb) for Serpens North, there are anomalous concentrations of Cu, but these concentrations are significantly lower than in other areas. For example, in a study conducted in Lac Sheen using hydroxylamine hydrochloride partial leach technique, the copper concentrations in the samples were found to be in the ppm ranges (<30 ppm - >71 ppm) (Cook et al., 1992). Similarly, studies conducted

in the Great Dyke, Zimbabwe, soil samples were found to be characterised by Cu concentrations greater than 470 ppm and up to 750ppm (Evans et al., 1994).

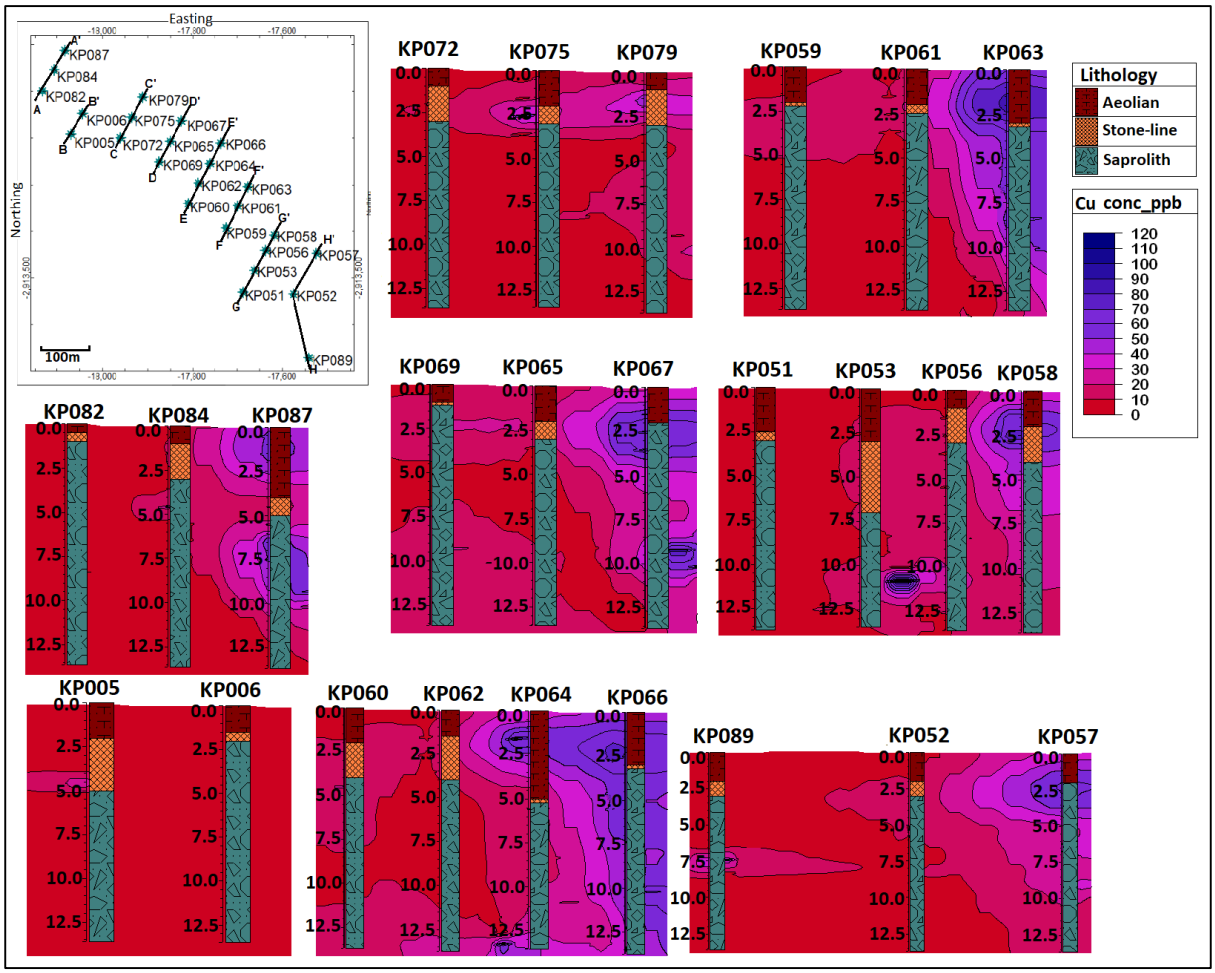

Figure 4.22: Copper distribution across the Serpens North deposit and the corresponding horizons down the soil profile.

Nickel (Ni) is usually concentrated in silicate and oxide minerals, notably olivine, pyroxenes, and some iron oxides because during fractionation it is partitioned into these early forming minerals by substituting for Fe^{2+}, thus Ni is enriched in mafic-ultramafic rocks and depleted in intermediate and felsic rocks (Reeder, et al., 2006). If, however, there are sufficiently high sulphur contents in the magma, the sulphide phase separates early, and in this case, Ni can be found associated with sulphide minerals (Reeder, et al., 2006). Additionally, Ni sulphides

can be formed by the reaction of pre-existing silicates with sulphides; with Ni forming separate phases or being incorporated into pyrrhotite largely and to lesser extent pyrite (Reeder, et al., 2006). Nickel is usually adsorbed by soil phases such as, Fe and Mn oxides, layered silicates, organic substances, and clays.

In a number of the boreholes, the Ni concentrations are highest mainly in the lower aeolian sand, stone-line and upper saprolith, while the lower saprolith is generally characterised by background concentrations (0 – 45ppb). In Serpens North; anomalous concentrations of Ni (> 45ppb) occur in boreholes KP052, KP058, KP063, KP087, directly over the ore body, KP064 in the proximity of the ore body and KP069, distal to the ore body as shown in Figure 4.23 below. Unlike Cu, Ni does not show extensive vertical dispersion. In addition, there is no significant lateral dispersion of the element. The concentrations of nickel in Serpens North suggest a depletion of the element in the parent rock. Similar to the observations made in the case of Cu, Ni concentrations are significantly lower than in other areas. In Lac Sheen, for example, the Ni concentrations range from 30 ppm - > 81 ppm (Cook et al., 1992).

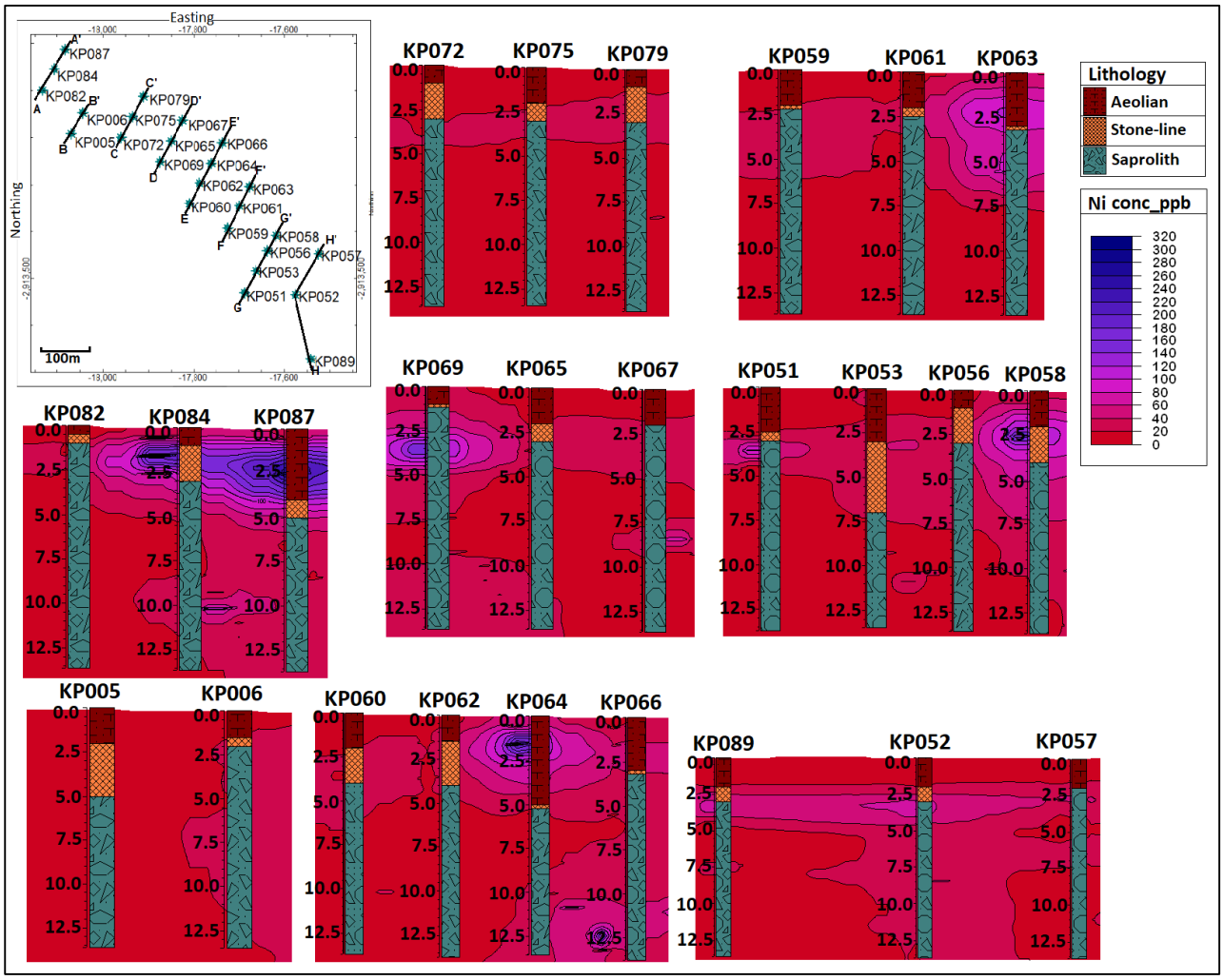

Figure 4.23: Spatial dispersion of nickel across the Serpens North deposit and the corresponding horizons down the soil profile.

Cobalt (Co), exhibits both chalcophile and siderophile properties and is mainly partitioned into sulphides and sulpharsenide phases forming rare minerals such as smaltite (Co, Ni) $As_{2-2.5}$, cobaltite (Cu, Fe) AsS, linnaeite (Co, Ni)$_3S_4$ and also occurring as an accessory element in olivine, pyroxenes, amphiboles, micas, garnets and sphalerite (Reeder, et al., 2006). Cobalt may also occur in iron sulphides, including pyrite, arsenopyrite, pyrrhotite and oxide mineral accessory minerals such as magnetite (Reeder, et al., 2006). In Serpens North, as shown in Figure 4.24, anomalous concentrations of cobalt (>125ppb) occur in boreholes that were drilled directly over the ore body (KP052, KP058, KP063, KP067, and KP079) and some boreholes that are proximal to the ore body (KP057, KP064, KP066). Strong anomalous Co

concentrations (> 186ppb) mainly occur within the lower aeolian sand and stone-line, while anomalies occur within the upper saprolith and occasionally the middle section of the saprolith. Compared to nickel, cobalt shows more significant dispersion trains in a few boreholes, although most boreholes are still characterised by background concentrations.

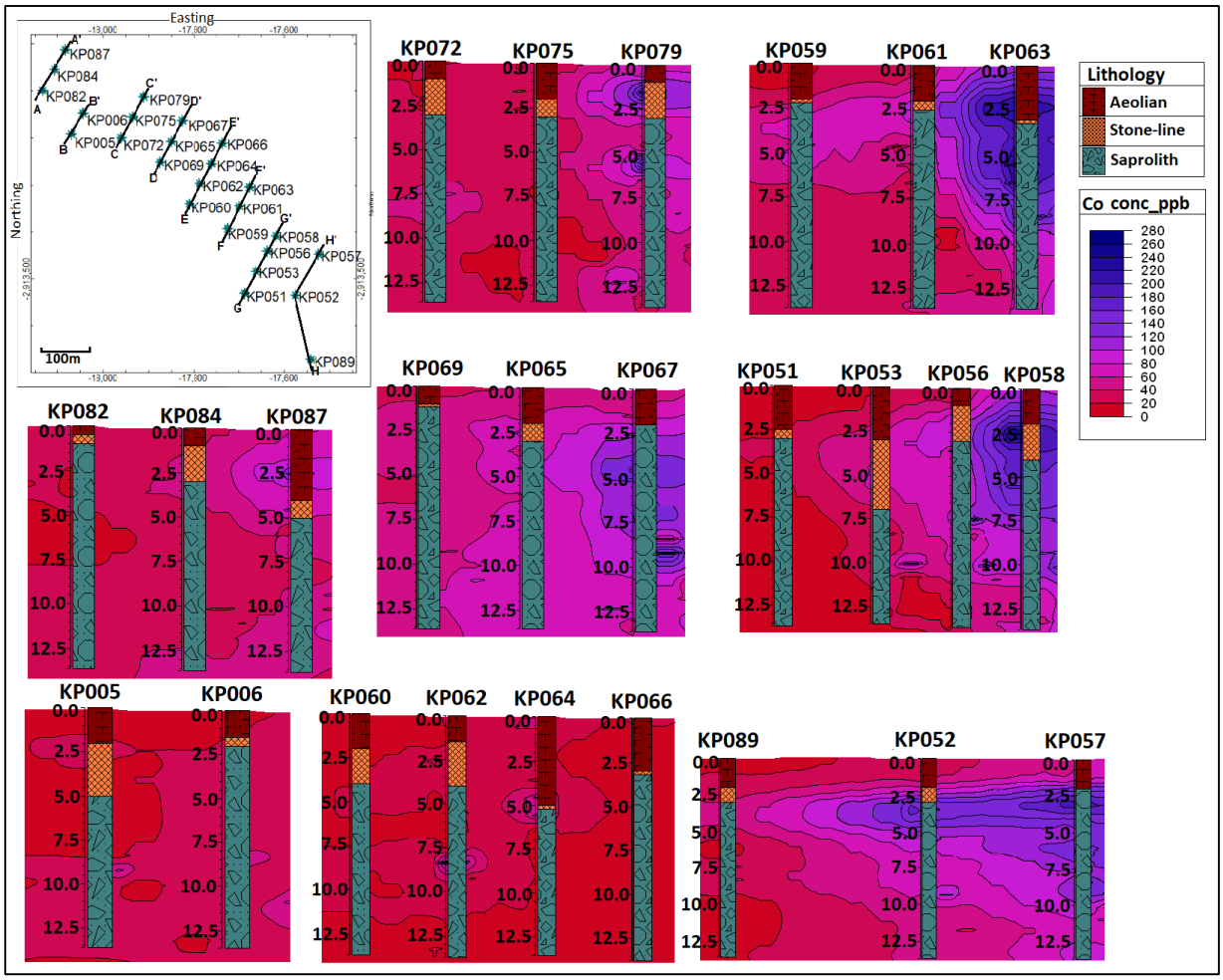

Figure 4.24: A cross-section showing the distribution of cobalt across the Serpens North deposit and the corresponding horizons down the soil profile.

4.10.5.2 Geochemical dispersion of ore elements (Pt, Pd, and Au) in Serpens North Prospect

In Serpens North, anomalous concentrations (> 65ppb) of platinum are largely observed within the lower to middle saprolith in boreholes including; KP006 and KP057 drilled proximal

to the ore body (Figure 4.28). An anomaly can also be observed in the mid-section of the saprolith in borehole KP089. Based on the sections produced through spatial interpolation (Figure 4.25 below), there is a limited dispersion of Pt, with concentrations in most samples lying within the background range of concentration (0 - 65ppb). These observations are consistent with the widely accepted notion that platinum is a relatively immobile element in surficial environments (Cook et al., 1992; Evans et al., 1994; Hattori, 2004).

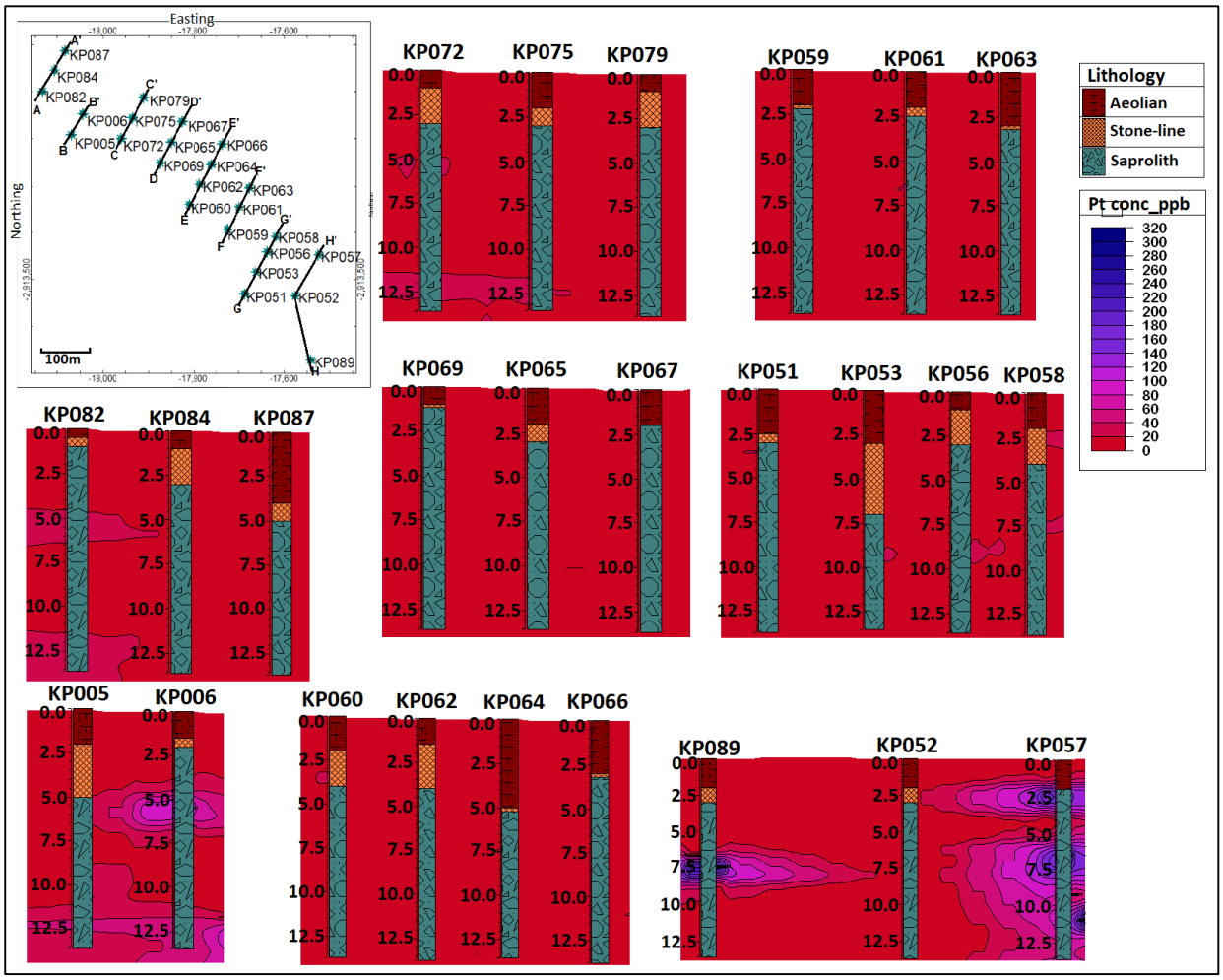

Figure 4.25: Platinum distribution across the Serpens North deposit and the corresponding horizons down the soil profile.

Palladium is also dispersed further from the ore body compared to the pathfinder elements as suggested by the anomalous concentrations in boreholes that are distal to the ore body. In boreholes drilled directly over the mineralised zone, Pd concentrations are mostly within background ranges (0 - 54ppb). Occasional enrichment of palladium is observed within the

middle to lower part of the saprolith in boreholes KP0005, KP006, KP053, KP059, KP065, KP069 and KP082 (Figure 4.26), away from the mineralised zone. This suggests that Pd is significantly mobile within regolith materials in Serpens North. The high mobility of palladium relative to platinum in the weathering environment was suggested in studies conducted in the Great Dyke (Evans et al., 1994) and the temperate regions of Lac des Ilse (Hattori, 2004). These observations are however contrary to observations made in the hot, dry region of Ora Banda, where Pd was found to be mobile over short distances and partly retained in ferruginous zones and the underlying saprolite (Gray et al., 1996).

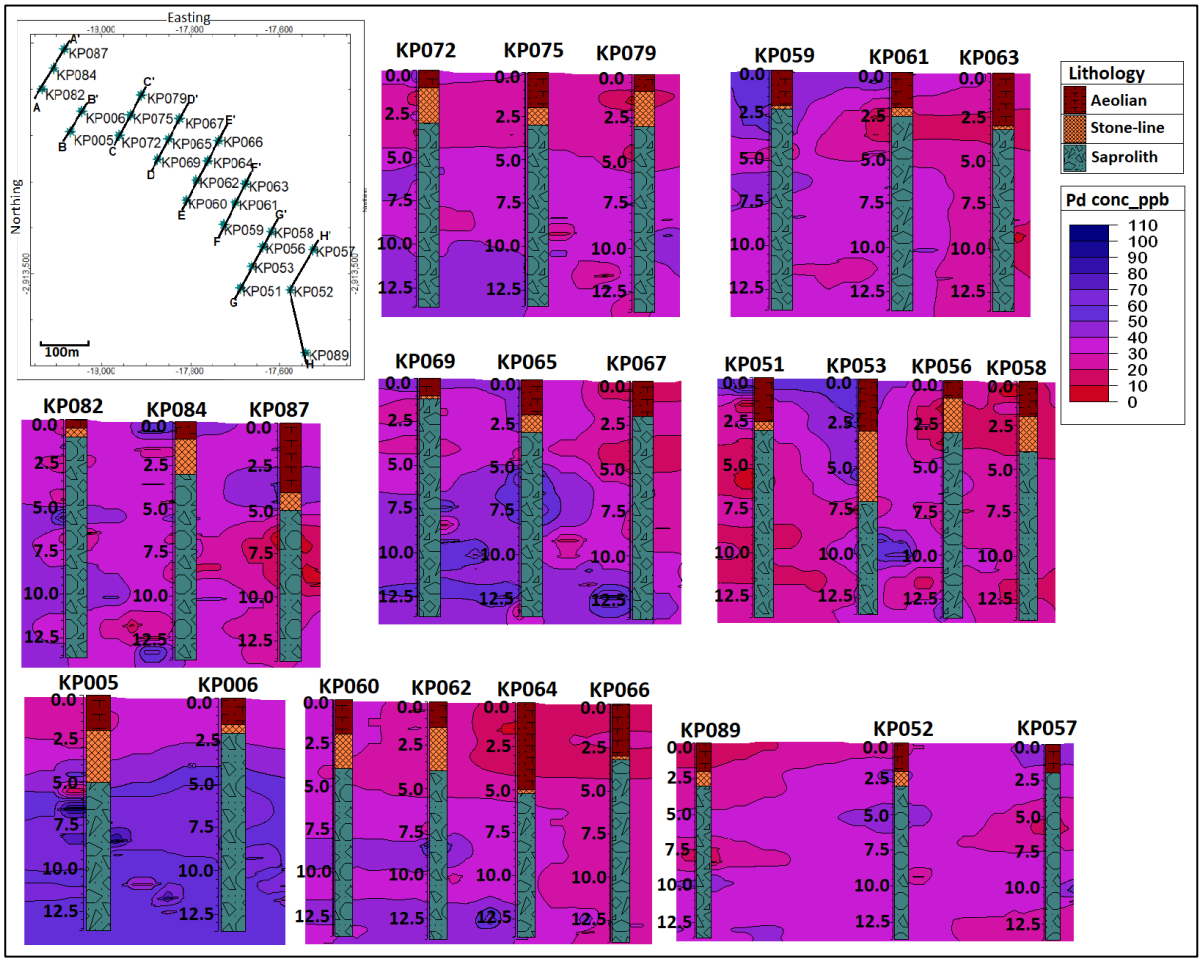

Figure 4.26: Geochemical distribution of palladium across the Serpens North deposit and the corresponding horizons down the soil profile.

Anomalous concentrations (> 5ppb) of Au occur in the upper part of the aeolian sand in borehole KP067. Unlike the other ore elements mentioned above, anomalous Au concentrations occur in some boreholes drilled over the orebody and those in the proximity of the ore body. The mobility of gold is much more restricted to the saprolith, comparable to Pt and Pd. In general, gold is depleted across the area exhibiting mostly background concentrations (0 – 5ppb), except in boreholes KP063, and KP079 drilled directly over mineralisation and KP006, KP062, KP064 proximal to the mineralised zone the upper saprolith (Figure 4.27). According to Butt et al. (2000), Au anomalies generally range between 5 – 300 ppb. In Gawler craton, anomalies are > 10 ppb, and maximum concentrations are over 50 ppb and even reach > 300 ppb (Butt et al., 2000).

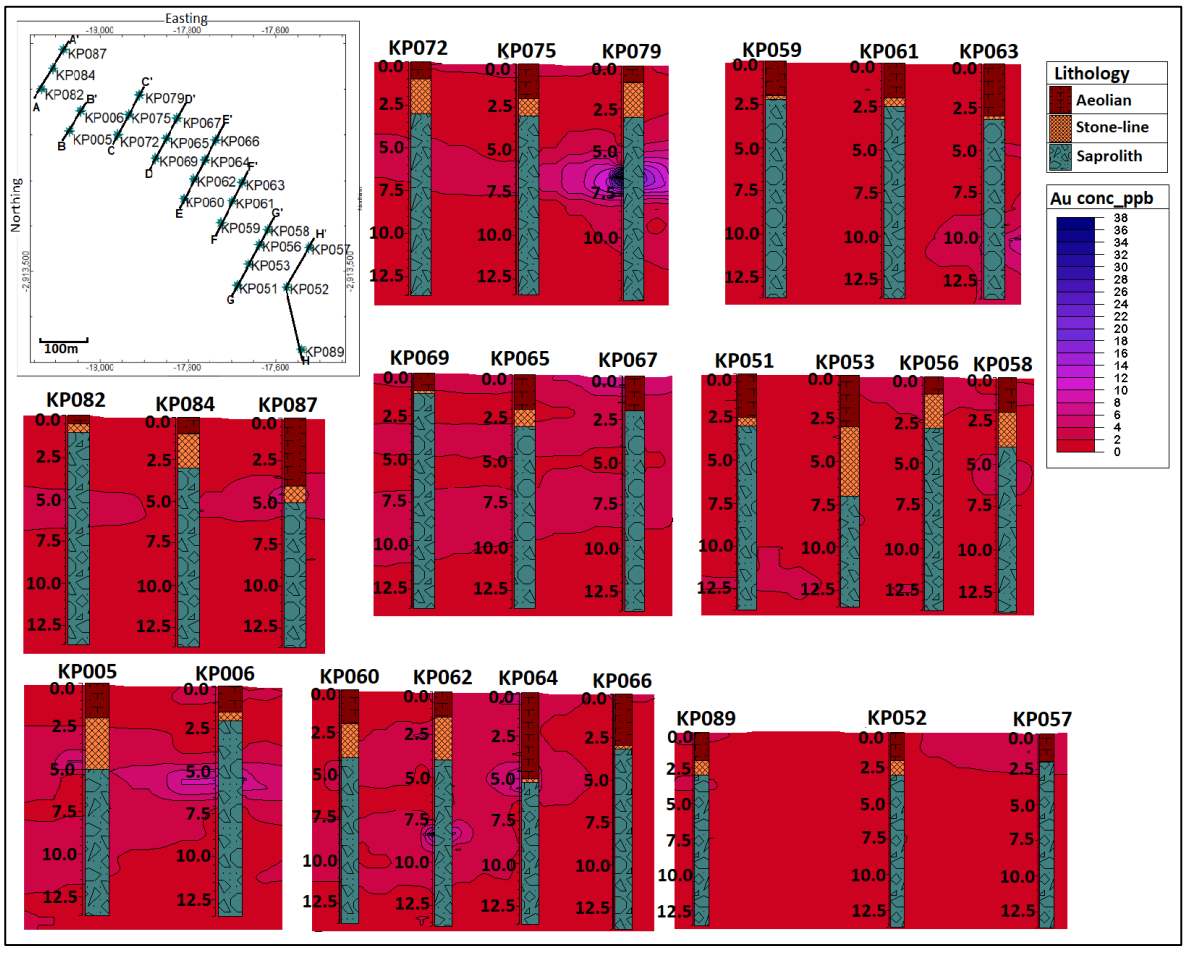

Figure 4.27: Geochemical distribution of gold across the Serpens North deposit and the corresponding horizons down the soil profile.

4.10.5.3 Geochemical dispersions of pathfinder elements in the Sirius Prospect (As, Cu, Co, Ni)

In the Sirius Prospect, an area characterised by the occurrence of calcretes, (Figure 4.28 below), the enrichment of arsenic occurs within the lower saprolith in borehole KP095. The upper saprolith and calcrete horizons are characterised by anomalous arsenic concentrations (> 3.6ppb) in boreholes KP092 and KP097. In borehole KP091, where the calcrete horizon is absent, arsenic enrichment extends into the aeolian sand. Some boreholes are characterised by arsenic enrichment in the upper saprolith and calcrete, but anomalies do not extend into the overlying aeolian sand, suggesting that the arsenic is immobilised and thus precipitated in the calcrete layer due to increase in pH associated with dissolution of carbonates. In general, arsenic concentrations are subdued across the entire prospect.

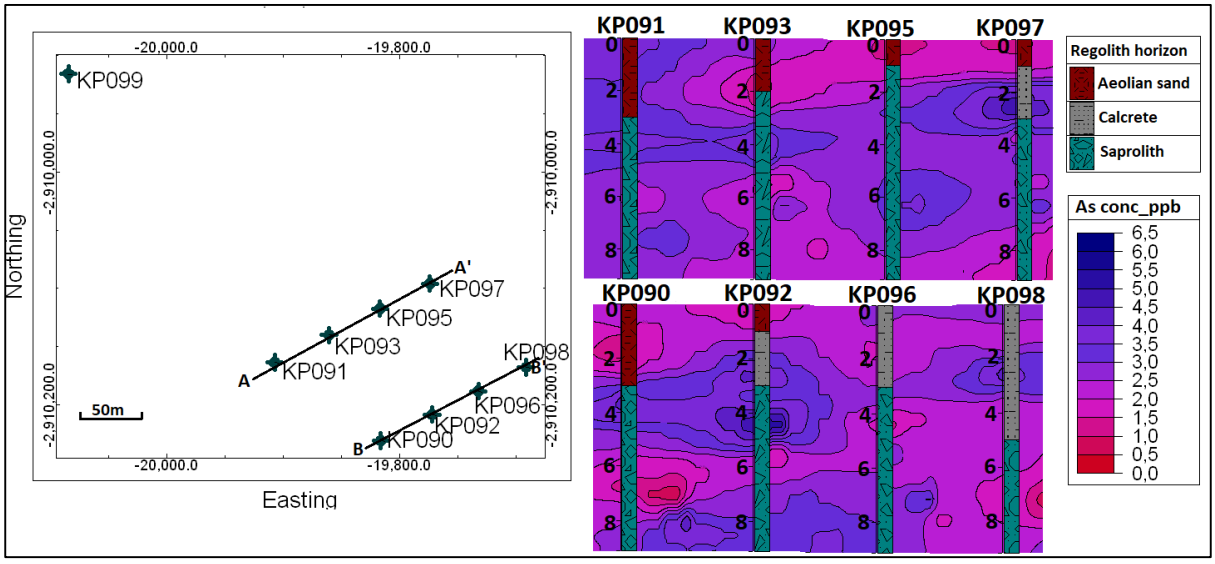

Figure 4.28: Geochemical distribution of arsenic across the Sirius deposit and the corresponding horizons down the soil profile.

In Sirius, most boreholes are characterised by background and below background concentrations of Cu (< 69 ppb), as shown in Figure 4.29 below. However, boreholes KP092 and KP095 are characterised by Cu enrichment in the saprolith horizon, and in KP095 the Cu

enrichment extends from the saprolith into the overlying lower aeolian sand. Borehole KP091 is characterised by Cu concentrations that are below background concentrations.

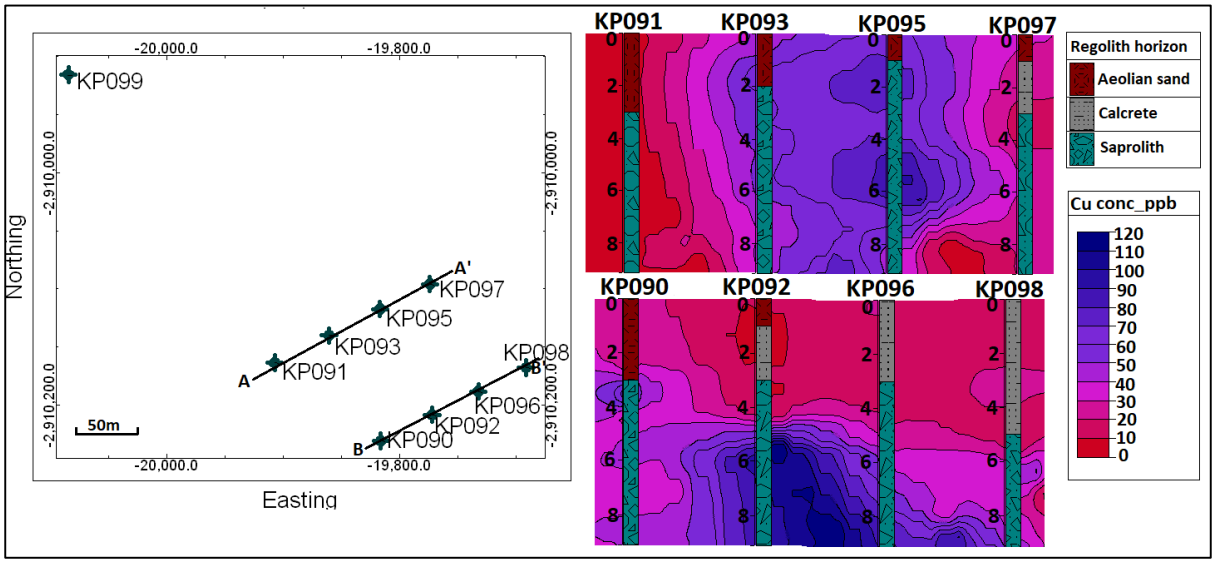

Figure 4.29: Geochemical distribution of Cu across the Sirius deposit and the corresponding horizons down the soil profile.

The distribution of nickel in Sirius as represented in Figure 4.30. The area is characterised by nickel enrichment within the saprolith in borehole KP090 (> 12.7), while in borehole KP097, the lower calcrete horizon is characterised by Ni enrichment. The upper part of the aeolian sand in KP097 is also enriched in Ni. The nickel geochemical signatures are substantially subdued in the Sirius Prospect.

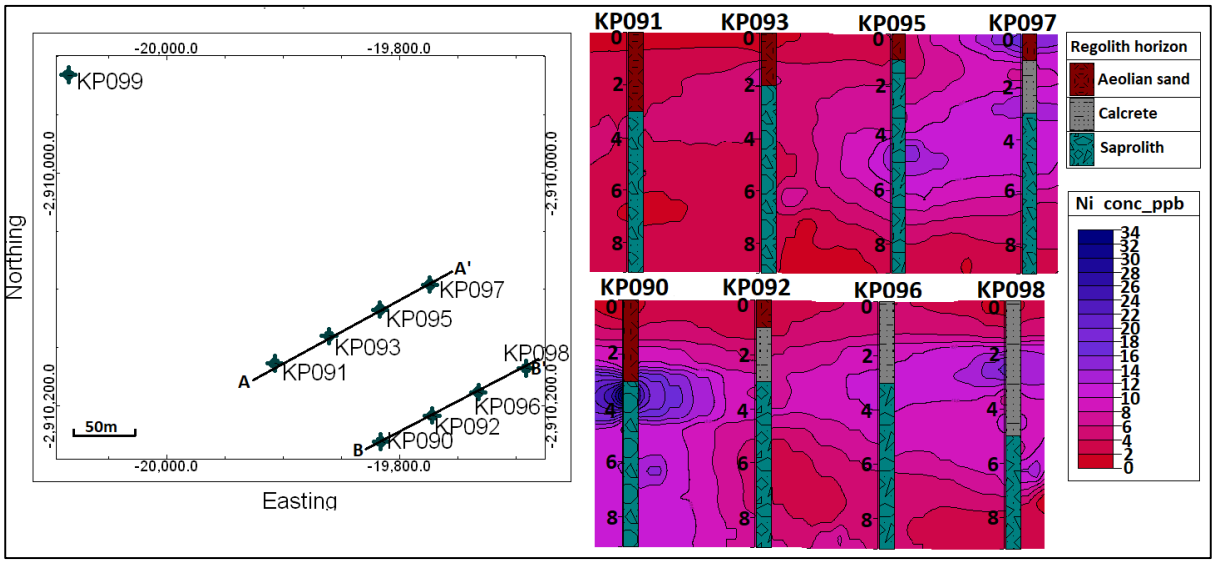

Figure 4.30: Geochemical distribution of Ni across the Sirius deposit and the corresponding horizons down the soil profile.

In Sirius, the geochemical signatures of Co are subdued except in two boreholes in traverse B-B' (Figure 4.31). Boreholes KP090 and KP092 are characterised by anomalous concentrations (> 11ppb) of cobalt in the lower saprolith. Dispersion halos extend outwards into the upper saprolith. Spatial interpolation sections of cobalt concentrations show that the dispersion trains could extend to the upper horizons in areas that were not sampled. Slight Co enrichment occurs within the calcrete and upper aeolian sand in boreholes KP097 and KP093 respectively.

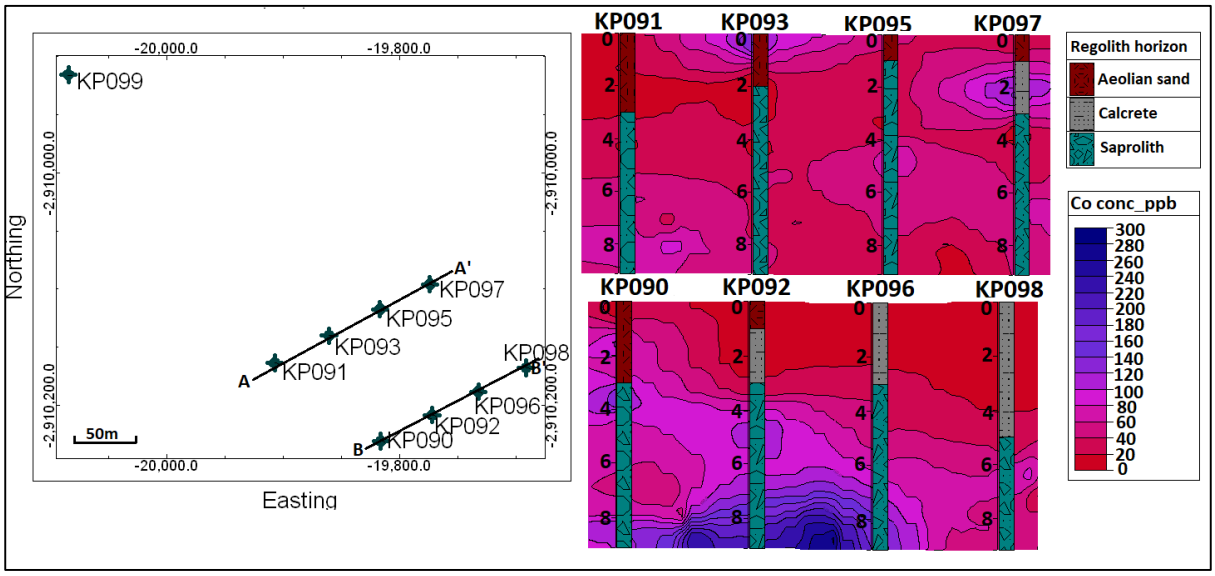

Figure 4.31: Geochemical distribution of Co across the Sirius deposit and the corresponding horizons down the soil profile.

4.10.5.4 Geochemical dispersions of ore elements in Sirius Prospect (Pt, Pd, and Au)

In Sirius, unlike in Serpens North, the signatures of Pt and Au are poorly expressed in most boreholes, as shown in Figures 4.32 and 4.33 respectively. Platinum anomalies (> 40ppb) occur in boreholes KP092 and KP093 within the saprolith, while in KP093 the enrichment extends to the aeolian sand horizon indicating vertical dispersion of the element. The Pt signatures attenuate in the calcrete horizon, but the overlying aeolian sand is characterised by occasional anomalous concentrations. Considering that Pt is relatively immobile (Cook et al., 1992; Evans et al., 1994; Hattori, 2004), it would be implausible for the element to be mobilised in solution in the calcrete layer where pH conditions are alkaline. Thus, the Pt anomalies could have been formed prior to the formation of the calcrete layer, or they could represent anomalies from the source of the transported material. Occasional gold anomalies (> 4.5ppb) can be observed within the saprolith in borehole KP095, drilled directly over the ore body as well as in KP091 and KP096, proximal to the ore body. In general, the Au signatures are weak (0-4.5ppb) throughout the area. Calcrete has always been regarded as a

diluent, which depresses geochemical signatures. In addition, they also introduce an alkaline environment into the host regolith material, which reduces the mobility of elements and restricts the formation of anomalies (Lintern , 2010). However, studies conducted in Cobar and Copper Blow-Galena Hill in Australia, suggest that calcretes can be a major sink for Au and they were used successfully to identify underlying Au deposits (McQueen et al., 1999). The results from the Sirius Prospect do not indicate the enrichment of Au in the horizon except in borehole KP096, suggesting that Au signatures have been diluted by the carbonates. Pd signatures are weak (0-62.5ppb) in Sirius (traverse B-B' shown n Figure 4.34), while mostly slight enrichment within the saprolith in KP093, KP095, and KP099. Further up in the soil profile in KP091 and KP096 anomalous concentrations can be observed in the aeolian sand. The weak Pd signatures can be attributed to the high mobility of the element, suggesting that the element could have been completely leached and removed from the profile.

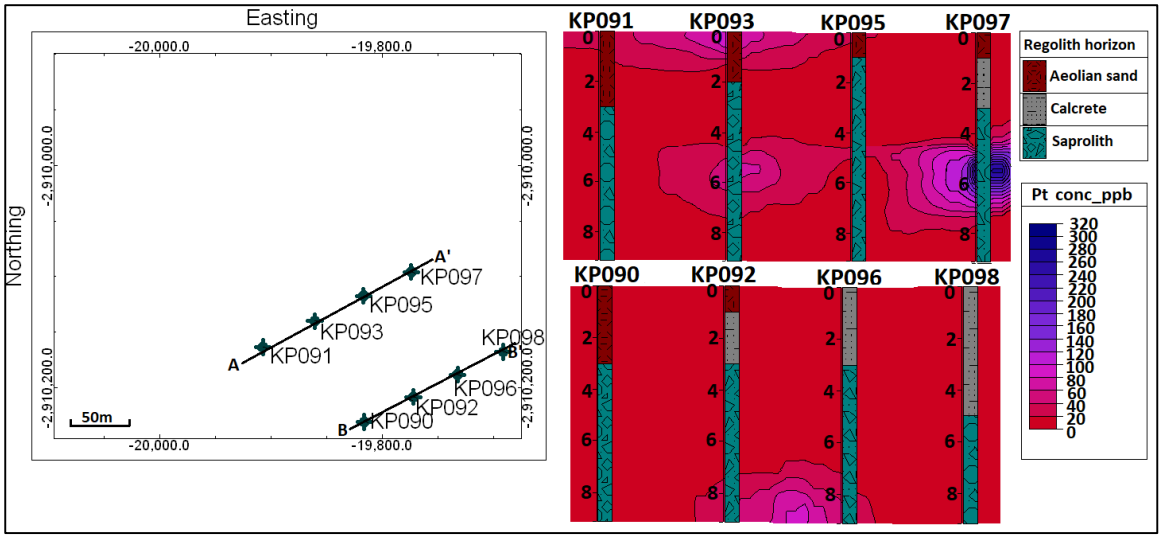

Figure 4.32: Geochemical distribution of Pt across the Sirius deposit and the corresponding horizons down the soil profile.

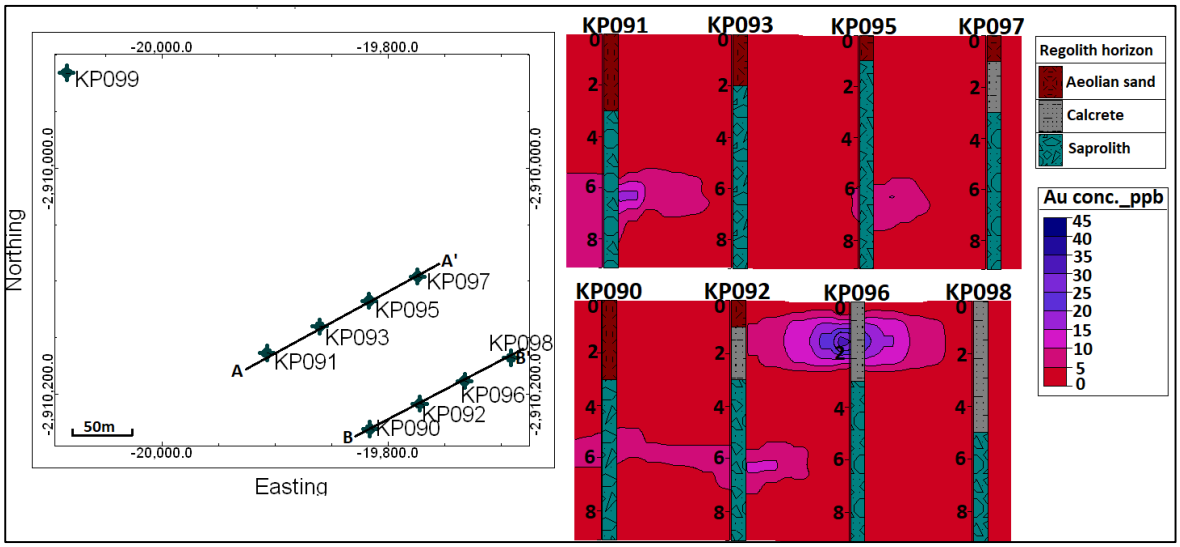

Figure 4.33: Geochemical distribution of Au across the Sirius deposit and the corresponding horizons down the soil profile.

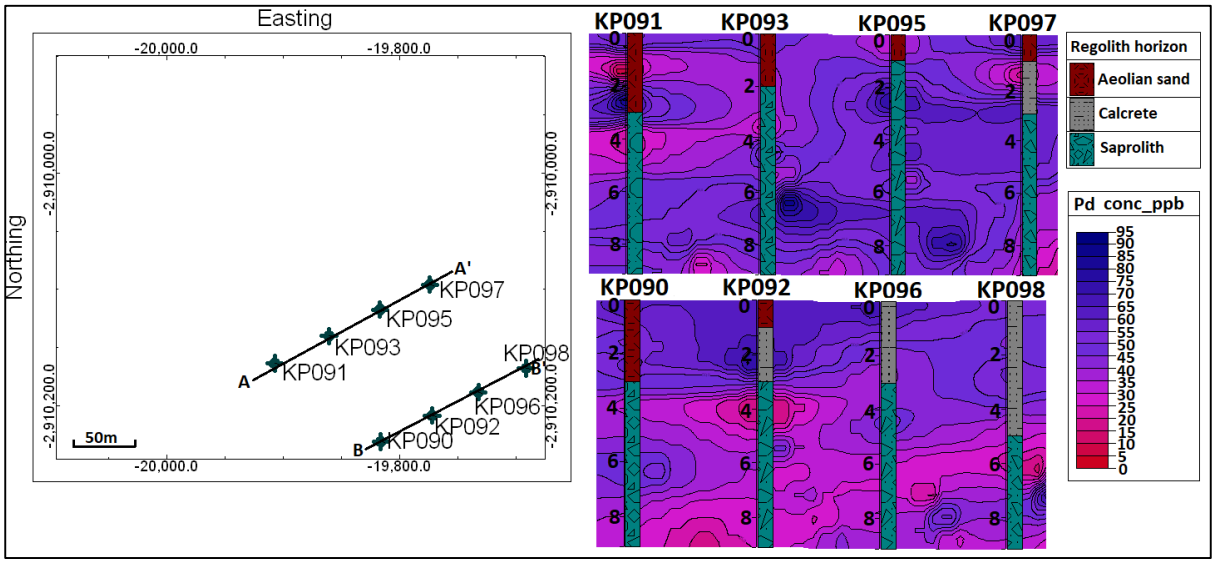

Figure 4.34: Geochemical distribution of Pd across the Sirius deposit and the corresponding horizons down the soil profile.

4.11 SUMMARY OF FINDINGS

I. In Serpens North Prospect, Cu, Ni, and Co always occur in close association. In the aeolian sand, the enrichment of these elements is dependent on the availability of Fe_2O_3, while in the stone-line and saprolith, they are dependent on the availability of both Fe_2O_3 and MnO. The concentration of Pt is controlled by the availability of MnO

as demonstrated by their association in the PCA, and as suggested by the strong correlation between the two elements. Palladium and Au do not show significant associations with any oxides within the aeolian sand, stone-line, and saprolith, suggesting that its enrichment is not dependent on any of these oxides. Based on the sections, arsenic enrichment is mostly within the saprolith and the element is characterised by lateral dispersion. While arsenic is leached from the profiles directly overlying the mineralised zone, anomalies do occur in boreholes that are proximal and distal to the mineralised zone. Copper displays vertical dispersion rather than lateral dispersion. Anomalous concentrations of Cu occur mostly in the upper saprolith, stone-line, and aeolian sand. Similarly, Ni anomalies occur in the lower aeolian sand, stone-line and upper saprolith, mostly occurring in boreholes drilled directly above mineralisation. In addition, Co is also enriched in the aeolian, stone-line, upper saprolith and is dispersed only to areas proximal to the mineralised zone. The dispersion of the ore elements (Pt, Pd, and Au), is mostly confined to the saprolith. While palladium is removed from the profile directly over the mineralised zone, anomalous concentrations occur in some boreholes distal to the mineralised zone. Platinum and Au however, are more restricted in mobility, with occasional anomalies in boreholes drilled directly over and proximal to the mineralised zone.

II. In the Sirius Prospect, the main soil phases that seem to be controlling the enrichment of trace elements are CaO, Al_2O_3, MnO, Fe_2O_3, with no particular oxide showing a consistent affinity for any particular elements. In the calcrete horizon, the statistically significant correlations are between Ca and Fe oxides with Pt and Au respectively. In the saprolith, weak but statistically significant element associations between Al_2O_3

and trace elements including Co and Cu; while MnO and arsenic also have a weak, significant correlation. The mobility of arsenic is influenced by the calcrete horizon which affects the alkalinity of the water that acts as a transporting medium for elements. Thus, where the calcrete horizon is present arsenic signatures attenuate in the calcrete. Where the calcrete horizon is absent, Cu is dispersed vertically, with anomalies occurring throughout the profile. In the profiles where a calcrete layer is present, the Cu anomalies are confined to the saprolith. The Ni signatures in Sirius are weak compared to Serpens North, with anomalies only reaching 33.5ppb. Where occasional anomalies occur, they occur in the upper saprolith, calcrete, and aeolian sand horizons. Platinum anomalies occur in some boreholes within the saprolith and in one borehole within the aeolian sand, but the calcrete horizon shows no Pt enrichment. Gold anomalies mostly occur in the lower-mid saprolith, and in one borehole, an anomaly occurs in the calcrete horizon. Slight Pd anomalies occur in the saprolith and the aeolian sand occasionally.

5 DISCUSSION

5.1 OVERVIEW

Chemical weathering results in the redistribution of elements within the surficial environment. Progressive chemical weathering, for example, results in the depletion of the cations Ca^{2+}, Na^{+}, Mg^{2+} and K^{+} (which are highly mobile); while cations such as Si^{4+}, Al^{3+} and Fe^{3+} are retained (McQueen, 2006). Weathering processes operating over periods result in the alteration of primary minerals of the parent rock such as feldspars, amphiboles, pyroxenes, etc. to clay minerals including kaolinite, montmorillonite, smectite, and vermiculite (Cox, et al., 1995). With progressive weathering, the resulting secondary minerals are mostly rich in aluminium oxides, while highly mobile cations are removed (Cox, et al., 1995). A number of indices have been used to determine the degree of weathering in regolith including, chemical index of alteration, CIA (Nesbitt & Young, 1982), K_2O/ Al_2O_3 versus MgO/ Al_2O_3, (McQueen, 2006)), index of chemical variability (ICV) (Cox, et al., 1995) , amongst other indices.

While paleo-climate significantly influences the nature of regolith characteristics (Butt, 2005), it is important to note that the shallow regolith profile in the Serpens North and Sirius does not suggest previous deep weathering from past climatic conditions, which could have overprinted some of the more recent geochemical signatures and influenced the nature of the regolith significantly. As much as the currently active climate should be considered as the most contributing factor in the secondary geochemical dispersion of elements, the

mobilization of elements is likely to be minimal due to the semi-arid to arid conditions that currently exist. Thus, the role of the paleoclimate, like the regolith materials in the area, cannot be entirely dismissed.

The use of geochemical data as a surrogate for mineralogy in cases where X-ray diffraction or infra-red spectral analysis is not available was suggested, mainly because it is difficult to identify minerals in soil samples because they are generally fine-grained and pulverised in drill cuttings in the absence of these techniques (McQueen (2006); Arhin, et al. (2017)). While the classification of regolith materials using whole-rock geochemical data cannot substitute regolith mapping, it gives new insight into the nature of regolith in the area of study, and it is clear that these two reinforce each other and should be used concurrently to better understand regolith materials.

5.2 REGOLITH CHARACTERISATION IN SERPENS NORTH AND SIRIUS

5.2.1 Major and trace element patterns in the weathering environment: Serpens North Prospect

The results of the regolith material plot in Figure 4.5 (after McQueen, 2006) show that although the area has an arid- semi-arid climate, significant weathering has taken place. This is demonstrated by the geochemistry of the saprolith samples, mainly exhibiting significantly high Mg/Al ratios, which indicate that the samples are enriched in MgO. Most of the saprolith samples also have low K/Al ratios, indicating very low K_2O in these samples. This suggests that there has been a slow removal of cations, with Mg being retained; coupled with replacement

of other divalent cations by Mg+ cations with progressive weathering; resulting in a saprolith horizon with much higher MgO concentrations. According to Lewins et al., 2008; the study area was subjected to intense carbonate alteration, which resulted in the alteration of the precursor rocks. This is likely to have resulted in the formation of talc-carbonates, which probably resulted in an increase in Mg content of the precursor rocks and subsequently resulted in Mg enrichment in the saprolith. This is also an indication of the presence of smectite in the profile, which is characterised by high Mg concentrations and occurs in the lower part of the saprolith.

The main elements that dominate all three regolith horizons are SiO_2, Fe_2O_3, and Al_2O_3. According to Tonui et al. (2003), this is a common phenomenon in regolith terrains. The dominance of oxides such as hematite, goethite, and quartz, as well as aluminosilicates such as kaolinite, which host these elements are the main products of weathering (Tonui et al., 2003). In addition, the saprolith also contains slightly high MgO and CaO (geomean concentrations of 2.81 and 2.45 wt.% respectively), indicating that the underlying parent rock is also rich in Mg and Ca. Trace elements including Ni, Co, Pb, Zn, and Sr occur in very low concentrations compared to other areas such as the regolith overlying the Great Dyke (Cu and Ni) (Evans, et al., 1994), but they are well within ranges similar to those of Thunderdome prospect, Australia (Tonui, et al., 2003). The bulk geochemical data suggest that element associations vary in the different horizons. In the aeolian sand horizon, Zn, V, Sr, Rb, Ni, Co, and Ba are not found associated with any major soil phases, suggesting that these elements are probably retained in a different phase, perhaps organic matter. In the stone-line, aluminium-rich clays (Ce, Nd, Co, and Ba), carbonates (Zr), secondary Fe oxides (Ni), and

manganese oxides (Sr, Rb, and Y) as well as residual primary silicates (Pb, and V), seem to be controlling the enrichment of trace elements in the regolith. Based on both the PCA and Pearson's correlation, there seems to be a decoupling of most trace elements from Fe oxides in the saprolith and their association with oxides of aluminium (Co, Ni, Zn, V) and silica (Ba, Pb, Ce, Nd, and Y), which suggests that secondary Fe oxides not incorporate trace elements into their chemical structures. The data suggest that aluminium-rich clays incorporate trace elements that are released from the less stable primary minerals such as pyroxenes and amphiboles into their complex chemical structures. Some trace elements are retained in potassium-rich feldspars (which according to Cox et al. (1995) are relatively stable in the weathering environment), as suggested by association of trace elements with SiO_2 and K_2O. This is contrary to observations that were made in Thunderdome Prospect (Tonui, et al., 2003), for example, where Fe oxides are associated with trace elements such as Co, Cu, Zn, and Ni.

The differences in the CIA across the different boreholes which do not show any particular trend indicate that regolith is heterogeneous, due to variations in weathering intensities. As a result, the distribution of trace elements is more complex and possibly does not show uniform trends. Some of the regolith materials have been significantly weathered as shown by CIA values up to 90 while other samples have only been slightly weathered in a few samples, with CIA values as low as 36 and up to 75 in most samples, while other samples have CIA values ranging from 75 to 85 indicating a moderate degree of weathering. The A-CN-K plot shows that across some profiles there has been an addition of CaO and Na_2O as indicated by the enrichment of these oxides in some saprolith samples and a correspondingly low concentration of these elements in a few of the saprolith samples. The ICA index, which seems

to be largely affected by the enrichment of iron, can be regarded as indicating zones of ferruginisation in this case. These zones could be important for the enrichment of trace elements that are linked to mineralisation due to the abundance of iron oxides that scavenge trace elements.

5.2.2 Major and trace element patterns in the weathering front: Sirius Prospect

The boreholes drilled in the Sirius Prospect intercept the regolith at 10 meters. In Sirius, a similar trend to that of Serpens North, where the ratio of MgO / Al_2O_3 is high can also be observed although in Sirius the variation within the samples is lower. In this area, however, there is an occurrence of pedogenic carbonates (Ca and Mg). The occurrence of carbonates is demonstrated in the geochemistry of some samples, where some of the calcrete samples form a distinct group that is characterised by high CaO and a corresponding high LOI. These pedogenic carbonates were not encountered in Serpens North. Thus the carbonates can be attributed to the dissolution and mobilisation of calcium and magnesium from a more Ca and Mg-rich parent rock (Ca-rich plagioclase feldspars) and their subsequent accumulation in paleochannels in Sirius. While the majority of saprolith samples from Serpens North have MgO concentrations less than 5 wt.%, the majority of saprolith samples from Sirius have concentrations ranging from 5 wt.% and up to more than 7.5 wt.%, which suggests that the parent rock in Sirius is more Mg-rich.

Based on the PCA and Pearson's correlation matrix of the bulk geochemical data, there is a strong relationship between major secondary soil phases and a number of trace elements. Iron oxides have strong correlations with trace elements such as Zn, V, Pb, Co, Ba, and Y in the aeolian sand, which is an indication of the elements that are retained in secondary oxides during weathering. Trace elements are also retained in iron oxides in the calcrete horizon (which is characterised by high Fe_2O_3 concentrations with a geomean of 9.6 wt.%). Within the saprolith, the association of trace elements such as Co, Pb, Ba, Ce, and Nd with LOI suggests that these trace elements are hosted in carbonates because the high LOI in the saprolith can be attributed to the presence of carbonates (Heiri et al., 2001; Frangipane et al., 2009).

In general, the occurrence of regolith carbonates in Sirius, which were not observed in Serpens North, suggests a difference in underlying bedrock composition. From the geochemistry of the samples, it is evident that the underlying bedrock in Sirius is richer in calcium and relatively higher in magnesium compared to Serpens North. The Ca and Mg-rich parent rock has over time been exposed to groundwater, which resulted in chemical weathering and through evaporation and subsequent capillary action, carbonates were mobilised and then precipitated in the soil moisture zone.

5.3 DISTRIBUTION OF PATHFINDER AND ORE ELEMENTS IN SERPENS NORTH

In Serpens North Prospect, Cu, Ni, and Co always occur in close association. Based on PCA plots and Pearson's correlation, in the aeolian sand horizon, the enrichment of these trace elements is dependent on the availability of Fe_2O_3, while in the stone-line and saprolith, they are dependent on the availability of both Fe_2O_3 and MnO. The enrichment of Pt is controlled by the availability of MnO as demonstrated by their association in the PCA, and as suggested by the strong correlation between the two elements. Palladium and Au do not show any significant associations with any oxides within the aeolian sand, stone-line, and saprolith, suggesting that their enrichment is not dependent on any of these soil phases, but possibly other soil phases such as clays.

The distribution of arsenic suggests that this element is highly mobile in this environment. However, the dispersion is lateral rather than vertical, as evidenced by the enrichment of the element in boreholes that are distal to the mineralised zone. Generally, boreholes drilled directly over mineralisation, and occasionally those proximal to the mineralised zone are characterised by anomalous Cu concentrations, KP054, KP058, KP063, KP067, KP087 and

KP057, KP062, KP064, KP066 respectively; while distal to the mineralised zone, KP053 shows a strong Cu anomaly. The Ni dispersion trains mimic those of Cu because these ore related trace elements are usually found in close association. Similarly, Co is also enriched in the lower part of the aeolian sand, stone-line as well as the upper saprolith, however, the lateral dispersion of Co does not extend to the distal part of the mineralised zone. The three elements seem to be enriched within the aeolian sand and the underlying, thin stone-line horizon and mostly within the upper saprolith. This can be attributed to the cyclical mobilization of the trace elements from the ore body by processes such as hydromorphic dispersion and capillary action mainly in an upward direction, but also in a lateral direction. In the case of upward mobilization, the minimal rainfall in the semi-arid area results in the downward mobilization of elements during the wet summers and their successive precipitation within the lower aeolian sand, stone-line as well as the upper saprolith. However, anomalous concentrations of these elements occur occasionally within the lower saprolith.

The PGEs (Pt and Pd), are mostly dispersed laterally, and dispersion trains extend further away from the mineralized zone. While the upward mobilisation of Pt mostly extends to the middle part of the saprolith, Pd is mostly mobilised all the way to the aeolian sand. Moreover, the boreholes drilled over the mineralised zone are characterised by background concentrations of the two PGEs indicating that the elements known to be relatively immobile have been mobilised in this weathering environment. Gold, on the other hand, seems to have limited dispersion trains with most of the anomalies occurring over the mineralised zone and in its proximity although some occasional anomalies occur further away from the ore body.

In the aeolian sand, both Fe- and Mn-oxides determine the dispersion patterns of elements such as Cu, Au, Co, Ni, Pt, Pd, and Pt. The dispersion of arsenic and Pd in the stone-line horizon seems to be controlled by Fe- and Mn- oxides, while the other trace elements are not associated with these soil phases. In general, Cu and Co show significant anomalies, while Ni signatures are weaker throughout the prospect. Compared to studies conducted in Lac Sheen (Cook, et al., 1992)and the Great Dyke (Evans, et al., 1994) for example, the average concentrations of trace elements in Serpens North prospect are significantly lower.

5.4 DISTRIBUTION OF PATHFINDER AND ORE ELEMENTS IN SIRIUS

Arid to semi-arid environments are characterised by minimal organic matter (which limits the amount of humic acids), and calcium carbonate accumulation, hence the soils are generally neutral to strongly alkaline (van Berkel, 1982). The Sirius deposit is characterised by the occurrence of carbonates. The enrichment of elements is therefore mostly confined to the saprolith, although in some boreholes enrichment extends into the overlying calcrete and aeolian sand.

Carbonates are regarded as a diluent that depresses the geochemical signatures and introduces an alkaline environment into the host regolith material which reduces the mobility of elements and restricts the formation of epigenetic anomalies (Lintern , 2010). A study carried out in Bounty, Australia, a gold deposit, successfully used calcrete as a sampling medium for Au exploration (Lintern, 1989 as cited in Lintern, 2010). According to Lintern (2010), there was a significant correlation between Au and Ca, but Fe and many other

elements were diluted by the calcrete. Where a calcrete layer is present, anomalies in the aeolian sand were possibly formed prior to the formation of the calcrete layer.

Unlike in Serpens North, the signatures of Pt and Au are poorly expressed in most boreholes. Nonetheless, Pt seems to exhibit preferential vertical dispersion. The calcrete horizon is depleted in Pt, but the overlying aeolian sand is characterised by occasional anomalous concentrations. Considering that Pt is relatively immobile (Cook et al., 1992; Evans et al., 1994; Hattori, 2004), it would be implausible for the element to be mobilised in solution in the calcrete layer where pH conditions are alkaline. Therefore, the Pt anomalies possibly precede the formation of the calcrete layer. Alternatively, these anomalies could represent signatures from the source of the transported material. Good Au signatures occasionally occur within the saprolith in boreholes that were drilled directly over the ore body. In general, the Au signatures are weak throughout the prospect. Although studies have been conducted (e.g. Cobar and Copper Blow-Galena Hill in Australia), where calcretes were used successfully as sample medium in Au exploration (McQueen et al., 1999); results from the Sirius prospect do not indicate any significant Au anomalies in the horizon. Therefore, Au signatures have been diluted by the carbonates. Pd signatures are poorly expressed in Sirius, with mostly slight enrichment within the saprolith and occasionally in the aeolian sand. The reason why Pd concentrations are subdued can be attributed to the high mobility of the element, suggesting that the element could have been completely leached and removed from the profile. In addition, Pd could have been diluted by the carbonates found in the Sirius prospect.

In the Sirius Prospect, the main soil phases that seem to be controlling the enrichment of trace elements are CaO, Al_2O_3, MnO, Fe_2O_3, with no particular oxide showing a consistent affinity for any particular elements. In the calcrete horizon, the statistically significant correlations are between Ca and Fe oxides with Pt and Au respectively. In the saprolith, weak but statistically significant element associations between Al_2O_3 and trace elements including Co and Cu, while MnO and As also have a weak, significant correlation.

6 CONCLUSION

The main objectives of this study were to use major element data to characterise the regolith materials enclosing the PGE mineralisation in the Stella Layered Intrusion and ascertain the degree of weathering that has occurred. Furthermore, the study aimed to relate the weathering patterns in regolith to the distribution of pathfinder elements of PGEs and gold in areas proximal and distal to the mineralised zones.

Based on the results of McQueen's classification of regolith materials, it can be concluded that this form of classification can be used to further understand regolith although it cannot substitute field identification of regolith materials or X-Ray diffraction. Using geochemical data as a surrogate for techniques such as X-Ray diffraction in cases where the latter method is not available is indeed useful because it demonstrates that regolith materials are heterogeneous and complex. These are characteristics that cannot be determined only by regolith mapping. Using geochemical data helps in understanding how weathering processes have influenced the nature of regolith materials. From the results, it is clear that these samples have undergone weathering to an extent (incipient to moderate), and they have retained only some of the characteristics of the original protolith. The semi-arid conditions and the extensive aeolian cover prevents the deep weathering of the bedrock. However, the results suggest that there has been some notable (incipient to moderate) weathering and thus, the mobilisation and redistribution of elements.

In general, the upper aeolian sand is characterised by a depletion in the relatively mobile elements including CaO, Na_2O, K_2O, MnO, MgO, while the lower aeolian sand shows a slight

enrichment in these elements. This suggests that these mobile elements are leached from the upper horizon during rainy seasons and precipitated in the lower aeolian sand. Silica oxide which is less mobile, is enriched across the entire horizon. The concentration of Al_2O_3 is higher in the upper aeolian sand than the lower part, which suggests that the upper aeolian sand is more clayey than the lower part. The concentrations of CaO and Na_2O within the saprolith vary across boreholes again emphasing the heterogeneity of the regolith, although these two major oxides are closely associated with each other. Although K_2O is also a relatively mobile element, it is mostly not found associated with the previously mentioned oxides. However, a general enrichment of the major oxides is seen within the upper part of the saprolith compared to the lower part of this horizon.

Based on the PCA and the geochemistry of the saprolith, it can be deduced that the protolith of the overlying in-situ regolith is mafic because of the high FeO + MgO* concentrations of the samples. Gabbro is the major lithology found within the Stella Layered Intrusion, and the regolith geochemical data indicate that the regolith was derived from bedrock that has the characteristics of gabbro. The other lithology from which the regolith may be derived is mafic diabase, which is supported by the greenish nature of a few of the regolith samples from Serpens North. Additionally, a few samples from Serpens North have characteristics of a more K-feldspar-rich protolith as evidenced by the samples that plotted away from the FeO + MgO apex in the A-CNK-FM plot, and this could be attributed to the presence of a feldspathic pegmatoidal gabbro which forms part of the underlying rocks.

The technique that was used in the partial leaching of the samples is hydroxylamine hydrochloride. Although the technique gave positive results for both study areas, the geochemical signatures were less pronounced in Sirius. This is largely due to the presence of regolith carbonates, which usually increase pH of the partial leach solution upon their dissolution, thereby causing elements that are mobilised at low pH to precipitate out of solution. Considering that the elements of interest including Cu, Ni, Co, Pd, Pt, and Au are mobile under acidic environments, an increase in the pH of the solution due to these carbonates caused the elements to precipitate, and this diminished the geochemical signatures. Therefore, a different partial leach solution that is suitable for the leaching of carbonates, such as ammonium acetate is much more suitable. Alternatively, the hydroxylamine hydrochloride could be modified to include a buffer which can keep the pH of the solution constant during the leaching procedure.

The main horizons that are characterised by good anomalies that are most likely to yield positive results during exploration in Serpens North are the lower aeolian sand and the upper saprolith particularly for elements such as Cu, Co, Ni, and Pd. The lateral distance from the ore body should also be considered because the results show that the dispersion trains of Cu, Co and Ni mostly do not extend to the distal parts of the ore body. The ore elements (Pt& Au) seem to be relatively immobile in both Serpens North and Sirius, with occasional anomalies occurring in the lower to mid-saprolith, while Pd seems to be slightly mobile, with anomalies extending to the upper horizons and areas that are distal to the mineralised zone. Based on the analysis of the data using various methods such as the PCA and Pearson's

correlation matrix for example, Cu, Co, and Ni are not good indicators of mineralization in this specific study area because they are almost always found decoupled from the ore elements.

7 REFERENCES

Ackon, P., 2001. *Selective leach techniques as a tool for prospecting gold deposits concealed by aeolian regolith: A case study at the Blue Dot Mine, Amalia, Northwest Province, South Africa.,* University of the Western Cape, Cape Town: M.Sc Thesis (Unpublished), 127pp.

ALS Minerals, 2012). *Fire assay technical note.* Retrieved from https://www.alsglobal.com/-/media/als/resources/services-and-products/geochemistry/technical-notes/fire-assay- technical-note-2012.pdf, 4pp.

Amos, M., 2006. Flame and Vapour Generation Atomic Absorption Spectrometry. In *Encyclopedia of Analytical Chemistry.* John Wiley & Sons Ltd.

Analytikjena, 2014. *HS 55 Modular.* Jena, Germany: Analytik Jena AG.

Anand, R., 2001. Evolution, classification and use of ferruginous regolith materials in gold exploration, Yilgarn Craton, Western Australia. *Geochemistry: Exploration, Environment, Analysis,* Volume 1, pp. 221-236.

Anand, R. & Butt, C., 2010. A guide for mineral exploration through the regolith in Yilgarn Craton, Western Australia. *Australian Journal of Earth Sciences,* Volume 57, pp. 1015-1114.

Anand, R. & Paine, M., 2002. Regolith geology of the Yilgarn craton, Western Australia: Implications for exploration. *Australian Journal of Earth Sciences,* Volume 49, pp. 3-162.

Anhaeusser, C. R. & Walraven, F., 1997. *Polyphase crustal evolution of the Archean Kraaipan granite-greenstone terrane, Kaapvaal craton, South Africa,* Pretoria: Council for Geoscience 34pp.

Anhaeusser, C. R. & Walraven, F., 1999. Episodic granatoid emplacement in the Western Kaapvaal craton: evidence from the Archaean granite-greenstone terrane, South Africa. *Journal of African Earth Sciences; Vol 28,* pp. 289-309.

Arhin, E., 2013. *Use of regolith geochemistry to delineate gold mineralisation undercover: A case study in the Lawra belt, NW Ghana,* University of Leicester: Unpublished Thesis, 258pp.

Arhin, E., Zango, M. & Kazapoe, R., 2017. Characterizing and indexing regolith materials using geochemistry towards hidden mineral anomaly delineation: A case study of the Savannah region of Northwest Ghana. *Universal Journal of Geoscience,* 5(6), pp. 169-182.

Aspandiar, M., Anand, R. & Gray, D., 2008. *Geochemical dispersion mechanisms through transported cover: Implications for mineral exploration in Australia,* Bentley, Western Australia: Corporative Research Centre for Landscape Environments and Mineral Exploration, 84 pp.

Borggaard, O., 1981. Selective extraction of amorphous iron oxides by EDTA from soils from Denmark and Tanzania. *Soil science, 32*, 427-432.

Bowles, J. F., Gize, A. P. & Cowden, A., 1994. The mobility of the platinum-group elements in the soils of the Freetown Peninsula, Sierra Leone. *The Canadian Minerologist,* Volume 32, pp. 957-967.

Brandl, G., Cloete, M. & Anhaeusser, C. R., 2006. Archaean greenstone belts. In: M. R. Johnson, C. R. Anhaeusser & R. J. Thomas, eds. *The geology of South Africa.* Johannesburg/Council for Geoscience, Pretoria: Geological Society of South Africa, pp. 9-56.

Brand, N. & Butt, C., 2001. Weathering, element distribution, and geochemical dispersion in Mt. Keith, Western Australia: Implication for nickel sulphide exploration. *Geochemistry: Exploration, Environment, Analysis,* Volume 1, pp. 391-407.

Burke, K., Kidd, W. S. & Kusky, T., 1985. Is the Ventersdorp rift system of Southern Africa related to a continental collision between the Kaapvaal and Zimbabwe cratons at 2.64 Ga ago. *Tectonophysics,* Volume 115, pp. 1-24.

Butt, C., 1995. *Geochemical exploration for base metals in deeply weathered terrain.* Reproduced in: Ho S. E. & Amann W.J. (Eds). Recent developments in base metal geology and exploration Bulletin 16. Australian Institute of Geoscientists. pp. 17-31. (Also published in McConaghy T.F. & McInnes (Eds). Copper-zinc massive sulphide deposits in Western Australia. CSIRO Explores 2. CSIRO Exploration and Mining, Melbourne. pp. 81-101.

Butt, C., 2005. Geochemical dispersion, process and exploration models. In: C. Butt, I. Robertson, K. Scott & M. Cornelius, eds. *Regolith expression of Australian ore systems.* Perth; W.A: CRC LEME, pp. 81-106.

Butt, C.R.M., Lintern, M. & Anand, R., 2000. Evolution of regoliths and landscapes in deeply weathered terrain - implications for geochemical exploration. *Ore Geology Reviews,* Volume 16, pp. 167-183.

Butt, C.R.M., Williams, P.A., Gray, D.J., Robertson, I.D.M, Schorin, K.H., Churchward, H.M., McAndrew, J., Barnes, S.J., Tenhaeff, M.F.J., 1992. *Geochemical exploration for platinum-group elements in weathered terrain,* Wembley, Australia: CSIRO Exploration and Mining, 78pp.

Cameron, E. M.., Hamilton, S.M., Leybourne, M.I., Hall, G.E.M. & McClenaghan, M.E., 2004. Finding deeply buried deposits using geochemistry. *Geochemistry: Exploration, Environment, Analysis,* Volume 4, pp. 7-32.

Chao, T., 1984. Use of partial dissolution techniques in geochemical exploration. *Journal of Geochemical Exploration, Vol. 20,* pp. 101-135.

Chen, X., 2010a. Morphology and Occurrence. In: X. Chen, M. Lintern & I. Roach, eds. *Calcrete: Characteristics, distribution and use in mineral exploration.* Kensington, Western Australia: CSIRO Exploration and Mining, pp. 5-6.

Chen, X., 2010b. Origins. In: X. Chen, M. Lintern & I. Roach, eds. *Calcrete: Characteristics, distribution and use in mineral exploration.* Kensington, Western Australia: CSIRO Mining and Exploration, pp. 8-12.

Cook, N., Wood, S. & Zhang, Y., 1992. Transport and fixation of Au, Pt, and Pd around the Lac Sheen Cu-Ni-PGE occurrence in Quebec, Canada. *Journal of Geochemical Exploration,* Volume 46, pp. 187-228.

Cox, R., Lowe, D. R. & Cullers, R., 1995. The influence of sediment recycling and basement composition on evolution of mudrock chemistry in the southwestern United States. *Geochimica et Cosmochimica Acta,* 59(14), pp. 2919-2940.

D'Ulivo, A., 2018. *Atomic absorption spectrometry | Vapor generation.* Pisa, Italy: Elsevier.

Department of Rural, Environment and Agricultural Development, 2015. *Climate Support Programme (CSP)- Vulnerability Assessment,* North West Province: Pegasys Strategy and Development (Pty) Ltd, 104 pp.

Elipe, M. & Lopez-Querol, S., 2014. Aeolian sands: Characterization, options of improvement and possible employment in construction - The State-of-the-art. *Construction and Building Materials,* Volume 73, pp. 728-739.

Evans, D., Buchanan, D. & Hall, G., 1994. Dispersion of platinum, palladium, and gold from the Main Sulphide Zone, Great Dyke, Zimbabwe. *Transactions of the Institute of Mining and Metallurgy (Section B: Applied Earth Science),* Volume 103, pp. B57 - B67.

Fabris, A., Keeling, J. & Fidler R.W., 2009. Soil geochemistry as an exploration tool in areas of thick transported cover, Curnamona Province. *Geochemistry: Exploration, Environment, Analysis, pp. 32-40.*

Frangipane, G., Pistolato, M., Molinaroli, E., Guerzoni, S. & Tagliapietra, D., 2009. Comparison of loss on ignition and thermal analysis stepwise methods for determination of sedimentary organic matter. *Aquatic Conservation: Marine and Freshwater Ecosystems,* Volume 19, pp. 24-33.

Flowers, P., Theopold, K., & Langley, R., 2015. *Chemistry* (1st Edition ed.). OpenStax.

Fotheringham, A., 1989. Spatial interaction models: Formulations and applications. Kluwer, Boston: 224pp.

Fuchs, W. & Rose, A., 1974. The geochemical behavior of platinum and palladium in the weathering cycle in the Stillwater complex, Montana. *Economic Geology,* Volume 69, pp. 332-346.

Goldberg, K. & Humayun, M., 2010. The applicability of the Chemical Index of Alteration as a paleoclimatic indicator: An example from the Permian of the Parana basin, Brazil. *Palaeogeography, Palaeoclimatology, Palaeoecology,* Volume 293, pp. 175-183.

Gray, D., Schorin, K. & Butt, C., 1996. Mineral associations of platinum and palladium in lateritic regolith, Ora Banda Sill, Western Australia. *Geochemical Exploration,* Volume 57, pp. 245-255.

Grunsky, E., 2010. The interpretation of geochemical survey data. *Geochemistry: Exploration, Environment, Analysis,* Volume 10, pp. 27-74.

Grunsky, E., Drew, L. & Sutphin, D., 2009. Process recognition in multi-element soil and stream-sediment geochemical data. *Applied Geochemistry,* Volume 24, pp. 1602-1616.

Haddon, I. G., 2005. *The sub-Kalahari geology and tectonic evolution of the Kalahari basin, Southern Africa,* Johannesburg: Unpublished, 343pp.

Hall, G., 1998. Analytical perspective on trace element species of interest in exploration. *Journal of Geochemical Exploration,* pp. 1-19.

Hallberg, J., 1984. A geochemical aid to igneous rock type identification in deeply weathered terrain. *Journal of Geochemical Exploration, 20*, 1-8.

Hamilton, S., 2007. *A prospector's guide to the use of selective leach and other deep penetrating geochemical techniques in mineral exploration,* Ontario: Ontario Geological Survey, 39pp.

Hattori, K., & Cabri, L., 1992. Origin of platinum group mineral nuggets inferred from osmium-isotope study. *Canadian Mineralogist, 30*, 289-301.

Hattori, K., 2004. Using the high mobility of palladium in surface media in exploration for platinum group element deposits: Evidence from the Lac Des Iles region, Northwestern Ontario. *Economic Geology,* Volume 99, pp. 157-171.

Heiri, O., Lotter, A. & Lemcke, G., 2001. Loss on ignition as a method for estimating organic and carbonate content in sediments: reproducibility and comparability of results. *Paleolimnology,* Volume 2001, pp. 101-110.

Hollabaugh, C. L., 2007. Modification of Goldschmidt's geochemical classification of the elements to include arsenic, mercury, and lead as biophile elements. In: D. Sarkar & R. Hannigan, eds. *Concepts and applications in environmental geochemistry.* Amsterdam: Elsevier, pp. 9-31.

Hunter, D., Johnson, M., Anhaeusser, C. & Thomas, R., 2006. Introduction. In: M. Johnson, C. Anhaeusser & R. Thomas, eds. Johannesburg/Council for Geoscience, Pretoria: Geological Society of South Africa, pp. 1-7.

Jenne, E., 1987. *Sediment quality criteria for metals: 11 Review of methods for quantitative determination of important adsorbents and sorbed metals in sediments,* Washington D.C: U.S Environmental Protection Agency Criteria and Standards Division, 34pp.

Khider, K. & McQueen, K., 2005. *Geochemical discrimination of weathered bedrock in the Hermidale-Byrock region of Western NSW,* Canberra: CRC LEME, pp. 170-175.

Lambe, P., 1996. Residual soils. Landslides: investigation and mitigation. *Landslides investigation and mitigation, special report. Transportation Research Board, National Research Council 247* (pp. 507-524). Turner, K. & Schuster, R.

Land, M. & Ohlander, B., 2000. Chemical weathering rates, erosion rates and mobility of major and trace elements in a boreal granitic till. *Aquatic Geochemistry,* Volume 6, pp. 435-460.

Leuta, P. M., 2009. *The framework and geochemistry of regolith overlying the Sirius Platinum Group Elements mineralization in the Stella Layered Intrusion, South Africa,* University of the Western Cape: Unpublished Thesis, 126 pp.

Lewins, J., Hunns, S. & Budenhorst, J., 2008. *The Kalahari Platinum Project,* s.l.: The Southern African Institute of Mining and Metallurgy, pp. 355-366

Li, J. & Heap, A. D., 2014. Spatial interpolation methods applied in environmental sciences: A review. *Environmental modelling and software,* Volume 53, pp. 173-189.

Lintern, M., 1989. *Study of the distribution of gold in soils at Mt Hope, Western Australia.* Division of Exploration geoscience, Perth: CSIRO Australia.

Lintern, M., 2010. Calcrete sampling for mineral exploration. In: X. Chen, M. Lintern & I. Roach, eds. *Calcrete: Characteristics, distribution and use in mineral exploration.* Kensington, Western Australia: CSIRO Mining and Exploration, pp. 13-108.

Lintern, M., 1999. *Study of the distribution of gold in soils at Mt Hope, Western Australia,* Division of Exploration Geoscience, Perth: CSIRO Australia, 36 pp.

Lintern, M., 2002. Calcrete sampling for mineral exploration. *Calcrete: Characteristics, distribution, and use in mineral exploration,* pp. 31-109.

Loftus-Hills, G., & Solomon, M., 1967. Cobalt, nickel and selenium in sulphides as indicators of ore genesis. *Mineralium Deposita, 2*, 228-242.

Lu, G. Y. & Wong, D. W., 2008. An adaptive inverse-distance weighting spatial interpolation technique. *Earth Systems & GeoInformation Sciences,* Volume 34, pp. 1044-1055.

Luoma, S., & Bryan, G., 1981. A statistical assessment of the form of trace metals in oxidised sediments employing chemical extractants. *Science of the Total Environment, 17*, 165-196.

Ma, J., Wei, G., Xu Y., Long W. & Sun W., 2007. Mobilisation and redistribution of major and trace elements during extreme weathering of basalt in Hainan Islands, South China. *Geochimica et Cosmochimica Acta,* Volume 71, pp. 3223-3237.

Mahala, N. (2008). *Comparative analysis of gold by fire assay and aqua regia techniques.* University of the Western Cape: Unpublished Thesis, 37pp.

Maier, W., 2005. Platinum-group element (PGE) deposits and occurrences: Mineralisation styles, genetic concepts, and exploration criteria. *Journal of African Earth Sciences,* Volume 41, pp. 165-191.

Mann, A., 2009. *Ligand based soil extraction geochemistry,* Bentley, Western Australia: s.n., 9 pp.

Mann, A., Birrell, R., Fedikow, M. & de Souza, H., 2005. Vertical ionic migration: Mechanisms, soil anomalies, and sampling depth for mineral exploration. *Geochemistry: Exploration, Environment, Analysis,* Volume 5, pp. 201-210.

Mazzucchelli, R., 1972. Secondary geochemical dispersion patterns associated with nickel sulphide deposits at Kambalda, Western Australia. *Journal of Geochemical Exploration,* Volume 1, pp. 103-116.

McCurdy, D., & Sibakoti, T., 2011. *Hydride Generation Atomic Absorption Spectrophotometry (HGAAS) for the Determination of Lead (Pb).* [cited 2019 Aug 28]. Available from https://www.researchgate.net/publication/313660539: Truman State University CHEM 322 Lab Manual.

McGillis, J., 1967. The silver content of caliche on alluvial fans as a regional guide to areas of silver and gold mineralisation in the basin and range province. Nevada. USA: Part fulfilment of MSc. Thesis. 30pp.

McQueen, K. G., 2006. *Unravelling the regolith with geochemistry,* Australia National University: CRC Leme, pp. 230-235.

McQueen, K., Hill, S. & Foster, K., 1999. The nature and distribution of regolith carbonate accumulations in Southeastern Australia and their potential as a sampling medium in geochemical exploration. *Geochemical Exploration,* Volume 67, pp. 67-82.

McQueen, K. & Scott, K., 2008. Rock weathering and structure of the regolith. In: K. Scott & C. Pain, eds. *Regolith Science.* Canberra: CSIRO, pp. 103-124.

Middelburg, J., van der Weijden, C. & Woittiez, J., 1988. Chemical processes affecting the mobility of major, minor and trace elements during weathering of granitic rocks. *Chemical Geology,* Volume 68, pp. 253-273.

Mitas, L., & Mitasova, H., 1999. Spatial interpolation. In P. Longley, M. Goodchild, D. Maguire, & D. Rhind (Eds.), *Geographic Information Systems. 2nd Edition. Vol 1: Principles and Technical Issues* (pp. 481-492).

Mpuru, T., 2009. *The framework and geochemistry of regolith overlying the Serpens North platinum group elements - mineralization in the Stella greenstone belt, Northwest Province, South Africa,* Cape Town: Unpublished, 106 pp.

Nesbitt, H. & Wilson, R., 1992. Recent chemical weathering of basalts. *American Journal of Science,* Volume 292, pp. 740-777.

Nesbitt, H. & Young, G., 1984. Prediction of some weathering trends of plutonic and volcanic rocks based on thermodynamic and kinetic considerations. *Geochimica et Cosmochimica Acta,* Volume 48, pp. 1523-1534.

Nesbitt, H. & Young, G., 1989. Formation and diagenesis of weathering profiles. *The Journal of Geology,* 97(2), pp. 129-147.

Nesbitt, W. & Young, G., 1982. Early Proterozoic climates and plate motions inferred from major element chemistry of lutites. *Nature,* Volume 299, pp. 715-717.

Netterberg, F., 1967. Some roadmaking properties of South African calcretes. (pp. 77-81). Cape Town: 4th Regional Conference for Africa on Soil Mechanics and Foundation Engeneering.

Netterberg, F., 1969. *Ages of calcretes in South Africa.* CSIR. Pretoria, South African Archaeological Society, pp. 88-92.

Okujeni, C., Akon, P., Baugaard, W. & Langa, N., 2005. Controls of element dispersion in aeolian sand and calcrete-dominated regolith associated with gold mineralisation in the Kraaipan greenstone belt, South Africa. *Geochemistry: Exploration, Environment, Analysis,* Volume 5, pp. 223-231.

Patchineelam, S., 1978. Coprecipitation of heavy metals with $CaCO_3$: an example from polluted Elbe river (FRG). *Chemistry Erde, 37*, 221-225.

Platinum Australia Limited. (2007). *Kalahari Platinum Project.* Unpublished, 75pp

Poujol, M., Anhaeusser, C. & Armstrong, R., 2002. Episodic granitoid emplacement in the Archaean Amalia- Kraaipan terrane, South Africa: confirmation from single zircon U-Pb geochronology. *African Earth Sciences,* Volume 35, pp. 147-161.

Price, J. & Velbel, M., 2003. Chemical weathering indices applied to weathering profiles developed on heterogenous felsic metamorphic parent rocks. *Chemical Geology,* Volume 202, pp. 397-416.

Pye, K. & Tsoar, H., 2009. *Aeolian sand and sand dunes.* s.l.: Springer, 458 pp.

Reeder, S., Taylor, H., Shaw, R. & Demetriades, A., 2006. Introduction to the chemistry and geochemistry of elements. In: R. Salminen, ed. *Geochemical Atlas of Europe.* Espoo, Finland: Geological Survey of Finland, pp. 49-293.

Regassa, A. et al., 2014. Characterising weathering intensity and trends of geological materials in the Gilgel catchment, Southwestern Ethiopia. *Journal of African Earth Sciences,* Volume 99, pp. 568-580.

Robb, L., Brandl, G., Anhaeusser, C. & Poujol, M., 2006. Archaean granitiod intrusions. In: M. Johnson, C. Anhauesser & R. Thomas, eds. *The geology of South Africa.* Johannesburg/Council for Geoscience, Pretoria: The Geological Society of South Africa, pp. 57-94.

Rockware, 2017. *Home: Reference: Solid Modeling Reference: Solid Modeling Methods: Solid Modeling Methods.* [Online]
Available at: https://help.rockware.com/rockworks17/WebHelp/solid_model_algorithms.htm
[Accessed 24 05 2018].

S.A.C.S., 1980. South African Committee for Stratigraphy; Stratigraphy of South Africa, Part 1 (comp L.E. Kent. Lithostratigraphy of the Republic of South Africa. South West Africa/ Namibia & the Republics of Bophuthatswana, Translei & Venda: Handbook OF Geological Survey of South Africa, 8.

Stribryn, B. et al., 2000. Unconventional PGE occurrences and PGE mineralization in the Great Dyke: metallogenic and economic aspects. *Mineralium Deposita,* Volume 35, pp. 260-281.

Sykes, L., Gani, F. & Vally, Z., 2016. Statistical terms Part 1: the meaning of the Mean, and other statistical terms commonly used in medical research. *South African Dental Journal,* 71(6), pp. 274-278.

Tankard, A., Jackson, M., Erikson, K., Hobday, D., Hunter, D., & Minter, W., 1982. Crustal evolution of Southern Africa (3.8 billion years of earth history). Berlin-Heidelberg: Springer. 523pp.

Taylor, G. & Eggleton, R., 2001. *Regolith Geology and Geomorphology.* Chichester; New York: John Wiley & Sons Ltd, 375 pp.

Thompson-Becker, E., & Luoma, S., 1985. Temporal fluctuations in grain size, organic materials and iron concentrations in intertidal surface sediments of San Francisco Bay. *Hydrobiologia, 129*, 91-107.

Tonui, E., de Caritat, P. & Leyh, W., 2003. Geochemical signature of mineralisation in weathered sediments and bedrock, Thunderdome prospect, Broken Hill Region, Western New South Wales, Australia: implications for mineral exploration under cover. *Geochemistry: Exploration, Environment, Analysis,* Volume 3, pp. 263-280.

Torres, J., Santos, P., Ferrari, C., Kremer, C., & Kremerv, E., 2017. Solution chemistry of arsenic anions in the presence of metal cations. *Solution Chemistry,* 46(12), pp. 2231-2247.

Towett, E., Shepherd, K., Tondoh, J., Winowiecki, L., Lulseged, L., Nyambura, M., Sila, A., Vagen, T-G., Cadisch, G., 2015. Total elemental composition of soils in Sub-Saharan Africa and relationship with soil-forming factors. *Geoderma Regional,* Volume 5, pp. 157-168.

Tsalev, D., 2010. Atomic absoption spectrometry (Flame, Electrothermal, Vapour generation) in environmental, biological and food analysis. In L. Simeonov, M. Kochuboski, & B. Simeonova (Eds.), *Environmental heavy metal pollution and effects on child mental development: Risk assessment and prevention strategies* (pp. 171-202). Springer.

Valiani, Z. & Rezaee, P., 2014. Chemical characteristics, provenance determination and genesis conditions of clay deposits of Kahrizak formation (Early- Late Pleistocene), East of Tehran, Iran. *GSTF International Journal of Geological Sciences,* 1. (2), pp. 15-22.

van Berkel, F., 1982. *Geochemical exploration in arid and semi-arid environments,* Rhodes University: Unpublished, 159 pp.

Varga, A., Szakmany, G., Raucsik, B. & Mathe, Z., 2005. Chemical composition, provenance, and early diagenetic processes of playa lake deposits from the Boda Siltstone Formation (Upper Permian), SW Hungary. *Acta Geologica Hungarica,* 48(1), pp. 49-68.

Winter, H., 1976. A lithostratigraphic classification of the Ventersdorp succession. *Geological Society of South Africa Trans, 79*, 31-48.

Xueqiu, W., 1998. Leaching of mobile forms of metals in overburden: development and application. *Journal of Geochemical Exploration,* Volume 61, pp. 39-55.

Zientek, M. L., Causey, J. D., Parks, H. L. & Miller, R. J., 2010. *Platinum-group elements in Southern Africa- Mineral inventory and an assessment of undiscovered mineral resources,* Virginia: US Geological Survey, 126 pp.

8APPENDICES

Appendix 1: Major element data used to calculate the ICV and CIA of the in-situ regolith sample in boreholes KP051- KP059, Serpens North.

Hole ID	From	To	Al2O3	# of mols	Fe2O3	# of mols	MnO	# of mols	MgO	# of mols	CaO	# of mols	Na2O	# of mols	K2O	# of mols	TiO2	# of mols	ICV	CIA
KP051	4	5	18,37	0,18	4,51	0,03	0,00	0,000	1,32	0,03	0,60	0,01	2,12	0,03	2,83	0,03	0,27	0,00	0,77	70,60
KP051	8	9	18,88	0,19	3,12	0,02	0,01	0,000	1,03	0,03	0,57	0,01	2,39	0,04	2,62	0,03	0,21	0,00	0,67	70,76
KP051	11	12	16,15	0,16	6,10	0,04	0,05	0,001	1,71	0,04	0,83	0,01	2,00	0,03	1,78	0,02	0,21	0,00	0,95	70,62
KP051	13	14	10,27	0,10	28,63	0,18	0,22	0,003	4,16	0,10	1,40	0,02	0,02	0,00	0,03	0,00	0,36	0,00	3,13	79,76
KP052	4	5	6,67	0,07	13,06	0,08	0,19	0,003	15,45	0,38	3,21	0,06	0,04	0,00	0,05	0,00	0,19	0,00	8,08	52,85
KP052	7	8	6,67	0,07	14,50	0,09	0,20	0,003	15,33	0,38	3,17	0,06	0,04	0,00	0,02	0,00	0,18	0,00	8,16	53,30
KP052	12	13	5,11	0,05	13,67	0,09	0,19	0,003	21,84	0,54	4,68	0,08	0,12	0,00	0,00	0,00	0,15	0,00	14,30	37,03
KP053	9	10	11,50	0,11	11,04	0,07	0,08	0,001	1,86	0,05	0,55	0,01	0,06	0,00	2,07	0,02	0,53	0,01	1,38	77,47
KP053	12	13	20,36	0,20	4,32	0,03	0,07	0,001	1,25	0,03	0,30	0,01	0,13	0,00	5,83	0,06	0,24	0,00	0,66	74,21
KP054	9	10	15,28	0,15	51,34	0,32	0,07	0,001	3,33	0,08	2,02	0,04	0,37	0,01	0,65	0,01	5,15	0,06	3,46	75,46
KP054	11	12	20,94	0,21	23,68	0,15	0,10	0,001	2,00	0,05	2,69	0,05	1,47	0,02	2,12	0,02	1,61	0,02	1,53	68,56
KP054	13	14	18,41	0,18	7,47	0,05	0,04	0,001	1,31	0,03	2,13	0,04	2,90	0,05	0,76	0,01	0,44	0,01	0,99	66,04
KP056	3	4	14,14	0,14	21,94	0,14	0,21	0,003	2,83	0,07	5,03	0,09	0,52	0,01	0,55	0,01	1,12	0,01	2,37	57,19
KP056	5	6	11,46	0,11	29,92	0,19	0,26	0,004	4,14	0,10	7,46	0,13	0,58	0,01	0,43	0,00	1,43	0,02	4,08	43,34
KP056	9	10	12,15	0,12	25,31	0,16	0,20	0,003	3,02	0,08	5,30	0,09	0,28	0,00	0,35	0,00	0,99	0,01	2,95	53,70
KP056	13	14	11,22	0,11	28,41	0,18	0,16	0,002	4,94	0,12	6,78	0,12	0,66	0,01	0,45	0,00	1,24	0,02	4,13	44,69
KP057	5	6	12,81	0,13	33,14	0,21	0,13	0,002	1,70	0,04	2,29	0,04	0,21	0,00	0,68	0,01	2,11	0,03	2,62	70,90
KP057	9	10	17,61	0,17	28,97	0,18	0,10	0,001	1,62	0,04	4,38	0,08	1,12	0,02	1,15	0,01	2,33	0,03	2,09	61,48
KP057	13	14	20,44	0,20	16,91	0,11	0,09	0,001	1,74	0,04	5,35	0,10	1,56	0,03	0,93	0,01	0,84	0,01	1,45	60,58
KP058	2	3	9,19	0,09	30,32	0,19	0,50	0,007	0,33	0,01	0,67	0,01	0,13	0,00	0,44	0,00	0,69	0,01	2,58	82,82
KP058	4	5	17,99	0,18	21,37	0,13	0,13	0,002	1,83	0,05	3,88	0,07	0,53	0,01	1,09	0,01	1,08	0,01	1,61	66,42
KP058	6	7	17,33	0,17	19,18	0,12	0,12	0,002	1,80	0,04	3,56	0,06	0,58	0,01	0,97	0,01	1,12	0,01	1,55	67,21
KP058	8	9	17,41	0,17	19,49	0,12	0,09	0,001	2,21	0,05	4,22	0,08	0,51	0,01	0,80	0,01	0,92	0,01	1,65	64,99
KP058	12	13	17,31	0,17	10,48	0,07	0,08	0,001	2,06	0,05	4,34	0,08	1,36	0,02	0,87	0,01	0,43	0,01	1,37	61,00
KP058	13	14	10,47	0,10	54,67	0,34	0,16	0,002	2,80	0,07	1,22	0,02	0,07	0,00	0,32	0,00	4,06	0,05	4,79	79,59
KP059	5	6	9,58	0,09	17,61	0,11	0,20	0,003	7,61	0,19	2,64	0,05	0,04	0,00	0,09	0,00	0,25	0,00	3,76	65,92
KP059	9	10	8,53	0,08	20,71	0,13	0,00	0,000	10,35	0,26	2,11	0,04	0,08	0,00	0,04	0,00	0,20	0,00	5,12	68,00
KP059	13	14	5,35	0,05	13,93	0,09	0,13	0,002	20,24	0,50	5,08	0,09	0,10	0,00	0,00	0,00	0,13	0,00	13,06	36,29

Appendix 2:Major element data used to calculate the ICV and CIA in boreholes KP060- KP067, Serpens North.

Hole ID	From	To	Al2O3	# of mols	Fe2O3	# of mols	MnO	# of mols	MgO	# of mols	CaO	# of mols	Na2O	# of mols	K2O	# of mols	TiO2	# of mols	ICV	CIA
KP060	2	3	5,15	0,05	24,06	0,15	0,08	0,001	0,22	0,01	0,09	0,00	0,05	0,00	0,30	0,00	0,25	0,00	3,29	90,13
KP060	4	5	7,64	0,07	7,25	0,05	0,07	0,001	0,67	0,02	0,23	0,00	0,06	0,00	1,11	0,01	0,31	0,00	1,12	81,73
KP060	6	7	9,46	0,09	8,39	0,05	0,06	0,001	1,32	0,03	0,24	0,00	0,04	0,00	1,66	0,02	0,29	0,00	1,21	80,49
KP060	8	9	11,24	0,11	27,44	0,17	0,00	0,000	3,86	0,10	0,87	0,02	0,01	0,00	2,04	0,02	0,83	0,01	2,86	74,66
KP060	11	12	13,40	0,13	23,40	0,15	0,00	0,000	3,42	0,08	1,19	0,02	0,03	0,00	2,96	0,03	0,89	0,01	2,25	71,25
KP060	14	15	9,61	0,09	24,89	0,16	0,00	0,000	3,55	0,09	1,33	0,02	0,05	0,00	0,23	0,00	0,97	0,01	3,00	77,86
KP061	6	7	18,40	0,18	10,07	0,06	0,06	0,001	2,49	0,06	2,27	0,04	1,40	0,02	1,15	0,01	0,41	0,01	1,14	70,55
KP061	11	12	15,66	0,15	16,07	0,10	0,13	0,002	3,84	0,10	6,38	0,11	0,73	0,01	0,45	0,00	0,36	0,00	2,16	54,11
KP062	3	4	3,23	0,03	26,39	0,17	0,08	0,001	0,25	0,01	0,09	0,00	0,03	0,00	0,09	0,00	0,15	0,00	5,61	91,33
KP062	6	7	12,24	0,12	16,93	0,11	0,14	0,002	5,66	0,14	4,22	0,08	0,17	0,00	0,18	0,00	0,30	0,00	2,77	60,05
KP062	9	10	14,05	0,14	17,61	0,11	0,12	0,002	3,15	0,08	1,16	0,02	0,06	0,00	1,23	0,01	0,35	0,00	1,66	79,81
KP062	12	13	20,28	0,20	5,63	0,04	0,00	0,000	2,26	0,06	0,43	0,01	0,19	0,00	5,12	0,05	0,27	0,00	0,80	75,37
KP063	4	5	13,33	0,13	24,25	0,15	0,14	0,002	2,51	0,06	3,20	0,06	0,20	0,00	0,60	0,01	0,96	0,01	2,26	66,22
KP063	6	7	10,34	0,10	31,83	0,20	0,00	0,000	2,32	0,06	3,46	0,06	0,09	0,00	0,36	0,00	1,16	0,01	3,33	60,25
KP063	8	9	12,15	0,12	26,87	0,17	0,16	0,002	3,51	0,09	4,38	0,08	0,36	0,01	0,68	0,01	1,30	0,02	3,06	56,65
KP063	10	11	18,73	0,18	18,68	0,12	0,09	0,001	2,05	0,05	5,40	0,10	1,50	0,02	1,24	0,01	1,61	0,02	1,76	57,90
KP063	13	14	16,05	0,16	21,95	0,14	0,02	0,000	2,94	0,07	5,80	0,10	1,21	0,02	0,79	0,01	0,94	0,01	2,25	54,50
KP064	3	4	18,88	0,19	16,54	0,10	0,09	0,001	1,63	0,04	3,76	0,07	0,75	0,01	0,81	0,01	1,15	0,01	1,34	67,85
KP064	5	6	20,75	0,20	15,91	0,10	0,06	0,001	1,96	0,05	5,35	0,10	1,26	0,02	0,95	0,01	1,03	0,01	1,41	61,82
KP064	7	8	18,91	0,19	22,29	0,14	0,09	0,001	2,35	0,06	4,72	0,08	1,32	0,02	1,23	0,01	2,16	0,03	1,86	61,01
KP064	9	10	17,98	0,18	23,76	0,15	0,10	0,001	2,84	0,07	4,12	0,07	0,82	0,01	0,71	0,01	1,61	0,02	1,90	65,16
KP064	11	12	16,38	0,16	22,25	0,14	0,13	0,002	2,77	0,07	4,79	0,09	0,83	0,01	0,77	0,01	1,64	0,02	2,10	60,05
KP064	13	14	11,61	0,11	24,50	0,15	0,17	0,002	4,12	0,10	4,59	0,08	0,23	0,00	0,08	0,00	0,83	0,01	3,11	56,88
KP065	7	8	16,82	0,17	24,97	0,16	0,08	0,001	2,42	0,06	5,07	0,09	1,05	0,02	1,01	0,01	1,82	0,02	2,17	58,28
KP065	12	13	15,21	0,15	21,92	0,14	0,10	0,001	3,09	0,08	6,22	0,11	0,68	0,01	0,37	0,00	1,32	0,02	2,40	54,24
KP066	3	4	11,42	0,11	28,07	0,18	0,00	0,000	2,28	0,06	2,82	0,05	0,12	0,00	0,28	0,00	1,35	0,02	2,72	66,97
KP066	7	8	9,58	0,09	27,74	0,17	0,00	0,000	3,45	0,09	3,60	0,06	0,18	0,00	0,09	0,00	0,88	0,01	3,60	58,04
KP066	10	11	10,09	0,10	29,87	0,19	0,24	0,003	3,86	0,10	5,35	0,10	0,21	0,00	0,12	0,00	1,41	0,02	4,08	49,76
KP066	14	15	11,42	0,11	22,08	0,14	0,17	0,002	3,58	0,09	5,76	0,10	0,72	0,01	0,62	0,01	1,12	0,01	3,25	48,10
KP067	3	4	13,89	0,14	33,64	0,21	0,16	0,002	1,84	0,05	2,43	0,04	0,24	0,00	0,52	0,01	2,43	0,03	2,51	72,10
KP067	4	5	12,48	0,12	35,47	0,22	0,18	0,003	1,97	0,05	2,93	0,05	0,17	0,00	0,29	0,00	2,07	0,03	2,92	67,82
KP067	6	7	18,38	0,18	23,31	0,15	0,11	0,002	1,66	0,04	4,95	0,09	1,09	0,02	0,87	0,01	1,50	0,02	1,79	61,03
KP067	8	9	14,16	0,14	30,05	0,19	0,07	0,001	2,58	0,06	4,60	0,08	0,80	0,01	0,43	0,00	1,63	0,02	2,69	58,24
KP067	10	11	14,14	0,14	40,80	0,26	0,19	0,003	2,74	0,07	3,37	0,06	0,73	0,01	0,41	0,00	3,57	0,04	3,22	64,56
KP067	13	14	17,52	0,17	21,43	0,13	0,07	0,001	1,98	0,05	5,61	0,10	1,45	0,02	0,65	0,01	1,15	0,01	1,92	56,86
KP069	3	4	8,91	0,09	31,48	0,20	0,16	0,002	3,34	0,08	1,94	0,03	0,05	0,00	0,25	0,00	0,53	0,01	3,74	69,67
KP069	7	8	12,42	0,12	18,02	0,11	0,27	0,004	3,84	0,10	5,84	0,10	0,65	0,01	0,66	0,01	1,67	0,02	2,91	50,04
KP069	10	11	8,87	0,09	31,34	0,20	0,00	0,000	2,56	0,06	3,21	0,06	0,06	0,00	0,19	0,00	1,08	0,01	3,84	59,13
KP069	13	14	9,10	0,09	29,89	0,19	0,24	0,003	3,42	0,08	6,38	0,11	0,17	0,00	0,13	0,00	1,39	0,02	4,60	43,11

Appendix 3: Major element data used to calculate the ICV and CIA of boreholes KP069- KP087, Serpens North.

Hole ID	From	To	Al2O3	# of mols	Fe2O3	# of mols	MnO	# of mols	MgO	# of mols	CaO ǂ	of mols	Na2O ǂ	of mols	K2O	# of mols	TiO2	# of mols	ICV	CIA
KP072	3	4	8,78	0,09	25,13	0,16	0,15	0,002	3,41	0,08	3,41	0,06	0,43	0,01	0,21	0,00	0,47	0,01	3,71	55,22
KP072	5	6	9,34	0,09	24,34	0,15	0,00	0,000	4,78	0,12	3,02	0,05	0,06	0,00	0,07	0,00	1,30	0,02	3,74	62,25
KP072	8	9	10,87	0,11	23,70	0,15	0,17	0,002	3,67	0,09	3,87	0,07	0,19	0,00	0,08	0,00	0,64	0,01	3,03	59,40
KP072	12	13	11,50	0,11	11,46	0,07	0,08	0,001	4,04	0,10	1,10	0,02	0,58	0,01	0,16	0,00	0,11	0,00	1,82	78,62
KP075	7	8	20,93	0,21	3,60	0,02	0,04	0,001	2,43	0,06	3,00	0,05	2,65	0,04	1,66	0,02	0,49	0,01	0,99	64,32
KP075	9	10	17,77	0,17	18,52	0,12	0,00	0,000	1,92	0,05	1,23	0,02	0,58	0,01	1,04	0,01	0,51	0,01	1,22	80,48
KP075	13	14	12,89	0,13	22,69	0,14	0,00	0,000	3,49	0,09	3,74	0,07	0,27	0,00	0,38	0,00	0,82	0,01	2,48	62,74
KP079	3	4	12,64	0,12	35,29	0,22	0,18	0,002	2,41	0,06	2,46	0,04	0,11	0,00	0,27	0,00	2,46	0,03	2,92	71,92
KP079	5	6	11,40	0,11	34,51	0,22	0,14	0,002	3,38	0,08	2,62	0,05	0,17	0,00	0,61	0,01	2,37	0,03	3,47	66,64
KP079	7	8	12,69	0,12	26,20	0,16	0,00	0,000	2,26	0,06	4,32	0,08	0,35	0,01	0,25	0,00	1,21	0,02	2,58	59,30
KP079	9	10	12,27	0,12	41,46	0,26	0,00	0,000	3,68	0,09	3,33	0,06	0,51	0,01	0,37	0,00	3,91	0,05	3,92	62,72
KP079	11	12	18,59	0,18	17,48	0,11	0,10	0,001	2,26	0,06	5,98	0,11	1,29	0,02	1,44	0,02	0,94	0,01	1,76	56,10
KP079	13	14	12,40	0,12	36,35	0,23	0,00	0,000	3,34	0,08	3,19	0,06	0,33	0,01	0,43	0,00	2,92	0,04	3,40	64,56
KP082	2	3	14,76	0,14	11,81	0,07	0,04	0,001	1,32	0,03	0,30	0,01	0,16	0,00	3,24	0,03	0,17	0,00	1,05	77,46
KP082	5	6	11,16	0,11	21,19	0,13	0,04	0,001	1,70	0,04	0,58	0,01	0,06	0,00	1,60	0,02	0,14	0,00	1,88	79,40
KP082	8	9	5,42	0,05	33,81	0,21	0,82	0,012	1,65	0,04	0,39	0,01	0,04	0,00	0,23	0,00	0,17	0,00	5,21	84,01
KP082	13	14	10,98	0,11	24,22	0,15	0,13	0,002	4,24	0,11	3,76	0,07	0,04	0,00	0,01	0,00	0,82	0,01	3,12	61,40
KP084	3	4	12,26	0,12	23,69	0,15	0,17	0,002	2,53	0,06	3,53	0,06	0,15	0,00	0,27	0,00	1,16	0,01	2,46	63,80
KP084	6	7	11,56	0,11	22,21	0,14	0,16	0,002	3,75	0,09	3,59	0,06	0,14	0,00	0,15	0,00	0,72	0,01	2,75	62,58
KP084	11	12	11,98	0,12	18,70	0,12	0,16	0,002	4,34	0,11	4,23	0,08	0,31	0,00	0,08	0,00	0,68	0,01	2,70	59,12
KP087	6	7	13,70	0,13	29,31	0,18	0,00	0,000	2,30	0,06	1,11	0,02	0,13	0,00	0,69	0,01	0,98	0,01	2,10	82,18
KP087	8	9	13,30	0,13	40,60	0,25	0,00	0,000	2,52	0,06	1,10	0,02	0,11	0,00	1,01	0,01	2,20	0,03	2,89	80,21
KP087	10	11	16,39	0,16	17,15	0,11	0,10	0,001	3,65	0,09	4,38	0,08	0,94	0,02	0,72	0,01	0,82	0,01	1,93	61,43
KP087	13	14	8,01	0,08	30,99	0,19	0,00	0,000	4,31	0,11	1,19	0,02	0,05	0,00	0,08	0,00	0,48	0,01	4,20	77,40

Appendix 4: Major element concentrations in residual soils and calculations of the CIA and ICA used to estimate the degree of weathering within the Sirius deposit.

Hole ID	From	To	Al2O3	ǂ of mols	Fe2O3	ǂ of mols	MnO	ǂ of mols	MgO	ǂ of mols	CaO	ǂ of mols	Na2O	ǂ of mols	K2O	ǂ of mols	TiO2	ǂ of mols	ICV	CIA
KP090	3	4	11,62	0,11	23,52	0,15	0,41	0,006	2,04	0,05	1,16	0,02	0,28	0,00	0,54	0,006	0,80	0,01	2,14	70,62
KP090	4	5	12,32	0,12	27,59	0,17	0,00	0,000	6,46	0,16	3,16	0,06	0,53	0,01	0,19	0,002	1,25	0,02	3,44	79,76
KP090	5	6	11,61	0,11	27,94	0,17	*	*	7,23	0,18	4,27	0,08	0,73	0,01	0,13	0,001	1,57	0,02	*	83,80
KP090	6	7	11,09	0,11	27,12	0,17	*	*	8,74	0,22	3,72	0,07	0,25	0,00	0,11	0,001	1,16	0,01	*	75,15
KP090	7	8	12,92	0,13	31,59	0,20	*	*	6,52	0,16	4,07	0,07	1,47	0,02	0,21	0,002	1,86	0,02	*	52,85
KP090	8	9	14,46	0,14	30,46	0,19	*	*	7,30	0,18	4,04	0,07	1,92	0,03	0,25	0,003	1,59	0,02	*	53,30
KP090	9	10	14,55	0,14	30,48	0,19	*	*	7,89	0,20	4,68	0,08	2,06	0,03	0,24	0,003	1,57	0,02	*	37,03
KP092	2	3	8,72	0,09	11,00	0,07	*	*	2,61	0,06	1,96	0,03	0,16	0,00	0,46	0,005	0,65	0,01	*	80,32
KP092	3	4	10,72	0,11	28,80	0,18	*	*	2,93	0,07	2,09	0,04	0,52	0,01	0,66	0,007	1,23	0,02	*	77,47
KP092	4	5	12,55	0,12	34,14	0,21	*	*	5,54	0,14	1,70	0,03	1,13	0,02	0,46	0,005	1,54	0,02	*	74,21
KP092	5	6	12,55	0,12	36,56	0,23	*	*	5,72	0,14	2,36	0,04	1,20	0,02	0,41	0,004	1,82	0,02	*	84,87
KP092	6	7	14,06	0,14	34,06	0,21	*	*	5,70	0,14	1,84	0,03	1,56	0,03	0,74	0,008	1,19	0,01	*	87,65
KP092	7	8	13,94	0,14	34,60	0,22	*	*	7,00	0,17	1,91	0,03	1,70	0,03	0,58	0,006	1,38	0,02	*	74,40
KP092	8	9	13,35	0,13	37,32	0,23	*	*	7,54	0,19	2,05	0,04	1,74	0,03	0,32	0,003	1,63	0,02	*	69,46
KP092	9	10	13,64	0,13	36,93	0,23	*	*	6,73	0,17	2,55	0,05	2,01	0,03	0,25	0,003	1,52	0,02	*	70,55
KP096	1	2	6,54	0,06	7,29	0,05	*	*	2,46	0,06	23,37	0,42	0,08	0,00	0,47	0,005	0,56	0,01	*	68,56
KP096	2	3	9,33	0,09	12,01	0,08	0,01	0,000	2,36	0,06	3,70	0,07	0,18	0,00	0,70	0,007	0,88	0,01	2,42	66,04
KP096	3	4	8,52	0,08	10,33	0,06	0,05	0,001	2,46	0,06	1,82	0,03	0,10	0,00	0,58	0,006	0,70	0,01	2,10	77,25
KP096	4	5	8,77	0,09	11,00	0,07	0,04	0,001	2,56	0,06	1,50	0,03	0,11	0,00	0,60	0,006	0,70	0,01	2,05	57,19
KP096	5	6	9,03	0,09	20,27	0,13	0,07	0,001	2,99	0,07	2,73	0,05	0,21	0,00	0,54	0,006	0,72	0,01	3,04	43,34
KP096	6	7	9,90	0,10	31,88	0,20	0,24	0,003	6,97	0,17	3,35	0,06	0,47	0,01	0,18	0,002	0,89	0,01	4,70	53,70
KP096	7	8	9,34	0,09	30,13	0,19	0,12	0,002	5,89	0,15	5,70	0,10	0,63	0,01	0,07	0,001	1,66	0,02	5,13	44,69
KP096	8	9	9,91	0,10	35,47	0,22	0,14	0,002	8,82	0,22	3,48	0,06	0,60	0,01	0,02	0,000	1,11	0,01	5,44	86,54
KP096	9	10	10,05	0,10	37,27	0,23	0,17	0,002	9,41	0,23	3,30	0,06	0,73	0,01	0,02	0,000	1,52	0,02	5,67	87,79
KP098	1	2	4,49	0,04	6,39	0,04	*	*	2,46	0,06	26,21	0,47	0,03	0,00	0,38	0,004	0,33	0,00	*	61,48
KP098	2	3	4,64	0,05	6,30	0,04	*	*	3,54	0,09	28,21	0,50	0,01	0,00	0,35	0,004	0,30	0,00	*	60,58
KP098	3	4	4,49	0,04	7,87	0,05	*	*	3,63	0,09	27,69	0,49	0,03	0,00	0,34	0,004	0,32	0,00	*	83,55
KP098	4	5	5,46	0,05	9,50	0,06	*	*	3,09	0,08	21,22	0,38	0,05	0,00	0,39	0,004	0,43	0,01	*	84,12
KP098	5	6	8,67	0,09	7,74	0,05	*	*	3,19	0,08	1,94	0,03	0,14	0,00	0,84	0,009	0,94	0,01	*	82,82
KP098	6	7	8,14	0,08	6,27	0,04	*	*	2,11	0,05	1,65	0,03	0,19	0,00	0,87	0,009	0,84	0,01	*	66,42
KP098	7	8	10,31	0,10	14,97	0,09	*	*	4,20	0,10	4,74	0,08	0,68	0,01	0,54	0,006	1,01	0,01	*	67,21
KP098	8	9	11,31	0,11	20,26	0,13	*	*	5,64	0,14	5,27	0,09	1,35	0,02	0,16	0,002	1,03	0,01	*	64,99

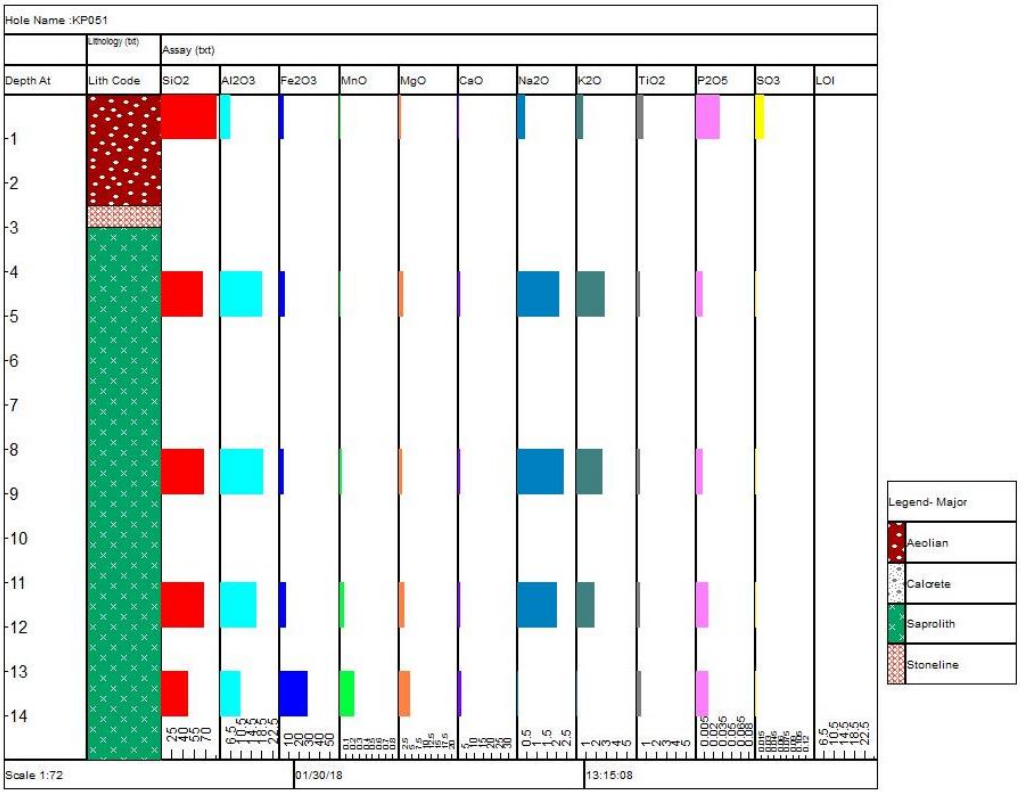

Appendix 5:The downhole distribution of major elements in borehole KP051 in Serpens North.

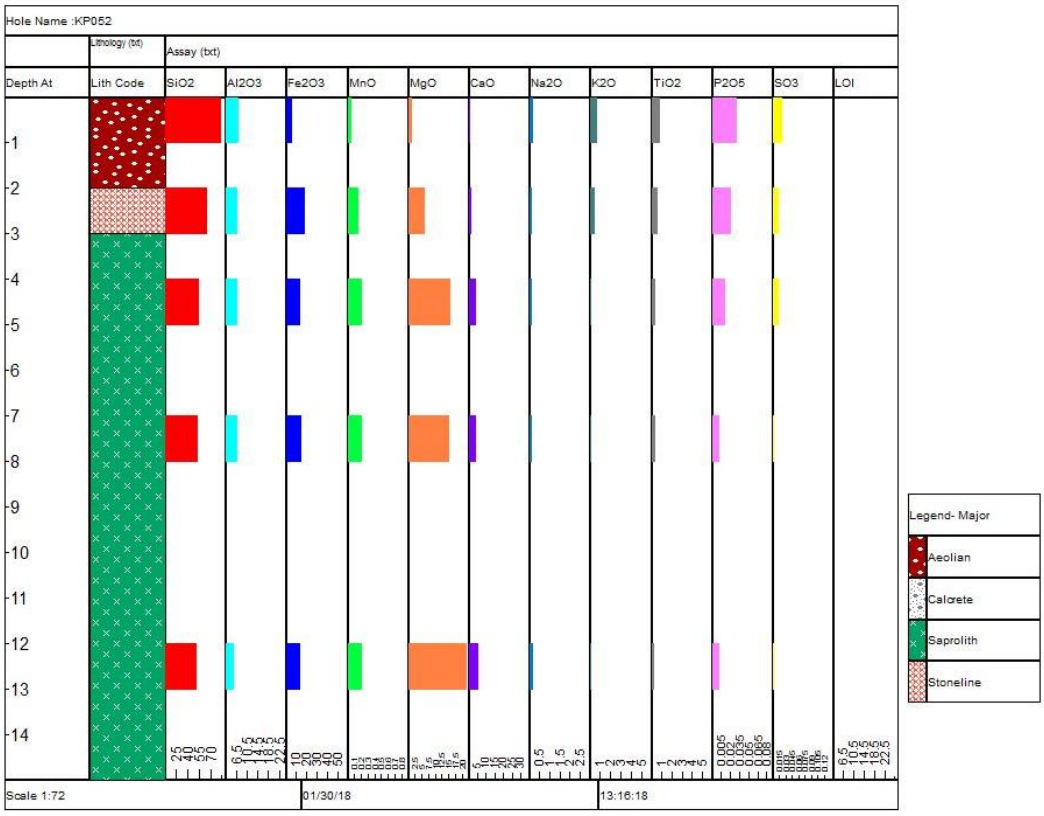

Appendix 6: Major element distribution in borehole KP052 IN Serpens North.

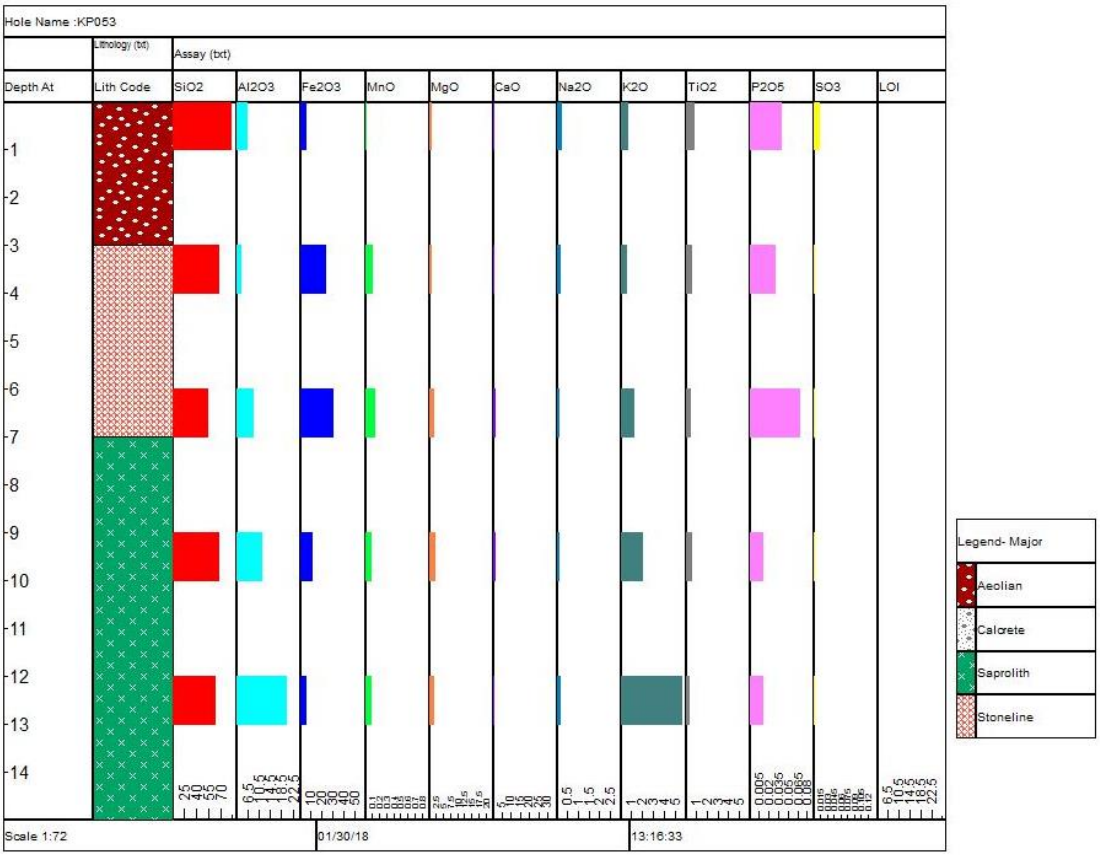

Appendix 7: Downhole concentrations of major elements in KP053 in Serpens North.

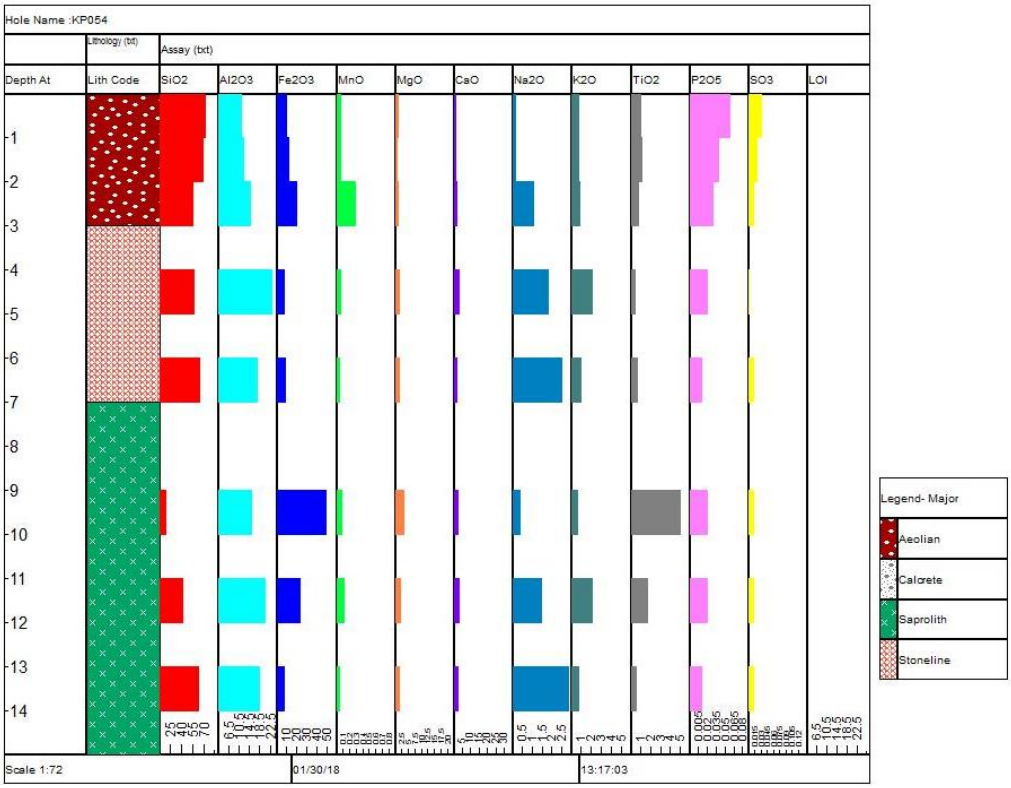

Appendix 8: The downhole distribution of major elements in borehole KP054, Serpens North.

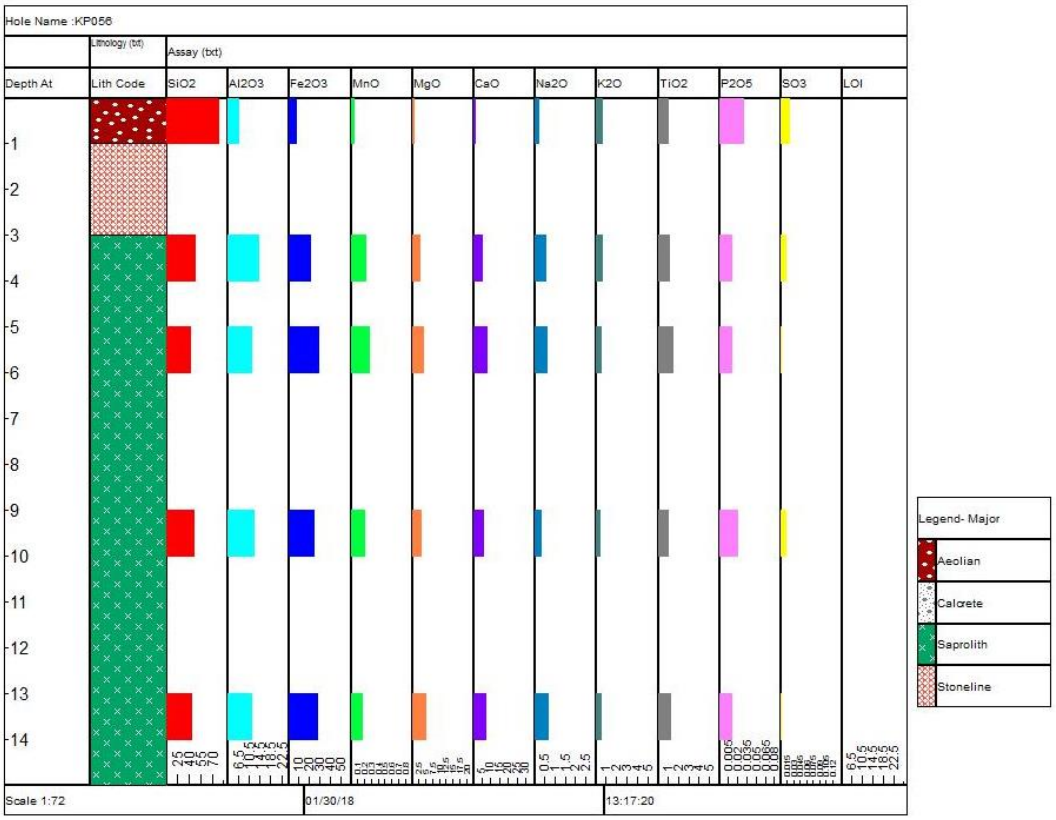

Appendix 9: The distribution of major elements in borehole KP056, in Serpens North.

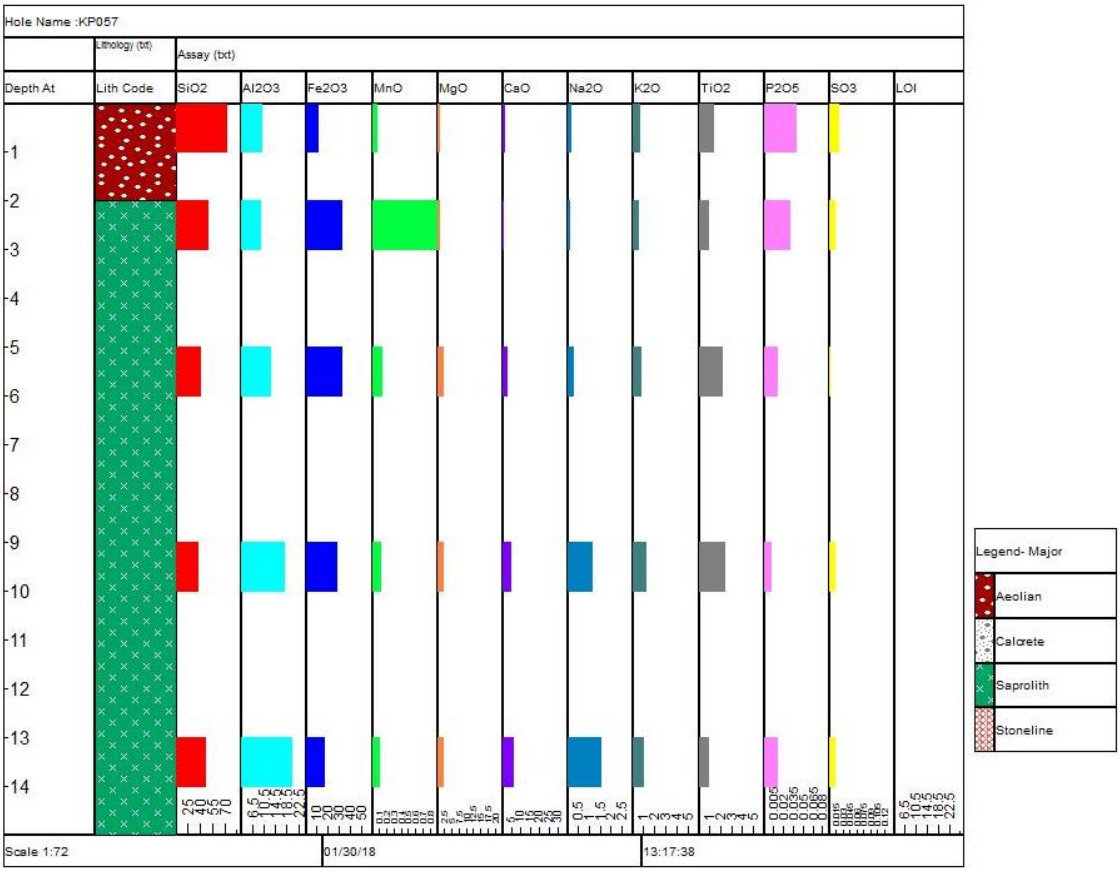

Appendix 10: The downhole distribution of major elements in borehole KP057, Serpens North.

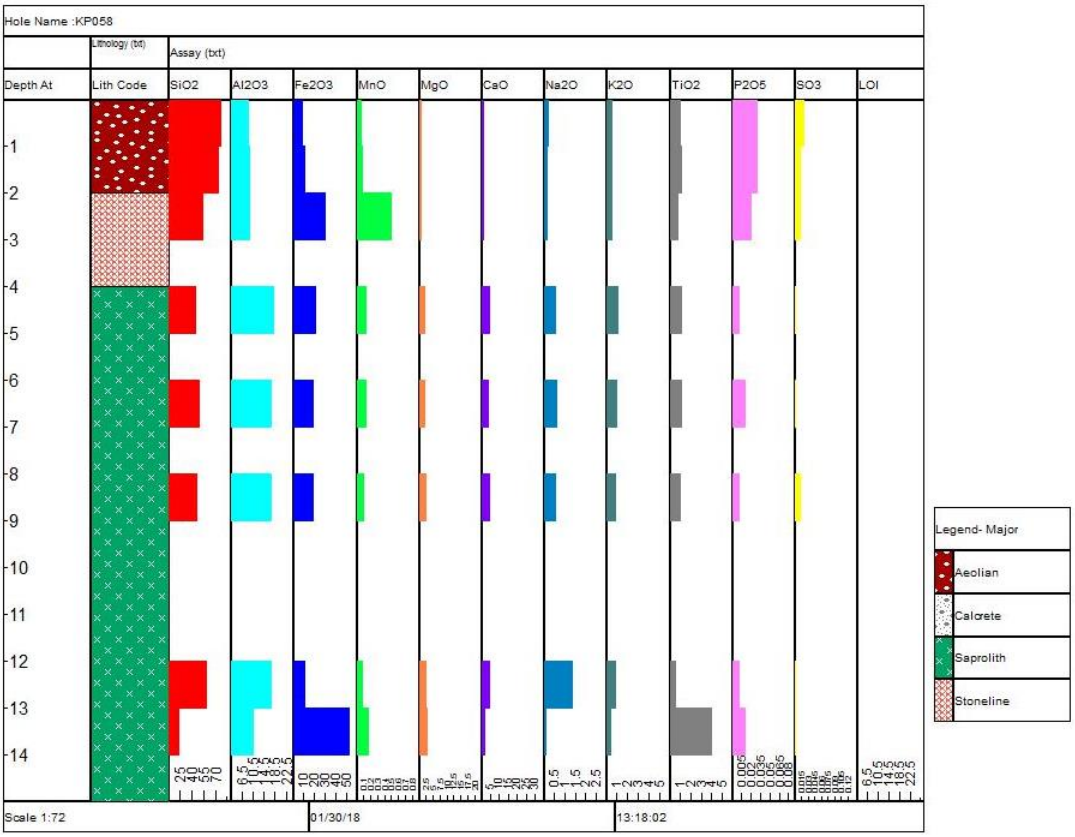

Appendix 11: The downhole distribution of major elements in borehole KP058, Serpens North.

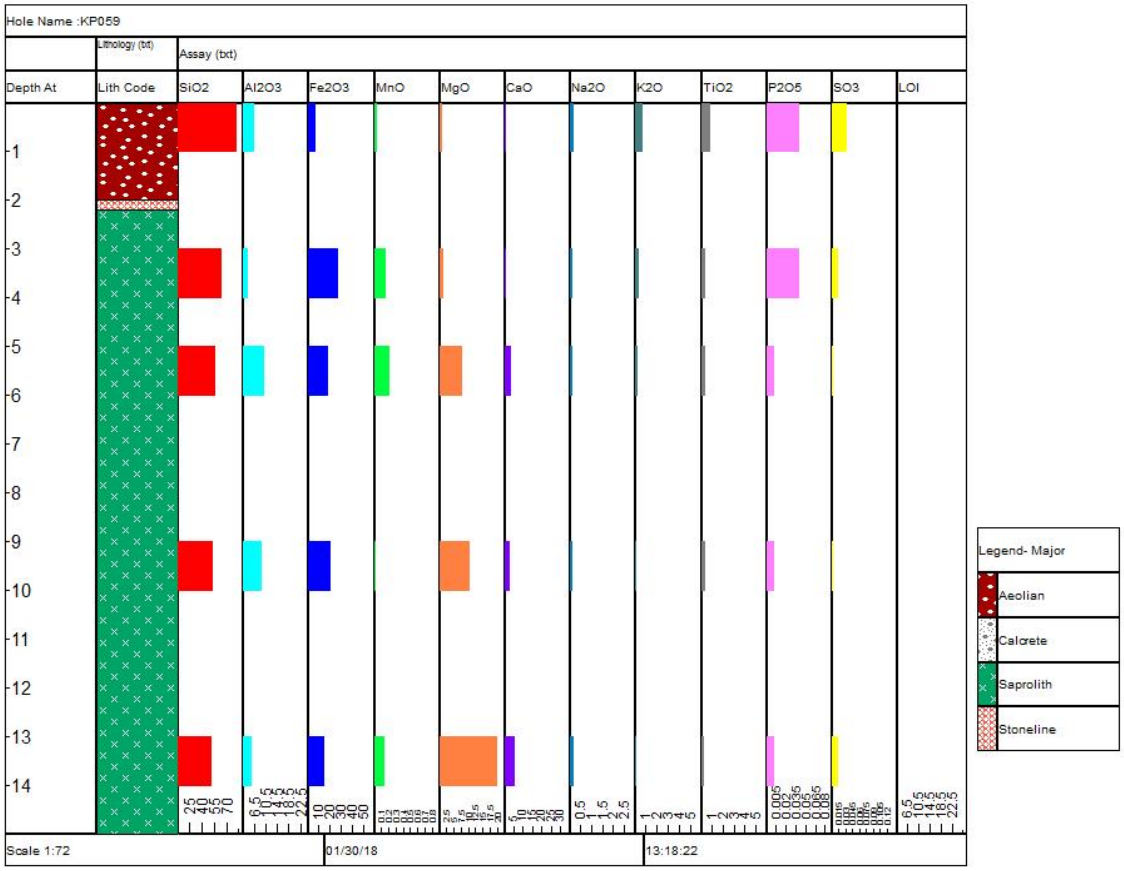

Appendix 12: The downhole distribution of major elements in borehole KP059, Serpens North.

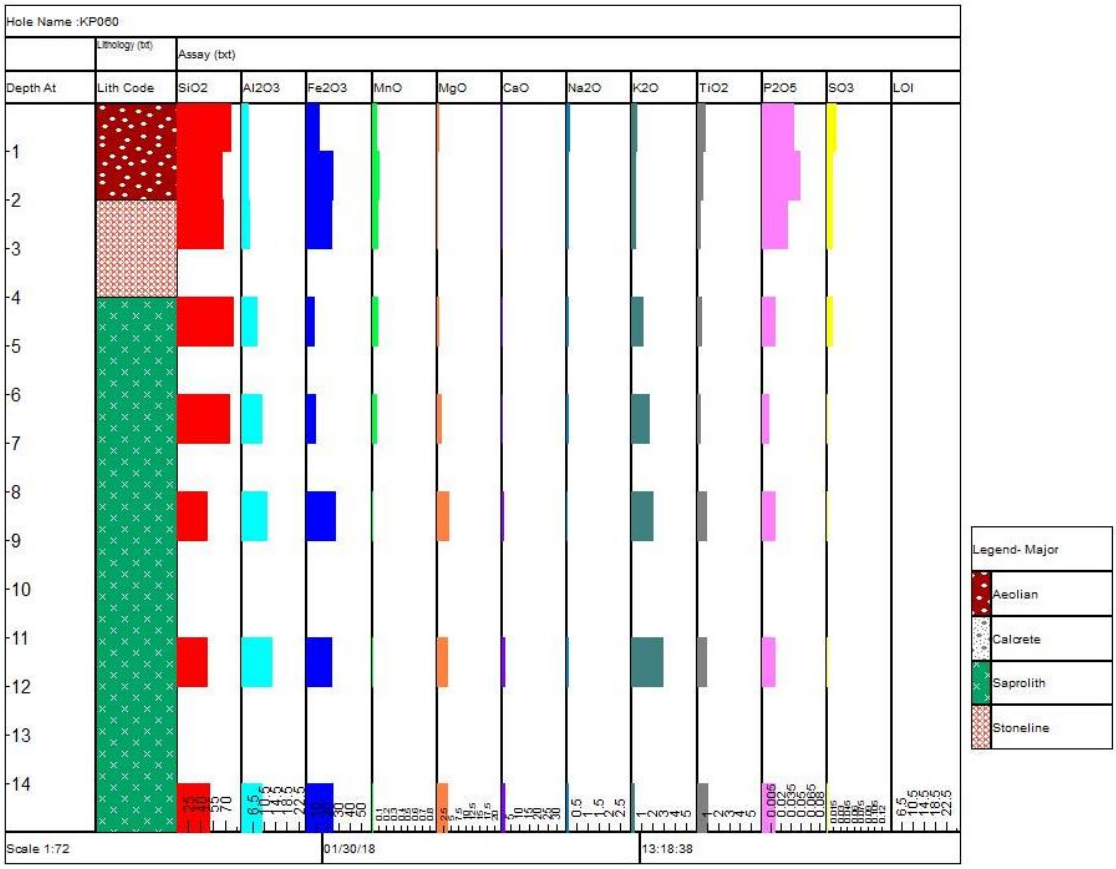

Appendix 13: The downhole distribution of major elements in borehole KP060, Serpens North.

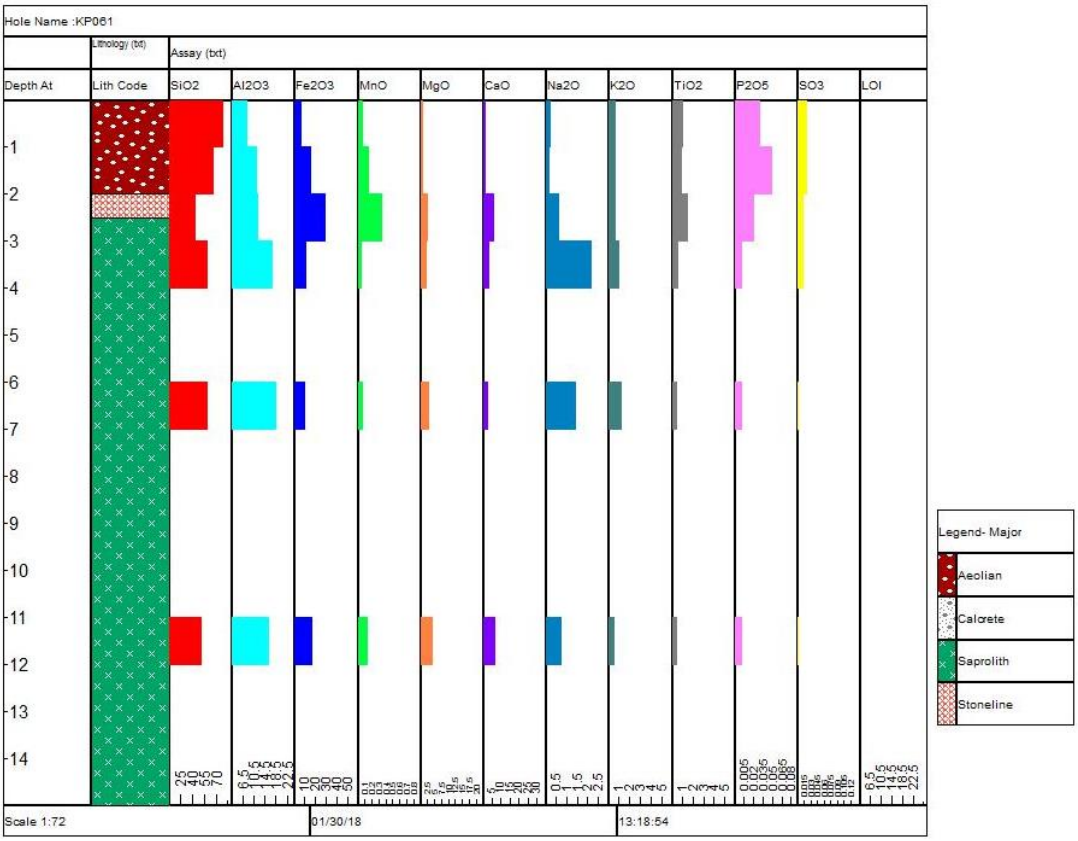

Appendix 14: The downhole distribution of major elements in borehole KP061, Serpens North.

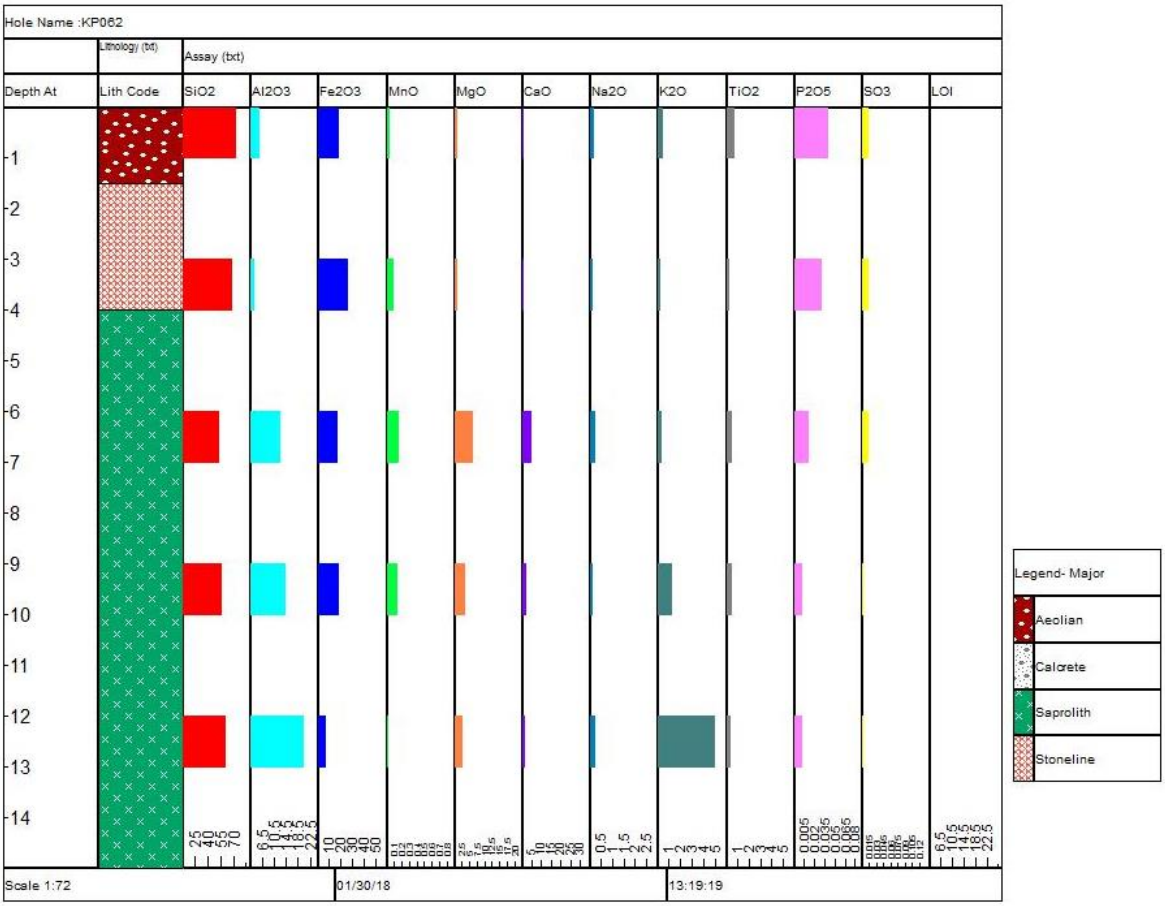

Appendix 15: The downhole distribution of major elements in borehole KP062, Serpens North.

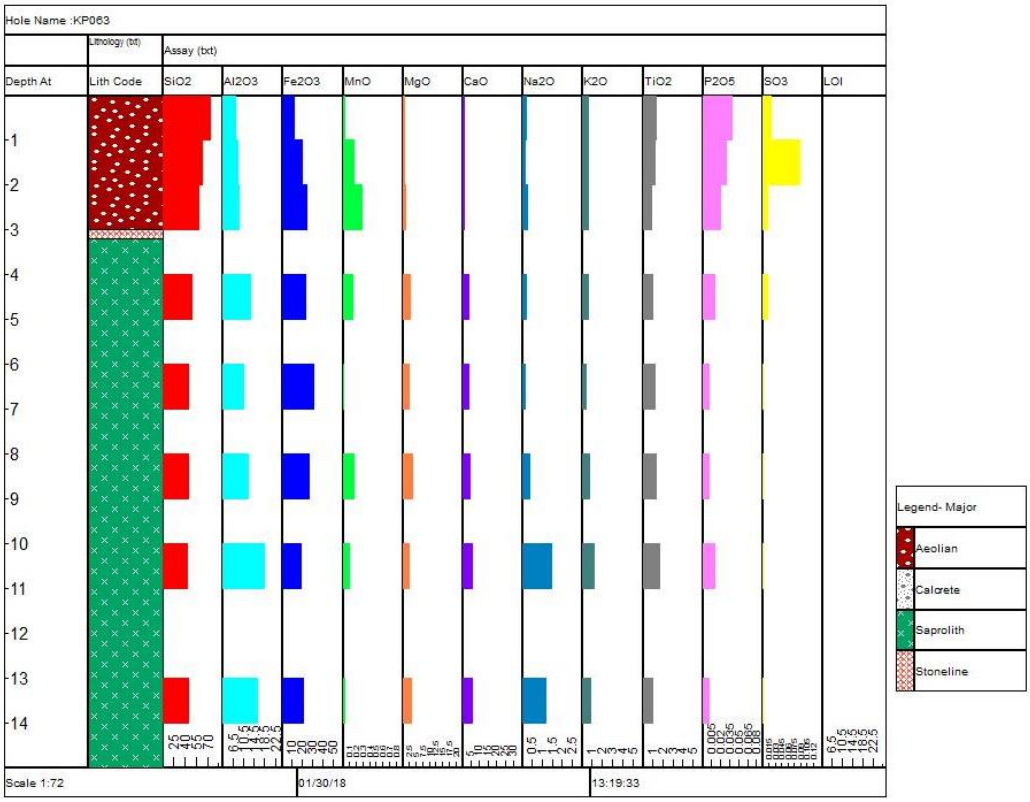

Appendix 16: The downhole distribution of major elements in borehole KP063, Serpens North.

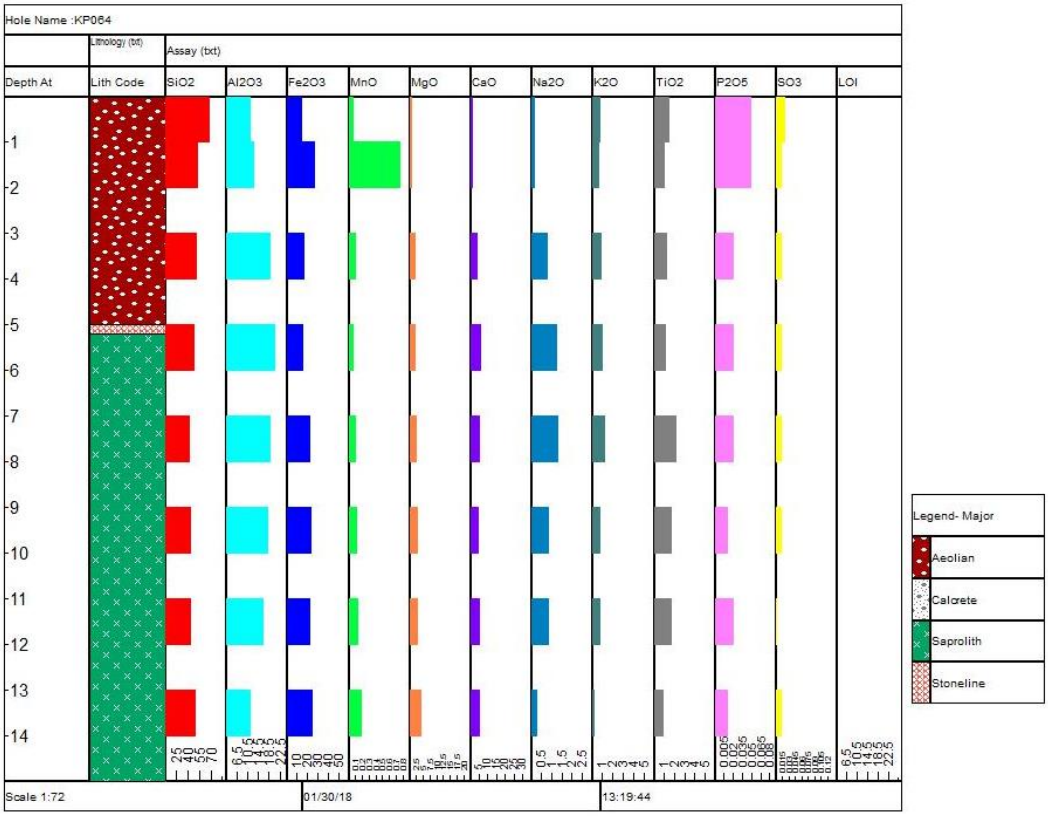

Appendix 17: The downhole distribution of major elements in borehole KP064, Serpens North.

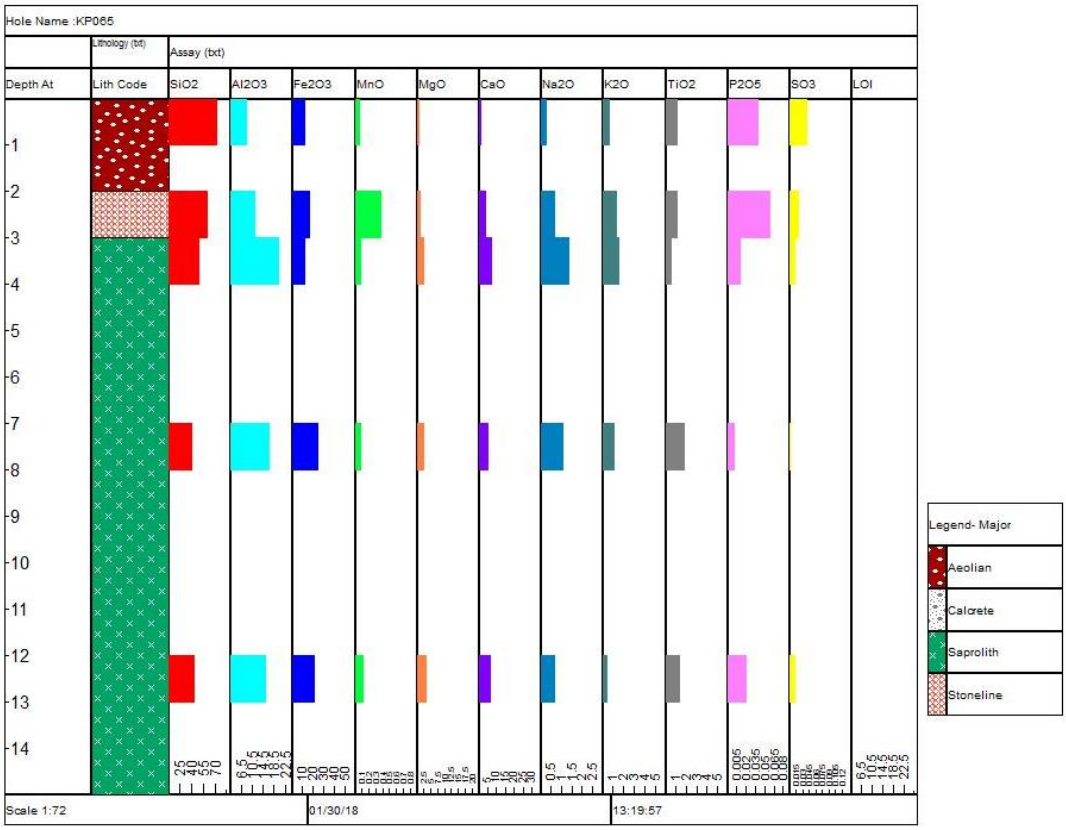

Appendix 18: The downhole distribution of major elements in borehole KP065, Serpens North.

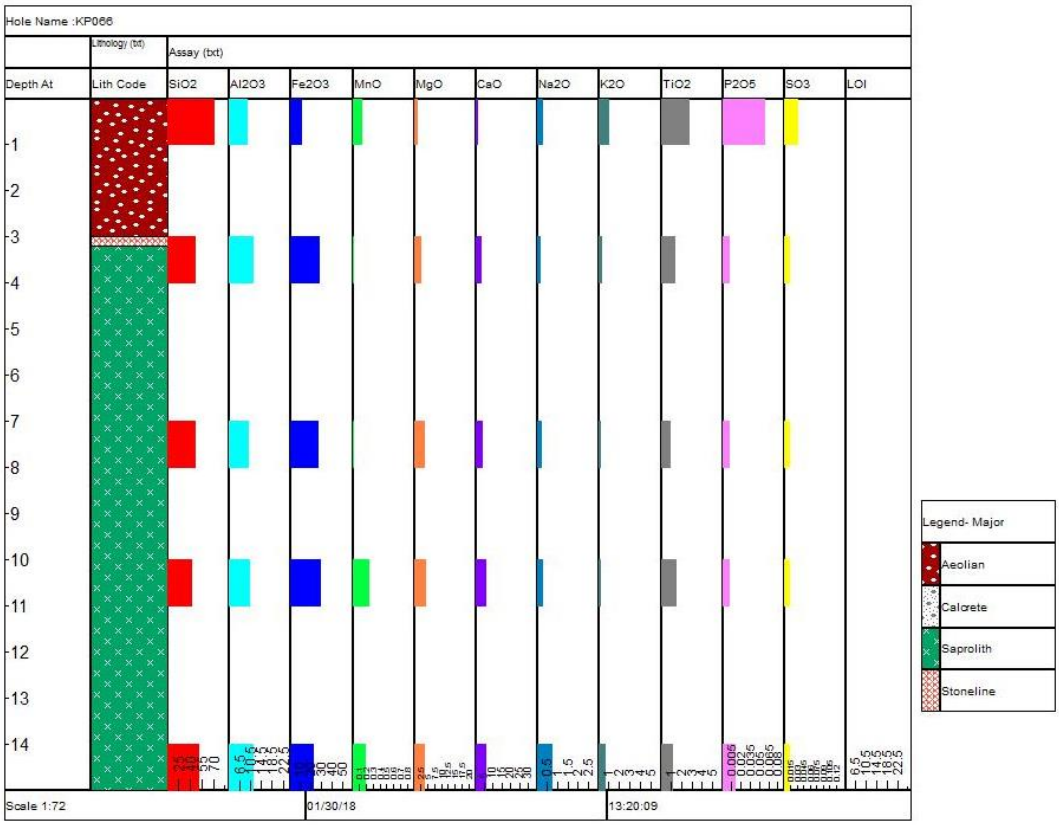

Appendix 19: The downhole distribution of major elements in borehole KP066, Serpens North.

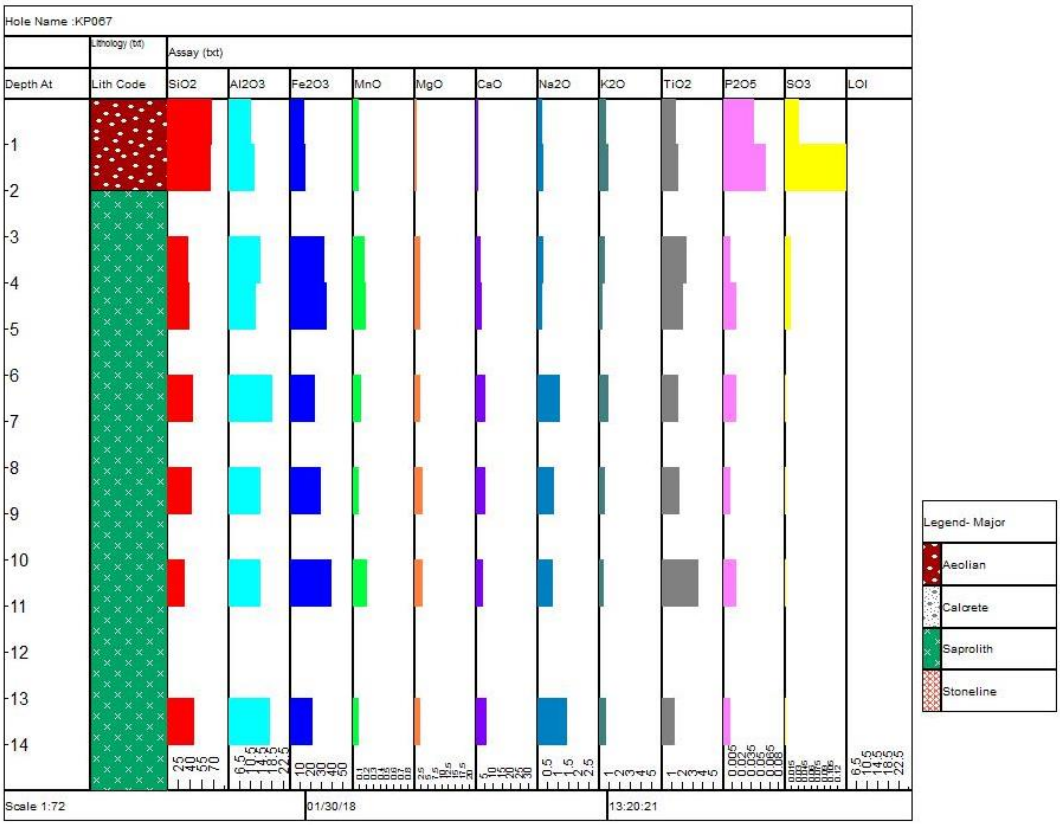

Appendix 20: The downhole distribution of major elements in borehole KP067, Serpens North.

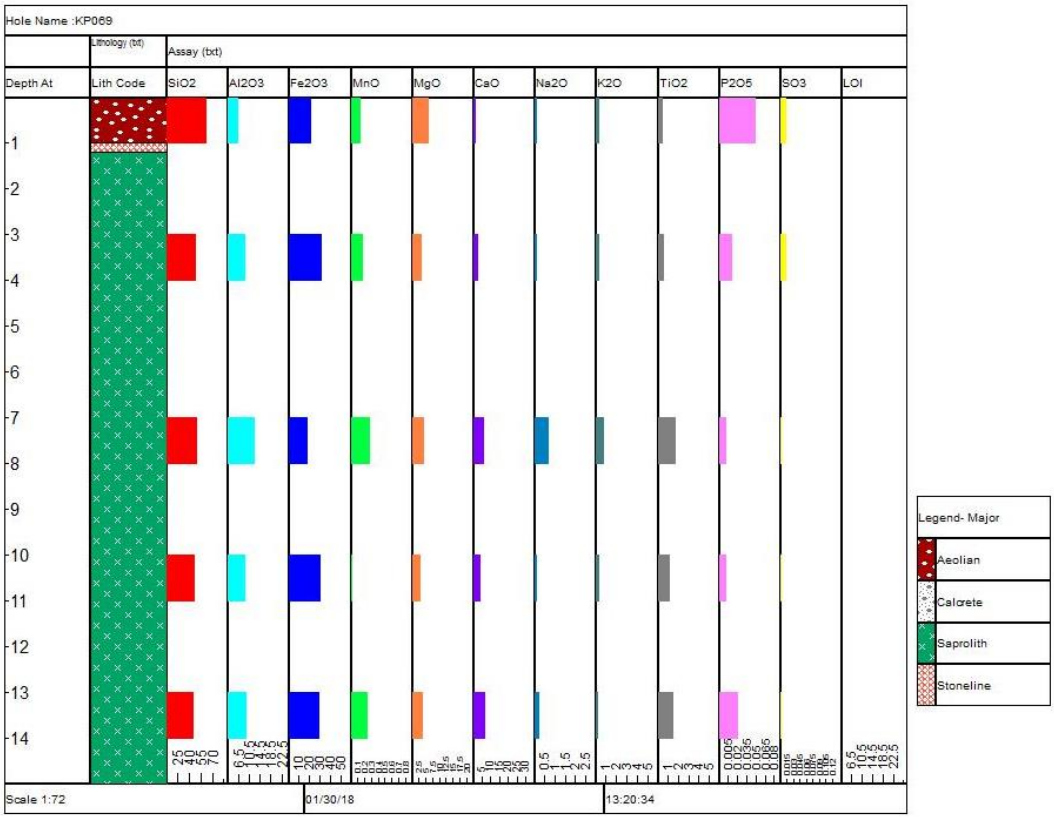

Appendix 21: The downhole distribution of major elements in borehole KP069, Serpens North.

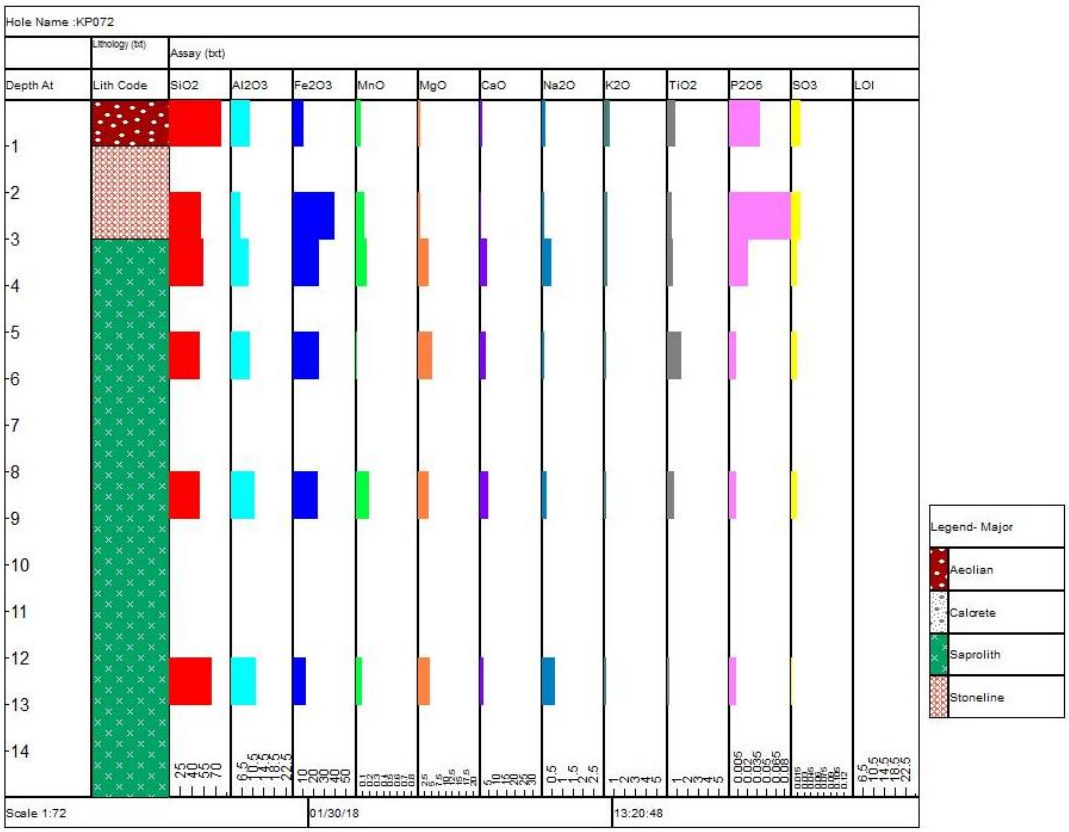

Appendix 22: The downhole distribution of major elements in borehole KP072, Serpens North.

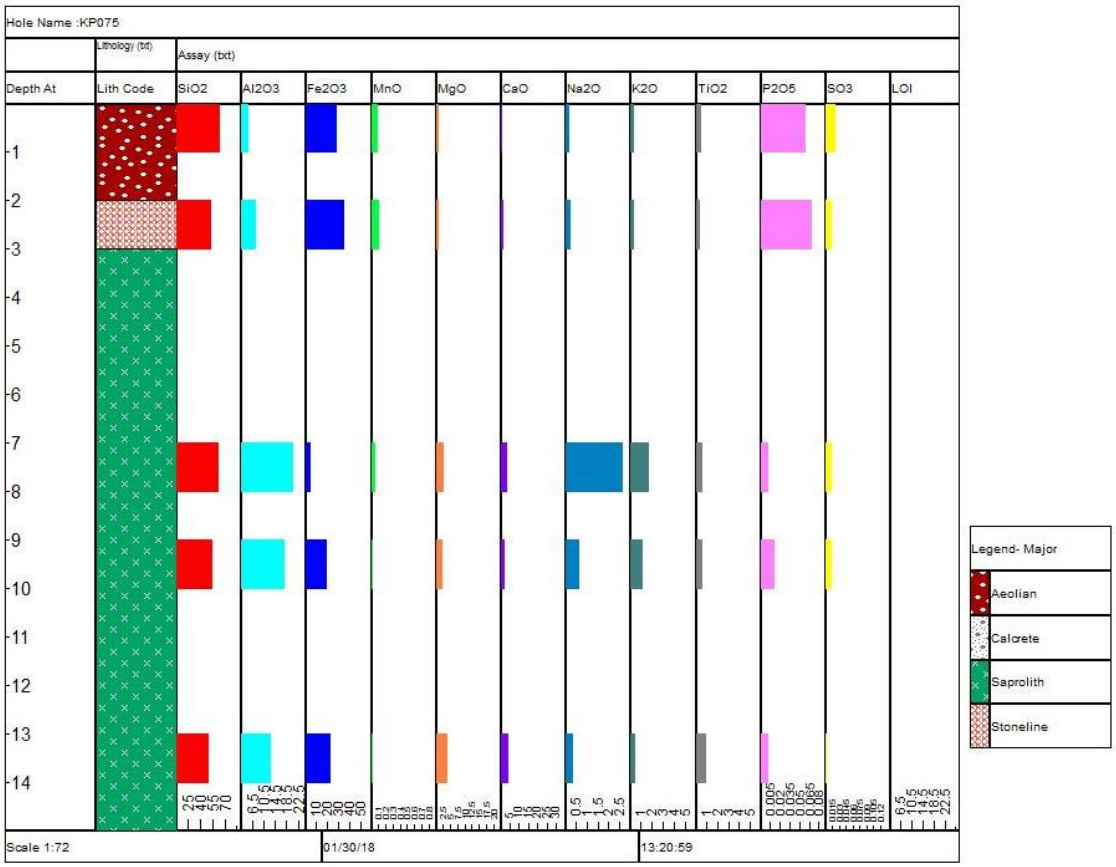

Appendix 23: The downhole distribution of major elements in borehole KP075, Serpens North.

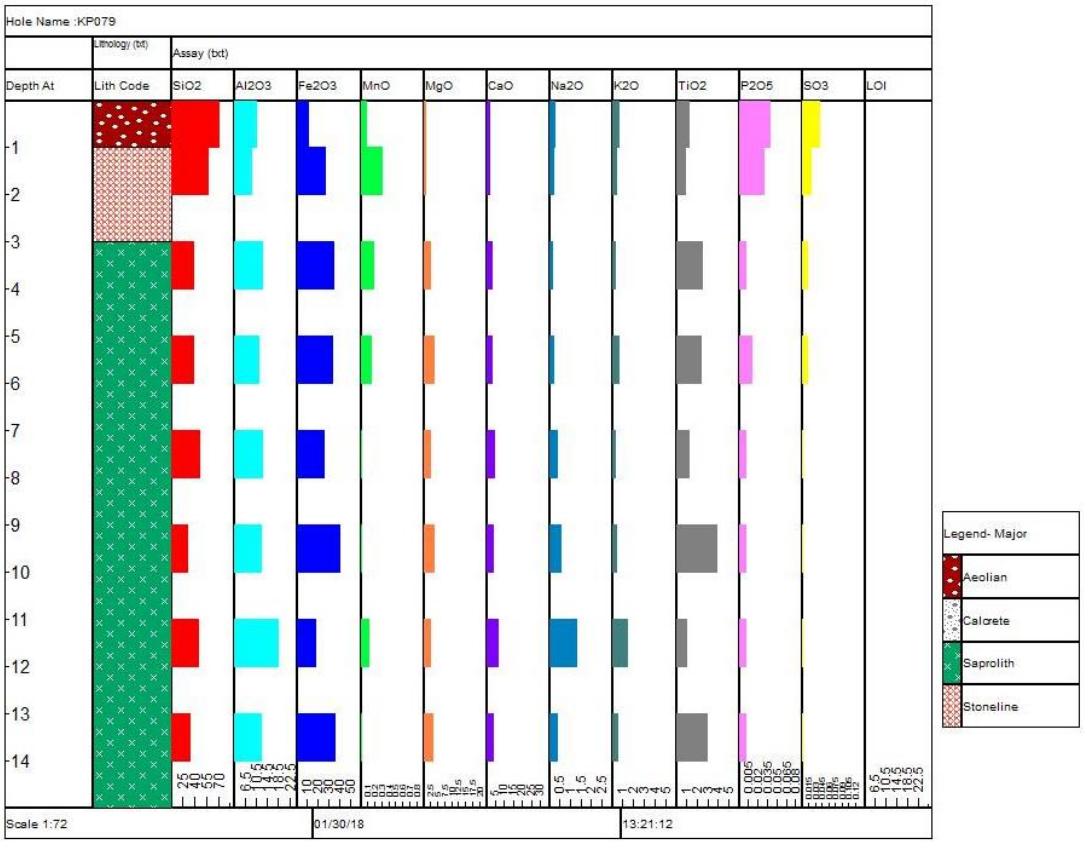

Appendix 24: The downhole distribution of major elements in borehole KP079, Serpens North.

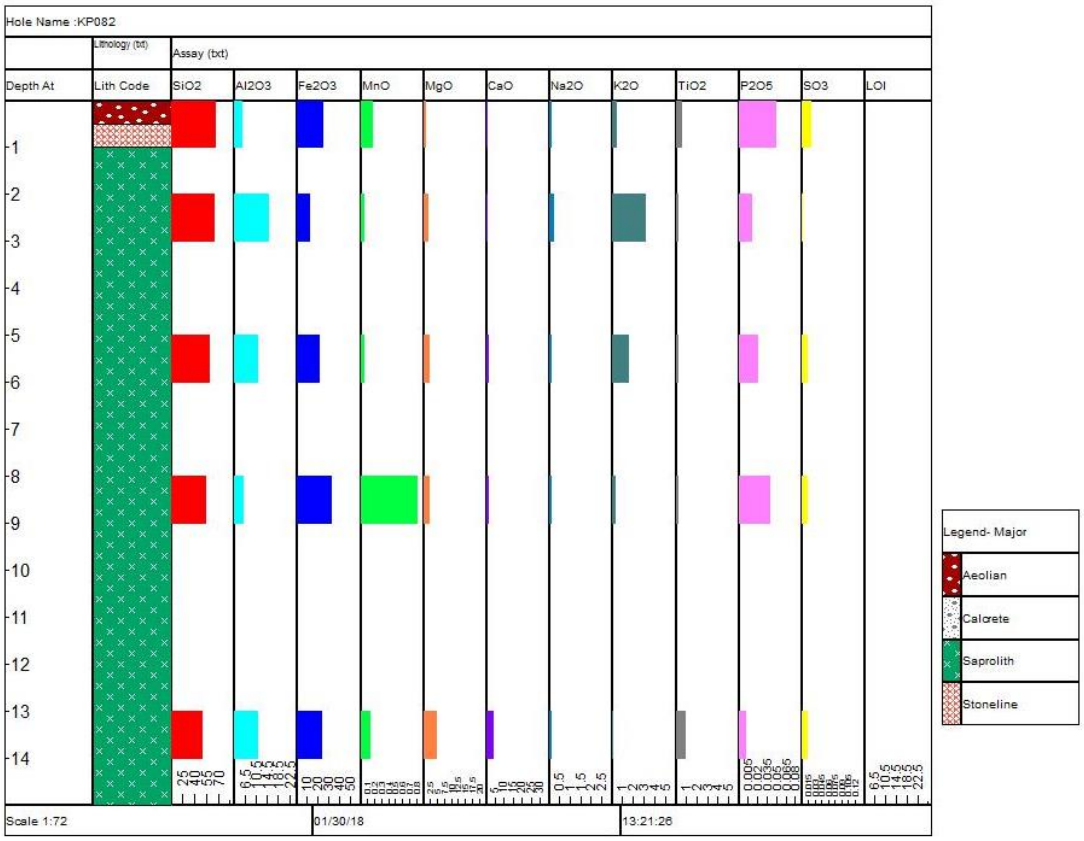

Appendix 25: The downhole distribution of major elements in borehole KP082, Serpens North.

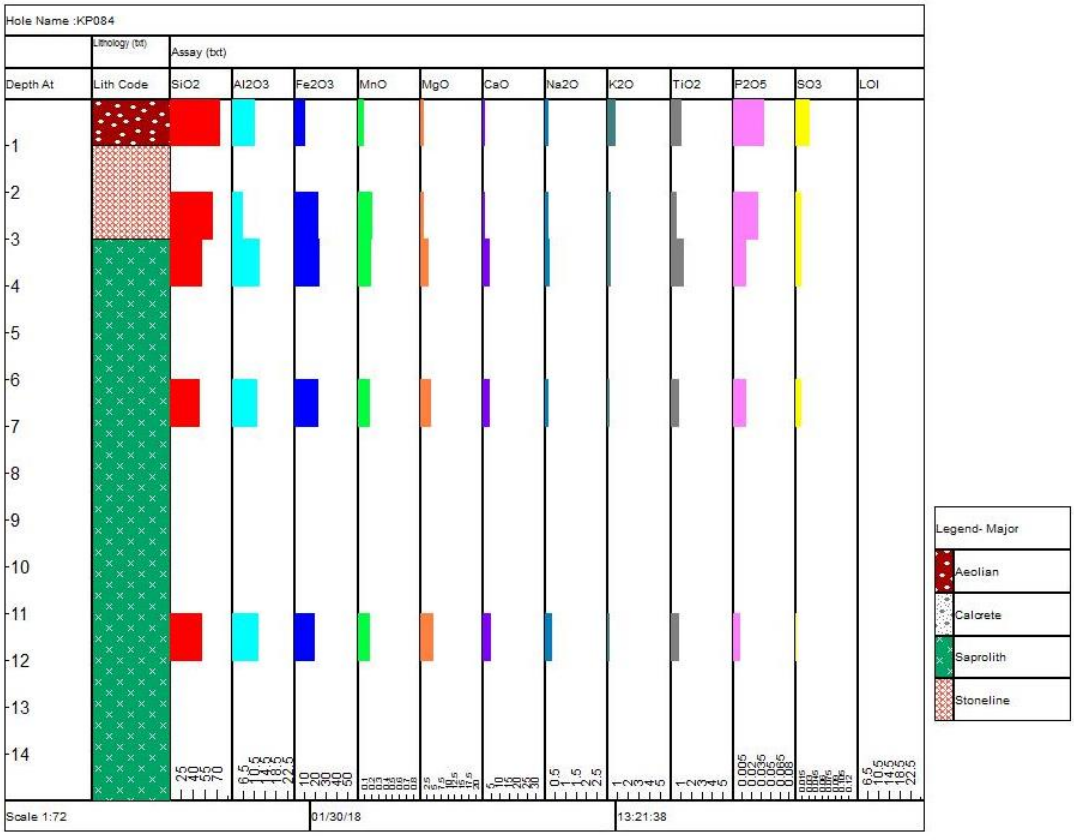

Appendix 26: The downhole distribution of major elements in borehole KP084, Serpens North.

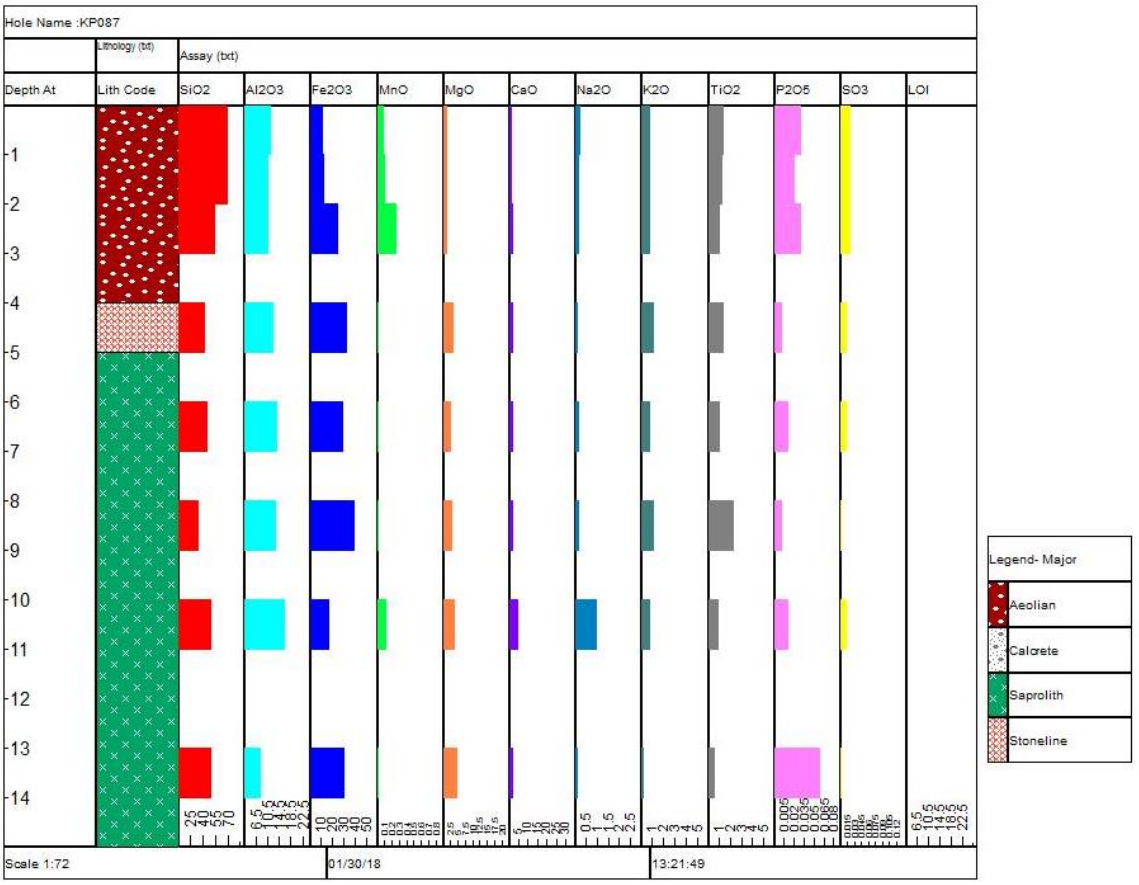

Appendix 27: The major element concentrations in borehole KP087, Serpens North.

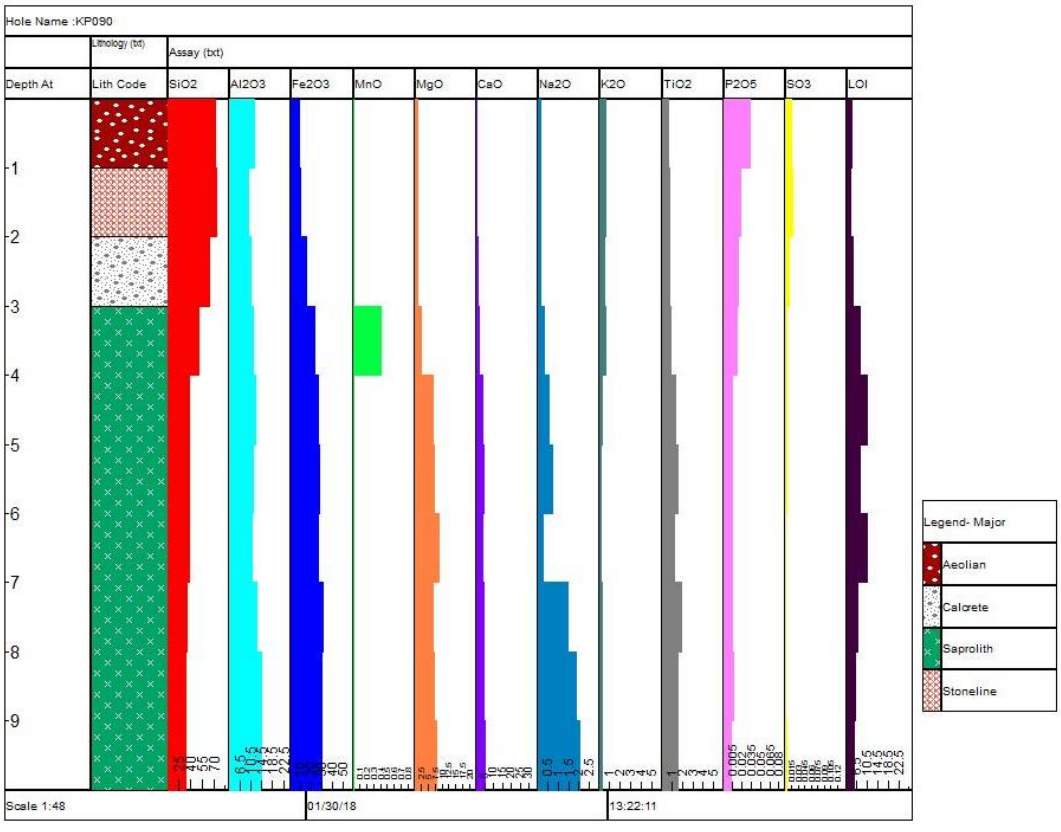

Appendix 28: The downhole distribution of major elements in KP090, Sirius.

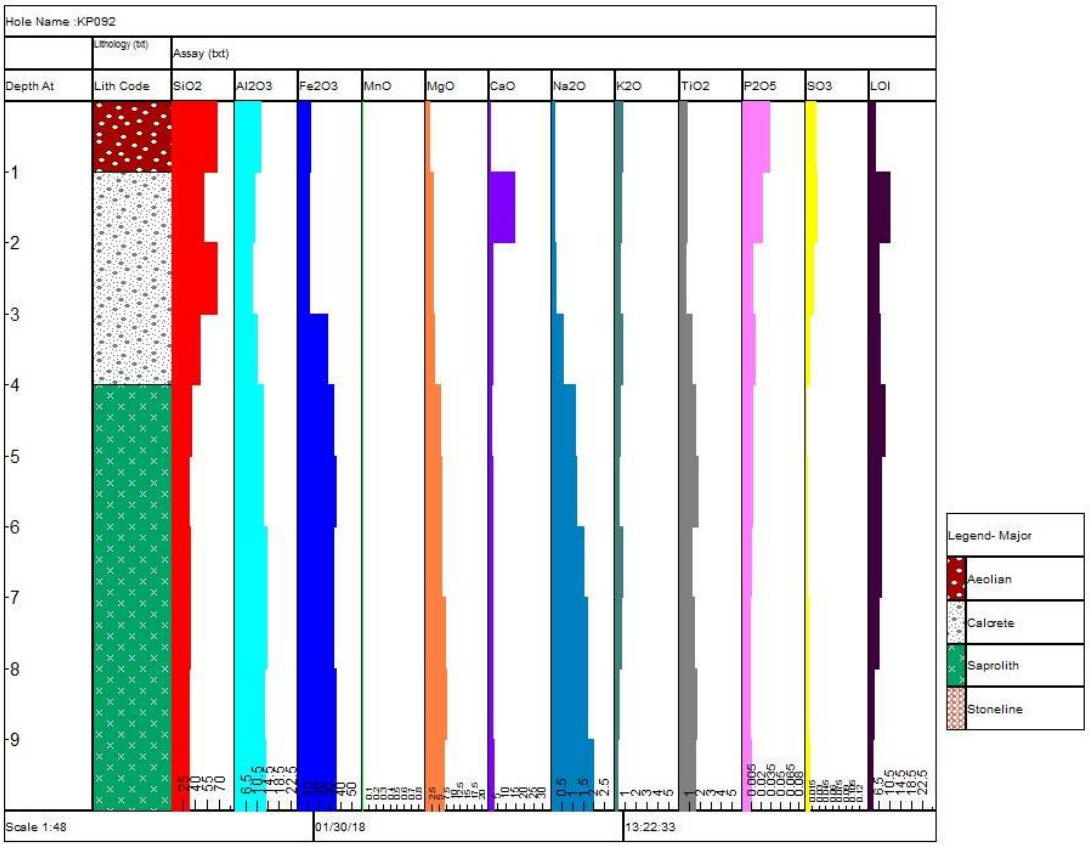

Appendix 29: Downhole distribution of major elements in KP092, Sirius.

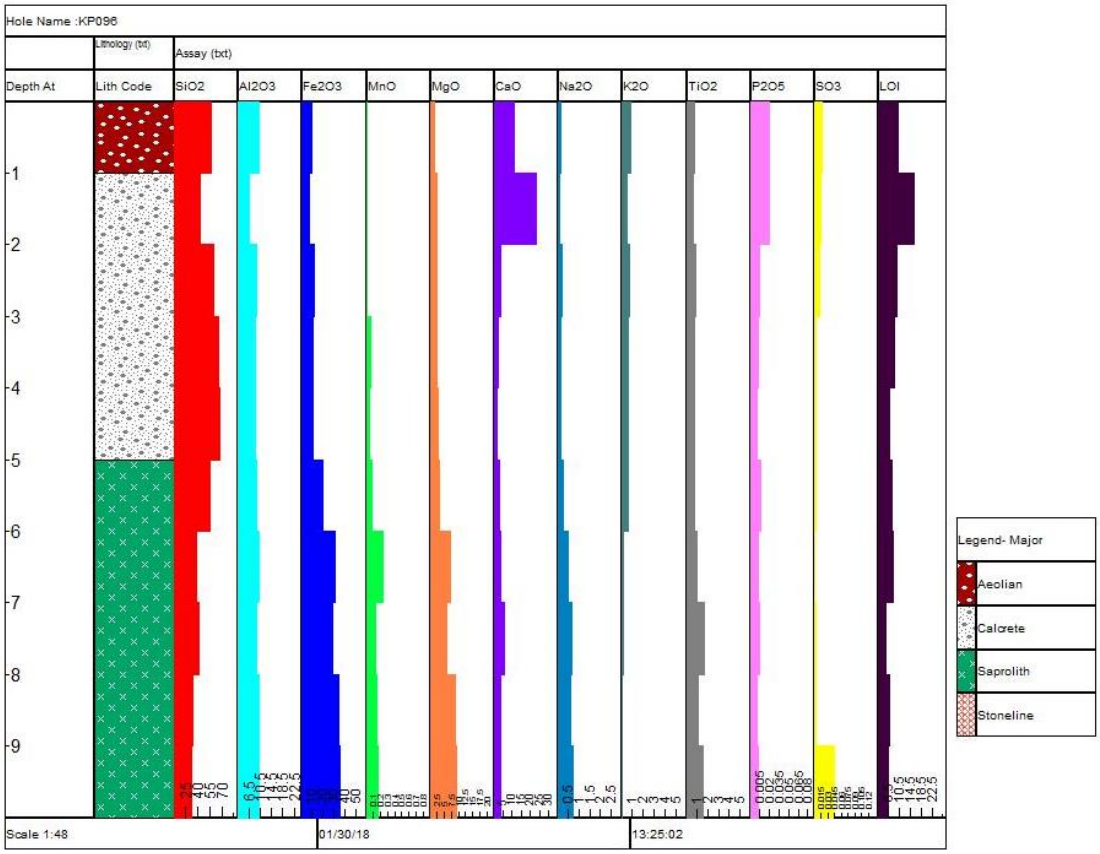

Appendix 30:The downhole distribution of major elements in borehole KP096, Sirius.

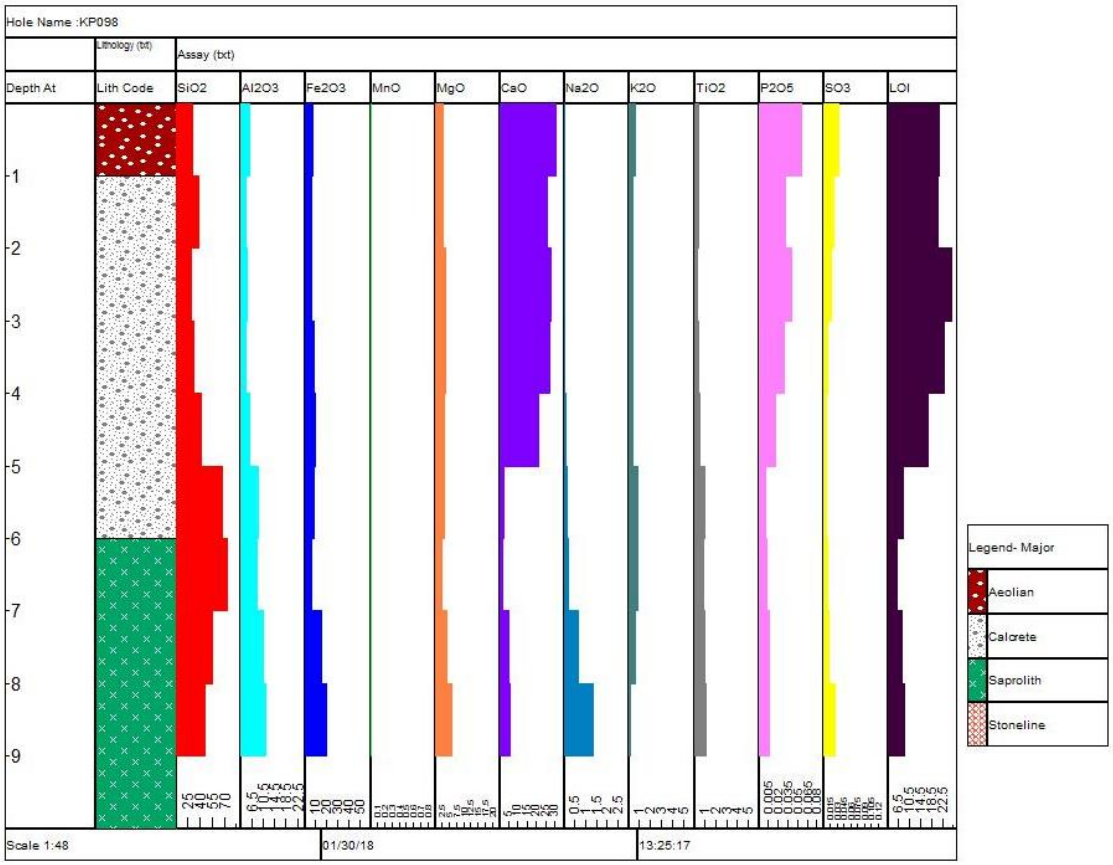

Appendix 31: The downhole distribution of major elements in borehole KP098, Sirius.

Appendix 32: Contribution of each variable in all samples from Serpens North Prospect (%).

	PC1	PC2	PC3	PC4	PC5	PC6	PC7	PC8	PC9	PC10
Major oxide										
SiO2	10,561	1,616	11,473	1,743	0,439	1,983	2,076	0,105	0,489	1,262
Al2O3	7,337	8,922	2,090	6,327	0,297	4,564	0,030	0,787	0,157	0,919
Fe2O3	1,435	9,180	17,687	0,314	0,095	2,629	0,491	0,009	1,969	2,927
MnO	0,687	5,373	7,151	0,079	10,007	0,758	0,348	16,051	1,973	6,305
MgO	1,921	0,092	0,553	2,675	6,401	23,177	3,389	3,819	6,346	23,230
CaO	12,844	0,171	0,109	2,426	0,191	5,433	0,842	5,898	1,471	0,212
Na2O	5,119	4,101	6,167	2,316	0,173	0,523	8,238	0,457	1,305	0,139
K2O	0,287	7,183	3,007	5,291	2,376	5,981	8,834	4,765	0,111	2,285
TiO2	2,078	0,334	9,990	0,474	7,947	17,640	4,125	8,263	0,525	0,883
P2O5	10,485	1,578	0,536	10,247	0,010	0,063	0,092	1,147	6,844	0,678
SO3	4,371	1,456	2,043	4,510	0,109	3,165	3,210	17,861	15,761	4,586
Trace elements										
Ba	0,316	10,647	8,114	1,342	5,784	1,005	1,511	4,736	7,121	1,312
Ce	3,528	11,618	2,167	4,538	1,534	0,008	8,282	2,381	0,035	1,384
Co	5,078	8,488	3,204	8,419	0,045	0,288	8,505	0,063	0,125	0,702
Nd	1,854	12,993	1,016	6,785	2,458	0,065	9,820	1,198	0,785	0,962
Ni	3,014	0,056	2,958	9,312	1,243	11,268	2,116	0,662	6,872	12,870

Pb	0,299	4,049	3,790	0,720	1,494	11,158	0,041	7,316	20,884	20,991
Rb	3,380	0,918	0,016	1,973	11,759	1,477	13,874	2,536	7,209	0,255
Sr	3,084	2,874	2,544	2,309	12,845	0,531	12,562	8,663	1,585	3,597
V	6,939	1,458	0,921	9,890	1,611	6,903	3,128	7,399	13,694	0,788
Y	0,133	1,814	6,894	0,206	23,916	0,349	3,341	1,356	0,276	9,077
Zn	8,609	0,472	5,187	13,221	0,420	1,030	4,096	3,737	4,151	0,419
Zr	6,641	4,609	2,385	4,881	8,845	0,004	1,048	0,790	0,312	4,216

Appendix 33: Contribution of the variables from the aeolian sand samples in Serpens North (%)

	PC1	PC2	PC3	PC4	PC5	PC6	PC7	PC8	PC9
Major oxides									
SiO2	4,785	4,858	0,544	11,868	1,073	0,319	0,306	10,602	2,104
Al2O3	9,077	0,023	0,000	1,785	0,349	4,484	2,537	8,206	5,010
Fe2O3	0,665	6,216	0,000	31,131	2,172	0,220	0,150	2,765	0,072
MnO	0,347	4,756	1,821	27,147	0,537	17,085	1,859	5,021	0,545
MgO	8,548	1,027	2,134	0,047	0,060	0,556	0,220	3,190	0,151
CaO	8,821	1,420	0,605	0,028	0,885	1,497	0,205	2,762	0,996
Na2O	8,692	0,767	0,525	0,493	1,273	6,062	0,927	5,437	0,681
K2O	8,803	0,056	2,598	0,478	0,001	0,497	0,428	0,012	2,288
TiO2	0,392	7,628	12,541	0,161	1,009	4,528	7,003	1,263	14,599
P2O5	5,328	2,807	0,677	2,571	7,047	2,673	36,899	6,151	20,712
SO3	5,277	0,433	5,063	0,260	2,825	12,684	28,935	1,535	25,521
Trace elements									
Ba	5,364	1,866	5,398	3,770	1,062	8,728	0,708	7,802	6,946
Ce	1,633	7,848	6,909	3,992	4,581	6,654	1,712	0,248	3,049
Co	6,519	3,944	0,365	5,568	0,427	3,193	0,360	1,230	0,199
Nd	0,726	11,697	6,243	0,928	4,625	0,777	3,516	7,098	7,370
Ni	5,702	6,068	0,369	0,206	0,804	14,168	0,557	0,139	0,134
Pb	5,905	0,397	6,592	0,368	10,722	0,053	8,162	0,152	2,806
Rb	4,603	9,630	0,001	0,073	4,936	0,121	1,462	1,082	2,974
Sr	0,359	3,439	13,313	0,530	22,352	9,963	0,610	2,547	0,041
V	1,374	11,958	2,779	3,975	7,388	0,788	0,175	2,413	2,722
Y	6,439	1,493	2,954	0,040	15,290	1,002	1,586	18,357	0,774
Zn	0,628	11,483	6,434	3,108	1,447	3,934	0,441	2,758	0,240
Zr	0,015	0,184	22,135	1,476	9,134	0,014	1,243	9,231	0,066

Appendix 34: Contribution of each variable to the principal components in stone lines- Serpens North (%).

	PC1	PC2	PC3	PC4	PC5	PC6	PC7	PC8
Major elements								
SiO2	1,135	5,551	10,274	6,692	0,005	2,559	0,001	14,631
Al2O3	9,891	0,005	0,242	0,008	1,531	11,002	0,086	0,961
Fe2O3	7,779	1,524	1,822	4,781	2,062	0,275	0,167	4,051
MnO	1,340	2,892	12,944	10,144	0,691	0,169	0,018	2,183
MgO	5,059	5,076	3,332	0,639	10,677	0,116	4,544	1,872
CaO	1,380	6,580	9,321	1,293	12,652	0,414	0,060	5,815
Na2O	9,253	0,019	1,226	0,011	2,851	11,925	0,134	0,015
K2O	9,928	0,605	0,517	0,157	0,398	3,921	6,602	0,135
TiO2	0,049	0,069	21,578	6,767	1,608	0,156	0,603	6,626
P2O5	6,779	1,906	4,530	0,716	4,209	7,317	0,455	2,528
SO3	1,276	1,127	0,089	21,352	6,884	10,350	14,824	0,326
Trace elements								
Ba	5,510	2,615	0,332	4,142	2,941	4,731	22,161	13,491
Ce	6,631	0,241	0,795	5,030	13,920	2,064	1,407	6,210
Co	8,638	1,093	2,459	0,038	0,665	5,096	0,582	8,724
Nd	5,898	0,349	1,351	8,949	8,711	4,902	3,141	0,653
Ni	3,609	3,252	11,543	0,032	1,522	10,717	0,960	0,933
Pb	2,507	13,553	0,117	1,912	0,550	4,295	0,627	4,932
Rb	0,002	5,985	7,957	3,008	2,792	12,071	26,752	13,693
Sr	1,730	12,877	0,023	0,945	12,487	0,498	5,712	0,188
V	2,619	9,067	0,373	7,483	7,158	2,310	0,006	1,159
Y	0,132	5,078	6,896	15,690	0,180	3,865	7,800	1,767
Zn	4,518	11,229	0,437	0,201	2,908	0,044	0,036	0,530
Zr	4,335	9,307	1,841	0,011	2,596	1,201	3,324	8,578

Appendix 35: Contribution of each variable to the principal components in saprolith-Serpens North (%).

	PC1	PC2	PC3	PC4	PC5	PC6	PC7	PC8	PC9	PC10
Major oxides (wt.%)										
SiO2	4,619	2,952	13,556	5,775	1,875	2,009	0,147	0,549	2,625	0,641
Al2O3	0,708	13,580	1,148	12,989	0,229	0,239	0,191	0,661	0,414	3,979
Fe2O3	1,049	10,815	13,311	1,643	0,129	3,136	1,014	0,156	0,054	0,551
MnO	1,001	11,029	0,002	4,712	7,017	0,948	0,000	13,571	3,561	1,877
MgO	0,011	0,810	0,004	11,013	11,038	15,924	0,001	1,026	20,269	9,725
CaO	7,446	1,645	0,988	2,755	6,230	0,003	15,340	0,844	1,418	0,045
Na2O	4,663	7,775	3,034	2,202	1,627	0,599	2,967	10,965	0,036	0,211
K2O	3,881	4,122	6,083	6,095	0,779	6,244	3,244	3,762	0,187	0,021
TiO2	3,196	1,496	14,771	9,325	1,401	1,413	2,744	0,000	1,353	0,292
P2O5	2,082	3,433	1,180	1,498	19,114	7,810	3,586	5,219	11,947	1,943
SO3	1,317	1,564	0,111	1,264	16,601	5,556	2,855	17,056	19,366	7,548
Trace elements (ppm)										
Ba	5,695	3,810	12,356	0,191	0,720	0,086	7,256	1,676	0,238	2,041

Ce	11,425	3,058	2,481	1,378	0,002	5,767	0,679	2,087	7,401	0,293
Co	0,020	8,919	13,439	0,960	6,102	1,661	0,374	0,100	0,204	0,620
Nd	7,110	7,314	3,085	0,812	1,199	4,015	3,267	0,322	9,184	0,352
Ni	1,409	4,538	0,069	16,274	1,124	2,830	0,835	9,826	0,423	1,029
Pb	4,399	0,060	5,945	8,629	0,016	0,097	0,281	16,137	13,423	6,650
Rb	5,720	0,795	3,042	2,412	0,034	11,158	5,720	1,012	2,260	15,905
Sr	6,883	0,036	0,111	1,179	3,696	16,553	15,328	1,839	0,006	3,742
V	5,039	6,245	0,800	0,047	14,395	0,441	10,527	0,066	0,342	6,951
Y	1,332	2,743	4,336	2,236	1,437	1,669	18,749	0,320	4,275	27,722
Zn	10,432	3,092	0,064	3,936	3,499	6,701	4,189	2,767	0,019	2,656
Zr	10,562	0,170	0,083	2,676	1,737	5,140	0,706	10,037	0,993	5,206

Appendix 36: Correlation between elements across the Serpens North regolith profiles.

Element	SiO2	Al2O3	Fe2O3	MnO	MgO	CaO	Na2O	K2O	TiO2	P2O5	SO3	Ba	Ce	Co	Nd	Ni	Pb	Rb	Sr	V	Y	Zn	Zr
SiO2	1	-.402**	-.809**	-.177*	-.285**	-.621**	-0,105	0,108	-.587**	.466**	.346**	-.195*	-0,041	-.355**	-0,089	-0,094	0,054	0,091	-.310**	-.339**	-0,035	-.383**	.489**
Al2O3	-.402**	1	-0,108	-0,151	-0,110	.473**	.709**	.531**	.206*	-.483**	-.217**	.214*	0,116	.184*	.196*	0,013	-0,114	-0,062	.395**	.235**	0,079	.209*	-0,147
Fe2O3	-.809**	-0,108	1	.281**	0,049	.219**	-.304**	-.362**	.561**	-0,085	-.187*	0,121	0,016	.212*	0,015	-0,051	0,021	0,024	0,122	.255**	0,027	.268**	-.374**
MnO	-.177*	-0,151	.281**	1	0,032	0,061	-0,156	-.201*	-0,017	0,131	-0,013	0,013	-0,050	0,011	-0,036	0,074	-0,054	-0,035	0,146	-0,059	.223**	0,055	-0,130
MgO	-.285**	-0,110	0,049	0,032	1	.378**	-0,106	-.212*	-0,112	-.427**	-.245**	-0,039	-0,051	.208*	-0,040	.448**	-0,008	-.200*	-0,043	-0,058	-0,091	0,075	-.283**
CaO	-.621**	.473**	.219**	0,061	.378**	1	.340**	-0,164	.230**	-.548**	-.290**	0,113	-0,073	.367**	-0,014	0,140	-0,075	-.256**	.328**	.259**	-0,012	.376**	-.392**
Na2O	-0,105	.709**	-.304**	-0,156	-0,106	.340**	1	.290**	-0,018	-.301**	-.177*	0,088	-0,085	0,111	-0,014	0,049	-.208*	-0,061	.286**	0,164	0,026	0,105	-0,072
K2O	0,108	.531**	-.362**	-.201*	-.212*	-0,164	.290**	1	-0,122	-0,143	-0,104	0,075	0,148	-0,165	.172*	-0,039	-0,004	0,154	0,035	-0,098	0,060	-0,086	0,098
TiO2	-.587**	.206*	.561**	-0,017	-0,112	.230**	-0,018	-0,122	1	-0,121	0,064	0,048	0,076	.213*	0,134	-0,082	-0,077	-0,052	0,162	.348**	0,026	.218**	-0,072
P2O5	.466**	-.483**	-0,085	0,131	-.427**	-.548**	-.301**	-0,143	-0,121	1	.493**	-.230**	-0,101	-.239**	-0,120	-0,140	-0,018	0,105	-.174*	-0,084	-0,036	-.183*	.330**
SO3	.346**	-.217**	-.187*	-0,013	-.245**	-.290**	-.177*	-0,104	0,064	.493**	1	-0,151	-0,075	0,055	-0,115	-0,123	0,076	-0,031	-0,080	0,153	-0,052	-0,013	0,161
Ba	-.195*	.214*	0,121	0,013	-0,039	0,113	0,088	0,075	0,048	-.230**	-0,151	1	.280**	.452**	.265**	-0,011	.224**	.229**	0,093	0,056	.347**	-0,001	-0,066
Ce	-0,041	0,116	0,016	-0,050	-0,051	-0,073	-0,085	0,148	0,076	-0,101	-0,075	.280**	1	.203*	.915**	0,059	.189*	0,013	-0,083	0,040	0,061	0,014	0,057
Co	-.355**	.184*	.212*	0,011	.208*	.367**	0,111	-0,165	.213*	-.239**	0,055	.452**	.203*	1	.191*	.217**	0,145	-.287**	0,053	.590**	.179*	.512**	-.388**
Nd	-0,089	.196*	0,015	-0,036	-0,040	-0,014	-0,014	.172*	0,134	-0,120	-0,115	.265**	.915**	.191*	1	.209*	0,053	-0,018	-0,003	0,062	0,105	0,092	0,042
Ni	-0,094	0,013	-0,051	0,074	.448**	0,140	0,049	-0,039	-0,082	-0,140	-0,123	-0,011	0,059	.217**	.209*	1	-.187*	-.239**	0,052	-0,107	-0,062	.173*	-.248**
Pb	0,054	-0,114	0,021	-0,054	-0,008	-0,075	-.208*	-0,004	-0,077	-0,018	0,076	.224**	.189*	0,145	0,053	-.187*	1	0,061	-0,128	0,026	0,115	-0,145	0,153
Rb	0,091	-0,062	0,024	-0,035	-.200*	-.256**	-0,061	0,154	-0,052	0,105	-0,031	.229**	0,013	-.287**	-0,018	-.239**	0,061	1	0,078	-0,141	0,119	-0,156	.215*
Sr	-.310**	.395**	0,122	0,146	-0,043	.328**	.286**	0,035	0,162	-.174*	-0,080	0,093	-0,083	0,053	-0,003	0,052	-0,128	0,078	1	0,032	0,010	.409**	-.358**
V	-.339**	.235**	.255**	-0,059	-0,058	.259**	0,164	-0,098	.348**	-0,084	0,153	0,056	0,040	.590**	0,062	-0,107	0,026	-0,141	0,032	1	0,006	.744**	-.374**
Y	-0,035	0,079	0,027	.223**	-0,091	-0,012	0,026	0,060	0,026	-0,036	-0,052	.347**	0,061	.179*	0,105	-0,062	0,115	0,119	0,010	0,006	1	-0,071	0,045
Zn	-.383**	.209*	.268**	0,055	0,075	.376**	0,105	-0,086	.218**	-.183*	-0,013	-0,001	0,014	.512**	0,092	.173*	-0,145	-0,156	.409**	.744**	-0,071	1	-.688**
Zr	.489**	-0,147	-.374**	-0,130	-.283**	-.392**	-0,072	0,098	-0,072	.330**	0,161	-0,066	0,057	-.388**	0,042	-.248**	0,153	.215*	-.358**	-.374**	0,045	-.688**	1

**. Correlation is significant at the 0.01 level (2-tailed).

*. Correlation is significant at the 0.05 level (2-tailed).

Appendix 37: Correlation of elements in aeolian sand in the Serpens North Prospect.

Element	SiO2	Al2O3	Fe2O3	MnO	MgO	CaO	Na2O	K2O	TiO2	P2O5	SO3	Ba	Ce	Co	Nd	Ni	Pb	Rb	Sr	V	Y	Zn	Zr
SiO2	1	-.583**	-.787**	-.659**	-.347*	-.569**	-.471**	-.361*	0,059	-0,072	0,027	-.411*	0,156	-.367*	0,214	-.533**	-.369*	-0,136	-0,316	-0,317	-0,023	-.372*	.406*
Al2O3	-.583**	1	-0,008	0,331	0,145	.725**	.684**	.807**	0,257	-0,317	0,091	.403*	-0,044	.378*	-0,088	0,289	.428*	0,057	.397*	.347*	0,104	0,298	-0,065
Fe2O3	-.787**	-0,008	1	.586**	0,159	0,050	-0,007	-0,215	-0,251	.358*	-0,074	0,214	-0,146	0,147	-0,207	.378*	0,026	0,148	0,138	0,151	-0,028	0,282	-.494**
MnO	-.659**	0,331	.586**	1	0,057	0,181	0,184	0,209	-0,009	0,168	-0,103	0,066	0,265	0,226	0,054	0,358	-0,126	-0,065	.376*	0,155	-0,034	.366*	-.346*
MgO	-.347*	0,145	0,159	0,057	1	.344*	0,208	0,069	-0,183	-0,105	-0,087	0,070	-0,102	0,076	-0,145	.783**	.398*	-0,111	-0,057	-0,049	-0,060	-0,057	-0,037
CaO	-.569**	.725**	0,050	0,181	.344*	1	.853**	.814**	-0,040	-.402*	-0,092	.421*	-0,230	0,263	-0,243	0,323	.609**	0,080	0,225	0,157	0,017	0,114	-0,031
Na2O	-.471**	.684**	-0,007	0,184	0,208	.853**	1	.767**	-0,097	-.409*	-0,134	0,288	-0,236	0,157	-0,233	0,172	.591**	0,076	0,103	0,100	0,011	0,006	0,108
K2O	-.361*	.807**	-0,215	0,209	0,069	.814**	.767**	1	.346*	-0,270	0,088	0,311	0,083	.370*	0,038	0,188	.410*	0,025	0,338	.360*	0,035	0,259	0,069
TiO2	0,059	0,257	-0,251	-0,009	-0,183	-0,040	-0,097	.346*	1	0,190	.348*	-0,117	.674**	0,260	.858**	-0,115	0,156	-0,025	0,079	.489**	0,120	0,182	0,238
P2O5	-0,072	-0,317	.358*	0,168	-0,105	-.402*	-.409*	-0,270	0,190	1	0,320	-0,195	0,310	0,109	0,447	0,008	-0,291	-0,128	0,042	0,281	-0,120	0,186	-0,256
SO3	0,027	0,091	-0,074	-0,103	-0,087	-0,092	-0,134	0,088	.348*	0,320	1	-0,017	-0,054	.740**	0,492	-0,208	0,149	-0,216	0,006	.746**	-0,120	0,321	-0,179
Ba	-.411*	.403*	0,214	0,066	0,070	.421*	0,288	0,311	-0,117	-0,195	-0,017	1	-0,027	.463**	-0,181	0,327	0,280	.689**	.559**	.450**	0,009	.700**	-.521**
Ce	0,156	-0,044	-0,146	0,265	-0,102	-0,230	-0,236	0,083	.674**	0,310	-0,054	-0,027	1	0,032	.929**	0,169	-0,002	0,021	0,095	0,151	0,025	0,087	0,195
Co	-.367*	.378*	0,147	0,226	0,076	0,263	0,157	.370*	0,260	0,109	.740**	.463**	0,032	1	0,273	0,202	0,346	0,003	.432*	.896**	-0,074	.720**	-.526**
Nd	0,214	-0,088	-0,207	0,054	-0,145	-0,243	-0,233	0,038	.858**	0,447	0,492	-0,181	.929**	0,273	1	0,096	0,048	-0,101	0,088	0,480	-0,086	0,124	0,228
Ni	-.533**	0,289	.378*	0,358	.783**	0,323	0,172	0,188	-0,115	0,008	-0,208	0,327	0,169	0,202	0,096	1	0,176	0,103	.390*	0,100	-0,044	.404*	-.439*
Pb	-.369*	.428*	0,026	-0,126	.398*	.609**	.591**	.410*	0,156	-0,291	0,149	0,280	-0,002	0,346	0,048	0,176	1	0,075	-0,113	0,271	0,130	-0,051	0,181
Rb	-0,136	0,057	0,148	-0,065	-0,111	0,080	0,076	0,025	-0,025	-0,128	-0,216	.689**	0,021	0,003	-0,101	0,103	0,075	1	0,176	0,230	0,104	.465**	-0,176
Sr	-0,316	.397*	0,138	.376*	-0,057	0,225	0,103	0,338	0,079	0,042	0,006	.559**	0,095	.432*	0,088	.390*	-0,113	0,176	1	0,308	-0,052	.747**	-.760**
V	-0,317	.347*	0,151	0,155	-0,049	0,157	0,100	.360*	.489**	0,281	.746**	.450**	0,151	.896**	0,480	0,100	0,271	0,230	0,308	1	-0,014	.736**	-.377*
Y	-0,023	0,104	-0,028	-0,034	-0,060	0,017	0,011	0,035	0,120	-0,120	-0,120	0,009	0,025	-0,074	-0,086	-0,044	0,130	0,104	-0,052	-0,014	1	-0,033	0,031
Zn	-.372*	0,298	0,282	.366*	-0,057	0,114	0,006	0,259	0,182	0,186	0,321	.700**	0,087	.720**	0,124	.404*	-0,051	.465**	.747**	.736**	-0,033	1	-.760**
Zr	.406*	-0,065	-.494**	-.346*	-0,037	-0,031	0,108	0,069	0,238	-0,256	-0,179	-.521**	0,195	-.526**	0,228	-.439*	0,181	-0,176	-.760**	-.377*	0,031	-.760**	1

**. Correlation is significant at the 0.01 level (2-tailed).

*. Correlation is significant at the 0.05 level (2-tailed).

Appendix 38: Correlation of elements within the stone lines in Serpens North.

Element	SiO2	Al2O3	Fe2O3	MnO	MgO	CaO	Na2O	K2O	TiO2	P2O5	SO3	Ba	Ce	Co	Nd	Ni	Pb	Rb	Sr	V	Y	Zn	Zr
SiO2	1	-0,156	-.627**	-0,439	-0,038	-0,416	0,192	-0,157	-0,456	-0,368	0,141	0,235	-0,048	.623*	0,036	0,243	0,051	0,304	-0,017	-0,140	-0,308	0,009	-0,164
Al2O3	-0,156	1	-.646**	-0,167	0,151	.570*	.847**	.846**	0,123	-.530*	-0,112	0,276	.678*	-0,239	.648*	-0,368	-0,103	-0,167	0,479	0,218	0,048	-0,263	0,410
Fe2O3	-.627**	-.646**	1	0,435	-0,248	-0,236	-.791**	-.510*	0,176	.756**	-0,001	-0,337	-0,392	-0,297	-0,387	0,044	0,025	-0,075	-0,273	-0,013	0,232	0,225	-0,230
MnO	-0,439	-0,167	0,435	1	-0,164	-0,029	-0,356	-0,200	0,505	-0,091	0,006	0,009	-0,078	-0,291	-0,052	-0,210	0,255	0,006	0,250	0,111	.895**	0,261	-0,184
MgO	-0,038	0,151	-0,248	-0,164	1	0,288	0,063	0,159	0,141	-0,342	-0,211	-0,300	0,272	0,104	0,202	.638*	0,228	-0,334	-0,290	-0,206	-0,164	0,051	-0,011
CaO	-0,416	.570*	-0,236	-0,029	0,288	1	0,428	0,349	0,431	-0,463	-0,116	-0,027	0,167	-0,247	0,069	-0,191	-0,248	-0,145	0,114	0,033	-0,102	-0,354	.528*
Na2O	0,192	.847**	-.791**	-0,356	0,063	0,428	1	.570*	-0,141	-.561*	-0,171	0,482	.615*	0,182	.665*	-0,254	-0,015	-0,053	0,270	0,158	-0,068	-0,393	0,436
K2O	-0,157	.846**	-.510*	-0,200	0,159	0,349	.570*	1	0,045	-0,348	-0,146	0,104	0,411	-0,370	0,181	-0,458	-0,219	-0,059	0,398	-0,025	-0,004	-0,309	0,385
TiO2	-0,456	0,123	0,176	0,505	0,141	0,431	-0,141	0,045	1	-0,363	0,409	-0,022	0,022	-0,452	-0,077	-0,307	0,043	0,026	-0,076	0,358	0,249	0,006	0,218
P2O5	-0,368	-.530*	.756**	-0,091	-0,342	-0,463	-.561*	-0,348	-0,363	1	0,092	-0,409	-0,446	-0,197	-0,417	0,203	-0,088	-0,176	-0,203	-0,145	-0,141	0,154	-0,256
SO3	0,141	-0,112	-0,001	0,006	-0,211	-0,116	-0,171	-0,146	0,409	0,092	1	-0,264	-0,296	-0,188	-0,297	-0,012	-0,049	0,048	0,134	0,377	-0,069	0,270	-0,247
Ba	0,235	0,276	-0,337	0,009	-0,300	-0,027	0,482	0,104	-0,022	-0,409	-0,264	1	0,565	0,056	.634*	-0,492	0,061	.623*	0,129	0,197	0,208	-0,296	0,292
Ce	-0,048	.678*	-0,392	-0,078	0,272	0,167	.615*	0,411	0,022	-0,446	-0,296	0,565	1	0,238	.894**	-0,363	0,369	0,024	-0,163	0,463	0,100	-0,431	0,472
Co	.623*	-0,239	-0,297	-0,291	0,104	-0,247	0,182	-0,370	-0,452	-0,197	-0,188	0,056	0,238	1	0,493	0,311	0,468	-0,212	-0,473	0,089	-0,198	-0,063	-0,056
Nd	0,036	.648*	-0,387	-0,052	0,202	0,069	.665*	0,181	-0,077	-0,417	-0,297	.634*	.894**	0,493	1	0,033	0,120	-0,173	-0,123	0,317	0,182	-0,236	0,280
Ni	0,243	-0,368	0,044	-0,210	.638*	-0,191	-0,254	-0,458	-0,307	0,203	-0,012	-0,492	-0,363	0,311	0,033	1	0,071	-0,413	-0,249	-0,368	-0,278	0,475	-0,517
Pb	0,051	-0,103	0,025	0,255	0,228	-0,248	-0,015	-0,219	0,043	-0,088	-0,049	0,061	0,369	0,468	0,120	0,071	1	-0,313	-0,150	.510*	0,318	0,284	-0,255
Rb	0,304	-0,167	-0,075	0,006	-0,334	-0,145	-0,053	-0,059	0,026	-0,176	0,048	.623*	0,024	-0,212	-0,173	-0,413	-0,313	1	-0,037	-0,181	0,033	-0,330	0,167
Sr	-0,017	0,479	-0,273	0,250	-0,290	0,114	0,270	0,398	-0,076	-0,203	0,134	0,129	-0,163	-0,473	-0,123	-0,249	-0,150	-0,037	1	0,179	0,371	0,405	-0,332
V	-0,140	0,218	-0,013	0,111	-0,206	0,033	0,158	-0,025	0,358	-0,145	0,377	0,197	0,463	0,089	0,317	-0,368	.510*	-0,181	0,179	1	0,147	0,327	-0,100
Y	-0,308	0,048	0,232	.895**	-0,164	-0,102	-0,068	-0,004	0,249	-0,141	-0,069	0,208	0,100	-0,198	0,182	-0,278	0,318	0,033	0,371	0,147	1	0,210	-0,198
Zn	0,009	-0,263	0,225	0,261	0,051	-0,354	-0,393	-0,309	0,006	0,154	0,270	-0,296	-0,431	-0,063	-0,236	0,475	0,284	-0,330	0,405	0,327	0,210	1	-.923**
Zr	-0,164	0,410	-0,230	-0,184	-0,011	.528*	0,436	0,385	0,218	-0,256	-0,247	0,292	0,472	-0,056	0,280	-0,517	-0,255	0,167	-0,332	-0,100	-0,198	-.923**	1

****. Correlation is significant at the 0.01 level (2-tailed).**

***. Correlation is significant at the 0.05 level (2-tailed).**

Appendix 39: Correlation of elements within the saprolith horizon in Serpens North.

Element	SiO2	Al2O3	Fe2O3	MnO	MgO	CaO	Na2O	K2O	TiO2	P2O5	SO3	Ba	Ce	Co	Nd	Ni	Pb	Rb	Sr	V	Y	Zn	Zr
SiO2	1	-0,120	-.836**	-0,158	-0,032	-.433**	0,104	.326**	-.855**	0,101	-0,118	0,000	0,090	-.213*	-0,060	0,073	0,163	0,108	-.213*	-.311**	0,027	-.234*	.221*
Al2O3	-0,120	1	-.291**	-.459**	-.445**	.211*	.693**	.525**	0,168	-.328**	-0,056	0,073	-0,045	-0,024	0,138	-0,106	-.240*	-0,037	.308**	0,138	0,096	0,102	0,042
Fe2O3	-.836**	-.291**	1	.377**	-0,111	0,093	-.433**	-.483**	.759**	0,135	0,174	0,031	-0,008	0,146	0,011	-0,201	0,041	0,046	0,054	.258*	-0,040	0,143	-0,114
MnO	-0,158	-.459**	.377**	1	0,121	-0,009	-.399**	-.364**	-0,009	.384**	0,010	-0,059	0,021	-0,071	-0,104	-0,028	0,088	-0,005	-0,081	-0,118	-0,072	-0,079	0,058
MgO	-0,032	-.445**	-0,111	0,121	1	.207*	-.258*	-.307**	-0,195	-0,071	-0,081	-0,150	-0,033	0,107	-0,060	.444**	-0,080	-.219*	-0,152	-0,162	-0,112	-0,068	-0,177
CaO	-.433**	.211*	0,093	-0,009	.207*	1	.221*	-.376**	0,203	-.262*	0,038	-0,069	-0,210	.268*	-0,009	0,097	-0,190	-.380**	.299**	0,199	-0,003	.354**	-.380**
Na2O	0,104	.693**	-.433**	-.399**	-.258*	.221*	1	.235*	-0,019	-0,189	-0,074	-0,058	-.311**	-0,004	-0,147	0,052	-.404**	-0,075	.274**	0,148	0,055	0,188	-0,050
K2O	.326**	.525**	-.483**	-.364**	-.307**	-.376**	.235*	1	-0,181	-0,141	-.246*	0,031	0,122	-.276*	0,172	-0,010	-0,063	.208*	-0,058	-0,174	0,081	-0,165	0,207
TiO2	-.855**	0,168	.759**	-0,009	-0,195	0,203	-0,019	-0,181	1	-0,181	0,173	0,058	-0,077	0,167	0,047	-0,116	-0,141	-0,059	0,192	.313**	0,000	0,191	-0,142
P2O5	0,101	-.328**	0,135	.384**	-0,071	-.262*	-0,189	-0,141	-0,181	1	0,195	-0,006	0,035	-0,046	-0,136	-0,202	-0,049	.266*	-0,093	0,060	-0,035	0,029	0,093
SO3	-0,118	-0,056	0,174	0,010	-0,081	0,038	-0,074	-.246*	0,173	0,195	1	-0,014	0,013	0,023	-0,112	-0,181	-0,138	-0,060	0,107	0,108	0,045	0,131	-0,083
Ba	0,000	0,073	0,031	-0,059	-0,150	-0,069	-0,058	0,031	0,058	-0,006	-0,014	1	.289*	.455**	0,217	-0,053	0,212	0,096	-0,101	-0,069	.495**	-.282**	.288**
Ce	0,090	-0,045	-0,008	0,021	-0,033	-0,210	-.311**	0,122	-0,077	0,035	0,013	.289*	1	0,176	.869**	0,055	.349**	0,130	-.230*	-0,184	0,157	-0,193	.263*
Co	-.213*	-0,024	0,146	-0,071	0,107	.268*	-0,004	-.276*	0,167	-0,046	0,023	.455**	0,176	1	.264*	0,095	0,167	-.336**	-0,135	.520**	.341**	.361**	-0,181
Nd	-0,060	0,138	0,011	-0,104	-0,060	-0,009	-0,147	0,172	0,047	-0,136	-0,112	0,217	.869**	.264*	1	0,186	0,248	0,073	-0,092	-0,048	0,169	-0,007	0,233
Ni	0,073	-0,106	-0,201	-0,028	.444**	0,097	0,052	-0,010	-0,116	-0,202	-0,181	-0,053	0,055	0,095	0,186	1	-0,187	-.315**	-0,046	-0,045	-0,077	0,187	-.250*
Pb	0,163	-.240*	0,041	0,088	-0,080	-0,190	-.404**	-0,063	-0,141	-0,049	-0,138	0,212	.349**	0,167	0,248	-0,187	1	0,066	-0,083	-0,082	0,108	-0,172	0,161
Rb	0,108	-0,037	0,046	-0,005	-.219*	-.380**	-0,075	.208*	-0,059	.266*	-0,060	0,096	0,130	-.336**	0,073	-.315**	0,066	1	0,099	-.214*	0,155	-.323**	.450**
Sr	-.213*	.308**	0,054	-0,081	-0,152	.299**	.274**	-0,058	0,192	-0,093	0,107	-0,101	-.230*	-0,135	-0,092	-0,046	-0,083	0,099	1	-0,095	-0,082	.233*	-0,041
V	-.311**	0,138	.258*	-0,118	-0,162	0,199	0,148	-0,174	.313**	0,060	0,108	-0,069	-0,184	.520**	-0,048	-0,045	-0,082	-.214*	-0,095	1	-0,002	.758**	-.394**
Y	0,027	0,096	-0,040	-0,072	-0,112	-0,003	0,055	0,081	0,000	-0,035	0,045	.495**	0,157	.341**	0,169	-0,077	0,108	0,155	-0,082	-0,002	1	-0,144	0,184
Zn	-.234*	0,102	0,143	-0,079	-0,068	.354**	0,188	-0,165	0,191	0,029	0,131	-.282**	-0,193	.361**	-0,007	0,187	-0,172	-.323**	.233*	.758**	-0,144	1	-.636**
Zr	.221*	0,042	-0,114	0,058	-0,177	-.380**	-0,050	0,207	-0,142	0,093	-0,083	.288**	.263*	-0,181	0,233	-.250*	0,161	.450**	-0,041	-.394**	0,184	-.636**	1

****. Correlation is significant at the 0.01 level (2-tailed).**

***. Correlation is significant at the 0.05 level (2-tailed).**

Appendix 40: Contributions of each variable to the principal components across the regolith profiles in Sirius.

Element	PC1	PC2	PC3	PC4
SiO2	4,966	3,831	5,021	0,174
Al2O3	4,264	0,387	10,428	8,206
Fe2O3	3,863	2,346	13,071	0,071
MnO	0,837	12,803	4,378	2,509
MgO	6,307	1,105	2,228	3,898
CaO	4,760	1,074	3,111	14,504
Na2O	5,957	2,280	3,681	0,103
K2O	5,899	0,909	6,742	0,026
TiO2	6,411	0,814	1,821	4,793
P2O5	5,653	4,248	0,021	1,957
SO3	3,465	0,109	0,310	32,656
LOI	0,004	11,401	12,275	0,288
Ba	4,691	6,673	0,602	0,107
Ce	2,549	10,839	1,444	0,986
Co	0,536	14,949	0,342	4,376
Nd	2,565	9,477	4,261	0,724
Pb	4,169	6,915	2,242	0,516
Rb	4,675	0,888	12,338	0,030
Sr	4,287	0,908	3,904	17,386
V	3,481	4,404	10,703	0,018
Y	7,094	1,381	0,214	0,293
Zn	6,720	0,323	0,671	6,047
Zr	6,848	1,936	0,191	0,330

Appendix 41: Contributions of each variable to the principal components within the aeolian sand horizon in Sirius.

Element	PC1	PC2	PC3
SiO2	6,494	0,034	0,120
Al2O3	2,450	8,701	12,835
Fe2O3	6,497	0,000	0,250
MgO	6,253	0,456	1,358
CaO	6,024	0,965	1,980
Na2O	4,221	6,117	1,134
K2O	2,296	11,644	0,095
TiO2	3,328	8,751	0,289
P2O5	1,879	11,024	9,064
SO3	5,859	0,821	5,019
LOL	2,931	3,557	32,131
Ba	6,458	0,143	0,070
Ce	1,304	14,395	0,057
Co	6,463	0,110	0,160
Nd	0,143	17,613	0,016
Pb	3,858	3,273	20,598
Rb	3,070	9,450	0,368
Sr	6,424	0,023	1,150
V	6,402	0,220	0,466
Y	5,183	1,419	11,454
Zn	6,423	0,097	0,797
Zr	6,043	1,188	0,591

Appendix 42: Contributions of variables to the principal component in the calcrete horizon in Sirius.

Element	PC1	PC2	PC3	PC4	PC5	PC6	PC7	PC8	PC9	PC10
SiO2	4,792	7,497	0,197	0,619	5,691	1,045	1,720	5,827	0,009	0,417
Al2O3	7,481	1,814	0,000	0,052	5,229	0,877	1,562	0,082	13,737	0,369
Fe2O3	6,749	2,906	0,836	1,011	0,417	7,446	2,665	3,156	0,038	7,557
MgO	3,210	8,078	2,044	0,715	8,524	22,742	2,300	0,013	1,226	8,185
CaO	7,471	2,169	0,222	0,000	3,657	0,006	0,028	4,420	3,909	3,472
Na2O	5,065	6,196	1,556	5,152	0,000	2,349	1,495	2,780	1,145	1,795
K2O	7,541	0,000	0,286	0,000	22,517	0,233	0,643	4,580	1,021	3,157
TiO2	6,198	3,752	3,627	0,059	0,317	2,040	1,429	0,714	16,596	0,524
P2O5	5,750	3,259	1,241	6,360	12,053	1,966	0,652	4,708	0,117	4,058
SO3	0,300	0,099	31,356	43,454	2,516	1,160	0,045	2,156	0,886	0,467
LOI	7,538	1,879	1,195	0,361	1,886	0,340	4,045	0,137	1,881	1,777
Ba	6,140	3,934	0,016	0,007	0,210	0,909	0,057	20,577	16,779	20,192
Ce	2,356	8,360	9,448	1,831	2,060	4,149	12,128	16,547	1,621	13,217
Co	5,838	3,703	1,123	1,583	3,726	3,989	9,406	2,612	25,053	1,782
Pb	1,215	0,934	35,008	15,745	0,134	15,142	0,120	10,051	0,001	5,260
Rb	7,371	0,050	2,799	1,693	8,651	0,082	10,787	0,152	0,040	15,783
Sr	2,879	11,091	1,212	0,063	0,653	8,923	2,896	0,138	0,740	6,533
V	2,349	10,533	0,426	2,873	13,644	0,161	11,235	3,796	14,680	2,269
Y	0,002	12,773	1,203	7,325	2,398	24,124	33,209	1,024	0,501	0,163
Zn	5,687	3,125	6,057	2,868	2,295	0,166	2,674	16,523	0,000	0,691
Zr	4,070	7,846	0,147	8,228	3,421	2,154	0,905	0,005	0,021	2,332

Appendix 43: Contributions of variations to the principal components within the saprolith in Sirius.

Element	PC1	PC2	PC3	PC4
SiO2	4,966	3,831	5,021	0,174
Al2O3	4,264	0,387	10,428	8,206
Fe2O3	3,863	2,346	13,071	0,071
MnO	0,837	12,803	4,378	2,509
MgO	6,307	1,105	2,228	3,898
CaO	4,760	1,074	3,111	14,504
Na2O	5,957	2,280	3,681	0,103
K2O	5,899	0,909	6,742	0,026
TiO2	6,411	0,814	1,821	4,793
P2O5	5,653	4,248	0,021	1,957
SO3	3,465	0,109	0,310	32,656
LOI	0,004	11,401	12,275	0,288
Ba	4,691	6,673	0,602	0,107
Ce	2,549	10,839	1,444	0,986
Co	0,536	14,949	0,342	4,376
Nd	2,565	9,477	4,261	0,724
Pb	4,169	6,915	2,242	0,516
Rb	4,675	0,888	12,338	0,030
Sr	4,287	0,908	3,904	17,386
V	3,481	4,404	10,703	0,018
Y	7,094	1,381	0,214	0,293
Zn	6,720	0,323	0,671	6,047
Zr	6,848	1,936	0,191	0,330

Appendix 44: Pearson's correlation of elements across profiles in Serpens North Prospect.

Element	SiO2	Al2O3	Fe2O3	MgO	CaO	Na2O	K2O	TiO2	P2O5	SO3	LOI	Ba	Ce	Co	Nd	Pb	Rb	Sr	V	Y	Zn	Zr
SiO2	1,000	0,106	-.788**	-.825**	-.325**	-.448**	.352**	-.589**	0,091	0,078	-.347**	-.359**	-0,162	-.725**	0,182	0,022	.389**	-.730**	-.773**	-0,108	-.785**	.884**
Al2O3	0,106	1,000	0,013	0,151	-.544**	.474**	.579**	0,003	-.275**	-0,122	-.418**	.375**	0,179	0,144	-0,319	0,101	.673**	-0,021	0,016	.256*	.218*	-0,093
Fe2O3	-.788**	0,013	1,000	.743**	-.249*	.442**	-.452**	.772**	-.415**	-.217*	-.208*	.405**	.227*	.861**	-0,204	0,034	-.448**	.611**	.879**	-0,013	.874**	-.789**
MgO	-.825**	0,151	.743**	1,000	0,020	.560**	-.269**	.557**	-.351**	-0,044	0,024	.289**	0,141	.707**	-0,164	0,084	-.331**	.813**	.704**	0,008	.852**	-.897**
CaO	-.325**	-.544**	-.249*	0,020	1,000	-0,161	-0,155	-0,170	.546**	.251*	.771**	-.249*	-0,118	-0,188	0,212	-0,116	-.208*	0,187	-0,088	0,039	-0,181	-0,072
Na2O	-.448**	.474**	.442**	.560**	-0,161	1,000	-0,065	.430**	-.365**	0,057	-.199*	.271**	0,148	.538**	-0,090	0,186	-0,046	.560**	.531**	-0,147	.621**	-.638**
K2O	.352**	.579**	-.452**	-.269**	-0,155	-0,065	1,000	-.476**	0,138	-0,180	-0,001	0,115	-0,025	-.378**	-0,083	-0,181	.913**	-.491**	-.470**	.373**	-.334**	.271**
TiO2	-.589**	0,003	.772**	.557**	-0,170	.430**	-.476**	1,000	-.361**	-0,091	-.301**	.225*	.233*	.788**	-0,022	0,128	-.421**	.462**	.900**	-0,143	.733**	-.518**
P2O5	0,091	-.275**	-.415**	-.351**	.546**	-.365**	0,138	-.361**	1,000	.298**	.403**	-.242*	-0,099	-.365**	-0,082	-0,179	0,110	-.275*	-.289**	0,162	-.402**	.245*
SO3	0,078	-0,122	-.217*	-0,044	.251*	0,057	-0,180	-0,091	.298**	1,000	0,039	-.316**	-0,066	-.230*	0,262	-0,038	-0,163	0,084	-0,117	-0,188	-0,131	0,061
LOI	-.347**	-.418**	-.208*	0,024	.771**	-.199*	-0,001	-.301**	.403**	0,039	1,000	0,025	-0,169	-.224*	0,058	-0,140	-0,046	0,055	-0,160	.203*	-0,175	-0,119
Ba	-.359**	.375**	.405**	.289**	-.249*	.271**	0,115	.225*	-.242*	-.316**	0,025	1,000	.447**	.535**	0,212	0,190	0,181	0,177	.371**	.581**	.369**	-.327**
Ce	-0,162	0,179	.227*	0,141	-0,118	0,148	-0,025	.233*	-0,099	-0,066	-0,169	.447**	1,000	.342**	.539**	.310**	-0,021	0,126	.299**	.246*	0,182	-0,086
Co	-.725**	0,144	.861**	.707**	-0,188	.538**	-.378**	.788**	-.365**	-.230*	-.224*	.535**	.342**	1,000	-0,034	0,190	-.340**	.563**	.896**	0,054	.885**	-.681**
Nd	0,182	-0,319	-0,204	-0,164	0,212	-0,090	-0,083	-0,022	-0,082	0,262	0,058	0,212	.539**	-0,034	1,000	0,251	-0,160	-0,008	-0,099	0,095	-0,274	0,150
Pb	0,022	0,101	0,034	0,084	-0,116	0,186	-0,181	0,128	-0,179	-0,038	-0,140	0,190	.310**	0,190	0,251	1,000	-0,117	0,131	0,169	0,040	0,060	0,023
Rb	.389**	.673**	-.448**	-.331**	-.208*	-0,046	.913**	-.421**	0,110	-0,163	-0,046	0,181	-0,021	-.340**	-0,160	-0,117	1,000	-.497**	-.444**	.443**	-.327**	.344**
Sr	-.730**	-0,021	.611**	.813**	0,187	.560**	-.491**	.462**	-.275*	0,084	0,055	0,177	0,126	.563**	-0,008	0,131	-.497**	1,000	.586**	-0,060	.656**	-.783**
V	-.773**	0,016	.879**	.704**	-0,088	.531**	-.470**	.900**	-.289**	-0,117	-0,160	.371**	.299**	.896**	-0,099	0,169	-.444**	.586**	1,000	-0,067	.840**	-.698**
Y	-0,108	.256*	-0,013	0,008	0,039	-0,147	.373**	-0,143	0,162	-0,188	.203*	.581**	.246*	0,054	0,095	0,040	.443**	-0,060	-0,067	1,000	-0,074	0,009
Zn	-.785**	.218*	.874**	.852**	-0,181	.621**	-.334**	.733**	-.402**	-0,131	-0,175	.369**	0,182	.885**	-0,274	0,060	-.327**	.656**	.840**	-0,074	1,000	-.839**
Zr	.884**	-0,093	-.789**	-.897**	-0,072	-.638**	.271**	-.518**	.245*	0,061	-0,119	-.327**	-0,086	-.681**	0,150	0,023	.344**	-.783**	-.698**	0,009	-.839**	1,000

****. Correlation is significant at the 0.01 level (2-tailed).**

***. Correlation is significant at the 0.05 level (2-tailed).**

Appendix 45: Pearson's correlation of elements within the eaolian sand horizon in Sirius Prospect.

Element	SiO2	Al2O3	Fe2O3	MgO	CaO	Na2O	K2O	TiO2	P2O5	SO3	LOI	Ba	Ce	Co	Nd	Pb	Rb	Sr	V	Y	Zn	Zr
SiO2	1	.576*	-0,472	-.844**	-.749**	-0,261	-0,364	-0,028	-.633*	0,028	-.822**	-0,481	-0,346	-0,374	-0,104	0,022	.760**	-.956**	-.598*	-0,280	-0,482	.843**
Al2O3	.576*	1	0,326	-0,154	-.900**	0,276	0,326	.555*	-0,484	-.603*	-.892**	0,301	0,075	0,379	-0,602	0,443	.599*	-.752**	0,137	0,298	0,306	0,269
Fe2O3	-0,472	0,326	1	.802**	-0,227	.819**	.542*	.585*	0,041	-.656**	-0,083	.933**	0,346	.863**	0,148	.634*	-0,326	0,249	.918**	.613*	.956**	-.720**
MgO	-.844**	-0,154	.802**	1	0,327	.606*	.588*	0,377	0,506	-0,350	0,422	.860**	0,450	.776**	-0,011	0,378	-.556*	.726**	.853**	.589*	.840**	-.880**
CaO	-.749**	-.900**	-0,227	0,327	1	-0,318	-0,022	-0,421	.662**	0,480	.966**	-0,180	-0,072	-0,250	-0,085	-0,500	-.600*	.871**	-0,024	-0,184	-0,186	-0,401
Na2O	-0,261	0,276	.819**	.606*	-0,318	1	0,138	0,443	-0,143	-.671**	-0,173	.828**	0,590	.814**	0,697	.718**	-0,384	0,102	.765**	.556*	.836**	-.664**
K2O	-0,364	0,326	.542*	.588*	-0,022	0,138	1	.736**	0,349	-0,307	-0,049	.569*	-0,013	.523*	-0,707	0,067	0,155	0,189	0,422	0,419	.600*	-0,371
TiO2	-0,028	.555*	.585*	0,377	-0,421	0,443	.736**	1	-0,021	-0,460	-0,398	.599*	-0,082	.617*	-0,584	0,254	0,337	-0,183	0,397	.566*	.664**	-0,229
P2O5	-.633*	-0,484	0,041	0,506	.662**	-0,143	0,349	-0,021	1	0,430	.610*	0,134	-0,187	0,089	-0,690	-0,229	-0,314	.715**	0,325	0,070	0,073	-0,396
SO3	0,028	-.603*	-.656**	-0,350	0,480	-.671**	-0,307	-0,460	0,430	1	0,370	-.662**	-0,601	-.725**	-0,348	-.647**	0,121	0,208	-0,482	-.664**	-.699**	0,363
LOI	-.822**	-.892**	-0,083	0,422	.966**	-0,173	-0,049	-0,398	.610*	0,370	1	-0,050	0,279	-0,137	0,531	-0,380	-.727**	.917**	0,107	-0,066	-0,070	-0,492
Ba	-0,481	0,301	.933**	.860**	-0,180	.828**	.569*	.599*	0,134	-.662**	-0,050	1	0,528	.969**	0,060	.677**	-0,283	0,295	.879**	.765**	.976**	-.706**
Ce	-0,346	0,075	0,346	0,450	-0,072	0,590	-0,013	-0,082	-0,187	-0,601	0,279	0,528	1	0,568	0,950	.725*	-0,530	0,422	0,314	0,575	0,487	-0,503
Co	-0,374	0,379	.863**	.776**	-0,250	.814**	.523*	.617*	0,089	-.725**	-0,137	.969**	0,568	1	0,070	.674**	-0,193	0,186	.818**	.847**	.946**	-.633*
Nd	-0,104	-0,602	0,148	-0,011	-0,085	0,697	-0,707	-0,584	-0,690	-0,348	0,531	0,060	0,950	0,070	1	0,542	-0,817	0,184	0,257	-0,150	0,076	-0,398
Pb	0,022	0,443	.634*	0,378	-0,500	.718**	0,067	0,254	-0,229	-.647**	-0,380	.677**	.725*	.674**	0,542	1	-0,102	-0,136	.594*	.553*	.639*	-0,236
Rb	.760**	.599*	-0,326	-.556*	-.600*	-0,384	0,155	0,337	-0,314	0,121	-.727**	-0,283	-0,530	-0,193	-0,817	-0,102	1	-.757**	-0,462	-0,117	-0,280	.760**
Sr	-.956**	-.752**	0,249	.726**	.871**	0,102	0,189	-0,183	.715**	0,208	.917**	0,295	0,422	0,186	0,184	-0,136	-.757**	1	0,437	0,131	0,265	-.719**
V	-.598*	0,137	.918**	.853**	-0,024	.765**	0,422	0,397	0,325	-0,482	0,107	.879**	0,314	.818**	0,257	.594*	-0,462	0,437	1	.573*	.863**	-.774**
Y	-0,280	0,298	.613*	.589*	-0,184	.556*	0,419	.566*	0,070	-.664**	-0,066	.765**	0,575	.847**	-0,150	.553*	-0,117	0,131	.573*	1	.729**	-0,374
Zn	-0,482	0,306	.956**	.840**	-0,186	.836**	.600*	.664**	0,073	-.699**	-0,070	.976**	0,487	.946**	0,076	.639*	-0,280	0,265	.863**	.729**	1	-.743**
Zr	.843**	0,269	-.720**	-.880**	-0,401	-.664**	-0,371	-0,229	-0,396	0,363	-0,492	-.706**	-0,503	-.633*	-0,398	-0,236	.760**	-.719**	-.774**	-0,374	-.743**	1

*. Correlation is significant at the 0.05 level (2-tailed).

**. Correlation is significant at the 0.01 level (2-tailed).

Appendix 46: Pearson's correlation of elements within the calcrete horizon in the Sirius Prospect.

Element	SiO2	Al2O3	Fe2O3	MnO	MgO	CaO	Na2O	K2O	TiO2	P2O5	SO3	LOI	Ba	Ce	Co	Nd	Pb	Rb	Sr	V	Y	Zn	Zr
SiO2	1	.754**	-0,180	-.951*	-.634**	-.779**	-0,009	.685**	0,330	-.885**	-0,251	-.769**	0,102	-0,093	-0,167	-0,457	0,191	.512*	-.907**	-0,362	-.595**	-0,294	.861**
Al2O3	.754**	1	0,257	-.997**	-.664**	-.846**	0,383	.527*	.527*	-.773**	-0,147	-.865**	.487*	0,261	0,270	-0,325	0,247	.670**	-.657**	0,063	-0,277	0,075	.665**
Fe2O3	-0,180	0,257	1	.953*	0,246	-.464*	.766**	-.447*	.536*	-.510*	-0,242	-.458*	.608**	0,397	.877**	0,181	-0,261	-0,159	0,317	.564**	0,320	.910**	-.449*
MnO	-.951*	-.997**	.953*	1	.969*	0,643	0,925	-.982*	0,820	.c	-0,592	-0,061	0,646	1.000**	.972*	.c	-0,913	-0,928	.956*	0,934	0,528	.976*	-.961*
MgO	-.634**	-.664**	0,246	.969*	1	0,390	0,240	-.467*	0,080	.510*	0,011	.432*	-0,126	0,155	0,092	0,987	-0,386	-.760**	.749**	0,220	0,216	0,418	-.788**
CaO	-.779**	-.846**	-.464*	0,643	0,390	1	-.488*	-0,359	-.641**	.906**	0,357	.955**	-.469*	-0,197	-0,381	.999*	-0,008	-0,360	.611**	-0,025	0,358	-0,299	-.480*
Na2O	-0,009	0,383	.766**	0,925	0,240	-.488*	1	-0,008	.802**	-0,434	-0,139	-.506*	.726**	.658**	.766**	0,564	-0,069	0,051	0,213	.591**	0,177	.670**	-0,263
K2O	.685**	.527*	-.447*	-.982*	-.467*	-0,359	-0,008	1	.430*	-.693**	-0,165	-0,363	0,046	0,212	-0,371	0,783	0,358	.603**	-.674**	-0,275	-0,417	-.583**	.704**
TiO2	0,330	.527*	.536*	0,820	0,080	-.641**	.802**	.430*	1	-.545*	-0,175	-.677**	.608**	.615**	.505*	0,876	0,042	0,217	-0,115	0,317	-0,004	0,376	0,059
P2O5	-.885**	-.773**	-.510*	.c	.510*	.906**	-0,434	-.693**	-.545*	1	0,402	.879**	-0,293	-0,088	-0,236	-1.000*	-0,057	-0,405	.772**	0,137	.515*	-0,404	-.754**
SO3	-0,251	-0,147	-0,242	-0,592	0,011	0,357	-0,139	-0,165	-0,175	0,402	1	0,229	-0,109	-0,268	-0,072	-0,042	-0,122	-0,010	0,352	0,248	0,198	-0,145	0,001
LOI	-.769**	-.865**	-.458*	-0,061	.432*	.955**	-.506*	-0,363	-.677**	.879**	0,229	1	-.516*	-0,181	-.425*	0,853	-0,051	-0,404	.588**	-0,083	0,275	-0,307	-.509*
Ba	0,102	.487*	.608**	0,646	-0,126	-.469*	.726**	0,046	.608**	-0,293	-0,109	-.516*	1	.626**	.764**	0,148	0,249	.456*	0,076	.641**	.482*	0,365	0,008
Ce	-0,093	0,261	0,397	1.000**	0,155	-0,197	.658**	0,212	.615**	-0,088	-0,268	-0,181	.626**	1	.562*	0,237	0,361	0,301	0,176	.613**	0,420	0,243	-0,117
Co	-0,167	0,270	.877**	.972*	0,092	-0,381	.766**	-0,371	.505*	-0,236	-0,072	-.425*	.764**	.562*	1	-0,226	0,049	0,113	0,290	.770**	.504*	.733**	-0,295
Nd	-0,457	-0,325	0,181	.c	0,987	.999*	0,564	0,783	0,876	-1.000*'	-0,042	0,853	0,148	0,237	-0,226	1	-0,784	-0,457	0,665	0,316	-0,313	0,577	-0,900
Pb	0,191	0,247	-0,261	-0,913	-0,386	-0,008	-0,069	0,358	0,042	-0,057	-0,122	-0,051	0,249	0,361	0,049	-0,784	1	.610**	-0,249	0,083	0,264	-.455*	.463*
Rb	.512*	.670**	-0,159	-0,928	-.760**	-0,360	0,051	.603**	0,217	-0,405	-0,010	-0,404	.456*	0,301	0,113	-0,457	.610**	1	-.530*	0,197	0,062	-.442*	.733**
Sr	-.907**	-.657**	0,317	.956*	.749**	.611**	0,213	-.674**	-0,115	.772**	0,352	.588**	0,076	0,176	0,290	0,665	-0,249	-.530*	1	.464*	.558**	.441*	-.859**
V	-0,362	0,063	.564**	0,934	0,220	-0,025	.591**	-0,275	0,317	0,137	0,248	-0,083	.641**	.613**	.770**	0,316	0,083	0,197	.464*	1	.656**	.438*	-0,284
Y	-.595**	-0,277	0,320	0,528	0,216	0,358	0,177	-0,417	-0,004	.515*	0,198	0,275	.482*	0,420	.504*	-0,313	0,264	0,062	.558**	.656**	1	0,167	-0,388
Zn	-0,294	0,075	.910**	.976*	0,418	-0,299	.670**	-.583**	0,376	-0,404	-0,145	-0,307	0,365	0,243	.733**	0,577	-.455*	-.442*	.441*	.438*	0,167	1	-.603**
Zr	.861**	.665**	-.449*	-.961*	-.788**	-.480*	-0,263	.704**	0,059	-.754**	0,001	-.509*	0,008	-0,117	-0,295	-0,900	.463*	.733**	-.859**	-0,284	-0,388	-.603**	1

**. Correlation is significant at the 0.01 level (2-tailed).
*. Correlation is significant at the 0.05 level (2-tailed).

Appendix 47: Correlation of element within the saprolith horizon in the Sirius Prospect.

Element	SiO2	Al2O3	Fe2O3	MnO	MgO	CaO	Na2O	K2O	TiO2	P2O5	SO3	LOI	Ba	Ce	Co	Nd	Pb	Rb	Sr	V	Y	Zn	Zr
SiO2	1	0,052	-.914**	-0,212	-.831**	-0,236	-.374**	.388**	-.696**	0,212	0,003	-0,056	-.262*	-0,155	-.809**	0,149	0,061	.340**	-.637**	-.836**	0,028	-.878**	.872**
Al2O3	0,052	1	-.285*	-0,224	0,107	-0,244	.450**	.704**	-0,206	0,068	-0,056	-0,027	.329**	0,274	-0,034	-0,106	0,000	.780**	-0,061	-0,160	.380**	0,059	-0,063
Fe2O3	-.914**	-.285*	1	0,231	.685**	0,036	0,239	-.559**	.782**	-0,261	-0,082	-0,167	0,179	0,151	.837**	-0,182	-0,047	-.503**	.532**	.894**	-0,168	.837**	-.754**
MnO	-0,212	-0,224	0,231	1	0,138	0,168	0,084	-0,398	0,223	0,424	0,129	0,030	.548*	0,504	.857**	.914*	.561*	-0,360	0,235	0,342	0,268	0,087	0,004
MgO	-.831**	0,107	.685**	0,138	1	0,247	.415**	-.289*	.487**	-0,267	0,135	-0,096	0,072	0,134	.635**	-0,110	0,031	-.283*	.752**	.634**	-0,079	.819**	-.871**
CaO	-0,236	-0,244	0,036	0,168	0,247	1	0,061	-.299*	0,104	0,212	.354*	0,138	-0,221	-0,107	0,007	0,333	-0,016	-.322*	.446**	0,077	-0,064	0,072	-0,199
Na2O	-.374**	.450**	0,239	0,084	.415**	0,061	1	-0,031	.302*	-0,186	0,224	-0,239	0,087	0,126	.391**	0,114	0,147	0,009	.461**	.412**	-0,243	.482**	-.557**
K2O	.388**	.704**	-.559**	-0,398	-.289*	-.299*	-0,031	1	-.572**	0,198	-0,210	0,171	0,156	0,051	-.412**	-0,262	-0,251	.966**	-.522**	-.553**	.480**	-.366**	.282*
TiO2	-.696**	-0,206	.782**	0,223	.487**	0,104	.302*	-.572**	1	-0,266	0,010	-.344**	0,067	0,198	.765**	-0,041	0,086	-.459**	.397**	.933**	-0,218	.704**	-.478**
P2O5	0,212	0,068	-0,261	0,424	-0,267	0,212	-0,186	0,198	-0,266	1	0,164	0,064	-0,016	-0,033	-0,266	0,486	-0,217	0,186	-.291*	-.280*	0,204	-.303*	0,196
SO3	0,003	-0,056	-0,082	0,129	0,135	.354*	0,224	-0,210	0,010	0,164	1	-0,066	-0,236	0,037	-0,144	0,480	0,060	-0,231	0,204	-0,022	-0,187	-0,005	-0,114
LOI	-0,056	-0,027	-0,167	0,030	-0,096	0,138	-0,239	0,171	-.344**	0,064	-0,066	1	.279*	-0,234	-.271*	-0,129	-0,129	0,178	-0,174	-.277*	.324*	-0,187	0,018
Ba	-.262*	.329**	0,179	.548*	0,072	-0,221	0,087	0,156	0,067	-0,016	-0,236	.279*	1	.496**	.402**	0,353	0,095	.265*	-0,016	0,189	.628**	0,188	-0,121
Ce	-0,155	0,274	0,151	0,504	0,134	-0,107	0,126	0,051	0,198	-0,033	0,037	-0,234	.496**	1	.363**	0,465	.297*	0,096	0,098	0,267	0,225	0,184	0,004
Co	-.809**	-0,034	.837**	.857**	.635**	0,007	.391**	-.412**	.765**	-0,266	-0,144	-.271*	.402**	.363**	1	0,212	0,129	-.360**	.459**	.885**	-0,046	.858**	-.620**
Nd	0,149	-0,106	-0,182	.914*	-0,110	0,333	0,114	-0,262	-0,041	0,486	0,480	-0,129	0,353	0,465	0,212	1	0,452	-0,283	0,136	-0,026	0,229	-0,148	0,046
Pb	0,061	0,000	-0,047	.561*	0,031	-0,016	0,147	-0,251	0,086	-0,217	0,060	-0,129	0,095	.297*	0,129	0,452	1	-0,192	0,135	0,098	-0,076	0,007	0,086
Rb	.340**	.780**	-.503**	-0,360	-.283*	-.322*	0,009	.966**	-.459**	0,186	-0,231	0,178	.265*	0,096	-.360**	-0,283	-0,192	1	-.485**	-.476**	.551**	-.323*	.283*
Sr	-.637**	-0,061	.532**	0,235	.752**	.446**	.461**	-.522**	.397**	-.291*	0,204	-0,174	-0,016	0,098	.459**	0,136	0,135	-.485**	1	.496**	-0,166	.566**	-.715**
V	-.836**	-0,160	.894**	0,342	.634**	0,077	.412**	-.553**	.933**	-.280*	-0,022	-.277*	0,189	0,267	.885**	-0,026	0,098	-.476**	.496**	1	-0,231	.831**	-.643**
Y	0,028	.380**	-0,168	0,268	-0,079	-0,064	-0,243	.480**	-0,218	0,204	-0,187	.324*	.628**	0,225	-0,046	0,229	-0,076	.551**	-0,166	-0,231	1	-0,182	0,156
Zn	-.878**	0,059	.837**	0,087	.819**	0,072	.482**	-.366**	.704**	-.303*	-0,005	-0,187	0,188	0,184	.858**	-0,148	0,007	-.323*	.566**	.831**	-0,182	1	-.819**
Zr	.872**	-0,063	-.754**	0,004	-.871**	-0,199	-.557**	.282*	-.478**	0,196	-0,114	0,018	-0,121	0,004	-.620**	0,046	0,086	.283*	-.715**	-.643**	0,156	-.819**	1

**. Correlation is significant at the 0.01 level (2-tailed).

*. Correlation is significant at the 0.05 level (2-tailed).

Appendix 48: The collective contributions of variables to the principal components in the Serpens North Prospect (%).

	PC1	PC2	PC3	PC4	PC5	PC6	PC7	PC8	PC9	F10
Trace element (ppb)										
As	1,350	42,679	10,447	0,380	0,208	0,070	4,129	10,967	27,889	1,881
Fe	26,398	0,256	2,212	0,026	1,610	2,129	22,258	2,150	5,073	37,889
Mn	8,301	17,008	7,579	0,009	1,633	2,623	24,472	35,220	2,414	0,740
Cu	13,624	9,726	0,191	0,974	3,993	17,922	15,439	29,344	1,507	7,278
Co	25,874	4,191	2,570	0,368	1,602	1,281	14,506	0,772	10,177	38,660
Ni	11,554	2,048	3,360	4,166	16,304	40,685	5,305	3,178	9,590	3,812
Pd	5,074	9,400	4,306	3,280	41,304	14,474	13,116	0,469	8,562	0,016
Au	0,376	4,336	14,444	62,719	0,311	0,221	0,666	8,829	7,231	0,865
Pt	0,544	8,394	17,401	26,962	28,818	0,470	0,070	7,660	4,162	5,519
Hg	6,905	1,963	37,490	1,115	4,215	20,126	0,042	1,410	23,395	3,340

Appendix 49: Contributions of variables to the principal components within the Aeolian sand in the Serpens North Prospect (%).

	PC1	PC2	PC3	PC4	PC5	PC6	PC7	PC8	PC9
Trace elements (ppb)									
As	10,013	2,937	10,059	10,475	32,344	23,186	0,999	3,350	5,720
Fe	19,737	3,990	0,301	1,493	0,096	12,360	0,205	6,105	0,601
Mn	1,262	18,975	4,603	19,264	40,078	4,586	5,188	0,058	1,023
Cu	19,291	0,059	6,104	1,582	3,781	9,992	20,988	30,490	1,044
Co	20,602	1,705	0,341	1,442	0,214	11,726	14,865	7,523	41,343
Ni	12,260	7,898	8,175	18,795	0,355	0,016	13,028	3,413	31,620
Pd	3,336	18,117	4,290	19,854	11,143	20,569	21,123	0,083	0,824
Au	13,080	5,969	7,858	13,985	6,162	8,346	1,440	19,355	1,106
Pt	0,376	7,225	57,040	1,411	4,501	5,674	1,907	16,644	3,487
Hg	0,042	33,125	1,227	11,698	1,326	3,545	20,256	12,978	13,233

Appendix 50: Contributions of the variables to the principal component within the calcretes in Serpens North Prospect (%).

	PC1	PC2	PC3	PC4	PC5	PC6	PC7
Trace elements (ppb)							
As	9,655	14,671	0,631	20,063	17,409	20,171	7,440
Fe	5,353	0,945	33,836	11,472	0,027	0,110	15,603
Mn	19,844	0,552	1,163	1,613	1,771	10,752	22,752
Cu	14,729	11,021	0,156	1,338	11,633	0,628	0,366
Co	0,002	0,017	49,811	3,135	11,068	0,640	13,104
Ni	3,252	22,674	2,070	33,667	25,168	0,023	5,839
Pd	10,163	10,862	9,885	0,721	28,111	10,301	2,487
Au	20,476	0,561	0,029	0,059	0,041	14,177	28,552
Pt	16,013	3,618	0,601	22,248	3,517	2,549	0,708
Hg	0,514	35,079	1,818	5,685	1,255	40,649	3,150

Appendix 51: Contributions of the variables to the principal components in the saprolith horizon - Serpens North Prospect (%).

	PC1	PC2	PC3	PC4	PC5	PC6	PC7	PC8	PC9
Trace elements (ppb)									
As	3,287	40,065	0,088	1,853	3,764	2,768	9,485	13,580	25,032
Fe	22,780	2,194	4,230	0,411	6,533	20,587	0,253	0,100	0,605
Mn	14,695	6,152	8,073	0,075	8,567	1,050	0,007	56,570	3,582
Cu	8,723	11,725	0,628	8,907	3,501	51,853	1,371	3,217	3,605
Co	20,141	10,246	0,263	9,242	5,115	2,447	5,716	1,510	0,030
Ni	8,801	8,197	4,930	0,047	22,749	1,680	45,246	0,272	7,259
Pd	6,927	3,732	5,364	26,516	20,100	7,481	13,090	5,747	8,878
Au	2,481	6,943	0,131	49,633	8,105	10,500	13,500	1,831	6,792
Pt	0,750	1,627	60,101	1,619	3,645	1,196	2,387	15,948	12,059
Hg	11,414	9,119	16,191	1,695	17,920	0,437	8,944	1,224	32,157

Appendix 52: Collective contributions of variables to the principal components in the Sirius Prospect (%).

	PC1	PC2	PC3	PC4	PC5	PC6	PC7	PC8	PC9
Trace elements (ppb)									
As	2,915	1,286	44,000	7,155	8,148	32,600	0,095	3,799	0,003
Fe	33,256	2,462	0,175	0,053	0,372	0,315	9,473	14,385	39,507
Mn	35,411	0,773	0,130	0,144	0,101	1,708	4,908	2,561	54,264
Cu	4,772	32,854	10,945	2,033	2,215	0,069	1,424	45,610	0,079
Co	0,066	42,584	0,103	0,905	0,475	0,113	31,554	21,632	2,568
Ni	20,349	8,454	0,388	0,980	5,049	5,336	45,787	10,241	3,418
Pd	2,927	3,340	4,718	51,377	1,895	28,738	5,276	1,641	0,089
Au	0,301	0,890	33,004	32,564	5,370	27,721	0,020	0,066	0,064
Pt	0,004	7,357	6,537	4,790	76,375	3,401	1,463	0,066	0,009

Appendix 53: Contributions of variables to the principal components within the aeolian sand horizons in the Sirius Prospect (%).

	PC1	PC2	PC3	PC4	PC5	PC6	PC7	PC8	PC9
Trace elements (ppb)									
As	15,243	0,047	10,291	25,920	0,503	33,858	8,893	5,019	0,225
Fe	20,942	0,235	7,193	0,639	11,269	1,288	31,310	5,301	21,824
Mn	24,919	1,697	1,736	0,921	4,247	1,795	4,230	0,000	60,455
Cu	5,045	0,028	38,551	3,213	9,999	1,684	38,974	2,302	0,204
Co	0,511	44,273	0,753	3,225	1,678	0,054	0,771	44,548	4,186
Ni	18,407	0,976	9,230	1,692	1,332	40,625	13,521	2,575	11,643
Pd	5,268	7,641	19,508	0,168	64,755	0,302	1,378	0,519	0,461
Au	2,825	25,303	4,900	40,189	0,579	11,963	0,854	13,310	0,076
Pt	6,839	19,800	7,840	24,032	5,637	8,431	0,070	26,425	0,926

Appendix 54: Contributions of variables to the principal components in calcrete samples from the Sirius Prospect(%).

	PC1	PC2	PC3	PC4	PC5	PC6	PC7	PC8	PC9
Trace elements (ppb)									
As	0,278	17,311	33,643	0,220	2,886	34,992	0,393	10,156	0,121
Fe	20,201	10,036	1,553	1,784	9,296	0,370	32,371	1,488	22,901
Mn	29,999	1,655	0,010	0,000	1,633	3,946	2,224	6,252	54,281
Cu	0,706	5,638	47,523	0,076	7,664	24,398	8,960	1,098	3,937
Co	18,231	16,936	0,411	1,959	7,867	0,022	2,951	50,955	0,668
Ni	17,376	10,737	11,812	0,385	2,868	2,526	16,892	21,767	15,636
Pd	1,009	14,816	3,451	30,530	39,584	1,983	3,786	2,484	2,358
Au	1,968	15,967	1,285	37,531	9,958	21,977	7,618	3,658	0,038
Pt	10,232	6,905	0,311	27,515	18,244	9,786	24,803	2,142	0,062

Appendix 55: Pearson's correlation of trace elements for all samples obtained from the Serpens North prospect (HH data).

	As	Fe	Mn	Cu	Co	Ni	Pd	Au	Pt	Hg	Fe2O3	MnO	Al2O3
As	1	-.141*	-0,047	-.259**	-.260**	-0,065	-0,020	-.132*	-0,077	-0,133	-0,109	-0,057	-0,137
Fe	-.141*	1	-0,089	.412**	.590**	.409**	0,111	0,023	.174*	-.240**	-0,042	0,006	0,111
Mn	-0,047	-0,089	1	.206**	.240**	.160**	-0,008	-0,030	-0,002	0,108	-0,007	-0,037	-.231*
Cu	-.259**	.412**	.206**	1	.600**	.370**	-.202**	0,027	.155*	-.160*	.182*	0,021	0,106
Co	-.260**	.590**	.240**	.600**	1	.502**	-.142*	0,029	.153*	-.185**	0,136	0,011	0,007
Ni	-0,065	.409**	.160**	.370**	.502**	1	-0,024	0,034	.179**	-.131*	0,085	-0,021	0,123
Pd	-0,020	0,111	-0,008	-.202**	-.142*	-0,024	1	0,052	0,072	.158*	-0,091	-0,016	-0,104
Au	-.132*	0,023	-0,030	0,027	0,029	0,034	0,052	1	.165*	0,043	.213*	-0,058	0,136
Pt	-0,077	.174*	-0,002	.155*	.153*	.179**	0,072	.165*	1	-0,049	0,179	0,001	-0,006
Hg	-0,133	-.240**	0,108	-.160*	-.185**	-.131*	.158*	0,043	-0,049	1	.234*	-0,036	0,047
Fe2O3	-0,109	-0,042	-0,007	.182*	0,136	0,085	-0,091	.213*	0,179	.234*	1	.430**	-0,079
MnO	-0,057	0,006	-0,037	0,021	0,011	-0,021	-0,016	-0,058	0,001	-0,036	.430**	1	-0,101
Al2O3	-0,137	0,111	-.231*	0,106	0,007	0,123	-0,104	0,136	-0,006	0,047	-0,079	-0,101	1

*. Correlation is significant at the 0.05 level (2-tailed).

**. Correlation is significant at the 0.01 level (2-tailed).

Appendix 56: Pearson's correlation of trace elements within the aeolian sand horizon in Serpens North Prospect HH data.

	As	Fe	Mn	Cu	Co	Ni	Pd	Au	Pt	Hg	SiO2	Al2O3	Fe2O3	MnO	CaO
As	1	-.476*	-0,285	-.506**	-.538**	-0,310	0,390	-.466*	-0,414	0,237	0,364	-.450*	-0,198	-0,231	-0,053
Fe	-.476*	1	.442*	.785**	.905**	.775**	-0,329	.461*	.738**	-0,236	-.443**	0,336	.389*	.665**	0,001
Mn	-0,285	.442*	1	.363*	.496**	0,317	-.390*	-0,079	0,008	-0,388	-0,191	0,099	0,148	0,185	0,020
Cu	-.506**	.785**	.363*	1	.801**	.677**	-0,334	0,229	0,482	-0,282	-.383*	.363*	0,302	.490**	-0,071
Co	-.538**	.905**	.496**	.801**	1	.766**	-.376*	.435*	.748**	-0,243	-.500**	.471**	.374*	.694**	0,069
Ni	-0,310	.775**	0,317	.677**	.766**	1	-0,120	0,206	.643**	-0,168	-.522**	0,302	.505**	.724**	0,022
Pd	0,390	-0,329	-.390*	-0,334	-.376*	-0,120	1	-0,193	0,087	0,403	0,237	-0,211	-0,251	-0,149	0,022
Au	-.466*	.461*	-0,079	0,229	.435*	0,206	-0,193	1	.912**	0,067	-0,309	.371*	0,173	0,149	0,063
Pt	-0,414	.738**	0,008	0,482	.748**	.643**	0,087	.912**	1	0,214	-0,422	0,344	0,300	.898**	0,054
Hg	0,237	-0,236	-0,388	-0,282	-0,243	-0,168	0,403	0,067	0,214	1	0,275	-0,033	-.409*	-0,171	0,125
SiO2	0,364	-.443**	-0,191	-.383*	-.500**	-.522**	0,237	-0,309	-0,422	0,275	1	-.620**	-.798**	-.657**	-.583**
Al2O3	-.450*	0,336	0,099	.363*	.471**	0,302	-0,211	.371*	0,344	-0,033	-.620**	1	0,059	.353*	.724**
Fe2O3	-0,198	.389*	0,148	0,302	.374*	.505**	-0,251	0,173	0,300	-.409*	-.798**	0,059	1	.596**	0,083
MnO	-0,231	.665**	0,185	.490**	.694**	.724**	-0,149	0,149	.898**	-0,171	-.657**	.353*	.596**	1	0,188
CaO	-0,053	0,001	0,020	-0,071	0,069	0,022	0,022	0,063	0,054	0,125	-.583**	.724**	0,083	0,188	1

Appendix 57: Pearson's correlation of elements within the stone-line horizon in Serpens North Prospect.

	As	Fe	Mn	Cu	Co	Ni	Pd	Au	Pt	Hg	SiO2	Al2O3	Fe2O3	MnO	CaO
As	1	-0,019	0,099	-0,449	-0,391	-0,073	0,624	-0,180	-0,370	-0,413	0,151	-0,440	0,104	-0,266	-0,220
Fe	-0,019	1	0,404	.518*	.662**	.642**	-0,021	-0,292	0,349	-0,025	0,284	-0,141	-0,118	0,490	-0,122
Mn	0,099	0,404	1	-0,065	0,424	0,186	0,196	-0,179	0,264	0,332	0,251	-0,303	-0,019	0,369	-0,095
Cu	-0,449	.518*	-0,065	1	.715**	.649**	-0,044	-0,322	0,421	0,201	0,047	-0,144	0,150	0,375	-0,290
Co	-0,391	.662**	0,424	.715**	1	.731**	-0,149	-0,048	0,415	0,123	0,101	0,109	-0,139	.507*	-0,103
Ni	-0,073	.642**	0,186	.649**	.731**	1	0,413	0,063	0,049	0,123	0,065	0,070	-0,074	0,115	-0,208
Pd	0,624	-0,021	0,196	-0,044	-0,149	0,413	1	0,146	0,214	0,682	0,230	-.577*	0,322	-0,039	-.696*
Au	-0,180	-0,292	-0,179	-0,322	-0,048	0,063	0,146	1	0,072	-0,400	-0,164	.687**	-0,392	-0,219	0,326
Pt	-0,370	0,349	0,264	0,421	0,415	0,049	0,214	0,072	1	0,793	-0,354	-0,074	0,406	.927**	-0,325
Hg	-0,413	-0,025	0,332	0,201	0,123	0,123	0,682	-0,400	0,793	1	0,206	-0,474	0,390	0,126	-0,364
SiO2	0,151	0,284	0,251	0,047	0,101	0,065	0,230	-0,164	-0,354	0,206	1	-0,156	-.627**	-0,256	-0,416
Al2O3	-0,440	-0,141	-0,303	-0,144	0,109	0,070	-.577*	.687**	-0,074	-0,474	-0,156	1	-.646**	-0,192	.570*
Fe2O3	0,104	-0,118	-0,019	0,150	-0,139	-0,074	0,322	-0,392	0,406	0,390	-.627**	-.646**	1	0,350	-0,236
MnO	-0,266	0,490	0,369	0,375	.507*	0,115	-0,039	-0,219	.927**	0,126	-0,256	-0,192	0,350	1	-0,037
CaO	-0,220	-0,122	-0,095	-0,290	-0,103	-0,208	-.696*	0,326	-0,325	-0,364	-0,416	.570*	-0,236	-0,037	1

Appendix 58: Pearson's correlation of trace elements within the saprolith horizon in Serpens North Prospect.

	As	Fe	Mn	Cu	Co	Ni	Pd	Au	Pt	Hg	SiO2	Al2O3	Fe2O3	MnO	CaO
As	1	0,003	-0,077	-.293*	-.285*	-0,166	0,164	-0,010	-0,024	-0,072	0,217	-0,235	-0,147	0,109	-0,114
Fe	0,003	1	0,146	.549**	.730**	.469**	-0,186	-0,024	-0,283	-.297*	-.273*	0,006	.288**	0,151	0,090
Mn	-0,077	0,146	1	0,121	0,181	0,183	0,205	-0,048	-0,050	0,178	0,032	-.427**	0,127	0,206	0,065
Cu	-.293*	.549**	0,121	1	.623**	.267*	-.259*	0,160	-0,197	-0,123	-.360**	0,082	.368**	0,078	0,136
Co	-.285*	.730**	0,181	.623**	1	.499**	-0,047	-0,059	-0,104	-0,238	-.489**	0,118	.412**	0,200	.282**
Ni	-0,166	.469**	0,183	.267*	.499**	1	-0,045	-0,164	-0,116	-0,168	-0,171	-0,083	.241*	.215*	-0,019
Pd	0,164	-0,186	0,205	-.259*	-0,047	-0,045	1	0,260	0,226	0,083	0,021	-0,131	-0,053	-0,177	0,159
Au	-0,010	-0,024	-0,048	0,160	-0,059	-0,164	0,260	1	-0,049	.288*	0,007	0,161	-0,109	-0,206	0,203
Pt	-0,024	-0,283	-0,050	-0,197	-0,104	-0,116	0,226	-0,049	1	0,028	0,101	0,192	-0,130	0,018	0,145
Hg	-0,072	-.297*	0,178	-0,123	-0,238	-0,168	0,083	.288*	0,028	1	0,062	-.256*	-0,059	-0,127	0,049
SiO2	0,217	-.273*	0,032	-.360**	-.489**	-0,171	0,021	0,007	0,101	0,062	1	-0,148	-.824**	-0,063	-.448**
Al2O3	-0,235	0,006	-.427**	0,082	0,118	-0,083	-0,131	0,161	0,192	-.256*	-0,148	1	-.286**	-.305**	.240*
Fe2O3	-0,147	.288**	0,127	.368**	.412**	.241*	-0,053	-0,109	-0,130	-0,059	-.824**	-.286**	1	0,174	0,089
MnO	0,109	0,151	0,206	0,078	0,200	.215*	-0,177	-0,206	0,018	-0,127	-0,063	-.305**	0,174	1	0,108
CaO	-0,114	0,090	0,065	0,136	.282**	-0,019	0,159	0,203	0,145	0,049	-.448**	.240*	0,089	0,108	1

Appendix 59: Pearson's correlation of trace elements for all horizons from the Sirius Prospect.

	As	Fe	Mn	Cu	Co	Ni	Pd	Au	Pt	Al2O3	Fe2O3	MnO	CaO
As	1	0,169	-0,187	-0,108	-0,029	-0,014	-0,014	-0,052	-0,034	-0,124	-0,100	0,298	.207*
Fe	0,169	1	-.808**	.415**	0,109	-.320**	0,155	0,075	0,025	-.257*	-.257*	0,162	.218*
Mn	-0,187	-.808**	1	-0,151	0,148	.526**	-.226*	-0,085	0,013	.326**	.443**	0,021	-.392**
Cu	-0,108	.415**	-0,151	1	.559**	0,154	0,039	0,042	0,128	.250*	-0,057	0,041	0,026
Co	-0,029	0,109	0,148	.559**	1	.271**	-.238*	-0,031	0,190	.296**	0,189	0,257	-0,097
Ni	-0,014	-.320**	.526**	0,154	.271**	1	-0,092	-0,071	0,010	.242*	-0,004	0,410	-.239*
Pd	-0,014	0,155	-.226*	0,039	-.238*	-0,092	1	-0,016	-0,042	0,031	-0,172	-0,074	-0,072
Au	-0,052	0,075	-0,085	0,042	-0,031	-0,071	-0,016	1	-0,054	-0,039	-0,018	0,444	0,102
Pt	-0,034	0,025	0,013	0,128	0,190	0,010	-0,042	-0,054	1	0,067	-0,113	0,123	0,048
Al2O3	-0,124	-.257*	.326**	.250*	.296**	.242*	0,031	-0,039	0,067	1	0,013	-0,128	-.544**
Fe2O3	-0,100	-.257*	.443**	-0,057	0,189	-0,004	-0,172	-0,018	-0,113	0,013	1	0,282	-.249*
MnO	0,298	0,162	0,021	0,041	0,257	0,410	-0,074	0,444	0,123	-0,128	0,282	1	0,198
CaO	.207*	.218*	-.392**	0,026	-0,097	-.239*	-0,072	0,102	0,048	-.544**	-.249*	0,198	1

*. Correlation is significant at the 0.05 level (2-tailed).

**. Correlation is significant at the 0.01 level (2-tailed).

Appendix 60: Pearson's correlation of trace elements within the aeolian sand horizon in the Sirius Prospect.

	As	Fe	Mn	Cu	Co	Ni	Pd	Au	Pt	Al2O3	Fe2O3	CaO
As	1	0,181	-0,229	-0,453	-0,124	-0,394	0,501	-0,182	0,334	0,098	.577*	0,340
Fe	0,181	1	-.740**	0,415	0,176	-0,364	-0,114	-0,190	0,474	0,415	0,117	0,093
Mn	-0,229	-.740**	1	-0,066	0,186	.675**	-0,009	0,348	-0,423	-.594*	-0,121	-0,306
Cu	-0,453	0,415	-0,066	1	0,362	0,259	-0,513	0,315	0,110	0,268	-0,457	-.608*
Co	-0,124	0,176	0,186	0,362	1	-0,017	-0,178	-0,207	.635*	-0,405	-0,283	-0,383
Ni	-0,394	-0,364	.675**	0,259	-0,017	1	-0,012	0,377	-0,402	-0,116	-0,248	-0,341
Pd	0,501	-0,114	-0,009	-0,513	-0,178	-0,012	1	-0,100	-0,028	-0,205	0,252	0,351
Au	-0,182	-0,190	0,348	0,315	-0,207	0,377	-0,100	1	-0,519	0,046	-0,069	-0,081
Pt	0,334	0,474	-0,423	0,110	.635*	-0,402	-0,028	-0,519	1	0,122	-0,004	-0,086
Al2O3	0,098	0,415	-.594*	0,268	-0,405	-0,116	-0,205	0,046	0,122	1	0,224	0,003
Fe2O3	.577*	0,117	-0,121	-0,457	-0,283	-0,248	0,252	-0,069	-0,004	0,224	1	.646**
CaO	0,340	0,093	-0,306	-.608*	-0,383	-0,341	0,351	-0,081	-0,086	0,003	.646**	1

*. Correlation is significant at the 0.05 level (2-tailed).

**. Correlation is significant at the 0.01 level (2-tailed).

Appendix 61: Pearson's correlation of trace elements within the calcrete horizon in the Sirius Prospect.

	As	Fe	Mn	Cu	Co	Ni	Pd	Au	Pt	Al2O3	Fe2O3	CaO
As	1	0,568	-.647*	-.685**	-0,185	-0,274	.701**	-0,115	0,148	-0,435	-0,196	0,360
Fe	0,568	1	-.936**	-.774*	-0,559	-0,491	0,703	-0,212	0,715	-0,616	-0,228	0,462
Mn	-.647*	-.936**	1	.805**	0,446	.546*	-0,511	-0,046	-0,385	0,340	0,000	-0,222
Cu	-.685**	-.774*	.805**	1	.609*	0,485	-0,537	0,016	-0,288	0,469	0,160	-0,324
Co	-0,185	-0,559	0,446	.609*	1	0,497	-0,461	-0,156	-0,513	0,304	0,003	-0,240
Ni	-0,274	-0,491	.546*	0,485	0,497	1	-0,200	-0,095	-0,147	0,126	-0,090	-0,102
Pd	.701**	0,703	-0,511	-0,537	-0,461	-0,200	1	0,025	0,392	-0,079	0,248	-0,015
Au	-0,115	-0,212	-0,046	0,016	-0,156	-0,095	0,025	1	0,200	0,269	.716**	-0,376
Pt	0,148	0,715	-0,385	-0,288	-0,513	-0,147	0,392	0,200	1	-.771**	-0,310	.700*
Al2O3	-0,435	-0,616	0,340	0,469	0,304	0,126	-0,079	0,269	-.771**	1	.728**	-.879**
Fe2O3	-0,196	-0,228	0,000	0,160	0,003	-0,090	0,248	.716**	-0,310	.728**	1	-.802**
CaO	0,360	0,462	-0,222	-0,324	-0,240	-0,102	-0,015	-0,376	.700*	-.879**	-.802**	1

*. Correlation is significant at the 0.05 level (2-tailed).

**. Correlation is significant at the 0.01 level (2-tailed).

Appendix 62: Pearson's correlation of elements within the saprolith horizon in the Sirius Prospect.

	As	Fe	Mn	Cu	Co	Ni	Pd	Au	Pt	Al2O3	Fe2O3	MnO	CaO
As	1	.258*	-0,179	0,012	0,194	0,164	-0,137	-0,021	-0,070	-0,100	0,041	.640**	0,057
Fe	.258*	1	-.859**	.416**	0,134	-.310**	0,151	.276*	-0,037	-.337**	-.321**	0,212	0,022
Mn	-0,179	-.859**	1	-0,225	0,093	.473**	-0,220	-0,230	0,079	.330**	.401**	-0,036	-0,208
Cu	0,012	.416**	-0,225	1	.558**	0,158	0,090	0,100	0,103	.303*	-0,183	0,117	-0,012
Co	0,194	0,134	0,093	.558**	1	.276*	-0,223	0,033	0,163	.331**	-0,104	0,304	-0,162
Ni	0,164	-.310**	.473**	0,158	.276*	1	-0,081	-0,169	0,086	0,231	0,026	0,381	-0,125
Pd	-0,137	0,151	-0,220	0,090	-0,223	-0,081	1	-0,025	-0,045	0,007	-0,135	-0,131	0,110
Au	-0,021	.276*	-0,230	0,100	0,033	-0,169	-0,025	1	-0,076	-0,066	-0,091	0,153	-0,055
Pt	-0,070	-0,037	0,079	0,103	0,163	0,086	-0,045	-0,076	1	-0,128	0,110	-0,145	0,028
Al2O3	-0,100	-.337**	.330**	.303*	.331**	0,231	0,007	-0,066	-0,128	1	-.237*	-0,128	-0,218
Fe2O3	0,041	-.321**	.401**	-0,183	-0,104	0,026	-0,135	-0,091	0,110	-.237*	1	0,282	0,081
MnO	.640**	0,212	-0,036	0,117	0,304	0,381	-0,131	0,153	-0,145	-0,128	0,282	1	0,198
CaO	0,057	0,022	-0,208	-0,012	-0,162	-0,125	0,110	-0,055	0,028	-0,218	0,081	0,198	1

*. Correlation is significant at the 0.05 level (2-tailed).

**. Correlation is significant at the 0.01 level (2-tailed).